VOLUME 120 NUMBER 1

THE ASTROPHYSICAL JOURNAL

AN INTERNATIONAL REVIEW OF SPECTROSCOPY AND ASTRONOMICAL PHYSICS

JULY 1954

BEHAVIOR OF MATTER IN SPACE . . . . . *Lyman Spitzer, Jr.* 1
ON "ELEPHANT-TRUNK" STRUCTURES IN THE REGION OF O ASSOCIATIONS *E. A. Frieman* 18
A STUDY OF THE ATMOSPHERES OF EARLY O AND Of STARS . . . *J. B. Oke* 22
EARLY-TYPE STARS IN THE DIRECTION OF THE GALACTIC CENTER *W. A. Hiltner* 41
PHOTOELECTRIC SPECTROPHOTOMETRY OF PLANETARY NEBULAE *William Liller and Lawrence H. Aller* 48
A SECOND PHOTOELECTRIC STUDY OF 16 LACERTAE . . . . *Merle F. Walker* 58
THE MAGNETIC VARIABLE HD 188041 . . . . . *Horace W. Babcock* 66
THE ABNORMAL ATMOSPHERE OF AG PEGASI *G. R. Burbidge and E. Margaret Burbidge* 76
THE WIDTH OF H_α IN SOLAR FLARES *Leo Goldberg, Helen W. Dodson, and Edith A. Müller* 83
EMISSION IN HYDROGEN BALMER LINES AND CONTINUUM IN FLASH SPECTRUM OF 1952 TOTAL SOLAR ECLIPSE AT KHARTOUM, SUDAN *R. Grant Athay, Donald E. Billings, John W. Evans, and Walter O. Roberts* 94
ACTIVE REGION PROMINENCES AND THE YELLOW CORONAL LINE *F. P. Dolder, W. O. Roberts, and D. E. Billings* 112
BRIGHT LATE M-TYPE STARS NEAR THE GALACTIC EQUATOR *J. J. Nassau and V. M. Blanco* 118
CARBON STARS AT THE GALACTIC EQUATOR IN A ZONE 4° WIDE *J. J. Nassau and V. M. Blanco* 129
VARIATIONS IN THE STELLAR LUMINOSITY FUNCTION. VI. A REGION IN MONOCEROS . . . . . *S. W. McCuskey* 139
THE VISCOSITY AND THERMAL CONDUCTIVITY OF A COMPLETELY IONIZED GAS . . . . . *Sydney Chapman* 151
THE SOLAR INTERNAL OPACITY AND CONSTITUTION . . *I. Epstein and L. Motz* 156
THE PROPAGATION OF SHOCK WAVES IN SELF-GRAVITATING GAS SPHERES *Zdeněk Kopal* 159
ON THE ELONGATION OF A FLUID SPHERE IN A UNIFORM EXTERNAL MAGNETIC FIELD . . . . . *Guro Ejellestad* 172

NOTES

POLARIZATION OF A HEAVILY OBSCURED CLUSTERING OF OB STARS IN CYGNUS . *W. A. Hiltner* 178
NOTE ON THE SPECTRUM OF 16 LACERTAE . . . *A. Van Hoof, M. De Ridder, and O. Struve* 179
PHYSICAL AND GALACTIC CHARACTERISTICS OF PLANETARY NEBULAE . . . *Hugh M. Johnson* 182
PHOTOSPHERIC MAGNETIC FIELDS PRECEDING OTHER SOLAR ACTIVITY . *Donald E. Billings* 184
A NOTE ON THE MOTION OF AURORAL STREAMERS . . . . . *Dean B. McLaughlin* 185
THE TEMPERATURE OF THE LOW CHROMOSPHERE . . . . . *Leo Goldberg* 185

ERRATUM 187

THE UNIVERSITY OF CHICAGO PRESS
CHICAGO, ILLINOIS, U.S.A.

July 1954 Vol. 120, No. 1

THE ASTROPHYSICAL JOURNAL

AN INTERNATIONAL REVIEW OF SPECTROSCOPY AND ASTRONOMICAL PHYSICS

Founded in 1895 by George E. Hale and James E. Keeler

Published in Collaboration with the American Astronomical Society

S. CHANDRASEKHAR
Managing Editor

GERARD P. KUIPER
Associate Editor

Yerkes Observatory of the University of Chicago

EDITORIAL BOARD

MARTIN SCHWARZSCHILD, JR. (1954-58)
Princeton University Observatory

G. HERZBERG (1952-56)
National Research Council, Ottawa

H. W. BABCOCK (1953-57)
Mount Wilson Observatory of the Carnegie Institution of Washington

FRED L. WHIPPLE (1952-54)
Harvard College Observatory

C. D. SHANE (1952-55)
Lick Observatory, University of California

The Astrophysical Journal is published bimonthly by the University of Chicago at the University of Chicago Press, 5750 Ellis Avenue, Chicago 37, Illinois, during January, March, May, July, September, and November. ¶Two volumes are published per year, one beginning with the January issue and the other beginning with the July issue. The subscription price is $6.00 per volume or $12.00 per year; the price of single copies is $3.00. (Orders for service of less than a volume will be charged at the single copy rate.) ¶Postage is prepaid by the publishers on all orders from the United States and its possessions. No extra charge is made for postage to countries in the Pan American Postal Union. ¶Postage is charged extra as follows: for Canada, 20 cents per volume, 40 cents per year (total $6.20 per volume, $12.40 per year); on single copies 5 cents (total $3.05); for all other countries in the Postal Union, 40 cents per volume, 75 cents per year (total $6.40 per volume, $12.75 per year), on single copies 10 cents (total $3.10). ¶Subscriptions are payable in advance. Please make all remittances payable to The University of Chicago Press, in United States currency or its equivalent by postal or express money orders or bank drafts.

The following is an authorized agent:

For the British Empire, except North America and Australasia: The Cambridge University Press, Bentley House, 200 Euston Road, London, N.W. 1, England. Prices of yearly subscriptions and of single copies may be had on application.

Claims for missing numbers should be made within the month following the regular month of publication. The publishers expect to supply missing numbers free only when losses have been sustained in transit, and when the reserve stock will permit.

Business correspondence should be addressed to The University of Chicago Press, Chicago 37, Illinois.

Communications for the editors and manuscripts should be addressed to: S. Chandrasekhar, Editor of THE ASTROPHYSICAL JOURNAL, Yerkes Observatory, Williams Bay, Wisconsin.

Line drawings and photographs should be made by the author, and all marginal notes such as co-ordinates, wave lengths, etc., should be included in the cuts. It will not be possible to set up such material in type.

One copy of the corrected galley proof should be returned as soon as possible to the editor, Yerkes Observatory, Williams Bay, Wisconsin. Authors should take notice that the manuscript will not be sent to them with the proof.

The cable address is "Observatory, Williamsbay, Wisconsin."

The articles in this journal are indexed in the *International Index to Periodicals*, New York, N.Y.

Applications for permission to quote from this journal should be addressed to The University of Chicago Press, and will be freely granted.

Microfilms of complete journal volumes are available to regular subscribers only and may be obtained at the end of the year. Orders and inquiries should be addressed to University Microfilms, 313 North First Street, Ann Arbor, Michigan.

Notice to subscribers: If you change your address, please notify us and your local postmaster immediately.

Entered as second-class matter, July 21, 1930, at the Post-Office at Chicago, Ill., under the Act of March 3, 1879.
Acceptance for mailing at special rate of postage provided for in United States Postal Act of October 3, 1917, Section 1103, amended February 28, 1925.
Copyright 1954 by the University of Chicago.

[PRINTED IN U.S.A.]

THE ASTROPHYSICAL JOURNAL

AN INTERNATIONAL REVIEW OF SPECTROSCOPY AND ASTRONOMICAL PHYSICS

VOLUME 120 JULY 1954 NUMBER 1

BEHAVIOR OF MATTER IN SPACE*

LYMAN SPITZER, JR.
Princeton University Observatory
Received March 12, 1954

I. INTRODUCTION

Study of the stars is one of man's oldest intellectual activities. Study of the matter between stars is one of the youngest. Even as recently as some thirty years ago, the existence of interstellar material was uncertain. In 1920, for example, a prominent astrophysicist, in an extensive discussion of the calcium absorption lines, now believed to be truly interstellar, concluded: "Hartmann's suggestion that the [calcium] clouds lie between the observer and the star . . . cannot be accepted. The hypothesis that the calcium cloud is a part of the star's atmosphere seems most satisfactory." Similarly, another well-known astronomer, in a thorough analysis of the absorption of light in interstellar space, wrote in 1923: "General absorption can at most amount to 2 magnitudes per kiloparsec; the true value is probably less than 0.1 magnitude per kiloparsec." We now know that absorption and scattering in the galactic plane actually amount, on the average, to at least 1.5 mag/kpc, very close to the extreme upper limit of thirty years ago.

In the last three decades enormous strides have been made in determining beyond a doubt the existence of matter between the stars and in estimating the amount of material present. The observational evidence has been obtained with three main techniques. Measures of interstellar emission lines, primarily the Balmer lines and the 21-cm line of neutral hydrogen, have given very basic information on the interstellar hydrogen gas. Spectroscopic measures of absorption lines have given invaluable data on the impurities present in the gas, particularly sodium and calcium. Photoelectric measures of the light from distant stars, which are usually somewhat obscured by the intervening clouds of solid particles, or grains, have indicated the sizes and distribution of these grains. The primary information obtained directly from these observations is brought together in Table 1. While many detailed facts have, of course, been omitted, this table includes most of the general information about interstellar matter which can be obtained directly from the observations, together with well-established physical laws. In particular, results dependent on assumed relative abundances of different atoms have not been included.

It is of interest that modern electronic techniques are responsible for a large part of the

* Seventh Henry Norris Russell Lecture of the American Astronomical Society delivered at Nashville, Tennessee, on December 27, 1953.

information in Table 1. Without the photoelectric cell and the electronic equipment needed for microwave reception, the only information remaining in Table 1 would be that obtained with the spectroscope, using this at its ultimate in either speed or resolution. Even here, it would seem that electronic techniques would be preferable. Most of the interstellar lines, other than the standard lines of sodium and ionized calcium, are very weak, usually not much exceeding some 10 mA in equivalent width. To detect so weak a line with a photographic spectrograph is difficult, and accurate measures are generally not possible.

TABLE 1

OBSERVATIONAL RESULTS ON INTERSTELLAR MATTER

A. HYDROGEN GAS	
Density	About 1 atom/cm^3 in spiral arms, with much lower values outside arms
Physical state	Ionization nearly complete within 20–150 parsecs of B and O stars (H II regions)
	Elsewhere hydrogen is predominantly neutral (H I clouds)
Temperature	Greater than 1000° in H II regions; temperature about 50° K in dense H I clouds
Velocities	Circular velocity of galactic rotation; turbulence 5–10 km/sec (r.m.s. radial velocity)
B. OTHER ELEMENTS IN GAS	
Density	Mean density of Na and Ca^+ about 3×10^{-9} atoms/cm^3
	$Fe, Ti^+, K, CH, CH^+, CN$ present with about same density
Velocities	Ca^+ present in clouds or currents of differing velocities
	Most of these clouds move with local circular velocity of galactic rotation, plus r.m.s. spread of 5–10 km/sec in radial velocity
	Straight line in galactic plane near sun intersects 10 such clouds per kiloparsec
	About 1 per cent of clouds have high random velocities, from 25 up to 95 km/sec
	Ratio of Ca^+ to Na greater in high-velocity clouds than in low-velocity clouds
C. GRAINS	
Size	Mean radius of optically important particles about 3×10^{-5} cm
	Distribution of radii highly similar in different regions
Density	Mean space density of optically important particles in local spiral arms about 10^{-26} gm/cm^3; density much less outside spiral arms
	Spatial distribution extremely irregular; concentrations range in size from 0.05 to 50 parsecs, with density varying by at least 10^4
Polarization	Grains somewhat elongated and tend to be oriented perpendicular to local spiral arms

In marked contrast, a photoelectric cell, looking at a width of a tenth of an angstrom and with an integrating time of an hour, could measure the equivalent width of an interstellar line in the spectrum of a 6th-magnitude star with a probable error of only 0.1 mA; this calculation is based on the performance of the 100-inch telescope and assumes a light-loss of 90 per cent in the light-path from telescope objective to the photosensitive surface. Such a technique would make possible accurate measures on weak lines, such as the line of neutral calcium at λ 4227, and might even permit a study of the abundance of neutral

oxygen, since the intensity of the forbidden line λ 6300 of interstellar oxygen might be as great as 0.1 mA in the spectrum of a star about 1 kiloparsec away. Moreover, even for the strong sodium lines, accurate measures of the doublet ratio would be extremely useful in discussing the relative distribution of grains and gas. Evidently it is from the further applications of such electronic techniques that marked progress may be expected in the future observational study of the interstellar gas.

The subject of the present paper is not, however, the important practical problem of observational techniques but rather the fascinating theoretical problem of how matter behaves in interstellar space. The task is the following. Given the data in Table 1, what can we infer about the various physical processes occurring in space, processes which cannot themselves be observed directly? Many fascinating problems arise when we try to carry out this general assignment. Here we shall consider primarily the following two questions: (1) What determines the temperature of the interstellar gas? and (2) How can we explain the random motions of the interstellar clouds? As we shall see, these questions are directly related, since thermal effects apparently are dominant in accelerating the interstellar material.

II. TEMPERATURE OF THE INTERSTELLAR GAS

In many ways interstellar space is as far from thermal equilibrium as can be imagined. The temperature found will depend entirely on the thermometer used. As shown by Eddington (1930) decades ago, a hypothetical material heated only by starlight and absorbing this light with equal efficiency in all wave lengths would cool off by its own radiation to about 3° K. On the other hand, the cosmic-ray particles, which are atoms moving at speeds close to that of light, have kinetic energies corresponding to trillions of degrees. Clearly, the concept of temperature is not very applicable to the stellar radiation field or to the cosmic-ray particles.

a) KINETIC EQUILIBRIUM

When we consider the random velocities of most of the atoms between the stars, we find that these velocities, at least, may be characterized by a temperature. In particular, we shall see that the distribution of the random velocities is closely Maxwellian, exactly as in a system which is in true thermal equilibrium. Thus if we define a kinetic temperature by the equation

$$\tfrac{3}{2}kT = \tfrac{1}{2}\overline{m\,v^2},$$

where v is the three-dimensional random velocity and the bar denotes an average over all atoms, each of mass m, then all properties of the gas depending on random motions of the atoms may be determined from T as though the system were in thermal equilibrium. This quantity T we shall therefore call the "temperature of the interstellar gas."

First, we must show that the velocity distribution is, in fact, Maxwellian. We know that such a distribution will result if elastic collisions predominate over inelastic ones. If kinetic energy is exchanged back and forth among atoms many times, without conversion into radiative energy or internal energy, then the same general probability considerations can be applied as in true thermal equilibrium, and the velocity distribution will be Maxwellian. Such a state of affairs we shall describe as "kinetic equilibrium." Let us therefore examine the relative number of elastic and inelastic collisions.

The rate of energy exchange in elastic collisions may be measured by the time t_E, defined by Chandrasekhar (1942) as the time required for the root-mean-square change of energy by a particle to equal the original energy. The rate of energy loss in inelastic collisions may be measured by the time t_I, defined as the time between inelastic impacts. To obtain the ratio t_I/t_E for electrons, we shall compute this quantity for an electron of kinetic energy $3kT/2$, on the assumption that an inelastic collision involves

an energy loss of half this kinetic energy. The value assumed for the inelastic cross-section may be taken from Spitzer and Savedoff (1953), for an ion of charge Z equal to 1 (with g_B, the weight of the upper level, equal to 3). Resultant values of this ratio are given in Table 2 for different electron temperatures for regions of ionized and neutral hydrogen. In ionized regions the electron density n_e is assumed to be 1 per cubic centimeter, while n_i, the density of ions with which inelastic collisions are possible, is assumed smaller by a factor of 10^3; this low abundance of elements other than hydrogen and helium cannot be regarded as proved for the interstellar gas, but seems very probable. In the regions of neutral hydrogen these two densities n_e and n_i are each assumed to equal 10^{-2} per cubic centimeter. In these *H* I regions the density of hydrogen molecules, whose vibrational state may be excited by electrons with more than 0.5 electron volts of energy, is assumed to be 100 times n_e.

The various assumptions made in deriving this table tend to maximize the effect of inelastic collisions, i.e., to decrease t_I. Yet the value of t_I is from 10^2 to 10^3 times greater than t_E. The numbers underlined in the table represent the values for the temperatures regarded as likely. The relatively low value of this ratio when the temperature rises above 1000°, with hydrogen still neutral, results from the excitation of H_2 molecules by elec-

TABLE 2

RELATIVE IMPORTANCE OF ELASTIC AND INELASTIC ENCOUNTERS

HYDROGEN	VALUES OF t_I/t_E WITH TEMPERATURE OF:		
	100°	1000°	10,000°
Ionized	3.0×10^9	3.6×10^8	$\underline{4.4\times10^7}$
Neutral	$\underline{3.5\times10^6}$	3.9×10^5	4.0×10^2

trons. Even in this extreme case, t_I is still sufficiently greater than t_E to insure kinetic equilibrium and a Maxwellian distribution of velocities. Since t_E is only a week or two at most, establishment of kinetic equilibrium should be very rapid. We conclude that the electron-velocity distribution is virtually certain to be nearly Maxwellian throughout the interstellar gas.

For the atoms of the gas, similar conclusions may be demonstrated for the *H* II regions. Moreover, the kinetic temperatures of all the atoms must be closely equal to the electron temperature. In *H* I regions the results are not quite so certain, and, while the hydrogen atoms are likely to have a Maxwellian velocity distribution, their mean kinetic energy may in certain extreme cases deviate significantly from the mean electron energy. Since such deviations do not seem very likely, we may usually neglect them and talk of a single temperature for all particles in the interstellar gas. Even the grains will usually have random velocities given by this kinetic temperature.

b) PROCESSES DETERMINING TEMPERATURE

Once the existence of a temperature has been established for the interstellar gas, it is relevant to investigate the processes which determine this temperature. In principle, these processes are very simple. The gas gains heat by absorption of light from the stars. It loses heat by radiation into space. The temperature automatically adjusts itself so that the heat gained equals the heat lost. If the temperature is too high, then the heat radiated exceeds the heat absorbed, and the temperature falls, while if the temperature is too low, the reverse happens, and the temperature rises. If we know how the absorption and radia-

tion of heat depend on the temperature, we can then find the temperature at which these processes are balanced.

As Eddington (1930) pointed out many years ago, the interstellar gas gains heat from starlight by means of the photoelectric effect. A neutral atom absorbs a photon, and an electron is ejected. The kinetic energy of this free electron is then available for heating the gas. The atoms which are capable of this process spend most of their time ionized. Thus the process consists of an electron colliding with the ion and being captured, emitting a photon. Then a stellar photon of high energy encounters the neutralized atom and is absorbed, with the electron going off with more energy than it had before it was captured. This process of electron capture followed by photoionization can occur with any element. Since hydrogen and helium are assumed to be vastly more abundant than any other elements, these two types of atoms provide most of the heating for the interstellar gas. Strömgren (1939) has showed that the ultraviolet radiation capable of ionizing hydrogen or helium is confined to roughly spherical regions around the early-type stars, a result given in Table 1. This theoretical prediction has been beautifully confirmed by observations made by Morgan and his collaborators at the Yerkes Observatory on such regions nearby and by Baade at the Mount Wilson and Palomar Observatories on such regions in M31. It follows directly that most of the heating of the interstellar gas must occur in these regions.

The cooling of the gas by radiation is quite a different story. Here atomic hydrogen plays a very minimum role, since this atom is a very poor radiator in visible and infrared light. As shown by Menzel and Aller (1941) for planetary nebulae, the dominant process of cooling is excitation of an atom by electron impact, followed by radiation of a photon, which carries away into space the energy lost to the atom by the colliding electron. All the excited states of the hydrogen atom lie some 10 volts or more above the ground level. Hence atomic hydrogen cannot radiate under electron bombardment unless the electrons have some 10 volts of energy, corresponding to a temperature well above 10,000° K. In helium the situation is even more extreme, with the lowest excited state lying about 20 volts above the ground level. Most other atoms, neutral or ionized, have levels with excitation energies ranging from a hundredth of an electron volt to several electron volts. These atoms can provide an important source of cooling. In addition, molecules and grains can radiate in the infrared and must also be considered as cooling agents.

c) TEMPERATURE OF *H* II REGIONS

Since oxygen is probably more abundant than any of the other atoms possessing low-lying energy levels and since most of the oxygen atoms in *H* II regions are probably singly ionized, the excitation of the O^+ excited level, 3.31 electron volts above the ground-level, is likely to be one of the chief sources of cooling in these regions. An atom excited in this way will jump down, after a wait of several hours, emitting a photon in the forbidden lines at λ 3727. Cross-sections for excitation of this level by electrons have recently been computed by Seaton (1953), who estimates an accuracy of about 40 per cent in his results. Since many previous computations gave results which were too great by an order of magnitude, the accuracy claimed by Seaton should represent a very great gain over previous work. From his results we can compute L_{ei}, the energy lost per electron per second in collisions with oxygen ions. From known quantum-mechanical formulae we can compute G_{ep}, the energy gained per electron per second in radiative encounters with protons, including energy losses in free-free transitions as well as electron captures and subsequent re-emission. The results are shown in Figure 4, where the dotted line represents G_{ep}, with the dashed line, L_{ei}. In this computation the proton density has been set equal to 1 per cubic centimeter, with the density of oxygen ions, to 10^{-3} per cubic centimeter. The distribution of ionizing radiation is taken to be that near a star of surface temperature 30,000°, corresponding to a star of spectral type about O9. The rise of the energy gain, G_{ep}, at the lower temperatures is due to the increase in electron-capture

cross-section with decreasing electron velocities. A slow electron is much more likely to be captured than a fast electron. The steep rise of L_{ei} with increasing temperature results from the fact that, at the temperatures shown, only a very small fraction of the electrons present have the 3.31 electron volts of energy required to excite the singly ionized oxygen atom. As the temperature increases, this fraction rises sharply, with a resultant rise in the rate of cooling.

Figure 1 shows that the equilibrium temperature under this assumption is about 8000° K. More important, the figure shows that large changes in the relative abundance of oxygen to hydrogen will not affect the temperature very greatly. If, for example, we

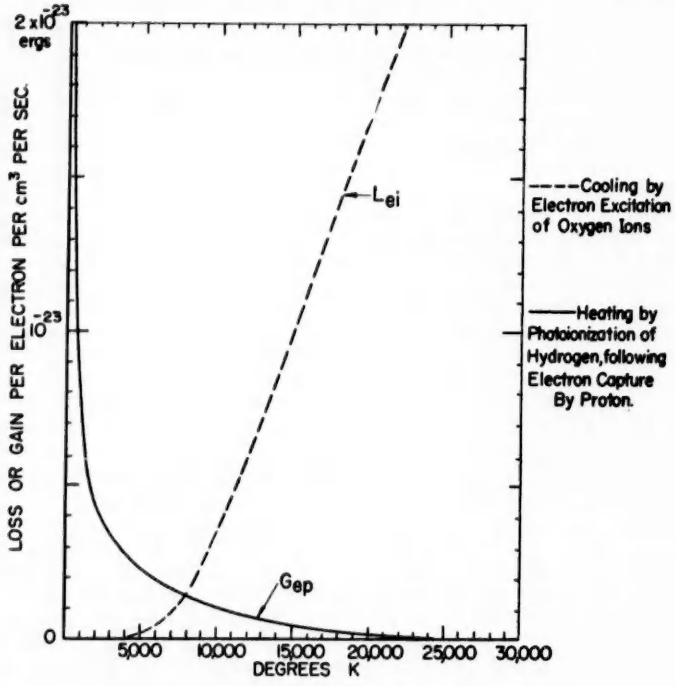

FIG. 1.—Heating and cooling in regions of ionized hydrogen

assume that this relative abundance is uncertain by a factor of 2, then the equilibrium temperature will lie between 7000° and 9000°. Evidently, if there is any appreciable amount of singly ionized oxygen present, the temperature cannot be much greater than about 15,000° K. Temperatures much lower than 8000° would be possible if there were some other cooling agent whose efficiency held up at lower temperatures. Neutral atoms are relatively ineffective, and the only other ion with probable high relative abundance and suitable low-lying excited levels is singly ionized nitrogen, which has an excited level at 1.89 electron volts. This excitation energy is a little over half the energy of the first excited level of O^+. Electron excitation of this level would depress the temperature to about 5000° K, if the abundance of N^+ were as great as that assumed here for O^+. If this happened, very few electrons would have enough energy to excite the oxygen ions, and

the forbidden lines of O^+ would not occur. The fact that these lines are actually observed in considerable strength indicates that the temperature is probably at least 8000° and either that the collisional cross-sections are much less than computed or that the abundance of N^+ is substantially less than that of O^+. The fact that the ionization potential of N^+ is 5.5 volts less than that of O^+ might account for this difference in relative ion abundance.

Evidently we are far from a precise numerical agreement between theory and observation for the temperatures of *H* II regions. The important physical processes seem clear, however, and a temperature somewhere in the general neighborhood of 10,000° K seems firmly indicated.

d) TEMPERATURE OF *H* I REGIONS

When we consider the regions where hydrogen is neutral, we find an entirely different picture. The chief heating mechanism, absorption of ultraviolet radiation by hydrogen atoms, is now absent, since the entire ultraviolet end of the spectrum, beyond 912 A, is completely missing as a result of the high ultraviolet opacity of the neutral hydrogen gas. In addition to hydrogen, the elements helium, nitrogen, oxygen, and neon will be completely neutral. Of the more abundant elements, carbon, with its ionization potential 2.3 electron volts less than that of hydrogen, can be ionized. Thus the free electrons will come from carbon, together with silicon and the metals, and the primary source of heating will be the photoionization of these same atoms. Cooling will be produced when an electron excites the low-lying levels of these ions, exactly as before. Since the heating has dimished so markedly, while the physical processes producing cooling are relatively unchanged by the neutralization of the hydrogen, it is evident that the temperature must drop until the electrons no longer have enough energy to excite the low-lying levels. We shall see that the resultant equilibrium temperature is in the neighborhood of 50° K.

If we neglect the presence of the neutral hydrogen atoms for the moment, the physical reason for this low temperature of *H* I regions is the relative inefficiency of heating by radiation as compared to cooling. We have seen that heating requires, first, that an electron be captured by an ion, in order that this same electron may be ejected from the atom by a photon of starlight. Electron capture, with the emission of radiation, is a very inefficient process. For electrons whose kinetic temperature is about 10,000° K, the cross-section for capture is about 10^{-21} cm², much less than the geometrical cross-section. Excitation of an ion by an electron is a very much more likely process, if the atom has a level whose excitation energy is less than the electron kinetic energy. The cross-section for such an event is about 10^{-17} cm² for electrons at 10,000°; this value is somewhat less than the geometrical cross-section of a neutral atom, but greater than the cross-section for radiative capture by a factor of 10,000. For every electron that is captured and then absorbs a stellar photon and heats up the gas, 10,000 electrons will excite the ionized atom, if the excited levels have energies low enough. Evidently the gas will cool until the electrons no longer have enough energy to excite the ions. In *H* II regions the heating is done by protons, which are at least 1000 times more abundant than the atoms doing the cooling. Thus with a moderate drop of the rate of cooling, produced by a fall of the temperature to about 10,000°, equilibrium is reached. In *H* I regions, where the ions responsible for the cooling must also provide the heating, the temperature must drop much further.

If the only low-lying excited levels were those we have already discussed, with excitation energies of several volts, the temperature would not have to drop very far before the rate of cooling fell practically to zero. In fact, most ions have low-lying levels about a hundredth of an electron volt above the ground-level, and the excitation of these can produce cooling even at 100° K. The heat lost to the gas in each excitation is small, and for this reason these levels are unimportant in *H* II regions. In *H* I regions, where both

heating and cooling are relatively much slower, these low-lying excited levels are very important.

To illustrate the type of behavior that may be expected, we may compute the heating and cooling for a gas composed of electrons and singly ionized carbon atoms. Since carbon is the most abundant atom that can be ionized in the *H* I region, other elements may at first be neglected. The ion C^+ has an excited level 0.0079 electron volts above the ground level. No information is available on the cross-section for collisional excitation of this level, but if we take reasonable values, following Spitzer and Savedoff (1953), we obtain the results shown in Figure 2. Here G_{ei}, shown by the solid line, represents the

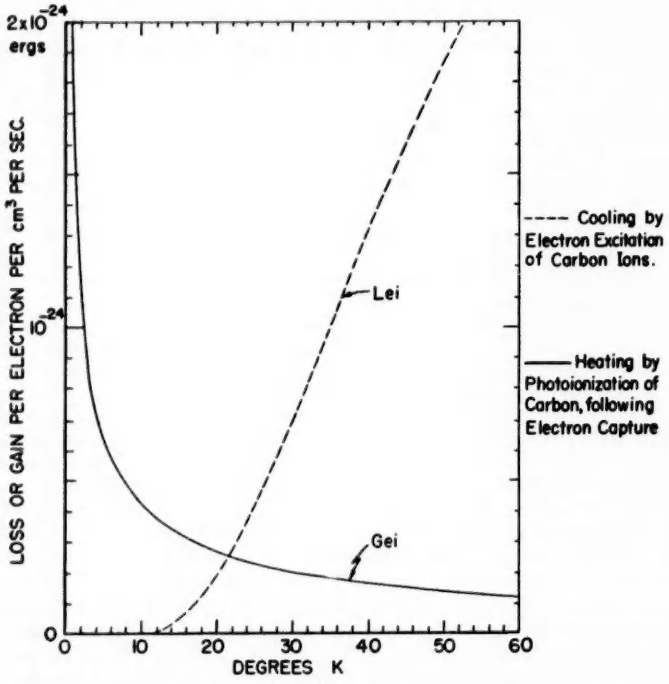

FIG. 2.—Heating and cooling by electrons in regions of neutral hydrogen

gain in energy per electron per second resulting from electron capture and subsequent reionization; L_{ei}, shown by the dashed line, represents the energy loss per electron per second resulting from ion excitation. To fix the vertical scale, the ion density has been set equal to $5 \times 10^{-3}/\text{cm}^3$; the relative position of the two curves is unaffected by the ion density. The color temperature of the ionizing radiation is taken to be 20,000° K.

Figure 2 indicates an equilibrium temperature of only 22° K. Again we see that relatively large changes in the assumed cross-section for collisional excitation will lead to only a small change in the equilibrium temperature. However, carbon ions may be much less abundant than we have assumed. It is possible that the carbon atoms are mostly neutral, although this does not seem very likely in a typical interstellar gas cloud. Another possibility is that a large fraction of the carbon atoms may be locked up in the

grains. For conditions in a typical gas cloud, a carbon ion will collide with a grain about once every 3×10^8 years, and there has thus been plenty of time for atoms to stick to grains. The rate at which atoms are given off from the grains depends partly on the rate of collisional evaporation, a process analyzed in detail by Oort and van de Hulst (1943), and partly on the rate of photodissociation at the surface of grains, a process which may also be of importance. Since these rates are difficult to compute theoretically, no definite conclusions can be drawn. While the observation of molecular *CH* in interstellar clouds indicates that some carbon vapor must be present,[1] the possibility that most of the carbon atoms may be locked up in the grains can certainly not be excluded.

To digress for a moment from the subject of interstellar temperatures, it may be noted that analysis of interstellar sodium and calcium suggests that many of the calcium atoms, also, are locked up in the grains. We have seen in Table 1 that the ratio of calcium ions to sodium atoms is higher in the clouds of high velocity than in the low-speed clouds. When these ratios are interpreted in terms of the ionization equilibrium theory, as applied by Strömgren (1948) to these conditions, we find that the ratio of calcium atoms, in all stages of ionization, to the corresponding number of sodium atoms has nearly the same value in the high-velocity clouds as in the earth and the stars. In the low-velocity clouds, on the other hand, this ratio is abnormally low. The result is consistent with the belief that in the low-velocity clouds calcium atoms are mostly locked up in the grains, while the sodium atoms are not. If the sodium atoms are expelled from grains, on absorption of a photon in the near ultraviolet, while calcium atoms are not, this result would be consistent with physical expectations. The normal ratio in high-velocity clouds could then be attributed to general evaporation or dissociation of the grains produced at the same time that the clouds were accelerated, since, as we shall shortly see, acceleration is apparently produced by an intense field of ultraviolet radiation. This working hypothesis seems to have a certain attractiveness.

Returning, now, to interstellar temperatures, if we admit the possibility that carbon ions may not be present in appreciable abundance, we must then consider the effects produced by other ions. The next most abundant elements with such low-lying levels in the singly ionized state are silicon and iron. Since the excitation energies of the lowest excited levels in these ions are 0.035 and about 0.05 electron volts, some five times the corresponding excitation energy in the carbon ion, the equilibrium temperature will be roughly five times as great as the value shown in Figure 2, or roughly 100° K. Evidently, a temperature not much greater than 100° K seems indicated in an *H* I region.

We have neglected so far the presence of neutral hydrogen atoms in these *H* I regions. Since these atoms probably outnumber all others except helium, by a factor of about 1000 to 1, this neglect may not always be justified. In fact, collisions involving hydrogen atoms or molecules may under certain conditions provide the dominant source of heating and cooling.

To consider heating first, a hydrogen atom may be ionized by a passing cosmic-ray particle. If the intensity of cosmic rays throughout space is the same as the measured intensity striking the earth, the kinetic energy carried off by the free electron amounts, on the average, to 4×10^{-30} ergs per neutral hydrogen atom per second. This value is shown by the solid line in Figure 3. To compare this rate of heating with that shown for electrons in Figure 2, we must multiply G_{ei} by n_e and G_{He} by n_H to obtain the energy gained per cubic centimeter per second. If the ratio n_e/n_H is about 2×10^{-4}, then the cosmic-ray heating amounts to only one-tenth the heating by starlight at an electron temperature of about 50° and is therefore unimportant on the basis of these assumptions. However, the cosmic-ray intensity in interstellar space is still quite uncertain, and the existence and magnitude of this supplementary heating are both quite uncertain.

Of the cooling mechanisms involving neutral hydrogen, one process is relatively sure,

[1] I am indebted to Dr. A. Schlüter for this suggestion, as well as for other helpful comments concerning this paper.

the other uncertain. We know that solid particles or grains are present in space, and their mean density is moderately well known from the work of van de Hulst (1949). When a hydrogen atom collides with a grain, it will tend to lose its initial kinetic energy and to leave with an energy characteristic of the internal temperature T_g of the grain. The value of T_g is not certain, but for any assumed T_g the rate of cooling may be computed with some accuracy.

The dashed line in Figure 3 shows the rate of cooling by this process for a grain temperature T_g of 20° K and for a particle density of grains ten times the average. For gas

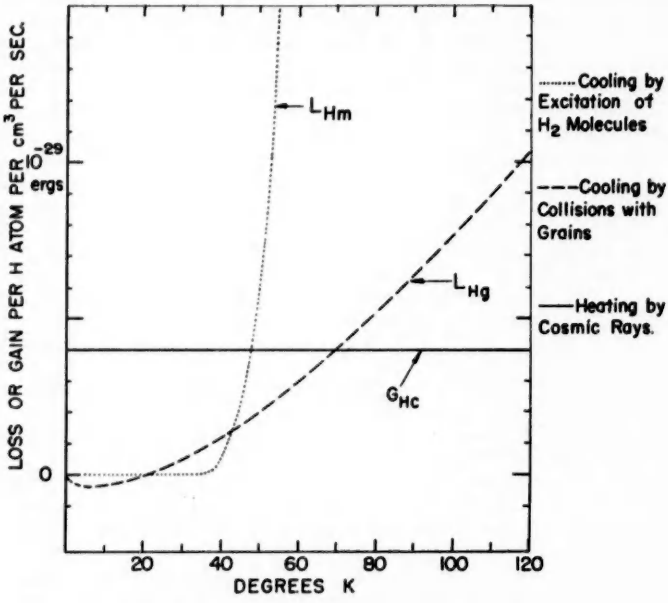

FIG. 3.—Heating and cooling by hydrogen atoms

temperatures considerably in excess of T_g, the computed cooling does not depend on T_g and should be reliable. The equilibrium temperature, if electron processes are unimportant and G_{Hc} and L_{Hg} are dominant, is about 70°. With a higher particle density for the grains, T would be reduced.

One last cooling process must be considered. If hydrogen molecules are present in the gas, collisions with hydrogen atoms will excite the molecular rotational levels and lead to radiation in the infrared. The rotational spectrum of the hydrogen molecule is not observed in the laboratory, as the transitions are forbidden. In interstellar space, however, the transition will take place, after a lapse of from one to a thousand years. The computed rate of cooling, for a particle density of 1 hydrogen molecule per cubic centimeter, is shown by the dotted line in Figure 3. Evidently, for temperatures greater than 50° K the cooling by this process is very rapid. We have no certain evidence that molecular hydrogen is present in interstellar space, but its formation seems likely, since the grains should provide an effective catalyst. If molecular hydrogen is present, it may well have no great effect on the equilibrium temperature, since cooling by ions and grains is more

efficient at temperatures between 20° and 40° K. If for some reason the temperature is increased, then the molecules come into action, cooling the gas much more rapidly than would otherwise be possible. For example, if a shock wave heats a gas cloud to 5000°, cooling by molecules will depress the temperature to about 2500° in roughly a thousand years, if the hydrogen density is 10 atoms and 1 molecule per cubic centimeter. This result is in contrast to the million years required for the same cooling without molecules. Since a thousand years is a very short time in interstellar space, it is clear that molecular cooling of the interstellar gas can be very rapid.

This discussion refers entirely to equilibrium conditions, with both heating and cooling produced by local influences. An additional source of heating in *H* I regions, recently proposed by Kahn (1953), is provided by collisions between clouds. Such collisions will certainly produce a kinetic temperature of several thousand degrees at the point of impact. At this high temperature, however, the increased rate of cooling may get rid of the additional thermal energy rather rapidly. Detailed computations on the mean temperature of *H* I clouds are not yet available; it is readily shown that under these conditions such an average temperature cannot exceed about 200° K.

While the theoretical study of interstellar temperatures has not yet yielded precise numerical values, a large difference of temperature between *H* II regions and dense *H* I clouds seems firmly established. With a temperature of about 10,000° in *H* II regions and perhaps about 50° in the *H* I clouds, the ratio of temperatures amounts to a factor of about 200. Since radio measures of the hydrogen emission line at 21 cm confirm the low temperature of the *H* I clouds, while the appearance of the forbidden line of O^+ confirms the high temperature of *H* II regions, this difference of temperature, which was first predicted theoretically, may be taken as observationally confirmed. As we shall see, this phenomenon should have important cosmogonic consequences.

III. MOTIONS OF THE INTERSTELLAR GAS

The observations summarized in Table 1 indicate that the interstellar gas, in addition to sharing in the general galactic rotation, is in a state of chaotic or turbulent motion. The average clouds have root-mean-square radial velocities between 5 and 10 km/sec, while occasional clouds have velocities ranging up to nearly 100 km/sec. Unlike the stars, the gas clouds will collide with one another relatively frequently, perhaps as often as once every 10,000,000 years. Since each collision must be highly inelastic, the motions would quickly die out if there were no force to sustain them. We shall see that, in a general way, the temperature differences which have been demonstrated between different parts of the gas are capable of maintaining these cloud velocities.

a) PRESSURE EQUILIBRIUM

Let us now examine the physical processes occurring in a gas in which there are large differences of temperature. One important effect which such a gas will show will be a tendency toward equalization of pressure in different regions. Since the gas pressure is proportional to the product of the density and the temperature, it follows that if the density is uniform, the temperature differences will produce large differences in pressure. The regions at high pressure will then tend to expand, compressing the remainder of the gas. If, for example, a region of the earth's atmosphere is suddenly heated to 200 times the temperature of the surrounding atmosphere, a violent explosion will result. If the heated region is 100 meters on a side, the effect will be comparable to the atomic bomb. Similarly, an interstellar cloud at high temperature will tend to expand.

In the absence of any abrupt change of temperature with time, such as is produced by a nuclear detonation, the gas will tend to come to pressure equilibrium. The high-temperature gas will expand until its pressure is equal to that in the surrounding region, and similarly the low-pressure gas will tend to be compressed. The speed with which pressure is equalized across the gas is given by the velocity of sound, and a pressure disturbance

will propagate outward at this velocity. In *H* II regions the sound velocity is about 17 km/sec, while in *H* I regions we obtain the much smaller value of 0.8 km/sec. Then in 10,000,000 years, which is about the time between collision among clouds, pressure should begin to be equalized over about 170 parsecs if the hydrogen is ionized, and about 8 parsecs if the hydrogen is neutral. The greater value is comparable with the dimensions of the luminous *H* II regions, while the smaller value is about the diameter of the small obscuring clouds, which presumably contain neutral hydrogen. While complete equality of pressure throughout the gas is not to be anticipated, we may expect a considerable tendency toward pressure equilibrium.

Such a tendency predicts at once that the regions of neutral hydrogen should be several hundred times as dense as the ionized regions, since this is about the ratio of probable temperatures. We thus arrive at a picture of *H* I clouds surrounded by a rarefied medium of much lower density. While the observations cannot be said to confirm such a picture unequivocally, Strömgren (1948) has shown, from an analysis of the interstellar absorption lines based on very reasonable assumptions, that the density of hydrogen within the clouds is probably about 10 atoms per cubic centimeter, while the density between the clouds is probably less by a factor of 100 or more. Actually, the atoms in this tenuous intercloud medium could be mostly neutral and still at a relatively high temperature, since at so low a density the time required for cooling, in the absence of H_2 molecules, is about a million years. We may conclude that as far as the data go, they are not inconsistent with the suggestion that the pressure in the interstellar gas tends to be uniform.

b) THERMAL ACCELERATING FORCES

We turn now to a consideration of the various ways in which thermal effects in the interstellar medium may produce motions. One mechanism is evident from the study of winds in our own atmosphere. These winds are entirely driven by thermal effects. Air is heated at the ground and expands under conditions of constant pressure. The expanded air is more buoyant than the surrounding denser air and tends to rise. The resulting air currents are then profoundly modified by the earth's rotation to give the observed winds. In the same way, interstellar gas which has been heated by an early-type star will tend to rise away from the galactic plane, buoyed up by the surrounding denser gas. Because of the spotty distribution of the O and B stars, the resultant cosmic winds should not be so systematic as the terrestrial winds, but they might be expected to become important near clusters of early-type stars. The gas velocity produced in this way might be expected to be comparable to the sound velocity in *H* II regions, or about 17 km/sec. This mechanism is clearly inadequate to account for the occasional much higher velocities observed by Adams (1949).

A second mechanism, which has been proposed by Oort (1953) and by Biermann and Schlüter (1953), relies on the dynamical effects of sudden heating. We have already seen that if the temperature of a gas is abruptly increased, an explosion results. One means for a sudden increase in temperature is the birth of one or more luminous O stars in a dense cloud. It is now rather generally accepted that the early-type stars are forming continuously from interstellar matter in the spiral arms, and the natural place for such stars to form is inside relatively dense clouds of neutral hydrogen. How rapidly the luminosity of a star will rise at its birth is uncertain, but it seems likely that the starlight, at least in the far ultraviolet, is "turned on," so to speak, relatively abruptly, perhaps in less than 10^5 years. The temperature and pressure in the surrounding clouds will rise equally abruptly. The result should be a violent explosion, shooting gas in all directions.

If there were no additional source of heat for the gas, once it was heated initially, the expansion would be adiabatic, and the gas would cool. In this case the velocity which might be attained by the ejected material would not exceed the sound velocity. Actually, the explosion is probably sufficiently leisurely so that the gas is maintained at a constant temperature by the heating and cooling mechanisms discussed above. In this isothermal

FIG. 4.—Detail of emission nebula M16, photographed with the Hale 200-inch telescope

case the expansion velocity may considerably exceed the sound velocity, though velocities exceeding 50 km/sec are not likely to be reached in this way.

A third mechanism, which should be capable of accelerating a few small clouds to very high velocities, might be called the "interstellar rocket." In an ordinary rocket, hot gases are ejected in one direction, accelerating the rocket in the other direction. The velocity attained may be much greater than the ejection velocity, provided that the amount of material ejected is larger than the final mass of the rocket. A dense cloud of neutral hydrogen constitutes a natural rocket when placed near a luminous star of high surface temperature. The stellar radiation heats up the surface of the cloud, on the side facing the star, to about 10,000°. The heated material expands and shoots away from the cloud; since only one side is heated, the gas will stream away predominantly in one direction—toward the hot star. The recoil from this stream of gas will then accelerate the cloud away from the star. The ejection velocity will be comparable with the speed of sound in an *H* II region, and if the cloud loses all but 1 per cent of its mass in this way, the remnant may be accelerated to a speed of about 80 km/sec, comparable with the highest speeds observed by Adams. This result assumes that the cloud is initially stationary relative to the star; if it is approaching the star initially, the final velocity is somewhat less.

With the explosion around a newly born O star accounting for the bulk of the cloud velocities and with supplementary rocket acceleration accounting for the occasional clouds of very high velocity, it appears from some rough computations by Oort and Spitzer (1954) that the observed cloud velocities may be accounted for. One direct result of the theory is that the clouds of very high velocity should mostly be approaching the earth rather than receding from it. Such clouds do not retain their high velocity very long, and they are most likely to be seen when they lie in the line of sight between the earth and the star whose radiation is reponsible for their motion. Clearly, they will be moving away from the star and toward the earth, and their radial velocities will be negative. Blaauw (1952) and Searle (1952) have noted the preponderance of negative cloud velocities, which are about twice as numerous as positive velocities for clouds with random velocities in excess of 15 km/sec. In terms of the present picture, this result finds a natural explanation.

c) RALEIGH–TAYLOR INSTABILITY

We have seen that the relatively dense clouds may be accelerated outward by the high pressure of the heated gas surrounding a hot star. If this picture is correct, one puzzling feature of the observed interstellar clouds may find a very natural explanation. It has been known for some time that many of the bright nebulae are characterized by tongues or "elephant trunks" of obscuring matter, extending from the surrounding dark nebulosity into the emitting regions and pointing in the general direction of the exciting star. Figure 4, which reproduces a plate taken by Humason with the 200-inch Hale telescope at the Palomar Observatory, shows a prominent feature of this sort in the emission nebula M16, NGC 6611.[2]

A recent analysis by Frieman (1954) shows that spikes of this approximate size and shape are a natural result of an assumed expansion of the hot gases in the luminous nebula. When the gas is heated and expands, it becomes less dense than the cool clouds which surround the nebula and which are being pushed radially outward. Thus at an early stage in the expansion we find a light gas pushing a denser one. It was shown theoretically by Lord Rayleigh (1899) many years ago that this state of affairs was unstable. The origin of this instability is physically obvious in the case of a thick layer of water supported from below by a layer of air. It is clear that any small displacement in an initially plane interface between the water and the air will grow until the water and air have finally exchanged places. This subject has been investigated anew by Taylor (1950)

[2] I am much indebted to Dr. Humason for his kind permission to include this reproduction here.

and by Lewis (1950), who obtained photographs of the interface between a liquid and a gas when the gas was pushing the liquid.

The results of the experiments by Lewis are portrayed in Figure 5. The light fluid below is pushing up the denser one above, and either supports it against the vertical force of gravity or accelerates it upward. In any case, the successive diagrams in Figure 5 indicate the progressive development of the Rayleigh-Taylor instability. When the disturbance is small, the first-order theory of Rayleigh and Taylor is applicable, and the disturbance increases exponentially with time. When the disturbance becomes compa-

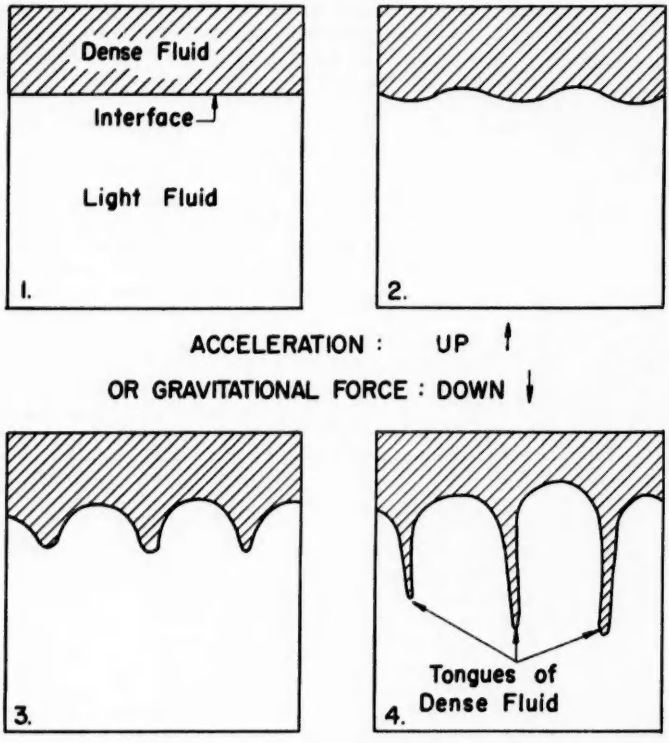

FIG. 5.—Development of Rayleigh-Taylor instability

rable with the wave length, the first-order theory is no longer applicable; but a theory of finite displacements developed by Layzer (1954), Frieman (1954), and others is in satisfactory agreement with the observations. According to this theory, thin spikes of the dense material fall through the lighter material, while thicker columns or "bubbles" of light material move into the heavier fluid. The problem is complicated by another type of instability which arises at the surface of the spikes, resulting from the discontinuity of velocity across the surface, and a great complication in the end result is entirely consistent with the theory.

Uncertainty about the physical conditions in actual emission nebulae and lack of

knowledge as to the initial irregularities when expansion began prevent a precise comparison between theory and observation. However, the general order of magnitude of the observed spikes and bubbles seems consistent with the theory. If the general point of view adopted here is correct and heated gases around hot stars are accelerating the surrounding dense clouds, spikes of this sort seem inevitable. The general agreement here between theory and observation lends added support to this whole viewpoint.

d) MAGNETIC FIELDS AND SPIRAL ARMS

Last, we come to one of the most fascinating topics encountered in the discussion of interstellar motions. The work of Alfvén (1950) and Fermi (1949) has shown that if a magnetic field is present between the stars, there must be a very intimate connection between this field and the cloud motions, since, under conditions in interstellar space, ionized particles cannot stray very far from a particular line of magnetic force. As a result, either the motions will greatly distort the magnetic field or the magnetic field will restrain the motions. A magnetic field of about 10^{-5} gauss seems to provide the dividing line. A field much less than this will have no effect on the main motions of the interstellar gas, while a much greater field will entirely control these motions.

The only clear evidence for the existence of an interstellar magnetic field is the polarization of light from reddened stars, a spectacular discovery by Hiltner (1949 and 1951) and by Hall (1949 and 1950). According to work by van de Hulst (1950), the amount of polarization can be explained if the grains are elongated and at least partially oriented. The only mechanism for orienting the grains which seems quantitatively plausible is by means of a magnetic field. An alternative theory, attributing the orientation to systematic motion of the grains through the gas, has been put forward by Gold (1952). According to Davis (1954), there is serious question as to whether the polarization data can actually be explained on the basis of Gold's ingenious theory. For magnetic orientation, two theories have been put forward. The one by Davis and Greenstein (1951) orients the particles perpendicular to the magnetic field by the dissipative mechanism of paramagnetic relaxation. The Spitzer-Tukey (1951) theory orients ferromagnetic grains parallel to the magnetic field in somewhat the same way that a compass is aligned parallel to the earth's magnetic field. However, both theories require rather high fields, greater than 10^{-5} gauss for the Greenstein-Davis version and still another order of magnitudce higher for the Spitzer-Tukey version.

There is some hope that the interstellar polarization can be explained with much lower fields, perhaps less than 10^{-6} gauss. Gorter has suggested informally that tiny ferromagnetic particles, so small that they constitute single domains, might be subject to a ferromagnetic relaxation many orders of magnitude greater than the paramagnetic relaxation. In the absence of laboratory evidence, which would require experiments on ferromagnetic particles no larger than the interstellar grains, this suggestion provides only a preliminary working hypothesis, which, if verified, would much simplify the entire subject. If the orientation method proposed in Pasadena can be applied to the ferromagnetic grains proposed at Princeton, the reduced magnetic field required would seem much more plausible than the larger fields which now are needed.

In any case, it seems clear from the observations that the magnetic field is intimately connected with the spiral arms, as shown in detail by Hoag (1949). If we look along the spiral arms (parallel to the axis of the arm), the polarization is small and randomly oriented, while the maximum polarization is found for light passing transversely across the spiral arm (perpendicular to the axis). Assuming orientation by some dissipative process, either paramagnetic or ferromagnetic, we see that the magnetic lines of force are preponderantly parallel to the axis of the spiral arm. This result, if accepted, is obviously a very basic one in our understanding of the nature of spiral arms.

There are two different ways in which this result may be interpreted. The first, due to Chandrasekhar and Fermi (1953), assumes that an approximately uniform and homoge-

neous magnetic field is present within the spiral arm, the line of force being mostly parallel to the axis of the arm. To maintain these lines of force parallel despite the motions of the clouds requires a field of 1.8×10^{-5} gauss, if we take, following Blaauw (1952), a root-mean-square cloud velocity of 7 km/sec in the line of sight, or 12 km/sec for the corresponding three-dimensional mean. This field is probably strong enough to orient the grains by the Davis-Greenstein mechanism.

There are several objections that may be made to this picture. First, it is rather surprising that such a large uniform field does not produce more striking effects in the appearances of the diffuse nebulae. Second, it is rather difficult to understand how such a uniform field could ever have been produced. Third, it is not a simple matter to prevent the lateral expansion of a spiral arm with so strong a uniform field. All these arguments are rather theoretical, however, and by no means conclusive.

There is an entirely different point of view from which these polarization results may perhaps be viewed. As Spitzer and Tukey (1951) have suggested, the magnetic field may be assumed to be highly chaotic, averaging out to zero over distances of less than 100 parsecs, but with a tendency for the lines of force to lie parallel to the spiral arm. The distribution of magnetic fields, exactly like the distribution of stellar velocities, would be ellipsoidal, with the average field, like the average random velocity, canceling out to zero in the average. The major axis of the magnetic ellipsoid would be parallel to the axis of the arm, while for the velocity ellipsoid the major axis points to the galactic center. The lines of force in such a distribution may be visualized by taking a loose tangled mass of string and stretching the entire mass in a particular direction. On the average, the strings will tend to be parallel to the direction of stretching.

The chief advantage of such a configuration is that this is exactly the type of distribution that might be expected to arise in a spiral arm. Batchelor (1950) and Schlüter and Biermann (1950) have shown that the random motions of the interstellar clouds will pull out the lines of force and produce an exponential increase in the magnetic-field strength until fields of the order of 10^{-6} gauss result. Such fields would apparently have a small scale and a spherical distribution. As implied by Cowling (1953), the differential rotation will stretch out a spiral arm, and this large-scale stretching of the lines of force will tend to produce an ellipsoidal distribution of magnetic fields, with the major axis of the ellipsoid parallel to the axis of the arm.

The chief disadvantage of this type of magnetic field is that the root-mean-square excess field parallel to the axis of the arm is not likely to be very great, perhaps no greater than 10^{-6} gauss. Such a field would be too weak, by at least an order of magnitude, to explain the observed polarization on the Davis-Greenstein theory. If ferromagnetic grains are present, however, and if ferromagnetic relaxation is as strong as proposed by Gorter, a field of about 10^{-6} gauss would be about right to explain the polarization data. Evidently, the model of small-scale magnetic fields, while it has many attractive features, is at best only another working hypothesis at the present time.

One final consequence of interstellar motions must be pointed out. According to Fermi (1949 and 1954), motion of the interstellar clouds can accelerate charged particles and account for the observed cosmic-ray spectrum. At the moment, this theory seems to offer the best hope of accounting quantitatively for the existence of cosmic rays. If this theory proves correct, it should be possible to use the existence of cosmic rays to deduce certain properties which the interstellar magnetic field must possess. At the present time there are too many uncertainties in the subject to permit any very definite conclusions in this respect.

In conclusion, we have seen that when an early-type star appears in a cloud of neutral gas, either by star formation or by relative motion, the photoionization of hydrogen has many important consequences. The free electrons ejected carry off several electron volts of energy and gradually heat up the material from its initial temperature of about 50° to roughly 10,000° K. As the pressure increases by a correspondingly large factor, very large

dynamical effects appear. The hotter gas pushes the cooler gas away, and the resulting instabilities account for at least some of the complicated contours of observed emission nebulosities. The resultant motions of the clouds may be responsible for the growth of an interstellar magnetic field. The motions of the clouds in the presence of such a field may well be responsible for the acceleration of a relatively small number of charged particles to cosmic-ray energies. Thus a wide variety of cosmic processes over enormous reaches of space may ultimately find a simple explanation in terms of temperature differences in the interstellar gas.

REFERENCES

Adams, W. S. 1949, *Ap. J.*, **109,** 354.
Alfvén, H. 1950, *Cosmical Electrodynamics* (Oxford: Clarendon Press).
Batchelor, G. K. 1950, *Proc. R. Soc., A.*, **109,** 405.
Bierman, L., and Schlüter, A. 1953, Paper read at Cambridge Symposium on Gas Dynamics of Interstellar Clouds.
Blaauw, A. 1952, *B.A.N.*, **11,** No. 436, 459.
Chandrasekhar, S. 1942, *Principles of Stellar Dynamics* (Chicago: University of Chicago Press), sec. 2.2.
Chandrasekhar, S., and Fermi, E. 1953, *Ap. J.*, **118,** 113.
Cowling, T. G. 1953, *Ciel et Terre*, **69,** 177.
Davis, L., Jr., and Greenstein, J. L. 1951, *Ap. J.*, **114,** 206.
Davis, L., Jr. 1954, *Vistas in Astronomy* (London: Pergamon Press).
Eddington, A. S. 1930, *Internal Constitution of the Stars* (Cambridge: At the University Press), chap. xiii.
Fermi, E. 1949, *Phys. Rev.*, **75,** 1169.
Fermi, E. 1954, *Ap. J.*, **119,** 1.
Frieman, E. 1954, *Ap.J.* (in press).
Gold, T. 1952, *M.N.*, **112,** 215.
Hall, J. S. 1949, *Science*, **109,** 166.
Hall, J. S., and Mikesell, A. H. 1950, *Pub. U.S. Naval Obs.*, **17,** 1.
Hiltner, W. A. 1949, *Science*, **109,** 165.
Hiltner, W. A. 1951, *Ap. J.*, **114,** 241.
Hoag, A. A. 1953, *A.J.*, **58,** 42.
Kahn, F. D. 1953, *Observatory*, **73,** 175.
Layzer, D. 1954 (in preparation).
Lewis, D. J. 1950, *Proc. R. Soc., A*, **202,** 81.
Menzel, D. H., and Aller, L. H. 1941, *Ap. J.*, **94,** 30.
Oort, J. H. 1953, Paper read at Cambridge Symposium on Gas Dynamics of the Interstellar Clouds.
Oort, J. H., and Spitzer, L., Jr. 1954, *Ap. J.* (in preparation).
Oort, J. H., and van de Hulst, H. C. 1946, *B.A.N.*, **10,** No. 376, 187.
Rayleigh, Lord. 1899, *Collected Papers* (Cambridge: At the University Press), **2,** 100.
Schlüter, A., and Biermann, L. 1950, *Zs. f. Naturforsch.*, **5a,** 237.
Searle, L. 1952, *Ap. J.*, **116,** 650.
Seaton, M. J. 1953, *Proc. R. Soc., A*, **218,** 400.
Spitzer, L., Jr., and Savedoff, M. P. 1950, *Ap. J.*, **111,** 593.
Spitzer, L., Jr., and Tukey, J. 1951, *Ap. J.*, **114,** 187.
Strömgren, B. 1939, *Ap. J.*, **89,** 526.
Strömgren, B. 1948, *Ap. J.*, **108,** 242.
Taylor, G. I. 1950, *Proc. R. Soc., A*, **201,** 192.
van de Hulst, H. C. 1949, *Rech. Astr. Obs. Utrecht*, Vol. **12,** Part 2.
van de Hulst, H. C. 1950, *Ap. J.*, **112,** 1.

ON "ELEPHANT-TRUNK" STRUCTURES IN THE REGION OF O ASSOCIATIONS*

E. A. FRIEMAN
Princeton University Observatory
Received February 8, 1954

ABSTRACT

A recent theory of Oort and Spitzer indicates that the O stars are born in regions of accumulation of interstellar *H* and further provides a mechanism for the acceleration of the interstellar clouds. It is shown here that the theory leads to the presence of the Rayleigh-Taylor hydrodynamic instability. The "elephant-trunk" structures observed in the region of the O associations are interpreted as manifestations of the instability in its asymptotic phase. Calculations are given of the linear dimensions to be expected for these structures and are in agreement with values obtained by measurement of Minkowski's photographs of NGC 2244.

I. INTRODUCTION

Oort (1953) has recently proposed a theory of the origin of O associations, and Oort and Spitzer (1954) a closely allied theory of the acceleration of the interstellar clouds by O stars. It is the purpose of this paper to show that these theories lead to a natural explanation of the "spikes" or "elephant-trunk" type of structure (van de Hulst 1953) seen in the region of the O associations. A particularly fine example of this phenomenon is exhibited in the diffuse nebula around the open cluster NGC 2244 in Monoceros, which has been described by Minkowski (1949).

These theories assume the O stars to have been formed in regions of interstellar gas so large as to preclude complete ionization of the whole mass by the O stars' radiation. The resulting high pressure in the Strömgren sphere causes a radial expansion of the ionized region, with an accompanying compression of the cool, neutral shell. Thus, at the interface, a sharp density gradient will tend to be built up. The conditions prevailing at the density transition layer are then just those which allow the development of the Rayleigh (1883)-Taylor (1950) hydrodynamic instability. It is suggested here that the spikelike structures seen are those characteristic of the instability in its asymptotic phase.

II. DYNAMICS OF THE INSTABILITY

Taylor instability occurs if there exists a perturbation on the interface between two fluids of different densities in the presence of an acceleration field directed from the lighter to the heavier fluid. D. J. Lewis (1950) has performed experiments on water-air interfaces which show that an initial perturbation rapidly grows to the point where it is characterized by long, narrow spikes extending into the lighter material, while the heavier material is penetrated by round-ended columns or "bubbles." A schematic picture of the development is given in Figure 1. The phenomenon also includes the presence of a second type of instability first considered by Helmholtz (1868). When two fluids are in relative motion with respect to each other, perturbations on the common interface are unstable. This instability obtains along the sides of the "spikes."

An examination of Minkowski's plates shows the same type of structure as that described by Lewis. It is therefore of interest to compute the linear dimensions to be expected for these structures on a hydrodynamical basis. Owing to the great variety of phenomena taking place, we can do no more than indicate orders of magnitude. In this

* This research was supported by funds of the Eugene Higgins Trust allocated to Princeton University.

direction we simplify the problem by considering one fluid and a vacuum, since Oort has indicated that a density ratio of 100 : 1 may well exist.

We now consider a small perturbation of amplitude η and wave number $k = \lambda^{-1}$ ($\lambda = \lambda/2\pi$ is the reduced wave length) as in Figure 1, *a*, and assume no motion in the *z*-direction. The potential energy of the configuration per unit thickness in the *z*-direction relative to the undisturbed fluid is of the order of ($\sim$ indicates order-of-magnitude equality)

$$\epsilon \sim (\lambda \eta \rho)\, \eta g\,. \tag{1}$$

The force is then given by

$$-\frac{\partial \epsilon}{\partial \eta} \sim -\lambda \rho \eta g\,. \tag{2}$$

This force acts on a region of extent λ in the *x*- and *y*-directions, so that we have, as our equation of motion,

$$(\lambda^2 \rho)\, \ddot{\eta} = -\lambda \rho \eta g\,. \tag{3}$$

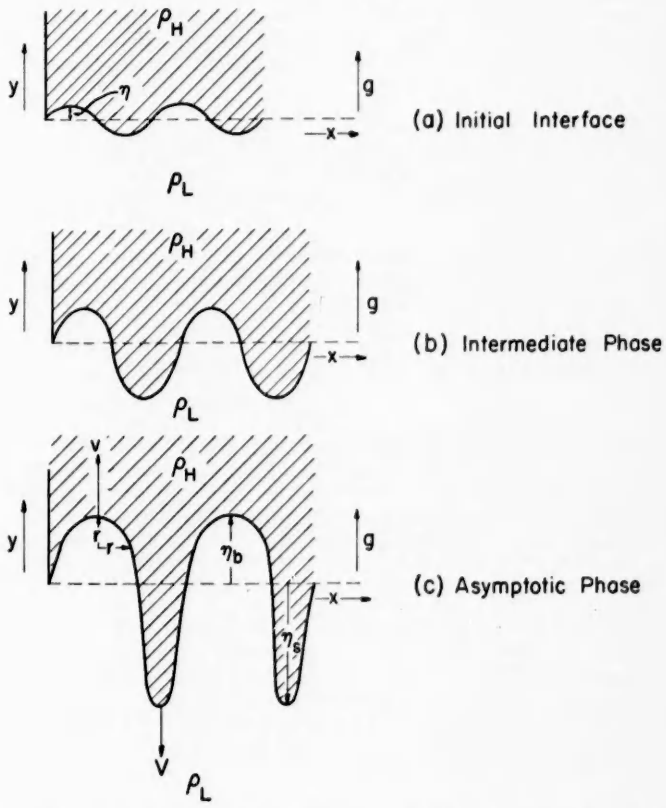

FIG. 1.—Development of Taylor instability. ρ_H and ρ_L are the densities of heavy and light fluids, respectively; g is the acceleration field; η, η_b, and η_s are the initial amplitude and the displacements of the bubble and spike, respectively; r is the radius of curvature; and v is the velocity at that point.

Equation (3), although derived in an approximate manner, is actually correct. The initial phase of development of the instability therefore occurs with an exponential growth, $\exp[(gk)^{1/2}t]$.

We now turn to consider the asymptotic growth in the same fashion. Figure 1, *c*, indicates the top of a bubble whose radius of curvature is r. The mass of fluid displaced by the rising bubble per unit width in the z-direction is of order ρr^2, so that the gravitational force is of order $\rho r^2 g$. The momentum imparted to the heavy material in a time δt is of order $(\rho r v \delta t)v$. The equation of motion is, therefore,

$$\rho v^2 r \sim g \rho r^2 , \tag{4}$$

leading to the result

$$v \sim (gr)^{1/2} . \tag{5}$$

This result has been obtained by more sophisticated methods by Davies and Taylor (1950) and is in substantial agreement with their experimental results and those of Lewis. The considerations regarding the asymptotic motion of the spike can also be obtained in a crude manner. Referring again to Figure 1, *c*, we see that the loss in potential-energy density is of order $-\rho g y$ in the neighborhood of the tip of the spike, and this must be equated to the gain in kinetic energy per unit volume, $\frac{1}{2}\rho V^2$. Thus we see that the spike is in free fall.

TABLE 1

COMPUTED LINEAR DIMENSIONS OF SPIKES AND BUBBLES
(All Lengths in Psc)

η_0	$a=1$			$a=\frac{1}{2}$		
	$\lambda \times 10^{-2}$	$\eta_b \times 10^{-1}$	η_s	$\lambda \times 10^{-2}$	$\eta_b \times 10^{-1}$	η_s
10^{-8}	1.6	2.5	1.9	1.7	2.5	1.9
10^{-6}	3.1	3.5	2.0	3.2	3.6	2.0
10^{-4}	7.5	5.8	2.25	7.8	6	2.3
10^{-2}	29	13.1	2.9	31	13.3	2.9

Lewis' experiments have shown, furthermore, that the transition range between the small-amplitude and asymptotic theories is of quite short duration as far as the motion of the bubble is concerned. Although the evidence is not so definite, the spike does seem to spend a longer time in the intermediate phase. One would, of course, expect that the small-amplitude theory would no longer be applicable when the amplitude became of the order of λ. We therefore approximate to the motion by assuming exponential growth until $\eta = a\lambda$ ($a = \frac{1}{2}$ and 1 for comparison purposes) and the asymptotic theory to hold thenceforth.

Further, we see that the small-amplitude theory predicts that the smallest wave lengths will grow the most rapidly, while the asymptotic velocity of penetration of the bubble indicates the reverse. Thus there must exist a particular wave length which an arbitrary disturbance will seek out and which will give maximum growth for a given initial amplitude and elapsed time. Since the free-fall motion of the spike is independent of λ, the bubble alone will determine the choice of the critical wave length. The critical wave length is then given by the solution of

$$\frac{t}{2}\left(\frac{g}{\lambda}\right)^{1/2} - \ln \frac{a\lambda}{\eta_0} = 1 - a , \tag{6}$$

where η_0 is the original amplitude.

III. COMPARISON WITH NGC 2244

Oort has given calculations based on the Monoceros nebula which indicate that the average radial velocity of the cool shell is approximately 13 km sec^{-1} and has assumed a time scale of 10^6 years. We have assumed these values to hold at the interface between the vacuum and the cool shell. Table 1 gives a representative sample of the linear dimensions of the bubble and spike and the associated wave lengths and was computed for an elapsed time of 10^6 years. The table illustrates the extreme insensitivity of the linear dimensions to large changes in the initial amplitude. Table 1 can be compared with estimates from Plates XX and XXI of Minkowski's paper. We have used the distance of

TABLE 2

MEASURED LINEAR DIMENSIONS OF SPIKES AND BUBBLES
(All Lengths in Psc)

Minkowski's Plates	λ	η_b	η_s
XX	0.4	0.9	2.3
XXI	0.3	0.3	1.1

1400 psc as given by Oort in calculating the linear dimensions (Table 2). It is seen that the order-of-magnitude agreement is good and that the value of $\eta_0 = 10^{-4}$ psc, which seems to agree most closely with the values in Table 2, is not unreasonable.

It is a pleasure to acknowledge the original suggestion of this hypothesis by Professor Lyman Spitzer, Jr., and his advice during the preparation of this paper.

REFERENCES

Davies, R. M., and Taylor, G. I. 1950, *Proc. R. Soc. A.*, **200**, 375.
Helmholtz, H. von; see Lamb, H. 1945. *Hydrodynamics* (New York: Dover Reprints), p. 373.
Lewis, D. J. 1950, *Proc. R. Soc. A.*, **202**, 81.
Minkowski, R. 1949, *Pub. A.S.P.*, **61**, 151.
Oort, J. H. 1953, unpublished. A preliminary account of this work was presented at the Second Symposium on Gas Dynamics of Interstellar Clouds, Cambridge, 1953.
Oort, J. H., and Spitzer, L., Jr. 1954, *Ap. J.* (in preparation).
Rayleigh. 1883, *Proc. London Math. Soc.*, **14**, 170.
Taylor, G. I. 1950, *Proc. R. Soc. A.*, **201**, 192.
van de Hulst, H. C. 1953, *Second Symposium on Gas Dynamics of Interstellar Clouds*. (Preliminary Comm., No. 9.) Cambridge, 1953.

A STUDY OF THE ATMOSPHERES OF EARLY O AND Of STARS*

J. B. Oke†
Princeton University Observatory
Received January 29, 1954; revised March 15, 1954

ABSTRACT

Spectrograms with a dispersion of 10.2 A/mm and covering the range from λ 3300 to λ 4900 have been obtained for eight early O and Of stars. Equivalent widths of nearly all measurable absorption lines have been obtained and are listed in Table 2. The equivalent widths have been analyzed, and it is found that the atmospheres can be described best by the data of Table 6. The very small effective gravity g_0, as measured by the gas pressure, is a result primarily of the large radiation pressure which nearly counterbalances gravity. Approximate values are obtained for the mass, luminosity, and radius of an Of star (listed in eq. [11]), which are in fairly good agreement with the observational evidence. The small value of log n_e in Table 6 does leave, however, a possible discrepancy in the breadths of the weaker hydrogen and helium lines, in the sense that the observed lines are too wide. This discrepancy is removed if the density of the atmosphere is increased by a factor of about 3. The emission lines of *N* III at λ 4634 and λ 4640 and the *He* II line at λ 4686 have also been studied. Typical profiles are shown in Figure 2. It is shown that the emission-line intensities are almost certainly varying in a few hours in the two stars for which adequate data are available. The proposal is made that the emission lines arise in the upper atmosphere of the stars rather than in an extended shell. Three circumstances suggest this: (1) the profiles of the emission and absorption lines are very similar in shape and breadth; (2) in one star, which is rotating rapidly, the emission lines show roughly the same rotational velocity as do the absorption lines; (3) the ratio of the emission equivalent widths of λ 4640 and λ 4634 indicates considerable self-absorption, which would not be expected for dilution factors much less than unity.

I. INTRODUCTION

The very hot stars can be divided spectroscopically into two classes—the Wolf-Rayet and P Cygni emission-line stars and the normal early O-type stars. The additional group of Of stars resembles the O stars in the apparent similarity of the absorption spectra, but differs in the appearance of several broad emission lines, particularly the *N* III lines at λ 4634 and λ 4640 and the *He* II line at λ 4686, the three lines which dominate the spectra of many Wolf-Rayet stars. For studies of the normal absorption-line stars we have the comprehensive works of Unsöld (1941) on the B0 star τ Scorpii and of Aller (1946) on the O9 star 10 Lacertae. Aller (1948) has made a similar analysis of the central stars of planetary nebulae. Many of these central stars are classed as Of stars, although, as will be seen, they are probably much less massive and luminous than the Of stars considered in this paper. Swings and Struve (1940*a*,*b*; Swings 1942) have studied the emission and absorption lines of several Of stars.

This study is aimed at answering the following questions: (1) What are the general properties of the O and Of stars as derived from the absorption lines? (2) Are the atmospheres of the O and Of stars different? (3) What can be inferred about the nature of the emission lines from the properties of the emission lines?

In Sections II and III the observational material to be used and the measurements made on this material are presented. Sections IV and V outline the analysis of the absorption-line measurements. Absorption-line breadths are discussed in Section VI. Section VII is concerned with the masses, luminosities, and radii of the stars. The final conclusions concerning the properties of the atmospheres are given in Section VIII. Abundances are discussed briefly in Section IX. Sections X, XI, and XII deal with the

* This investigation is based on plates taken by L. Spitzer, Jr., while a guest investigator at the Mount Wilson and Palomar Observatories.

† Now at the David Dunlap Observatory, Richmond Hill, Ontario.

emission lines from the standpoint of profiles and intensities, variability, and general properties, respectively. Section XIII briefly considers mechanisms which may play a role in causing the emission lines. The final conclusions concerning Of stars are given in Section XIV.

II. OBSERVATIONAL MATERIAL

Eight early O and Of stars were observed during the fall of 1952. While the stars have been classified both at Victoria and at Yerkes, only the Yerkes classification will be quoted in this paper. Seven of these stars, including three Of stars, have been classified by Morgan (cf. Johnson 1953). The remaining one, HD 190429N, has been listed as an Of star by Roman (1951). The four normal O stars were selected because of their relatively sharp lines. In Table 1 the stars are listed, with their visual magnitudes, Yerkes classification, and coudé numbers and dates of spectrograms obtained for each.

TABLE 1

OBSERVATIONAL DATA

HD (Name)	m_v	Sp. Type	Coudé Plate No. and Date in 1952
188001 (9 Sge)	6.3	O8f	8344 (Sept. 4), 8399 (Oct. 2), 8406 (Oct. 3), 8414 (Oct. 4), 8420 (Oct. 5), 8521 (Dec. 2)
190429N	6.6	O5f	8339 (Sept. 3), 8347 (Sept. 4), 8400 (Oct. 2), 8407 (Oct. 3), 8411 (Oct. 4), 8413 (Oct. 4), 8415 (Oct. 4), 8417 (Oct. 4), 8419 (Oct. 5), 8423 (Oct. 5)
190864	7.8	O6	8345 (Sept. 4), 8408 (Oct. 3), 8416 (Oct. 4)
192281	7.5	O5f	8346 (Sept. 4), 8412 (Oct. 4)
192639	7.0	O8f	8341 (Sept. 3), 8398 (Oct. 2), 8409 (Oct. 3), 8422 (Oct. 5)
34656	6.7	O7	8333 (Sept. 1), 8337 (Sept. 2), 8342 (Sept. 3), 8401 (Oct. 2), 8402 (Oct. 2), 8403 (Oct. 2), 8404 (Oct. 2), 8426 (Oct. 5)
46150	6.8	O6	8338 (Sept. 2), 8405 (Oct. 2)
47839 (S Mon)	4.7	O7	8427 (Oct. 5), 8428 (Oct. 5)

All spectrograms were taken with the 32-inch camera of the coudé grating spectrograph of the 100-inch telescope, which gives a dispersion of 10.2 A/mm. The spectrograph slit was set at a width of 120 μ, which corresponds to 34 μ on the plate. All spectra were widened to 0.35 mm on the plate. All exposures were made on Eastman IIa-O emulsion and covered the spectral range from λ 3300 to λ 4900. A step-slit calibration was put on each plate with the standard equipment of the coudé spectrograph. Microphotometer tracings were made from the plates. To reduce these tracings to an intensity scale, calibration-curves were obtained at four representative wave lengths, namely, $\lambda\lambda$ 4650, 4400, 4100, and 3930.

III. ABSORPTION-LINE EQUIVALENT WIDTHS

Since the equivalent widths of many lines were required, it was clear that the usual methods employed with microphotometer tracings would be too tedious. Since the central depths R_c of the lines are always small, rarely exceeding 0.35, and since the calibration-curves (in terms of log I) are sufficiently straight so that there is a single slope over one and sometimes over many lines, it was found empirically that the area as measured by a planimeter on the microphotometer tracing could be reduced to the equivalent width W by the relation,

$$W = \text{Const.}\ \frac{[\text{area}]\ [\text{slope (log } I/\text{unit deflection)}]}{1 + 0.37R_c}. \qquad (1)$$

TABLE 2

EQUIVALENT WIDTHS IN ANGSTROMS OF ABSORPTION LINES

λ	Identity	HD 188001	HD 190429N	HD 190864	HD 192281	HD 192639	HD 34656	HD 46150	HD 47839
4861	*Hβ, He* II	0.85	0.76	1.74	1.50	1.35	.....	2.28	1.94
4713	*He* I	0.25	.....	(0.14)	.....	0.24	0.24	.....	0.14
4619	*N* V	.....	0.16	.....	.....	.....	.....	.....	.....
4603	*N* V	.....	0.27	.....	.....	.....	.....	.....	.....
4541	*He* II	0.56	0.66	0.75	0.92	0.56	0.77	0.60	0.52
4534	*N* III	0.08	.....	(0.08)	.....	0.06	0.15	.....	.....
4523	*N* III	0.06	.....	(0.06)	.....	0.06	0.10	.....	.....
4514	*N* III	0.21	.....	0.09	.....	0.13	0.20	.....	0.08
4510	*N* III	0.16	.....	0.08	.....	0.12	0.18	.....	0.06
4471	*He* I	0.72	0.10	0.57	0.38	0.72	0.86	0.32	0.52
4387	*He* I	0.16	.....	0.10	.....	0.17	0.24	0.08	0.16
4340	*Hγ, He* II	1.25	1.22	1.90	1.76	1.48	1.89	1.94	2.06
4199	*He* II	0.38	0.44	0.49	0.88	0.47	0.57	0.43	0.40
4195	*N* III	.....	.....	0.10	.....	0.04	0.10	(0.16)	.....
4143	*He* I	0.09	.....	.....	.....	0.10	0.15	.....	.....
4116	*Si* IV	0.11	.....	.....	.....	0.11	0.07	.....	0.07
4101	*Hδ, He* II	1.39	0.94	1.54	2.09	1.41	1.56	1.84	1.86
4097	*N* III	0.60	0.11	0.40	.....	0.48	0.54	(0.31)	0.36
4088	*Si* IV	0.38	.....	0.18	.....	0.28	0.20	.....	0.16
4026	*He* I, *He* II	0.67	0.40	0.54	0.62	0.63	0.71	0.41	0.68
3970	*He, He* II	1.08	1.03	1.40	1.68	1.23	1.36	1.56	1.74
3964	*He* I	0.14	0.10	0.13	.....	0.13	0.18	(0.22)	0.26
3961	*O* III	0.10	.....	0.09	.....	0.13	0.10	(0.04)	0.14
3923	*He* II	0.29	0.37	0.34	0.58	0.36	0.46	0.23	0.19
3888	*H8, He* II	1.09	0.96	1.35	1.58	1.13	1.33	1.75	1.97
3867	*He* I	.....	.....	.....	.....	0.08	0.07	.....	.....
3858	*He* II	0.11	0.21	0.16	0.24	0.15	0.15	(0.11)	.....
3835	*H9, He* II	0.80	0.86	1.20	1.19	1.09	1.20	1.53	1.54
3819	*He* I	0.34	.....	0.18	0.18	0.27	0.36	0.20	0.28
3813	*He* II	0.14	0.11	0.09	0.16	(0.08)	0.10	0.08	(0.06)
3797	*H*10	0.85	0.65	0.98	1.02	0.80	1.00	1.23	1.44
3791	*O* III	0.20	.....	0.20	(0.18)	0.22	0.14	0.12	0.25
3774	*O* III	.....	.....	(0.14)	.....	(0.09)	.....	.....	.....
3770	*H*11	0.71	0.47	0.71	0.65	0.65	0.82	0.92	1.40
3759	*O* III	0.37	.....	0.34	.....	0.41	0.32	0.18	0.30
3757	*O* III	0.20	0.24	0.20	0.32	0.19	0.20	0.11	0.18
3754	*O* III, *N* III	0.08	.....	0.20	.....	0.17	0.17	0.20	0.20
3750	*H*12	0.55	0.52	0.54	0.48	0.58	0.65	0.60	0.92
3734	*H*13	0.41	0.31	0.42	0.40	0.56	0.52	0.40	0.74
3721	*H*14	0.33	0.18	0.23	0.21	0.45	0.30	0.20	0.46
3711	*H*15	0.33	.....	0.24	.....	0.34	0.16	(0.14)	0.36
3704	*H*16, *He* I	0.46	.....	0.29	.....	0.47	0.36	0.14	0.46
3634	*He* I	0.16	.....	(0.13)	.....	(0.26)	0.16	.....	0.12
3484	*N* IV	0.07	.....	(0.06)	.....	(0.13)	.....	(0.09)	.....
3482–4	*N* IV	.....	0.68	.....	(0.54)	.....	(0.13)	.....	(0.14)
3482	*N* IV	0.11	.....	(0.19)	.....	(0.20)	.....	(0.18)	.....
3478	*N* IV	0.20	0.60	0.27	0.56	0.24	(0.23)	(0.28)	0.10
3440	*O* III	.....	(0.17)	.....	.....	.....	.....	(0.13)	0.12
3411	*O* IV	.....	0.26	(0.11)	.....	.....	.....	(0.22)	0.06
3403	*O* IV	.....	(0.34)	(0.10)	.....	.....	.....	(0.27)	0.05
3374	*N* III	0.16	.....	(0.17)	.....	.....	(0.18)	(0.22)	(0.08)
3367	*N* III	0.25	.....	(0.20)	.....	.....	(0.22)	.....	(0.11)
3354	*N* III	0.29	.....	(0.18)	.....	.....	(0.15)	.....	(0.09)
3340	*O* III	0.30	.....	(0.24)	.....	.....	(0.45)	(0.28)	0.33
3312	*O* III	.....	.....	(0.20)	.....	.....	.....	.....	0.36

This formula was found to be accurate within 1 or 2 per cent, even for lines of quite different shapes and strengths. Consequently, all equivalent widths were determined by this method.

The results are listed in Table 2 for all the stars. We have tabulated the equivalent widths W, in angstroms, of the lines. Across the top are listed the HD numbers of the stars. Down the left are given the wave length and identification of the lines, two or more identifications denoting a blend. The equivalent widths for HD 188001, HD 190429N, and HD 192639 are based on three plates, while the equivalent widths for the other stars are based on two plates. All entries in parentheses denote either that the line was measured on only one plate or that the measurement is uncertain for other reasons, such as blending.

TABLE 3

PROBABLE ERRORS OF EQUIVALENT WIDTHS

HD	No. of Plates	p.e. of Mean		HD	No. of Plates	p.e. of Mean	
		$W \leq 0.3$	$W > 0.3$			$W \leq 0.3$	$W > 0.3$
188001	3	9%	0.025A	192639	3	7%	0.029A
190429N	3	9	.028	34656	2	8	.025
190864	2	9	.030	46150	2	13	.057
192281	2	13	0.040	47839	2	13	0.035

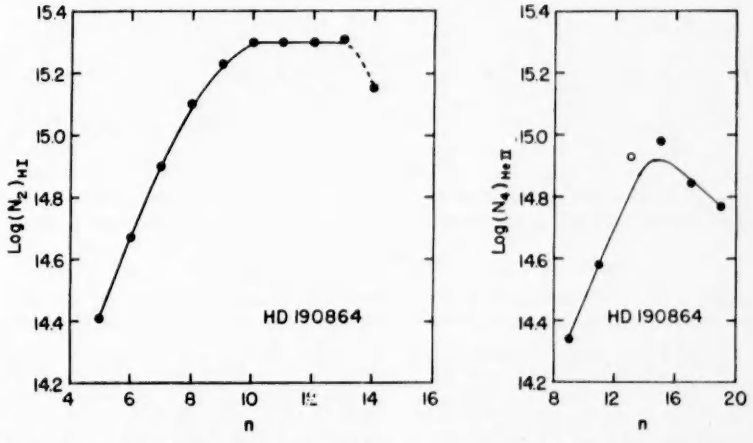

FIG. 1.—On the left is plotted the value of log $(N_2)_H$, as calculated from equation (2) for all the measurable Balmer lines. The lines are denoted by the usual Balmer number n. On the right is the corresponding plot for the Pickering series of *He* II. The open circle denotes λ 4026, which is blended and therefore too high. The plots are for the star HD 190864.

The probable errors of the equivalent widths were determined by comparing results from two or more plates of the same star. Since the probable errors appeared to be proportional to W for $W < 0.3$ and constant for $W > 0.3$, they were worked out on this basis. The probable errors of the mean equivalent widths are given in Table 3, along with the number of plates used in forming the mean. For $W \leq 0.3$, the probable errors

are given as percentages of the equivalent width, while for $W > 0.3$ they are given in angstrom units. The probable errors discussed above indicate only the internal accuracy of the measurements. There remains the question of the absolute accuracy of the equivalent widths. Measurements of some of the lines listed in Table 2 have been made for these stars by Petrie (1947) at Victoria. A comparison shows that there is a systematic difference amounting to 35 or 40 per cent, the Victoria equivalent width being larger. The internal consistency, on the other hand, seems fairly good. A difference of this order has been noted previously (Merrill, Sanford, Wilson, and Burwell 1937), but as yet no clear reason for it has been uncovered.

IV. NUMBERS OF ABSORBING ATOMS

H I

The numbers of atoms active in forming the Balmer lines can be estimated by a method used by Unsöld (1941). For weak lines we have

$$(N_2)_{H\,I} = \frac{W 10^{20}}{0.886 f \lambda^2}, \tag{2}$$

where λ is the wave length in angstroms, f is the oscillator strength, and $(N_2)_{H\,I}$ is the number of atoms above 1 cm² of the photosphere in the $n = 2$ level of hydrogen. If we use W for the strong hydrogen lines, equation (2) gives values of $(N_2)_{H\,I}$ which are too small because of the strong saturation effects. The last few resolved lines of the Balmer series, on the other hand, overlap, thus depressing the observed continuum and making W too small and consequently $(N_2)_{H\,I}$ also. The lines between these two extremes should give a good estimate of $(N_2)_{H\,I}$. The method is illustrated in Figure 1, where the values of log $(N_2)_{H\,I}$ calculated from equation (2) are plotted against the Balmer number n, for HD 190864. It should be noted that the *He* II Pickering series influences the Balmer lines only to $n = 7$ or 8, as can be inferred from the weakness of the *He* II lines at λ 3923 and λ 3858. One should be cautious about interpreting the flat portion of the curve, which is not present for all stars, as giving log $(N_2)_{H\,I}$, since the continuum may already be depressed. An inspection of the microphotometer tracings indicates, however, that the hydrogen lines do not have extensive wings, such as are present in somewhat later-type stars, and consequently the lines do not appear to be blended in the region where log $(N_2)_{H\,I}$ is determined. The values of log $(N_2)_{H\,I}$ have been taken, therefore, at the leveling-off part of the curves and are given in Table 4.

TABLE 4

NUMBERS OF ATOMS ABOVE THE PHOTOSPHERE

HD	log $(N_2)_{H\,I}$	log $(N_4)_{He\,II}$	log $[N(2^3P^o)]_{He\,I}$	log $\bar{\Gamma}[N(3s^3S)]/g]_{N\,IV}$	log $\{[N(3s^3P^o)]/g\}_{O\,III}$
188001	15.36	14.96	14.00	11.9	13.0
190429N	15.20	14.98	12.66	12.5	.....
190864	15.30	14.92	13.78	12.1	12.7
192281	15.28	15.17	13.6	12.4	.....
192639	15.44	15.00	14.04	12.2	12.6
34656	15.40	15.07	14.11	11.8	12.5
46150	15.40	14.84	13.64	12.1	.....
47839	15.57	14.72	13.84	(11.3)	12.7

He II

The method used above for hydrogen can be applied in precisely the same manner to the Pickering series of *He* II. Since every other line of the series coincides with a hydrogen

line, only half the lines can be used. Of these, λ 4026 is blended with *He* I. A sample plot is shown in Figure 1 for HD 190864. The open circle represents the blended line λ 4026. The drop of the curve for $n = 17$ and $n = 19$ cannot be due to overlapping lines but may be a result of a tendency to underestimate the equivalent widths of weak lines. The top points on the curves were assumed to give the correct values of log $(N_4)_{He\,II}$. The results for all stars are given in Table 4.

He I

The equivalent widths of the *He* I lines were used to construct a curve of growth. The lower energy levels of all measured lines are near enough together so that no excitation correction is needed. Although the measured lines do not define a good curve, it appears that the position of the linear portion of the curve of growth can be estimated with some reliability. In doing this, more weight was given to the $2^3P^o - n^3D$ series lines than to the others. It is perhaps noteworthy that the lines λ 3964 and λ 4713 appear too high in all plots. The linear part of the curve of growth was used to determine log $[N(2^3P^o)]_{He\,I}$, where $N(2^3P^o)$ is the number of atoms in the 2^3P^o level of *He* I. These values are given in Table 4. For the star HD 190429N the *He* I lines were so weak that only the line λ 4471 was measurable. It was assumed that this line was unsaturated. Likewise, for HD 192281 only the lines λ 4471 and λ 3819 could be measured. It was assumed that λ 3819 was unsaturated. The values of log $[N(2^3P^o)]_{He\,I}$ should be known within a range of 0.10–0.15.

OTHER IONS

The curve-of-growth method was also applied to *O* III, *O* IV, *N* III, and *N* IV. Oscillator strengths were computed by the method outlined by Bates and Damgaard (1949). From these curves of growth, estimates were made of log $[N(3s^3P^o)/g]_{O\,III}$ and log $[N(3s^3S)/g]_{N\,IV}$. These are given in Table 4. Curves of growth for *O* IV and *N* III were too poor to give any reliable estimates. In the case of *O* III and *N* III there is evidence that certain of the absorption lines are filled in by emission. Two lines of *Si* IV appear at λ 4088 and λ 4116. They appear in emission in HD 190429N. Only one star, HD 47839, showed carbon absorption lines of measurable strength. The lines found were λ 4647 and λ 4651 of *C* III.

ELECTRON DENSITY n_e

The electron density in the atmosphere may be found from the Stark-effect broadening of the Balmer lines according to the Inglis-Teller relation (Inglis and Teller 1939),

$$\log n = 23.26 - 7.5 \log n_m , \tag{3}$$

where n_m is the number of the last resolvable Balmer line and n is the positive ion density which is related to the electron density in hot O-type stars by the relation $n_e = 1.1n$. The factor 1.1 occurs if the ratio of hydrogen to helium, by numbers of atoms, is 10 to 1 and if both *H* and *He* II are almost completely ionized. Using equation (3), the stars yield values of log n_e ranging from 14.2 to 14.7. These values are maximum values, since if lines are broadened by other sources such as rotation, one would not resolve as many lines as otherwise would be resolved. In these stars it appears that this limit may have been reached.

V. PRINCIPAL FEATURES OF THE ATMOSPHERE

In Table 4 of Section IV we have assembled the data from which we can hope to get information concerning the atmospheres of these stars. It is evident that the main features of the atmosphere will depend chiefly on the hydrogen and helium observations and on the electron density. It is assumed that the numbers of atoms given in Table 4 really represent the true relative abundances in the atmosphere. This assumption implies that the atmosphere can be treated as a "thin layer" and also that the ions which are hard to

ionize are in the same regions as the ions which are easy to ionize. These assumptions can be removed only by constructing model atmospheres. Since we are interested in the very general properties of early O and Of stars, the above assumptions will be retained. We obtain these features in the following way. First we make an estimate of log n_e. Using this along with log $(N_4)_{He\,II}$ and log $[N(2^3P^o)]_{He\,I}$, we compute the temperature T by the Saha formula. Having n_e and T, we can compute numbers of atoms in any stage of ionization. In particular, we can get the total amount of hydrogen and helium above 1 cm^2 of the photosphere. If we make the reasonable assumption that hydrogen and helium make up 98 per cent of the total mass, we obtain X and Y, the masses per gram of hydrogen and helium, respectively. Since the continuous absorption coefficient is due to *H*, *He* I, *He* II, and electron scattering, we can compute the opacity per gram of stellar material for any wave length (we have done it for λ 4000). From this and the total mass above 1 cm^2 of the photosphere we obtain the optical depth τ_ν of the continuum. If one assumes that the observed lines are formed according to the Milne-Eddington model for pure absorption, then it can be shown (Unsöld 1941) that the central depth R_c of the strongest lines should equal the optical depth τ_ν. For Of stars here considered, this gives $\tau_\nu = 0.35$. This value is a minimum value, since if these lines are broadened by rotation or large-scale motions, as is likely in early O-type stars, the central depth is too small.

TABLE 5

PROPERTIES OF THE ATMOSPHERES FOR CASE A

HD	log n_e	T (° K)	log $(N_2)_{H\,I}$	X	Y	log H	log g_g
34656	14.04	34,200	16.5	0.55	0.43	9.6	3.3
46150	14.56	37,300	16.7	0.70	0.28	8.8	4.0

From a study of the Milne-Eddington model (Unsöld 1938) it is seen that an optical depth somewhere between 0.4 and 0.6 is reasonable. For early-type stars, the only model atmosphere available is for stars probably considerably fainter than Of stars (Underhill 1951). This atmosphere gives an optical depth of 0.45 for the visible region of the spectrum. In this paper it will be assumed that the optical depth should be about 0.6.

The other quantities of interest are the height of the atmosphere H, defined as the ratio of the total number of electrons above 1 cm^2 of the photosphere to the electron density, and the effective acceleration of gravity g_g as measured by the gas pressure. We obtain g_g from the relation,

$$g_g = \frac{2\,(N/N_e)\,n_e kT}{\rho H}, \tag{4}$$

where N/N_e is the ratio of the total number of particles to the total number of electrons and ρ is the density. The factor 2 is obtained from the assumption that the pressure at the bottom of the atmosphere is twice the average pressure.

The procedure just outlined was carried out by first assuming the values of log n_e which were given by the Stark-effect results in Section IV. This gave $\tau_\nu = 0.02$, an extremely small value. A similar but smaller discrepancy has been noticed previously by Unsöld (1941) and Aller (1946). Since we insist that τ_ν should be very nearly 0.6, we must assume either that the values of N for the various atoms are incorrect (case A) or that the values of n_e predicted by the Inglis-Teller relation are much too large (case B), or that both of these are working together.

First we consider case A, where log n_e as given by the Inglis-Teller relation is assumed correct. To obtain $\tau_\nu = 0.6$, we increase log $(N_2)_{H\,I}$, log $(N_4)_{He\,II}$, and log $[N(2^3P^o)]_{He\,I}$

by the same constant amount until we obtain the required τ_ν. In Table 5 we list in order log n_e, T, the new value of log $(N_2)_{H\,I}$, X, Y, log H, and log g_g for the two stars HD 34656 and HD 46150. We note that the numbers of atoms, N, must be increased by factors of 13 and 20 for the two stars. It might be argued that the values of log $(N_2)_{H\,I}$ and log $(N_4)_{He\,II}$, which are lower limits, have been underestimated by perhaps a factor of 2. Even allowing for this, there is still a discrepancy of a factor of 6–10. Hence it seems likely that incorrect values of the various N's can be only a small part of the trouble.

We next consider the other extreme alternative, case B, where log n_e alone is assumed incorrect. To obtain $\tau_\nu = 0.6$, we allow log n_e to be changed until the correct τ_ν is obtained. The results are given in Table 6, where we list in order the new values of log n_e,

TABLE 6

PROPERTIES OF THE ATMOSPHERES FOR CASE B

HD	log n_e	T (° K)	X	Y	log H	log g_g
188001	12.38	28,500	0.56	0.42	11.57	1.24
190429N	12.40	33,100	.60	.38	11.56	1.34
190864	12.32	28,800	.60	.38	11.66	1.16
192281	12.43	30,600	.51	.47	11.51	1.35
192639	12.45	28,700	.59	.39	11.51	1.32
34656	12.44	28,700	.53	.45	11.51	1.31
46150	12.41	29,200	.70	.28	11.55	1.34
47839	12.53	28,600	0.75	0.22	11.45	1.45

TABLE 7

HALF-WIDTHS IN ANGSTROMS OF LINES OF DIFFERENT ATOMS

HD	*N* III, *O* III	Weak *H* I	*He* II	*He* I	*N* III Emission λ 4634, λ 4640
188001	2.2	2.9	2.6	2.5	3.3
190429N	2.8	3.8	3.2	2.7	4.8
190864	1.7	3.3	2.7	2.0	2.9
192281	5	6	6	5	5
192639	2.4	3.3	2.6	2.2	3.1
34656	1.5	3.4	2.5	1.9	2.4
46150	2.0	4.3	2.9	3.4	3.3
47839	1.0	3.6	2.4	1.6	2.0

T, X, Y, log H, and log g_g for each star. We see that the value of n_e is 100 times smaller than in case A. With these new values of log n_e and T, both *H* I and *He* I are almost completely ionized and *He* II is partly ionized. The opacity is due almost entirely to electron scattering.

The results for case B in Table 6 indicate very low densities in the atmospheres and small effective gravities. Before the results for case B can be accepted, it is desirable to check these two features observationally. This is done in Sections VI and VII.

VI. ABSORPTION-LINE BREADTHS

According to case B, with a low value of log n_e, one would expect the weak lines to be rather sharp. From the curve of growth, one estimates the Doppler velocities to be about 10 km/sec or about 0.13 A. The instrumental profile is about twice as large. We actually find much greater breadths, as shown in Table 7, where we have tabulated half-widths in

angstroms. We give in order the half-widths of the weak absorption lines of *N* III and *O* III, of the unsaturated hydrogen lines, of the *He* II lines, and of the *He* I lines. The last column will be discussed later. We notice that the hydrogen lines are wider than the *He* II lines, which are, in turn, wider than the *N* III and *O* III lines. The *He* II lines are a little wider than the *He* I lines. The breadths of the narrowest lines suggest either rotation or large-scale motions. Only one star, HD 192281, shows conclusive evidence of rotation. For all the other stars one cannot estimate from the line profiles which effect is present.

We proceed on the assumption that large-scale motions are the broadening source. If we assume that these motions are primarily radial and that at the center of the star disk the time-averaged profile is Gaussian, then it can be shown readily that the half-width of the profile should be 1.4 times that of the observed line, which is formed by the integrated light over the hemisphere. This figure is based on a limb-darkening coefficient of 0.6.

The main problem is the excessive widths of the unsaturated hydrogen lines. At the densities involved for case B, collisional damping is small, as is radiation damping. It can be shown that the Stark effect for $H\gamma$ would produce a line having a width of 0.4–0.6 A. If this increases considerably as one goes from $H\gamma$ to $H10$, then the weaker hydrogen lines present no difficulty. If, on the other hand, Stark broadening does not increase appreciably from $H\gamma$ to $H10$, then there is a discrepancy. In this connection a puzzling fact is that HD 46150 and HD 47839 have hydrogen lines with appreciable wings; yet the increased density which this implies is not evident in the values of log n_e in Table 6.

One must conclude that for case B there may be a discrepancy in the breadths of the hydrogen lines. If this discrepancy does exist, it could be removed by decreasing τ_r from 0.6 to 0.2. This has the effect of increasing the density and thus the Stark broadening.

VII. SUPPORT OF THE ATMOSPHERE AND THE MASS-LUMINOSITY RELATION

For a bright main-sequence star one would expect an acceleration of gravity between 1000 and 10,000 cm/sec^2. The value which we get from the gas pressure is of the order of 20 cm/sec^2. Hence gas pressure supports only a small fraction of the atmosphere, the rest of the atmosphere being supported by radiation and turbulent pressure. Since we wish to work in terms of accelerations, we convert from pressures by the relation

$$g = \frac{P}{\rho H}. \tag{5}$$

We have

$$g = g_g + g_r + g_t\,, \tag{6}$$

where g is the acceleration of gravity, g_g is that given in Table 6, and g_r and g_t are the accelerations due to radiation and turbulence, respectively. First, we obtain suitable expressions for the g's in equation (6).

If we combine the law of gravitation and the ordinary black-body total-radiation law, we find,

$$\log g = \log \frac{m}{m_\odot} - 0.4\,(M_\odot - M_b) + 4 \log T - 10.59\,, \tag{7}$$

where $m/m_\odot$ is the mass of the star in solar units and $M_\odot$ and M_b are the absolute bolometric magnitudes of the sun and star, respectively.

It can readily be shown that

$$g_r = \frac{\kappa a T^4}{4}, \tag{8}$$

where κ is the mean opacity coefficient per gram. Since electron scattering is the chief source of opacity, we can set $\kappa = 0.3$.

The turbulent pressure is given by

$$P_t = \rho v^2 \tag{9}$$

which, by equation (5), becomes

$$g_t = \frac{v^2}{H}. \tag{10}$$

The velocity v should be the root-mean-square velocity. If, as has been assumed in Section VI, the velocity is given by a Gaussian distribution, then the value of v should be 0.7 of the half-half-width of the Gaussian distribution. We have already noted in Section VI that this half-half-width should be 1.4 times the actually observed half-half-width of weak lines. Together, v is given by the half-half-width of the weak lines and can be obtained from Table 7. We emphasize that the correct value of v depends on the assumed shape of the distribution-curve and also on the limb-darkening law. We should recall that if broadening is by rotation, then g_t will be absent. Fortunately, g_t is not the dominant contributor to g, and hence our results will be uncertain by at most a factor of 2.

The various g's have been computed for all stars and are given in Table 8. The sum

TABLE 8

ACCELERATIONS (CM/SEC^2)

HD	g_a	g_r	g_t	g	$\log m/m_\odot + 0.4M_b$
188001	20	370	190	580	−2.62
190429N	20	680	310	1010	−2.64
190864	10	390	90	490	−2.71
192281	20	490	250	760	−2.62
192639	20	380	250	650	−2.58
34656	20	380	100	500	−2.69
46150	20	410	160	590	−2.65
47839	30	370	50	450	−2.73

according to equation (6) is also given. Finally, the values of $\log (m/m_\odot) + 0.4M_b$, obtained from the value of $\log g$ and equation (7), are given.

A second relation between $m/m_\odot$ and M_b which can be applied is the mass-luminosity relation. Several different mass-luminosity laws have been published, the last being by Petrie (1951). He also compares the various relations which have been obtained. Employing the theoretical black-body bolometric correction, the average of these relations was combined with the values of $\log (m/m_\odot) + 0.4M_b$ in Table 8. The result is

$$\frac{m}{m_\odot} = 35\,, \qquad M_b = -10\,, \qquad \frac{R}{R_\odot} = 32\,. \tag{11}$$

The numbers in equation (11) can now be compared with the observational values. An absolute visual magnitude of −6 has been given by Roman (1951) for Of stars in Cygnus. For $T = 29{,}000°$ K, the theoretical black-body bolometric correction is 3 mag., which gives $M_b = -9$. Since the bolometric correction is rather uncertain and since the values of M_v, corrected for absorption, are somewhat uncertain, our value of M_b in equation (11) seems reasonable.

It is of interest to consider in detail the early-type binaries which have known masses,

luminosities, and radii. CC Cas is a system having a spectral type O8. J. A. Pearce (1931) has determined the spectroscopic orbit, and S. Gaposchkin (1940) has analyzed the light-curve. Gaposchkin gives for the two components, respectively, $m/m_\odot = 20$ and 10, $R/R_\odot = 7.3$ and 6.3, and $M_v = -3.2$ and -2.8. These stars are therefore much lighter and fainter than the stars being considered. HD 215835 consists of two O5 stars. J. A. Pearce (1949), from the spectroscopic orbit, gives minimum masses of 23.4 and 19.1 solar masses for the two components. The absolute visual magnitudes, -4.2 and -3.9, are known, since the binary is in a galactic cluster. Again these stars are fainter than stars being considered here.

The binary system 29 Canis Majoris contains an Of star as the brighter component. Kuiper, from a discussion of the observational data (1938), has given for this component $m/m_\odot = 44$, $M_b = -10$, and $R/R_\odot = 20$. These numbers are very similar to those in equation (11). Another binary system of interest is AO Cas, which contains two O8.5 stars. For the brighter component, Kuiper (1938) has given $m/m_\odot = 43$, $M_b = -10.3$, and $R/R_\odot = 23$. Using newer material, Wood (1948) obtains $m/m_\odot = 31$, $M_b = -9.1$, and $R/R_\odot = 19$. The spectroscopic orbit determined by Struve and Horak (1949) would give a mass nearer to that found by Kuiper. These values are consistent with those found in equation (11) if it is remembered that this star is somewhat later in spectral type than those for which equation (11) is intended to be applicable. It is perhaps noteworthy that, from a study of the light-curve of AO Cas, Hiltner (1949) has suggested the possibility that one of the stars may have a very extensive electron-scattering atmosphere like that postulated for the Wolf-Rayet binary V444 Cygni (Kron and Gordon 1950). This interpretation, if correct, is in agreement with the large value of H/R (equal to $\frac{1}{6}$) which is obtained from the values of H and R in Table 6 and equation (11), respectively.

The four binaries just discussed indicate that the properties of the stars studied in this paper should be associated only with the very bright O and Of stars. We must stress in conclusion that the values of M_b, m, and R for these early-type binaries are likely to be uncertain because of the difficult natures of their light-curves and of possible effects of gas streaming.

VIII. FINAL PROPERTIES OF THE ATMOSPHERE

From the discussions in Sections VI and VII it is now possible to determine whether the atmospheres of Of stars can be described by case B. A study of the Balmer lines indicates that the densities predicted by case B are consistent with the breadths of the Balmer lines, provided that the Stark broadening increases substantially as one goes to higher members of the Balmer series. If, on the other hand, the Stark broadening does not increase appreciably, then a density about three times higher than that given for case B is necessary. This can be obtained by choosing 0.2, rather than 0.6, for the optical depth. By studying the support of the atmosphere, it is found that the results for case B are in reasonably good agreement with observation. This agreement is not altered substantially by choosing $\tau_v = 0.2$ rather than 0.6. Until more is known about the Stark effect for the higher members of the Balmer series, it seems best to take the results for case B as describing the atmospheres of Of stars. These are given in Table 6. Additional results are listed in equation (11). It should be remembered, however, that there remains a possibility that the results in Table 6 are too extreme, in the sense that the densities in the atmospheres are too small by about a factor of 3.

IX. ABUNDANCES

In Table 9 are given the abundances of hydrogen, helium, nitrogen (from *N* IV lines), and oxygen (from *O* III lines), in terms of numbers of atoms. The results for nitrogen in HD 47839 are uncertain. The true relative abundances may be considerably different from those shown, since no account has been taken of the fact that lines of different atoms and ions may be formed in very different regions of the atmosphere. This difficulty can be

overcome only if a model atmosphere is obtained. From Table 9 one does note that the hydrogen-to-helium ratio changes by a factor of 3 among the stars listed. It seems extremely likely that these differences are due to real variations in composition. There is, however, a small possibility that the differences are due to some other unknown factor. In any case, one concludes that the stars listed in Table 9 are considerably different from one another in some respect. While the numbers for nitrogen are uncertain, there is some evidence that the nitrogen abundance is not constant for all the stars. The abundances for oxygen are nearly ten times smaller than those for 10 Lacertae and τ Scorpii.

X. EMISSION-LINE DATA

The Of stars show a large number of emission lines. Unfortunately, the only ones which are strong enough for detailed study are the *N* III lines at λ 4634 and λ 4640 and the *He* II line at λ 4686. Intensity profiles, in terms of the continuum, were constructed from the microphotometer tracings. Some typical profiles are given in Figure 2. The

TABLE 9

RELATIVE ABUNDANCES IN NUMBERS OF ATOMS

HD	*H*	*He*	*N*	*O*
188001	10,000	1,900	3.2	2.0
190429N	10,800	1,700	1.1	.....
190864	10,800	1,700	3.5	1.1
192281	9,000	2,100	3.6	.....
192639	10,500	1,800	2.1	0.6
34656	9,600	2,000	3.8	0.6
46150	12,600	1,200	6.3	.....
47839	13,800	980	(0.8)	1.1

profiles are given by the solid line. The zero positions of the lines were obtained by measuring the absorption lines on the tracings in much the same way as measuring a plate. (This can be done accurately with tracings made with the Mount Wilson microphotometer.) The zero positions, relative to the absorption lines, are indicated by triangles on the continuum lines in Figure 2. They should be accurate to 0.3 A.

The next problem is the question of correcting the emission profiles for underlying absorption. Unless one knows where and how the emission lines are formed, it is difficult to determine whether real absorption lines occur at the emission-line wave lengths. Since the spectra of some of the stars do show a strong absorption line at λ 4686 and some absorption in the neighborhood of λ 4634 and λ 4640 and since the spectra of two of these stars have been known to show absorption lines (Swings and Struve 1940*a*) at λ 4634 and λ 4640, it was decided that the emission lines, corrected for the absorption lines, would best describe the emission in the stars. The absorption line of *N* III at λ 4097 should be almost identical with λ 4634, the values of *Ngf* being the same. The emission line λ 4634 was therefore corrected by removing the effect of the λ 4097 line in the same star. The line λ 4640 has a value of *Ngf* which is twice as great as for λ 4634. Since it can be demonstrated that λ 4097 is on the square-root part of the curve of growth and since the line profiles are governed by large-scale motions (or rotation), the absorption at λ 4640 can be reconstructed by deepening the λ 4097 profile at all points by a factor of 1.4. This profile was used to correct the emission line at λ 4640. The corrected emission profiles are given in Figure 2 by the dashed lines. HD 192281 was not corrected, since the line λ 4097 was not resolved from *Hδ*. For HD 190429N the *N* III absorption lines are very weak, and no correction is necessary.

The underlying absorption of λ 4686 is more difficult to estimate, since no directly

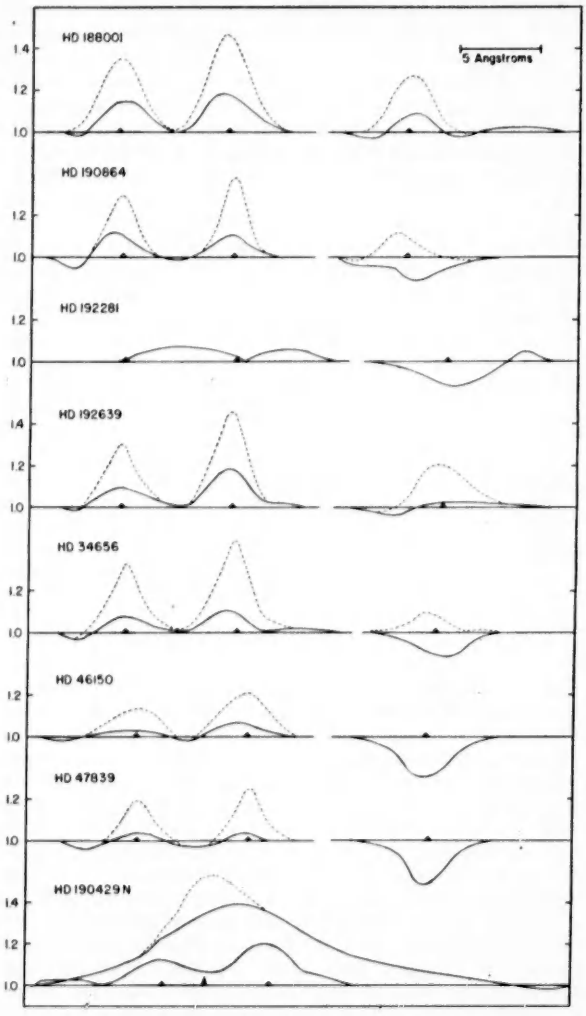

FIG. 2.—Representative line profiles are plotted in units of the continuum, the scale being given on the left. The horizontal wave-length scale is indicated by the distance of 5 A shown at the top of the figure. On the left are plotted the *N* III lines λ 4634 and λ 4640. On the right is plotted λ 4686 of *He* II. The solid curves indicate the observed profiles, the dashed curves the profiles corrected for the underlying absorption lines. It was not found possible to correct the lines in HD 192281. No correction is needed for the *N* III lines in HD 190429N. The *He* II line λ 4686 was assumed to be free of emission in HD 46150 and in HD 47839. The small solid triangles denote the zero positions of the lines. In HD 190429N, λ 4686, because of its great width, has been superposed over the *N* III lines. The tall triangle gives its zero position.

comparable lines are available. Since HD 46150 and HD 47839 showed λ 4686 as a strong absorption line of normal appearance, these profiles were used to correct the emission profiles in the other stars. Since HD 190429N is hotter than these two stars, this correction will not be too accurate. Since HD 192281 is broadened by rotation, no correction was applied. The corrected profiles are shown by dashed lines in Figure 2.

In addition to constructing profiles, the equivalent widths of the emission lines were determined. It was decided that these equivalent widths should include only the main body of the line, excluding violet or red absorption and emission features. The average equivalent widths in angstroms, corrected for the underlying absorption lines, are given in Table 10. For HD 192281 it was assumed that λ 4097 would have an equivalent width

TABLE 10

CORRECTED EQUIVALENT WIDTHS OF EMISSION LINES
(IN ANGSTROMS)

HD	*W*(4634)	*W*(4640)	*W*(4686)	*W*(4640)/*W*(4634)
188001	1.03	1.49	0.94	1.45
190429N	0.71	1.08	5.42	1.52
190864	0.65	0.90	0.24	1.38
192281	0.54	0.48	0.26	1.13
192639	0.87	1.25	0.71	1.44
34656	0.78	1.06	0.34	1.36
46150	0.45	0.62	0.00	1.38
47839	0.42	0.59	0.00	1.40

of 0.20 A. The emission equivalent widths were corrected accordingly. The ratio of the equivalent width of λ 4640 to λ 4634 is given in the last column.

XI. VARIABILITY OF THE EMISSION LINES

The variations of the *N* III line profiles take two forms: (*a*) the main part of the line varies considerably in shape; (*b*) the main lines are accompanied by emission and absorption satellites on the red and violet sides which come and go from plate to plate. The *He* II line λ 4686 shows rather similar changes.

A more quantitative way to study variability is to look for changes in the equivalent widths of the emission lines. We look for such changes in a sequence of four plates of HD 190429N taken on October 4–5, 1952, and in a similar sequence of four plates of HD 34656 taken on October 2–3, 1952. The equivalent widths of the three emission lines are plotted against time in Figure 3. From the probable error of a single equivalent width (about 0.04–0.05 A), which one can estimate from Table 3, it is seen that the curves, particularly those for HD 190429N, vary by considerably larger amounts. Also the fact that the curves vary in the same way for all lines strongly suggests that the changes in the equivalent widths are real. The time scale for the variations seems to be of the order of several hours. A second test of variability, which is basically the same, depends on dispersion calculations. We consider all the plates for a given star. We reduce all emission-line equivalent widths so that they are comparable to λ 4640. We now get the probable error of the mean of the three emission lines on each plate. This turns out to be nearly the same as that for the absorption lines, as should be the case if the lines vary together. We now take all the means for the one star and find the probable error of each individual mean on the basis of all the plates for the one star. For HD 190429N this probable error is four times as large as that derived from the three individual lines on the one plate. The factor is 2.5 for HD 34656. We again conclude that the emission-line

equivalent widths in HD 190429N are almost certainly variable, and may be variable in HD 34656. There remains the possibility that the variations are due to errors in the plate calibration-curves. A comparison of a great many calibration-curves shows, however, that the curves differ very little from plate to plate. The smallness of these differences makes it very unlikely that the equivalent widths can be in error by more than 3 or 4 per cent from this cause. It can therefore be concluded that the emission intensity is probably variable in HD 190429N, and may be variable in HD 34656.

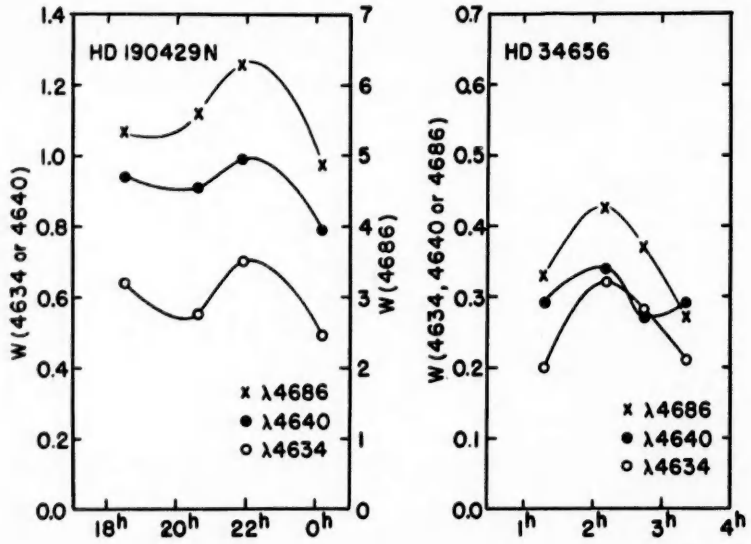

FIG. 3.—The three emission-line equivalent widths are plotted as a function of time (Pacific Standard time) for the stars HD 190429N and HD 34656, for each of which a series of four plates, closely spaced in time, had been obtained. The fact that the emission lines vary in phase is a strong indication that the variations are real. Although the λ 4640-curve for HD 34656 looks discordant, there is no reason for suspecting any of the points to be of low weight. The exposure times, on the average, were 50 minutes for HD 190429N and 37 minutes for HD 34656.

XII. PROPERTIES OF THE EMISSION LINES

We first consider the relation between the *He* II line λ 4686 and the *N* III lines λ 4634 and λ 4640. To do this the average equivalent width of λ 4634 and λ 4640 is plotted against that of λ 4686 for all stars. The plot is shown in Figure 4. The arrow denotes the point for HD 190429N which is far above the diagram. The six stars through which the curve is drawn are all of the same temperature, indicating a close relation between the *N* III and *He* II emission. HD 190429N and HD 192281, which are hotter objects, are displaced to the left of this curve. The most obvious explanation of this is that ionization is playing a role. At temperatures of 30,000° K the number of *N* III ions is decreasing rapidly and the number of *He* II atoms is changing little, with increasing temperature. If the *N* III emission is proportional to the number of *N* III ions, then the emission lines should be weaker by roughly the amount observed in these hotter stars. One cannot decide from this whether the emission arises in the atmosphere or in a shell above the atmosphere,

since dilution cannot be expected to show up in such calculations. More perhaps can be said if the mechanism producing the emission can be found.

Another feature of Figure 4 is the disappearance of λ 4686 emission, while λ 4634 and λ 4640 are still strong. The most likely reason for this is that the correction for the under-

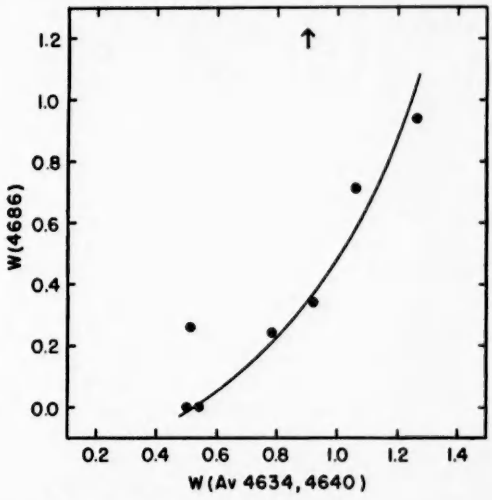

FIG. 4.—The equivalent width of the *He* II emission line λ 4686 is plotted against the average equivalent width of the *N* III emission lines λ 4634 and λ 4640. The data come from Table 10. The arrow indicates the point for HD 190429N which is far above the diagram. The curve is drawn through the six stars which have very nearly the same temperature.

lying absorption line has been underestimated for λ 4686. If this is the case, then the λ 4686 lines in HD 46150 and HD 47839 are actually already somewhat filled in by emission. This brings up the question of the division of early O-type stars into O and Of groups. HD 190864, HD 46150, and HD 47839, which on low dispersion appear to be normal O stars, actually are found on high dispersion to be Of stars. Thus O and Of stars form physically a continuous range of objects. In this group the O stars are the less active ones, in which emission does not fill the absorption lines, while the Of stars are the very active members with strong emission. We may conclude that, while the dividing line between O and Of stars is rather a formal one, still the two groups are, on the average, somewhat different physically.

We next consider the ratio of the equivalent widths of λ 4634 and λ 4640. The theoretical ratio of λ 4640 to λ 4634 in the absence of any saturation or absorption effects should be nearly 2. From Table 10 it is seen that the ratio, apart from that for HD 192281, is more like 1.4. This value has been obtained after applying rather large corrections for the absorption lines, these corrections having a ratio of 1.4. Unless, however, the emission ratio is also 1.4, one can expect large variations, which are a function of the emission-line strengths, in the uncorrected emission-line equivalent widths. Since this is not observed, the conclusion is that the true emission ratio is about 1.4. HD 192281 has a quite different ratio. This deviation of the observed ratio from the theoretical value of 2 shows that there must be considerable self-absorption of the emission lines. If the emission occurs in

a shell above the atmosphere, then, unless the dilution factor is close to unity, not enough atoms will be in a state to absorb the λ 4634 and λ 4640 emission, thus causing self-absorption. We can conclude that the emission cannot arise more than 1 or 2 stellar radii above the surface of the star.

Further information about the emission lines can be obtained by comparing their profiles with those of the absorption lines. Qualitatively, one notices that the emission fills in the absorption lines rather well, indicating that the shapes are similar. A more quantitative description is given in Table 7, where the half-widths of the emission lines (defined as for the absorption lines) are compared with half-widths of the absorption lines. The emission lines appear comparable in breadth to the moderately strong absorption lines. This suggests that the emission lines probably arise in regions where the fairly strong absorption lines are formed.

In the star HD 192281, which is rotating rapidly, it is found that the emission and absorption lines are similar in width and shape. This means that the emission and absorption lines must arise at nearly the same distance from the center of the star, since if the emission were farther out, the rotational velocity would be smaller and the lines narrower. This interpretation should be taken with caution, since the emission lines are shifted strongly to the red for some unknown reason.

In this section four properties of the emission lines have been discussed. In each case it is found that the feature is consistent with the view that the emission lines arise in the upper atmosphere of the star. While the first two features can perhaps be explained by a shell surrounding the star at a moderate distance, the last two features seem to require that the emission arise in the atmosphere. In conclusion, it is likely that the emission lines are formed in the upper atmosphere of Of stars.

XIII. ORIGIN OF THE EMISSION LINES

The *N* III emission lines have been discussed in terms of the Bowen fluorescence mechanism (Hynek 1951). If, however, we accept the results of the last section, this mechanism is not likely to work, since, although collisions are still unimportant, the induced upward transition probability is nearly as large as the spontaneous downward transition probability. This will tend to break up the mechanism very quickly. Other indications against this mechanism are, first, that the line λ 4097 of *N* III is a strong absorption line, even though it is the next step below λ 4640 in the cascading process, and, second, that the *O* III lines show only a little evidence of emission. There also remains the problem of many other emission lines for which no mechanism has been proposed. The *He* II line at λ 4686, unlike the others, is very probably produced by a resonance effect. A *He* II atom in the $n = 2$ state can be excited to the $n = 4$ state by absorbing Lyman-α, after which it may drop to the $n = 3$ level, giving λ 4686 emission. Lyman-α is almost certainly a strong emission line, since emission is observed in the Balmer lines. We conclude, provided that the emission is produced in the upper atmosphere of the star, that λ 4686 is the only emission line which is satisfactorily explained by selective mechanisms.

To look into some other sources of the emission lines, we consider the energies needed and available. We will make all calculations on the basis of $T = 30{,}000°$ K, $R/R_\odot = 32$, and the Planck radiation law. The amount of energy in the three strong emission lines is about 3×10^{35} ergs/sec. If it arises from the far ultraviolet radiation between 0 and λ A and if the processes are perfectly efficient, then we must go to λ = 450 A to get sufficient energy. If the processes are purely radiative, then we can estimate that a 4-volt photon will be obtained from an ultraviolet 40-volt photon, which means that we must have 3×10^{36} ergs/sec from the ultraviolet. This requires that we go to λ = 600 A. But at these wave lengths the photons do not have sufficient energy to ionize most of the atoms in question. Hence pure ionization and excitation processes are probably not the dominant ones. One possible solution to this difficulty is to postulate a strong ultraviolet

excess around 300–500 A. Such an ultraviolet excess has been suggested by Underhill (1951). If this excess were sufficient, it would ionize the atoms of interest and finally produce the emission lines. It is hard to see how this excess can arise in these bright Of stars, since the opacity, even in these regions, is primarily electron scattering.

Another possibility is that the longer-wave-length radiation (up to 900 A) sets the atmosphere in motion. This motion is finally reconverted into high-energy radiation by collisions. Taking an average velocity of about 100 km/sec (from half-widths of weak lines), the total energy in the atmosphere is 6×10^{39} ergs. This is used up roughly in the time required to traverse the atmosphere at a velocity of 100 km/sec. This time is 3×10^4 sec. The energy available from this source is therefore 2×10^{35} ergs/sec. Comparing this with the required energy of 3×10^{36} ergs/sec, we see that large-scale motions or turbulence are probably not adequate.

It is concluded that these rather simple mechanisms are not sufficient to explain the emission lines. It seems likely that a complex source of energy, for instance, shock waves, should be considered.

XIV. CONCLUSIONS

In the first part of this paper the absorption lines have been analyzed to obtain the essential features of the atmosphere. From this analysis two extreme cases can be distinguished, one with log n_e large (case A) and the other with log n_e small (case B). It is concluded that case B yields the best description of the atmosphere of an Of star, although there remains a possibility that the results for case B are too extreme in the sense that the densities are too low by about a factor of 3. Our choice of case B has the following implications: (1) Lines are broadened by large-scale motions or rotation. In addition, the hydrogen and helium lines are broadened by the Stark effect. (2) The Inglis-Teller relation does not give the correct electron density. This is possibly due to the fact that there is considerable broadening, apart from Stark broadening. (3) O5 and O7 stars have temperatures of roughly 33,000 and 29,000° K, respectively. These temperatures are rather lower than have been obtained by others. Petrie (1947) finds temperatures of 36,300 and 32,900° K for O5 and O7 stars, respectively. The differences are a result of the larger values of n_e used by Petrie. (4) The gas pressure is extremely small, owing primarily to the effects of radiation pressure. This makes the atmosphere 5 solar radii thick, or about one-sixth the radius of the star. Very low gas pressures, and hence low effective gravities, of the size found here for Of stars have been noted before in supergiant stars of later spectral type. Pannekoek (1937), for instance, has found very low effective gravities for A-type supergiants. He has shown that a small positive effective gravity can be obtained even if material is being blown away from the star. That a similar phenomenon is occurring in bright Of stars seems very possible. (5) The Of stars studied in this paper have bolometric absolute magnitudes of about -10 and masses of about 35 solar masses. These values are in fairly good agreement with observational values. If we compare these masses and absolute magnitudes with Aller's values for the nuclei of planetary nebulae (1948), namely, $M_b = -3$ and $m/m_\odot = 6$, it is clear that these objects are quite different from one another, even though their spectra are rather similar. The hydrogen-to-helium ratio is found to vary by a factor of 3 among the various stars. There is a possibility that these differences are caused by some agency other than composition.

In the second part of the paper the emission lines are discussed. It is found that the emission-line intensities have a total range of about 30 per cent during intervals of several hours in one and perhaps in two stars. Other properties of the emission lines, such as the breadths, ratios of intensities, and profiles, are consistent with the view that they arise in the upper atmosphere of the star. Several possible mechanisms for the production of the emission lines are discussed, but none of them appears to be satisfactory.

The author wishes to express his gratitude to Dr. Martin Schwarzschild for many stimulating discussions, and particularly to Dr. Lyman Spitzer, Jr., for obtaining the

plates used in this program and for his constant inspiration and guidance. Thanks are also due to Dr. Ira S. Bowen, director of the Mount Wilson and Palomar Observatories, for making this investigation possible, and to Dr. C. S. Beals for making available a considerable number of Victoria spectrograms. Finally, the author wishes to thank Princeton University for supporting this program through the Peyton Fellowship.

REFERENCES

Aller, L. H. 1946, *Ap. J.*, **104**, 347.
Aller, L. H. 1948, *Ap. J.*, **108**, 462.
Bates, D. R., and Damgaard, A. 1949, *Phil. Trans. R. Soc. London, A*, **242**, 101.
Gaposchkin, S. 1940, *Pop. Astr.*, **48**, 97.
Hiltner, W. A. 1949, *Ap. J.*, **110**, 443.
Hynek, J. A. 1951, *Astrophysics* (1st ed.; New York: McGraw-Hill Book Co., Inc.), p. 104.
Inglis, D. R., and Teller, E. 1939, *Ap. J.*, **90**, 439.
Johnson, H. M. 1953, *Ap. J.*, **118**, 370.
Kron, G. E., and Gordon, K. C. 1950, *Ap. J.*, **111**, 454.
Kuiper, G. P. 1938, *Ap. J.*, **88**, 472.
Merrill, P. W.; Sanford, R. F.; Wilson, O. C.; and Burwell, C. G. 1937, *Mt. W. Contr.*, No. 576; *Ap. J.*, **86**, 274.
Pannekoek, A. 1937, *B.A.N.*, **8**, 175.
Pearce, J. A. 1931, *Pub. Dom. Ap. Obs. Victoria*, **4**, 67.
Pearce, J. A. 1949, *A.J.*, **54**, 136.
Petrie, R. M. 1947, *Pub. Dom. Ap. Obs. Victoria*, **7**, 321.
Petrie, R. M. 1951, *Pub. Dom. Ap. Obs. Victoria*, **8**, 341.
Roman, N. G. 1951, *Ap. J.*, **114**, 492.
Struve, O., and Horak, H. G. 1949, *Ap. J.*, **110**, 447.
Swings, P. 1942, *Ap. J.*, **95**, 112.
Swings, P., and Struve, O. 1940*a*, *Ap. J.*, **91**, 546.
Swings, P., and Struve, O. 1940*b*, *Pub. A.S.P.*, **52**, 394.
Underhill, A. B. 1951, *Pub. Dom. Ap. Obs. Victoria*, **8**, 357.
Unsöld, A. 1938, *Physik der Sternatmosphären* (Berlin: J. Springer), p. 247.
Unsöld, A. 1941, *Zs. f. Ap.*, **21**, 1–84, 229–248.
Unsöld, A. 1942, *Zs. f. Ap.*, **22**, 229.
Wood, F. B. 1948, *Ap. J.*, **108**, 28.

EARLY-TYPE STARS IN THE DIRECTION OF THE GALACTIC CENTER*

W. A. HILTNER

Yerkes and McDonald Observatories

Received February 10, 1954

ABSTRACT

A group of OB stars in the direction of the galactic center has been observed for polarization, color, magnitude, and spectral type. The stars as a group have a distance modulus of 12.4 mag. or 3.0 kiloparsecs. The group is probably associated with a spiral arm inside the one isolated at 1.4 kiloparsecs from the sun. One star, HD 164019, located on a star cloud, appears to be more distant than all the others. The observed $m - M_0$ is 14.6 mag. and has an absorption of only 1.7 mag. The interstellar polarization is greatest for the more highly reddened stars. The relationship of the observed polarization and the visible obscuring clouds is well established. However, the distance of the obscuring cloud is still in doubt.

The group of blue giant stars discovered at the Observatorio de Tonantzintla (Morgan, González, and González 1953) has been observed for polarization, color, magnitude, and spectral type. The results from these observations are presented below.

OBSERVATIONAL MATERIAL

a) Polarization.—The observations for interstellar polarization were obtained with the same equipment as that employed earlier (Hiltner 1951) except that the RCA 1P21 photomultiplier was replaced with an EMI 5659, an end-on photomultiplier. This change was made in order to eliminate the necessity of any systematic corrections resulting from an inclined photocathode. Also, in the reductions of the observations, the graphical method for fitting the observations at distinct position angles to a sine-curve was replaced by least squares. Only two stars overlap with the previously reported polarization observations, HD 161103 and HD 160529. In these two cases the previously published values are effectively identical to the present observations.

b) Colors and magnitudes.—The color and magnitude observations were made with an RCA 1P21 photomultiplier and filters identical in number to those employed by Johnson and Morgan (1953) in establishing the (U, B, V) system. The amplifier was calibrated with a laboratory potentiometer. Atmospheric extinction was determined on four of the five nights on which this group of stars was observed. In the reductions, however, mean extinction coefficients were employed. Since the secant of the zenith distance of the group of stars under discussion was always large, nearly 2 at minimum, one star of the group (HD 161291) was employed as a secondary standard. Its color and magnitude were determined relative to 10 Lac and HR 8832 when the three stars were at nearly the same zenith distance.[1] Relative observations of colors and magnitude were obtained on four nights and are given in the following tabulation. The mean colors and magnitude were employed for determining nightly corrections to the observed colors and magnitudes of other members of the group. The mean corrections for $B - V$ and $U - B$ were 0.020 and 0.027 mag., respectively.

All observed natural colors were transferred to the (U, B, V) system. The transfer was based primarily on four stars, τ Her, ϵ CrB, 10 Lac, and HR 8832. In addition to these

* *Contributions from the McDonald Observatory, University of Texas*, No. 233.

[1] The magnitude of HR 8832 may be variable by 0.02 mag. In September, 1953, it was 0.021 mag. brighter than on three previous observing periods during which the star was used as a standard.

standard stars, early-type reddened stars were also observed, in order to check the transfer of the natural colors of these stars to the (U, B, V) system. More complete details will be given in a later paper. It will suffice here to state that, for the available data, the transfer appears to be linear and single-valued.

Three observations for colors and magnitude were obtained for each star on the program except HD 164019, HD 160529, CD−33°12155, and CD−33°12242, for which two observations were obtained. The internal agreement of the colors and magnitudes is entirely satisfactory. A probable error of a single color observation is ±0.007 mag. The systematic error, however, is more difficult to evaluate, but one not larger than 0.01 mag. seems to be indicated.

Date (1953)	V	$B-V$	$U-B$
June 5	8.898	+0.759	−0.251
7	8.885	+ .734	− .232
14	8.888	+ .758	− .269
15	8.872	+0.760	−0.251
Mean	8.886	+0.753	−0.251

c) Spectral classification.—Spectrograms of the stars under discussion were obtained by the author with the Cassegrain spectrograph of the 82-inch reflector. A new three-element camera lens with a focal length of 118 mm was used in conjunction with the two glass prisms. The average dispersion between $H\gamma$ and $H\delta$ is 100 A/mm. The exposure time is 80 minutes for a twelve-magnitude star on 103*a*-O emulsion and a spectrogram width of 0.60 mm. The spectrograms were kindly classified by Dr. W. W. Morgan.

SUMMARY OF THE OBSERVATIONAL MATERIAL

The observational material for the polarization, colors, magnitudes, and spectral types is collected in Table 1. The first column gives the number of the stars assigned by Morgan, González, and González (1953). Three additional stars are included and hence carry no number. The next six columns give the HD or CD number of the star, the 1900 right ascension and declination, the galactic longitude, latitude, and parallactic angle as computed from the Lund tables. The eighth, ninth, and tenth columns give the observed amount of polarization in magnitudes, the observed position angle of the electric vector maximum, and the position angle in galactic co-ordinates, respectively. The eleventh column is the spectral class on the MK system. The following three columns give the photometric data on the (U, B, V) system. The fifteenth column is the Q as computed from $Q = (U - B) - 0.886\,(B - V)$. The following columns give the assigned absolute magnitude, the color excess, and the distance modulus. The intrinsic colors adopted were those determined by Morgan, Harris, and Johnson (1953). An absorption of $3E_{B-V}$ was adopted in computing the corrected distance moduli (Morgan, Harris, and Johnson 1953).

DISTANCE OF THE GROUP

The distance moduli, as given in the eighteenth column, are plotted in Figure 1. The lower portion of the diagram is a plot of the stars in galactic co-ordinates, and in the upper portion the distance moduli are plotted with the galactic longitudes. It is obvious from the diagram that the stars as a group are much more distant than the spiral arm at 10.7 mag. or 1.4 kiloparsecs established by Morgan, Whitford, and Code (1953). If one is permitted to exclude all stars with a distance modulus less than 11.0 (on the assump-

TABLE 1

THE JOURNAL OF OBSERVATIONS

No.	Star (HD or CD)	1900 α	1900 δ	l	b	ϕ	p	θ	θ'	Sp.	V	$B-V$	$U-B$	Q	M_0	E_{B-V}	$m-M$
1.....	161061	17h38m3	−28°08′	328.23	−0.82	58.34	0.131	173°2	51°5	B2 III	8.47	+0.77	−0.31	−0.99	−4.1	1.01	9.54
2.....	161103*	17 38.5	−27 12	329.04	−0.27	58.36	.109	171.8	50.2	B2:pe (III–V)?	(8.69)	+0.44	− .69	−1.08	−3.3:	0.68	9.95:
3.....	161291	17 39.6	−27 11	329.19	−0.57	58.48	.144	179.8	58.3	B1 Ia*b*	8.89	+0.75	− .25	−0.92	−6.5	1.01	12.36
4.....	163065	17 49.1	−30 32	327.38	−4.07	59.67	.039	42.6	102.3	B1 Ia*b*	8.63	+0.37	− .54	−0.87	−6.5	0.63	13.24
5.....	164032	17 54.1	−29 49	328.57	−4.65	60.25	.013	29.4	89.6	B1 I*b*	7.48	+0.14	− .73	−0.86	−6.0	0.40	12.28
6.....	163453*	17 51.1	−28 14	329.60	−3.29	59.81	.041	15.5	75.3	B0.5:pe (V)?	9.28	+0.65	− .47	−1.03	−3.6:	0.93	10.09:
7.....	163454*	17 51.1	−31 00	327.19	−4.67	59.97	.031	53.2	113.2	B0.5:pe (V)?	8.24	+0.30	− .72	−0.98	−3.6:	0.58	10.10:
8.....	163667	17 52.2	−31 47	326.64	−5.27	60.16	.027	17.7	77.9	B0.5 III	8.76	+0.42	− .53	−0.90	−4.4	0.70	11.06
9.....	164019	17 54.0	−28 36	329.60	−4.02	60.15	.049	176.8	57.0	B0 Ia	9.31	+0.26	− .71	−0.94	−7.0	0.56	14.63
10.....	316204	17 39.0	−28 22	328.11	−1.07	58.44	.087	168.0	46.4	B2 III	9.29	+0.32	− .52	−0.80	−4.1	0.56	11.71
11.....	316232	17 39.4	−29 11	327.46	−1.58	58.50	.110	4.0	62.5	O9 IV	10.30	+0.68	− .37	−0.98	−4.8	0.99	13.13
12.....	316274	17 42.0	−27 43	329.02	−1.30	58.76	.040	3.7	62.5	B2 II	10.41	+0.72	− .14	−0.76	−5.0	0.96	12.53
13.....	316311	17 41.2	−28 55	327.90	−1.77	58.70	.059	172.4	51.1	B1 I*b*	10.24	+0.92	− .14	−0.95	−6.0	1.18	12.70
14.....	316325	17 42.0	−29 18	327.65	−2.12	58.81	.069	2.6	61.4	B1 IV	10.60	+0.62	− .29	−0.85	−3.8	0.88	11.76
15.....	316326	17 41.7	−29 17	327.64	−2.06	58.77	.066	5.5	64.3	B1 II	10.08	+0.62	− .32	−0.87	−5.1	0.88	12.54
16.....	316332	17 41.1	−29 36	327.29	−2.11	58.71	.040	16.0	74.7	B3 Ia	9.47	+1.38	+ .31	−0.91	−7.0	1.58	11.73
17.....	316341	17 42.2	−29 56	327.14	−2.48	58.85	.049	179.6	58.4	B0.5 V (pe)?	9.74	+0.42	− .50	−0.87	−3.6	0.70	11.24
18.....	316393	17 44.0	−28 28	328.60	−2.06	59.02	.048	0.4	59.4	B3 II–III	10.71	+0.39	− .38	−0.73	−4.1	0.59	13.04
19.....	316406	17 45.4	−28 46	328.50	−2.49	59.18	.055	0.0	59.2	B2 IV	10.51	+0.26	− .46	−0.70	−3.3	0.50	12.31
20.....	316409	17 45.1	−28 54	328.35	−2.49	59.15	.062	178.6	57.8	B1 V	10.56	+0.46	− .30	−0.71	−3.2	0.72	11.60
21.....	316436	17 44.8	−30 08	327.26	−3.07	59.16	.046	7.0	66.2	B3:pe (III–V)?	10.22	+0.59	− .18	−0.71	−2.8:	0.79	10.65:
22.....	316464	17 44.8	−30 37	326.86	−3.31	59.19	.057	163.6	42.8	B1 V (e)?	10.59	+0.50	− .44	−0.88	−3.2	0.76	11.51
23.....	316520	17 45.7	−28 45	328.55	−2.53	59.22	.051	0.9	60.1	B5:nn(e) (III–V)?	10.79	+0.33	− .28	−0.58	−2.2:	0.49	11.52:
24.....	316568	17 48.3	−29 43	328.00	−3.51	59.56	.033	11.6	71.2	B2pe (IV–V)	9.76	+0.25	− .62	−0.84	−3.0:	0.49	11.29:
25.....	316569	17 48.1	−29 47	327.92	−3.51	59.54	.027	11.5	71.0	B3 II	9.37	+0.30	− .49	−0.75	−4.5	0.50	12.37
26.....	316587	17 45.8	−29 55	327.55	−3.15	59.28	.011	155.4	34.7	B1:n(e) (V)	10.58	+0.33	− .49	−0.78	−3.2:	0.59	12.01:
27.....	316589	17 45.9	−30 02	327.40	−3.23	59.29	.026	19.0	78.3	B2nn(e) (III–V)	10.57	+0.31	− .48	−0.75	−3.3:	0.55	12.22:
28.....	316729	17 51.0	−29 34	328.48	−3.94	59.86	.031	16.4	76.3	B1n II:	9.94	+0.33	− .59	−0.88	−5.1	0.59	13.27
29.....	316786	17 53.0	−27 15	330.66	−3.15	59.97	.037	177.5	57.5	B5 IV	11.01	+0.31	− .22	−0.49	−2.2	0.47	11.80
30.....	.....	17 41.5	−29 30	327.43	−2.13	58.76	.065	24.8	83.6	B1 I*b*–II	10.87	+0.89	− .11	−0.90	−5.6	1.17	12.96
32.....	−29°13809	17 31.7	−29 03	326.68	−0.05	57.56	.098	157.5	35.1	O9 V	9.74	+0.68	− .34	−0.94	−4.2	0.99	10.97
33.....	.....	17 36.9	−28 37	327.56	−0.81	58.19	.131	178.4	56.6	B1nn (II–III)	10.56	+0.81	− .20	−0.92	−4.7:	1.07	12.05:
34.....	.....	17 38.8	−29 53	326.80	−1.83	58.44	.105	157.5	34.9	B0.5 I*b*	10.75	+1.10	+ .02	−0.96	−6.0	1.38	12.91
35.....	.....	17 41.2	−29 23	327.50	−2.01	58.72	.072	12.8	71.5	B0n III?	11.06	+0.70	− .34	−0.96	−4.5:	1.00	12.56:
36.....	.....	17 45.2	−29 54	327.51	−3.02	59.21	.054	11.3	70.5	B8 IV?	11.60	+0.41	− .02	−0.38	−1.7::	0.50	11.80:
37.....	.....	17 44.0	−30 08	327.17	−2.92	59.08	.034	169.1	48.2	B3 IV	11.31	+0.56	− .13	−0.63	−2.8	0.76	11.83
38.....	.....	17 45.6	−28 07	329.08	−2.10	59.18	.102	18.8	78.0	B1 I*b*–II	11.07	+0.77	− .23	−0.91	−5.6	1.03	13.58
.....	−33°12155	17 25.7	−33 16	322.45	−1.29	56.84	.054	179.7	56.5	B0 III	9.09	+0.79	− .28	−0.97	−4.5	1.09	10.32
.....	−33°12242	17 29.6	−33 49	322.42	−2.26	57.38	.118	51.7	109.1	B1 Ia	9.36	+1.16	+ .03	−0.98	−7.0	1.42	12.10
.....	160529*	17 35.3	−33 27	323.37	−3.07	58.13	0.150	19.9	78.0	A2 Ia+	6.67	+1.28	+0.35	−0.75	−8.4:	1.22	11.41:

* The following HD stars are noted:

HD 161103: The magnitudes are discordant. Probably variable. 1953, May 22.314, $V = 8.61$; June 5.292, $V = 8.51$; June 14.264, $V = 8.95$. The spectrum shows *Fe* II emission.
HD 163453: *Fe* II emission.
HD 163454: *Fe* II emission.
HD 160529: The spectrum indicates a luminosity considerably higher than α Cyg (A2 Ia) and probably at least as bright as 6 Cas (A3 Ia+), $V = -8.4$.

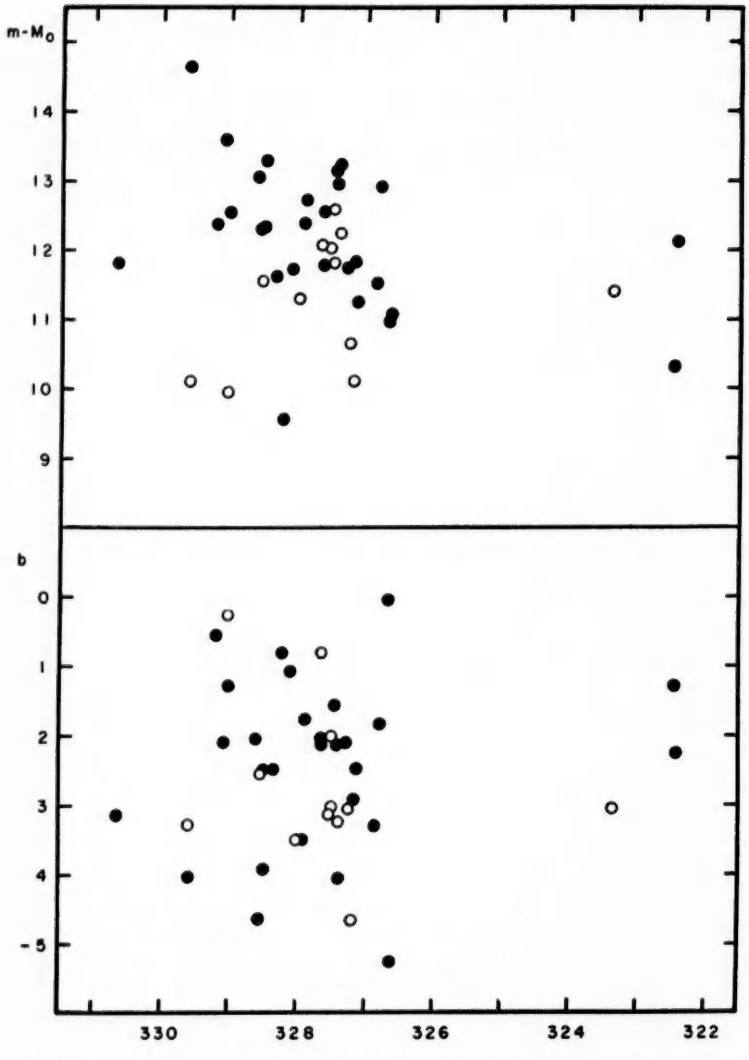

FIG. 1.—Distribution of stars in the direction of the galactic center. The lower portion represents the stars in galactic co-ordinates. In the upper portion the distance moduli are plotted with the galactic longitudes. Open circles represent stars for which the distance moduli are in doubt.

tion that these stars are associated with the arm at 10.7) and HD 160529 because of uncertainty in the absolute magnitude and all the stars with doubtful distance moduli, the mean distance modulus for the group is 12.4 or 3.0 kiloparsecs. The space-distribution diagram of early-type aggregates observed by Morgan, Whitford, and Code (1953) is shown in Figure 2, with the present group inserted in the diagram. Also the distance of the galactic center has been shifted from 9.0 to 8.3 kiloparsecs. The position of the present stars suggests that they are associated with a second inner spiral arm at a distance of 3.0 kiloparsecs.

Several stars are of special interest because of their apparent great distance, especially HD 164019, a B0 I*a* star with a distance modulus of 14.6. This star, as well as the others with distance moduli greater than 13.0 and outside the obscured area, has an absorption

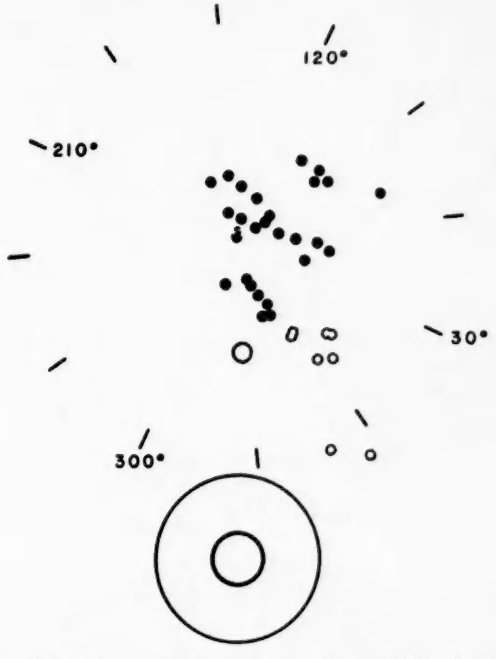

FIG. 2.—Space distribution of aggregates according to Morgan, Whitford, and Code (1953). The large open circle represents the stars discussed in the present paper. A distance to the galactic center of 8.3 kiloparsecs has been adopted.

of less than 2 mag., not significantly different from those with distance moduli less than 11.5 and also outside the obscured area. It follows that either the distances are not significantly different or that the absorption beyond a distance modulus of, say, 12.0 is small, or both. The former may be entirely correct, as assumed above in computing the mean distance. However, an error of five times the probable error in the distance modulus must be ascribed to that of HD 164019, in order to place it at the mean distance of the group. Baade (1950) also found that this region is remarkably clear. He obtained a photographic absorption of 2.8 mag. at a distance of $m - M_0 = 14.7$, corresponding to a distance of 8.7 kiloparsecs. A further search for early-type stars in this region should

either confirm or reject the presence of an early-type supergiant in or near the nuclear lens of the Galaxy.

INTERSTELLAR POLARIZATION

The polarization measurements are shown graphically in Figure 3. A direct photograph of the same area taken with a 5-inch Ross lens is reproduced in Figure 4. It is immediately obvious that all the stars with large polarization are situated in the obscured area, where the absorption is appreciably greater. This is borne out, in part, by the correlation of polarization and absorption as seen in Figure 5, where it is apparent that, in general, the polarization increases with absorption. This figure shows further that an absorption of about 1 mag. is not contributing effectively to the polarization. One star, HDE 316332, has an unusually large absorption, 4.7 mag., and small polarization, 0.040 mag. The absorption is over 1 mag. greater than the neighboring stars, although its polarization is similar. The correlation of the polarization with the obscuring cloud leaves little doubt that this obscuring cloud is a large contributor to the observed polarization.

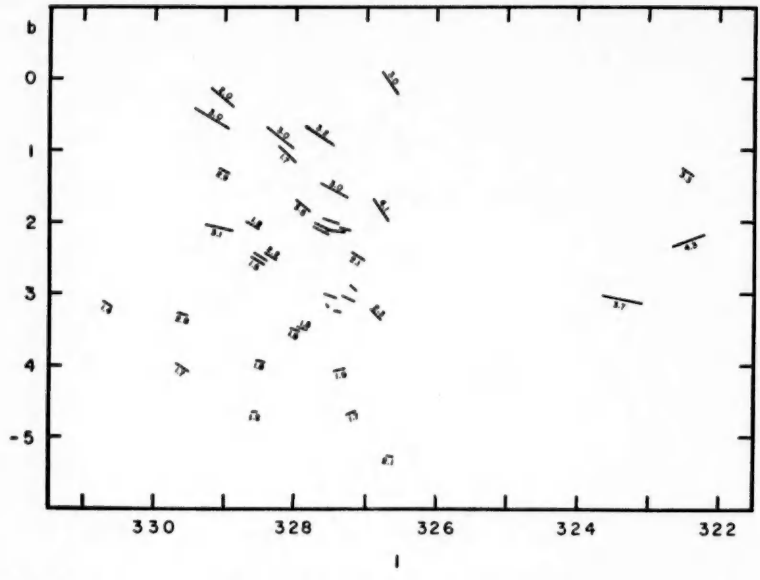

FIG. 3.—The polarization of stars in the direction of the galactic center. Each line represents a star. The length of a line is a relative measure of the interstellar polarization, and the direction of the line corresponds to the plane of vibration. The numbers beside the lines give the visual absorption.

Note that, as in the case of the absorption, the polarizations of the stars with observed distance moduli greater than 13.0 in the less obscured area are similar to those with observed distance moduli less than 11.5. Because of the absence of sufficient material on near-by stars, the distance of the polarizing and obscuring cloud remains in doubt. Polarization data on a few brighter stars tentatively place it in the first inner arm at 1.4 kiloparsecs.

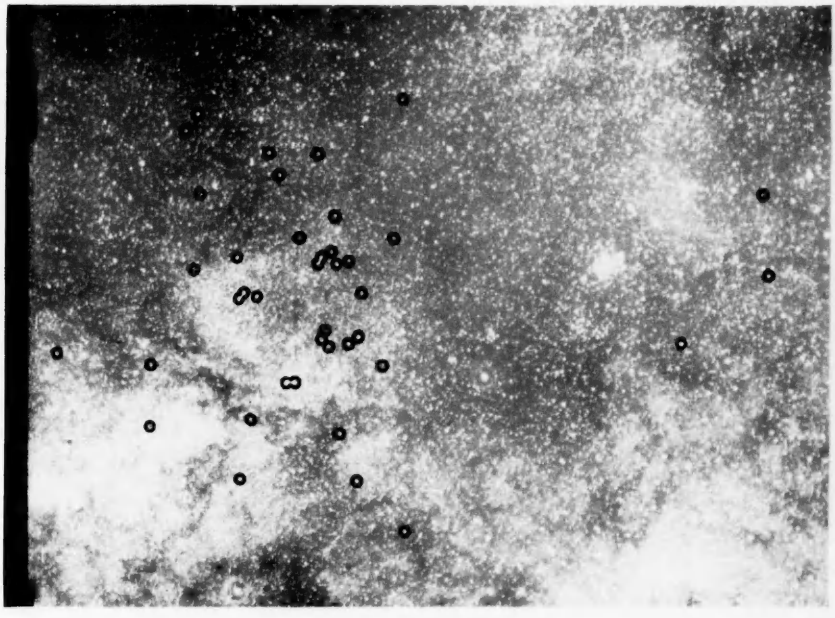

FIG. 4.—Positive reproduction of a Ross 5-inch plate taken at the McDonald Observatory by Mr. Thomas Gehrels. The stars in Table 1 are represented by black open circles. Galactic longitude increases toward the left, and latitude increases upward.

It is a pleasure to thank the Señoritas González for providing the author with the list of stars in advance of publication and for identification charts for the fainter stars; Dr. Morgan for kindly classifying the spectrograms; and the National Science Foundation for financial support.

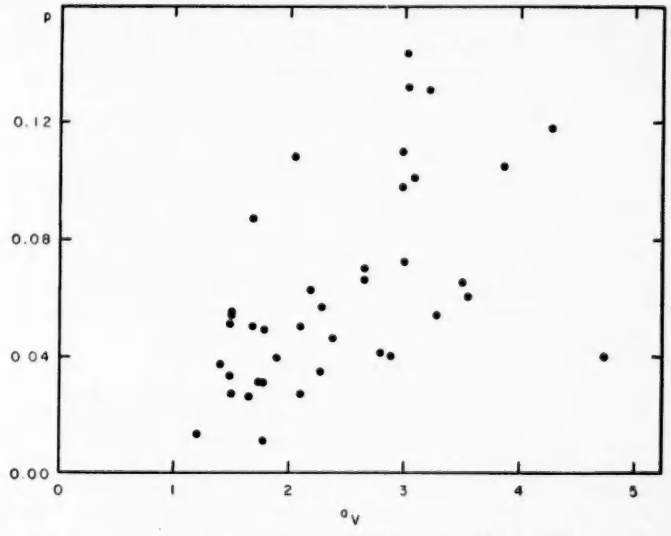

FIG. 5.—Polarization versus visual absorption in the direction of the galactic center

REFERENCES

Baade, W. A. 1950, *Pub. Obs. U. Michigan*, **10**, 7–17.
Hiltner, W. A. 1951, *Ap. J.*, **114**, 241–271.
Johnson, H. L., and Morgan, W. W. 1953, *Ap. J.*, **117**, 313–352.
Morgan, W. W.; González, G.; and González, G. 1953, *Ap. J.*, **118**, 345–346.
Morgan, W. W.; Harris, D. L.; and Johnson, H. L. 1953, *Ap. J.*, **118**, 92–105.
Morgan, W. W.; Whitford, A. E.; and Code, A. D. 1953, *Ap. J.*, **118**, 318–322.

PHOTOELECTRIC SPECTROPHOTOMETRY OF PLANETARY NEBULAE

WILLIAM LILLER AND LAWRENCE H. ALLER
The Observatory, University of Michigan, Ann Arbor, Michigan
Received January 22, 1954

ABSTRACT

Photoelectric spectrophotometric measures of the N_1, N_2, and $H\beta$ line intensities in twelve bright planetary nebulae have been made with the aid of the 10° objective prism on the Curtis Schmidt telescope. The absolute surface brightnesses are in good accord with results obtained by the filter photoelectric method. The mean N_1/N_2 intensity ratio is 3.03, while the $(N_1 + N_2)/H\beta$ intensity ratios are in excellent agreement with those found previously by MacRae and Stock and substantiate the photographic photometric measures made some years ago by one of us. The electron densities range from 10^3 to about 2×10^4 electrons/cm^3; they are of the same order of magnitude as those found some years ago by Menzel and one of us. The electron temperatures fall between 8000° and 20,000° K and show no strong correlation with the Zanstra temperature of the central star. This lack of correlation is in accordance with recent theoretical expectations.

I. INTRODUCTION

In the last thirty years the relative intensities of the principal monochromatic radiations of the planetary nebulae have been measured by a number of investigators. Measures or estimates of line intensities have been published by H. H. Plaskett (1929), Louis Berman (1930), Bowen and Wyse (1939; Wyse, 1942), R. Minkowski (1942), M. L. White (1952), and others, including one of the present writers (Aller 1941, 1951). Berman and one of us employed the slitless spectrographs on the Crossley reflector at the Lick Observatory and have given the relative total brightnesses of the monochromatic images. Others, using slit spectrographs, measured the relative intensities referred to some fixed point in the nebula or averaged in some rough fashion over the entire nebula.

These data, combined with estimates of the distances and surface brightnesses of the planetaries, have been utilized in conjunction with theories of physical processes to evaluate the densities, temperatures, and chemical compositions of the nebulae. With the Hebb and Menzel target areas for the collisional excitation of the metastable levels in O III, these observations gave electron temperatures in the neighborhood of 8000–10,000° K (Menzel *et al.* 1941). The electron densities appeared to lie in the neighborhood of 10^3–10^4 electrons/cm^3.

More recently Henri Andrillat (1950, 1952) has published, for a number of planetaries, electron temperatures that are in sharp disagreement with those found by others. He has not published the observational data used in his calculations of electron temperatures with the aid of the Hebb and Menzel target areas. His results require intensity ratios of the green nebular lines to 4363 markedly different from those previously obtained. The ratio of the green nebular line intensity to that of λ 4363, $I(N_1 + N_2)/I(\lambda\,4363)$, can be measured most conveniently by comparing 4363 with $H\gamma$ and $N_1 + N_2$ with $H\beta$. The $I(4363)/I(H\gamma)$ ratio can be measured reasonably well by photographic photometry; the $I(N_1 + N_2)/I(H\beta)$ ratio is much more difficult to establish, because the green nebular lines are often ten to twenty times as strong as $H\beta$ and fall in a spectral region where the sensitivity of the photographic emulsion changes rapidly with wave length.

Hence a check on the photographic spectrophotometry is very much to be desired. The photoelectric cell can reach the stronger lines easily, but the photometry of the fainter lines would be much more difficult. At least for the present, the spectrophotometry of the fainter lines would appear to require the use of the photographic plate. According-

ly, we decided to measure the intensity ratios of λ 5007(N_1), λ 4959(N_2), and $H\beta$ in as many nebulae as could be reached with our equipment in the late-summer observing season. Section II of this paper describes the observational procedures employed; Section III gives the methods of reduction, the results, and the comparison with those of other observers; Section IV treats of the intensity ratio of the green nebular lines; while in Section V we discuss the electron densities and temperatures obtained for the planetary nebulae. Photoelectric measures of the $I(N_1+N_2)/I(H\beta)$ ratio have been made previously by Donald MacRae and Jurgens Stock (1954). Their results are in excellent agreement with our own, as will be seen in Section III of this paper.

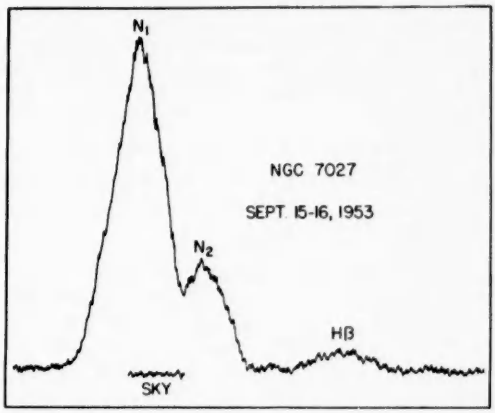

FIG. 1.—Photoelectric tracing of the spectrum of a planetary nebula. NGC 7027 represents a typical high-excitation object.

II. THE OBSERVATIONAL PROCEDURE

The 4° and 6° objective prisms of the Curtis Schmidt telescope, when used in their 10° combination, give a dispersion of 160 A/mm at $H\beta$. Because of the relatively short focal length of the telescope, the pair of [O III] images in the green will be completely separated only for planetaries with diameters less than 29″; the oxygen image at λ 4959 will overlap $H\beta$ only if the nebula is more than 62″ in diameter. Thus it is possible to measure photoelectrically the integrated intensities of the N_1, N_2, and $H\beta$ images of the majority of planetary nebulae with this equipment.

On the nights of September 13, 14, 15, and 16, 1953, we observed a total of thirteen planetaries by two different methods. The first consisted of securing spectral traces of all the nebulae by orienting the dispersion in the east-west direction and by driving the telescope in hour angle at a speed slightly different from the sidereal rate. Then the monochromatic nebular images slowly passed over a slit 0.17 mm wide, corresponding to 27 A at $H\beta$. Frequency-control equipment, designed by staff members of the McMath-Hulbert Observatory primarily for the widening of photographic spectra, provided the telescope motion in hour angle. This method is similar to that employed by MacRae and Stock (1954).

In addition, we measured the spectra of all but two of the planetary nebulae by taking individual deflections of the monochromatic nebular images and of the nebular and central star continua to the violet of $H\beta$ and to the red of the λ 5007 image of [O III]. Because the faintness of the nebulae often made it difficult to center the images accurately

in the diaphragm, we made no attempt to measure the N_1 and N_2 images separately in this fashion. The electronic equipment used in this investigation is identical with that described in a separate paper by one of us (Liller 1954). It was necessary to alter the optical design of the photometer, however, to accommodate the $f/3.5$ beam of the Curtis Schmidt.

Tracings of the spectra of α Lyrae and α Cygni secured at different zenith distances enable the determination of the atmospheric extinction and of the spectral response of the photometer plus the optical system of the telescope. In these reductions we have adopted the energy distributions published by R. C. Williams (1939) and by D. Barbier and D. Chalonge (1940).

Reproduced in Figure 1 is the spectral trace of the high-excitation planetary, NGC 7027. It is a rather small object; hence the separation of the N_1 and N_2 images is clear. The Ring Nebula in Lyra, NGC 6720, was the only nebula for which the diameter (70″) was too large to permit the measurement of the relative intensities of the green [*O* III] pair.

III. THE REDUCTION OF THE OBSERVATIONS

To convert the raw deflections of the N_1, N_2, and $H\beta$ lines into relative intensities, we took into account the effects of the spectral response of the photometer, the atmospheric

TABLE 1

OBSERVED DATA ON PLANETARY NEBULAE

Nebula (1)	α(1950) (2)	δ(1950) (3)	$I(N_1+N_2)/I(H\beta)$ (4)	n (5)	$I(N_1)/I(N_2)$ (6)	A'' (7)	log (S_1+S_2) (8)
NGC 6210	16^h42^m5	+23°9	15.1	2	2.95	4″	+0.55
NGC 6543	17 58.6	+66.6	8.86	2	3.04	10	− .05
NGC 6572	18 09.6	+ 6.8	15.6	2	3.11	7	+ .38
NGC 6803	19 29	+10.0	.....	.....	.....	2.5	− .16
NGC 6818	19 40.0	−14.3	11.6	1	3.00	9	− .35
NGC 6826	19 43.4	+50.4	9.32	3	3.18	13	− .57
NGC 7009	21 01.4	−11.6	16.1	3	2.72	9	+ .22
NGC 7027	21 05.2	+42.0	20.2	4	3.00	5	+ .36
NGC 7662	23 23.5	+42.3	18.2	4	3.02	8	+ .15
NGC 1535	4 11.7	−12.9	15.4	4	3.00	9	− .45
IC 2149	5 43.5	+46.1	5.4	3	2.90	6	− .68
IC 418	5 25.2	−12.7	1.78	2	3.40	6	−0.18

extinction, and the contribution made to the deflections by the continuous spectra of the nebulae and the central stars. As mentioned above, the first two corrections are easily derived from the tracings of Vega and Deneb. The intensity of the stellar and nebular continua required separate measures when the diaphragms were used. This background continuum can be measured directly from the slit tracings.

The diaphragm deflections and slit tracings gave $I(N_1+N_2)/I(H\beta)$ ratios that were in good agreement. We regarded the slit tracings as more reliable than the diaphragm deflections and assigned them greater weight. The final mean values are listed in column 4 of Table 1, and column 5 lists the number of observations secured on each object. The average probable error of a single result is ± 2.3 per cent. The $H\beta$ image of NGC 6803 was too faint to measure; about all that can be said is that it is several times fainter than N_2.

In Figure 2 we compare the values of $I(N_1+N_2)/I(H\beta)$ derived in this investigation with the values of this ratio found photoelectrically by MacRae and Stock (1954) (*circles*) and photographically by one of the present writers (Aller 1941, 1951) (*crosses*).

The two photoelectric investigations are in close agreement, reflecting the accuracy of the photoelectric measures. Also in good agreement, but showing a somewhat larger scatter, are the photographic results. There does not appear to be any systematic error in the latter results, only the random scatter that would naturally arise from the uncertainties in photographic photometry. If we assume that the photoelectric values are the true ones, we find that the mean error of a single photographic result is ± 18 per cent. NGC 1535 and 6818 show the largest errors. Both photographic determinations were based on one observation, and if these two nebulae are omitted, the mean error of a single photographic result drops to ± 12 per cent.

From the slit tracings we also determined the quantity $I(N_1)/I(N_2)$. For no planetary were the N_1 and N_2 lines completely separated, and it was necessary to construct "profiles" of at least one of the two lines, since it could not be safely assumed that the nebulae were spherically symmetric. Each profile was constructed by assuming the N_1 and N_2 images to be identical in shape and intensity distribution and by making the redward wing of the N_2 line geometrically similar to the redward wing of the N_1 line.

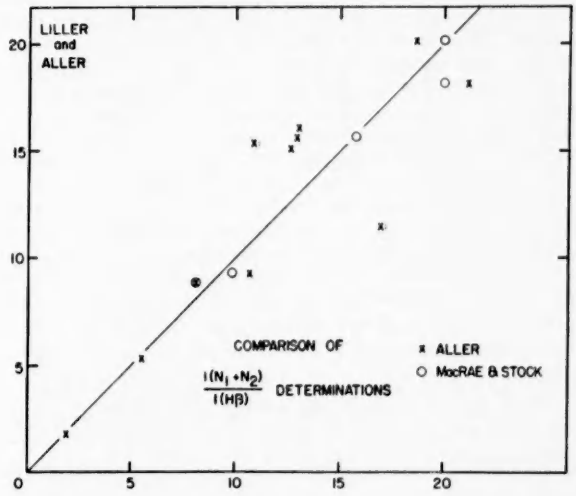

FIG. 2.—A comparison of the values of $I(N_1 + N_2)/I(H\beta)$ found by several observers. The open circles show the photoelectric results of MacRae and Stock; the crosses indicate the photographic determinations of one of us. Colons following two of the crosses mean that the photographic value is based on a single observation.

A subtraction of the area underneath the N_2 profile from the total area underneath the $N_1 + N_2$ tracing then gave the size of the N_1 deflection. As a further check, the spectra of a number of the nebulae were measured by constructing profiles in the above manner for both the [*O* III] lines.

The $I(N_1)/I(N_2)$ ratios are listed in column 6 of Table 1. NGC 1535 was observed twice; the spectra of the remaining planetaries were traced only once with a slit. As a result, it is difficult to tell whether the variation in this ratio from nebula to nebula is real or whether it is due to observational error. The largest source of error seems to arise from the uncertainty in drawing in the background continuum, and we are inclined to believe that the fluctuations are due to these errors.

Finally, by comparing the nebular tracings with the spectral tracings of Vega and Deneb, we can derive monochromatic surface brightnesses for the nebulae. Ambarzumian (1933) has described a method of deriving these surface brightnesses by comparing the intensities of the nebulae with the spectrum of a solar-type star. Therefore, we should like to find the relative intensities of the sun and Vega at the wave lengths of the green nebular lines. If we take the photovisual magnitude of Vega to be +0.03, as given by Johnson and Morgan (1953) and that of the sun to be −26.87, the mean of the values published by Kuiper (1938) and by De Vaucouleurs (1949), then the difference in the photovisual magnitudes (26.90) should correspond closely to the ratio of intensities of the two objects at the effective wave length of the International Photovisual System. The mean of the effective wave lengths is 5433 A, according to Seares and Joyner (1943). If we assume that both Vega and the sun radiate as black bodies over the limited wave-length range from 4860 to 5440, we should be able to calculate the ratio of intensities at the mean wave length of the N_1 and N_2 lines, λ 4995. Here we took the color temperatures of the two objects in this wave-length region to be 16,500° and 5700°. The resulting difference in magnitude at λ 4995 is 26.70, which is equivalent to an intensity ratio of 4.79×10^{10}. Hence we are able to calculate what the deflection would be from 1 A of the solar spectrum at the mean wave length of the green forbidden oxygen lines.

In calculating the mean surface brightnesses, we treated each nebula as an evenly illuminated disk of radius A. The values of the radii are those given by Curtis (1918) and are listed in column 7 of Table 1. The last column of this table lists the resulting surface fluxes of the planetary nebulae in the light of the green [*O* III] radiations. The units are the logarithms of the *fluxes* expressed in ergs/cm²/sec. Because of the uncertainties arising from the use of the effective wave lengths of the International Photovisual System, these values should not be expected to be of as high precision as those given elsewhere by one of us. However, these results give us an excellent independent check of the surface brightnesses derived photoelectrically with the use of narrow-band interference filters. The two sets of determinations have already been compared in the other paper, and we feel that the surface fluxes derived here should be given half the weight of the other values.

IV. THE INTENSITY RATIO OF THE GREEN NEBULAR LINES

The smaller planetaries should give the best determination of the N_1/N_2 ratio, but we have found no dependence of the value upon the size of the nebula. The mean ratio from 12 planetaries is 3.03 ± 0.11 (mean error). The chief error seems to arise from the uncertainty in drawing the background continuum.

Half a century ago, Wilsing and Scheiner (1902) found this ratio to be 2.5; many years later, H. H. Plaskett published a ratio of 2.73 (1929), while L. Berman found 2.63 (1930). Minkowski found a ratio of 2.99 ± 0.15 for the Orion nebula (1934).

Theoretical calculations of the $I(^1D_2-{}^3P_2)/I(^1D_2-{}^3P_1)$ ratio by Pasternack (1940) and independently by Shortley and his associates (1941) were based on the theory of intermediate coupling. They yielded an intensity ratio of 2.83. This theory, which assumes that the perturbation from the LS-coupling situation arises from the interaction of an electron's spin with its own orbit, gives results that contradict the observed intensity ratios in the $^4S-{}^2D$ transition of [*O* II]. The discrepancy was removed by later investigators, who took into account the effects of (spin)−(spin) interactions and of (spin of one electron)−(orbit of another) interactions (Aller *et al.* 1949). R. H. Garstang (1951) has applied this improved theory to the calculation of the energy levels and transition probabilities in the p^2 and p^4 configurations of *C* I, *N* II, *O* III, *F* IV, and *Ne* V and of *O* I, *F* II, and *Ne* III, respectively. He predicts an intensity ratio of 2.93. Thus our observational data favor Garstang's result, but the scatter is still comparable with the differences between the two theoretical predictions.

V. THE ELECTRON DENSITIES AND TEMPERATURES IN THE PLANETARY NEBULAE

Let S_{Bac} denote the flux in ergs/cm²/sec radiated by the nebula in a 20 A interval of the Balmer continuum near its limit (3630–3650 A). If the nebula can be approximated as a shell of thickness d and outer radius A, we define

$$D \equiv 3d\left[1 - \frac{d}{A} + \frac{d^2}{3A^2}\right]. \tag{1}$$

Further, if $N_i = N_e$, the electron density may be calculated from (Menzel and Aller 1941)

$$N_e = 1.68 \times 10^{10} S_{Bac}^{1/2} D^{-1/2} T_e^{3/4}. \tag{2}$$

If observations of S_{Bac} are not available or are not of sufficient accuracy, an estimate of N_e may be found from $H\beta$. The flux in $H\beta$ in ergs/cm²/sec is related to the electron density by

$$S_\beta = 7.37 \times 10^{-20} \frac{N_i N_e}{T_e^{3/2}} b_4(T_e)\, D e^{X_n}. \tag{3}$$

Here $b_4(T_e)$ is a factor that measures the departures of the population in the fourth level from the value appropriate to thermodynamic equilibrium at the temperature T_e (Menzel 1937, eq. [4]). Extensive measures of the Balmer lines in a large number of planetaries (Aller 1951) indicate that when corrections are made for the effects of interstellar absorption, Menzel and Baker's "model B" (1938) fits the observed Balmer decrement. In this model the central star radiates no energy in the Lyman lines, and each ultraviolet Lyman quantum absorbed in the nebula is ultimately degraded into a quantum of Lyman-α. The agreement between theory and observation justifies our use of the theoretical b_n's given by Menzel and Baker.

The electron temperature may be computed from the relative intensities of the 4363 and green nebular lines of [*O* III], provided that the target areas for collisional excitation are known. Earlier determinations of the electron temperature were based on Hebb and Menzel's calculations (1940). More recently, M. J. Seaton (1953) has calculated target areas for O^{++} and other ions by an improved theory. Using his results, we may derive rather easily the electron temperature in terms of the observed ratio of $I(N_1 + N_2)/I(4363)$.

The intensity ratio $I(\lambda\,4363)/I(N_1 + N_2)$ is related to the populations of the $^1S_0$ and $^1D_2$ levels by

$$\frac{I\,(4363)}{I\,(N_1 + N_2)} = \frac{N\,(^1S_0)\,A\,(^1S, {}^1D)\,h\nu\,(^1S, {}^1D)}{N\,(^1D_2)\,A\,(^1D, {}^3P)\,h\nu\,(^1D, {}^3P)}, \tag{4}$$

where A denotes the Einstein coefficient of spontaneous emission and ν the frequency.

The ratio $N(^1S_0)/N(^1D_2)$ depends on the electron density and temperature, the target-area parameters, Ω_{PS}, Ω_{PD}, and Ω_{DS}, and the Einstein A coefficients. Menzel, Aller, and Hebb (1941) give the necessary relationship as equation (9) of their paper. It is necessary to correct the last term in the denominator of their equation for a typographical error by replacing A_{PD} by Ω_{PD}, however. If we use

$$\Omega_{PS} = 0.195, \qquad \Omega_{PD} = 1.73, \qquad \Omega_{DS} = 0.61 \text{ (Seaton 1953)},$$

$$\left.\begin{aligned} A(^1S, {}^1D) &= 1.6 \qquad A(^1D, {}^3P_2) = 0.021 \\ A(^1S, {}^3P) &= 0.23 \qquad A(^1D, {}^3P_1) = 0.0071 \end{aligned}\right\} \text{(Garstang 1951)},$$

we obtain the following expression:

$$\frac{I(4363)}{I(N_1+N_2)} = 13.1\left\{\frac{1.012+2300\sqrt{T_e}/N_e}{1.01+2.70\times10^5\sqrt{T_e}/N_e}\right\}10^{-14,300/T_e} \sim 0.113\times10^{-14,300/T_e} \quad (5)$$

for such low densities as prevail in planetary nebulae.

The basic data needed for the calculations of the electron densities and temperatures are given in Table 2. For each nebula are given the average angular radius, A'', and the relative thickness of the shell, d/A, according to the data of Curtis (1918), the distance in parsecs from the work of Berman (1937), the quantity D, the logarithm of the mean flux in ergs/cm²/sec for the green nebular lines corresponding to the assumed angular size of the nebula, and in column 7 the ratio of the intensities of the green nebular lines and $H\beta$. All the data of column 6 are obtained from the photoelectric work, but for those nebulae not included in Table 1 we have used the photographic determinations of

TABLE 2*

BASIC DATA ON PLANETARY NEBULAE

Nebula (1)	A'' (2)	d/A (3)	r (Parsecs) (4)	$D\times10^{-11}$ (5)	log (S_1+S_2) (6)	log $[I(N_1+N_2)/I(H\beta)]$ (7)	log (S_{Bac}/S_β) (8)	$I(4363)$ $[H\beta=10]$ (9)	T_e (° K) (10)
NGC 1535	9″	0.3:	1720	1.52	−0.45	1.19	−0.80 (1) −0.72 (2)	1.75	14,300
IC 2149	6	1.0	2250	2.02	−0.68	0.74	−1.04 (3)	0.60 (2)	14,200
IC 418	6	0.2	1800	0.79	−0.18	0.25	−1.14 (1) −0.82 (4)	0.33	18,300
NGC 2392	23	0.2	860	1.44	−1.31	1.16	−1.62: (3)	3.0	19,600
NGC 3242	10	0.2	1640	1.20	+0.10	1.29	−1.10 (2)	2.1 (3)	17,700
IC 4593	5	1.0	2000	1.50	−0.44	0.88	−1.14 (2)	0.12 (5)	7,700
NGC 6210	4	1.0	1720	1.03	+0.56	1.18	−0.75 (4)	0.8 (5)	10,800
NGC 6543	10	0.2	1080	0.79	0.00	0.95	−1.07 (1)	0.32 (5)	9,500
NGC 6572	7	1.0	1230	1.29	+0.34	1.19	−1.17 (1)	1.5	13,500
NGC 6803	2.5	1.0	2640	0.98	−0.16	1.16	−0.6: (2)	1.07 (2)	12,800
NGC 6818	9	0.3	2380	2.10	−0.35	1.06	−1.00 (2)	1.6	15,700
NGC 6826	13	1.0	1050	2.04	−0.55	0.97	−1.12 (1)	0.55 (5)	11,200
NGC 7009	9	0.3	930	0.82	+0.15	1.21	−1.06 (1)	1.35	13,900
NGC 7027	5	1.0	2130	1.59	+0.40	1.30	−1.57 (1)	3.15	16,800
NGC 7662	8	0.2	1200	0.70	+0.08	1.26	−1.21 (1)	2.25	15,000

* The numbers in parentheses in cols. 8 and 9 refer to the source of the numerical data as follows:

1. D. H. Menzel and L. H. Aller, *Ap. J.*, **93,** 195, 1941.
2. L. H. Aller, *Ap. J.*, **113,** 125, 1951.
3. Heretofore unpublished values obtained at the Lick Observatory, 1943–1945, by one of us.
4. Slit-spectra observations obtained at the McDonald Observatory in 1945 by one of us.
5. L. H. Aller, *Ap. J.*, **118,** 547, 1953.

The $I(4363)$ values that are not followed by a number in parentheses were adopted from all data available to us, including isophotic contour measures of 4363 and 4340 on Mount Wilson data, and Minkowski and Aller's spectrophotometry of selected planetaries (*Ap. J.*, in press).

$I(N_1+N_2)/I(H\beta)$ made by one of us (Aller 1941, 1951). Column 8 gives log (S_{Bac}/S_β), the ratio of the flux in the 20 A interval of the Balmer continuum to the flux in $H\beta$, as determined by photographic photometry. Detailed references are given to the sources of the data. Most of the ratios are based on plates obtained with the quartz slitless spectrograph attached to the Crossley reflector at the Lick Observatory, although slit spectrograms obtained at the McDonald Observatory have also been used. The procedure then was to compare the intensity in the Balmer continuum with near-by Balmer lines whose

relative intensities are assumed to follow Menzel and Baker's model B. Since the position of the underlying continuum cannot be fixed with very great accuracy, either from slit or slitless plates, it is very difficult to determine S_{Bac}. Accordingly, we have estimated N_e both from S_{Bac} and from the photoelectric determinations of S_β. The chief uncertainty in the calculation of N_e then arises from the error in the distance of the planetary. Column 9 gives the intensity of λ 4363 [*O* III], referred to $H\beta$ as 10. These values are taken from slitless spectrograms obtained at the Lick Observatory and from slit spectrograms secured at the McDonald Observatory by one of us. Column 10 gives the value of the electron temperatures as computed with the aid of Seaton's cross-sections.

With the aid of these electron temperatures, S_{Bac}'s, S_β's, and assumed nebular distances, we now compute N_e by equations (2) and (3). The results are given in Table 3.

TABLE 3

CALCULATION OF ELECTRON DENSITIES IN PLANETARY NEBULAE

NEBULA	T_e (° K)	LOG b_4	LOG N_e			*Ap. J.*, **102**, 239, 1945	
			$H\beta$	Bac	Adopted	log N_e	T_e (° K)
(1)	(2)	(3)	(4)	(5)	(6)	(7)	(8)
NGC 1535	14,300	−0.55	3.40	3.55	3.44	3.98	11,600
IC 2149	14,200	−0.56	3.45	3.45	3.45		
IC 418	18,300	−0.43	4.20	4.19	4.20	4.04	9,700
NGC 2392	19,600	−0.40	3.05	2.82	3.04		
NGC 3242	17,700	−0.44	3.72	3.72	3.72	3.60	9,500
IC 4593	7,700	−1.02	3.46	3.33	3.46	3.63	7,000
NGC 6210	10,800	−0.72	3.93	4.05	3.94		
NGC 6543	9,500	−0.82	3.80	3.74	3.80	4.07	6,500
NGC 6572	13,500	−0.58	4.01	3.75	4.01	4.02	9,000
NGC 6803	12,500	−0.62	3.63	3.62	3.62		
NGC 6818	15,700	−0.50	3.46	3.50	3.47	3.50	9,400
NGC 6826	11,200	−0.70	3.35	3.30	3.34	3.65	8,200
NGC 7009	13,900	−0.57	3.81	3.80	3.80	4.31	8,900
NGC 7027	16,800	−0.46	3.69	3.46	3.69	3.77	9,600
NGC 7662	15,000	−0.52	3.81	3.75	3.80	4.12	10,000

Column 2 again gives the electron temperature for each nebula listed in column 1. Column 3 gives the corresponding log b_4. The values of log N_e found from S_β with the aid of equation (3) are given in column 4, while column 5 gives the values of log N_e deduced with the aid of log S_{Bac} by means of equation (2). Since the S_{Bac} values are subject to rather large uncertainties, the finally adopted values of log N_e are based primarily upon the $H\beta$ measurements. For comparison we give for these same nebulae the T_e and log N_e values derived from the older data.

The new electron temperatures are all higher than those previously assigned, partly because of the new cross-sections adopted and partly because no attempt had been made to correct the older observations of $I(4363)/I(N_1 + N_2)$ for space absorption. The new electron densities are of the same order of magnitude as those published in 1945. The effect of the lowering of the adopted surface brightness is compensated for by the increase in T_e.

A comparison of the log N_e values obtained from $H\beta$ and from the Balmer continuum (see Fig. 3) shows no systematic differences between the two sets of results. We conclude that the $H_{Bac}/H\beta$ ratio is in satisfactory agreement with the theory of the Balmer decrement as given by Menzel and Baker. This opinion differs from that of T. L. Page (1942),

who found that the intensity of the Balmer continuum as compared with that of $H\delta$ was less than the value predicted by the theory of a pure recombination spectrum.

In order to compare Andrillat's electron temperatures with our results, we must compute T_e from our data with the aid of the Hebb-Menzel target areas. The results are given in Table 4. If Seaton's cross-sections are used, Andrillat's electron temperatures would be much higher. Since the $I(4363)/I(H\beta)$ ratio can be measured photographically more easily than the $I(N_1 + N_2)/I(H\beta)$ ratio, one suspects that the discrepancy may lie in the latter ratio.

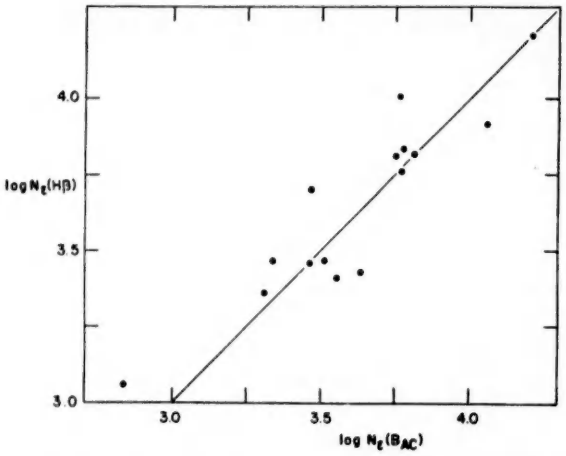

FIG. 3.—A comparison of the logarithms of the electron densities derived from the intensity measurements of $H\beta$ and of a 20 A interval of the Balmer continuum.

TABLE 4

ELECTRON TEMPERATURES DERIVED FROM HEBB AND MENZEL CROSS-SECTIONS

Nebula	T_e (Present Data) (° K)	T_e (Andrillat)	Nebula	T_e (Present Data) (° K)	T_e (Andrillat)
NGC 6543	7,850	9,500	NGC 7009	10,600	15,000
NGC 6572	10,000	15,000	NGC 7027	12,300	21,500
NGC 6803	9,800	16,500	NGC 7662	11,200	25,500

We find no strong correlation between the degree of excitation of the nebula and its electron temperature, although high-excitation nebulae tend, on the average, to have higher electron temperatures than do low-excitation nebulae. For example, IC 418, one of the low-excitation planetaries, almost certainly has a higher electron temperature than does NGC 7009. This result is in accordance with theoretical expectations (Aller 1953).

The mean values of S_β or $S_{N_1+N_2}$ employed in this paper may be replaced by more accurate values when use is made of the isophotic contours of the corresponding monochromatic images of these nebulae. Many years ago Berman derived such contours (1930) for a number of planetaries. Recently, Olin C. Wilson has secured slitless spectrograms

with the 100-inch coudé spectrograph, and R. Minkowski has obtained direct photographs with the 200-inch reflector that permit much more satisfactory isophotic contours to be derived. Many of these plates now are being analyzed with the isophotometer at the University of Michigan. Thus the intensity of a single line can ultimately be given in terms of an isophotic contour diagram, each closed curve of which corresponds to a known intensity expressed in ergs/cm^2/sec/unit solid angle. Finally, the surface brightnesses we have tabulated will also have to be corrected for space absorption. For some nebulae, such corrections may turn out to be large. In NGC 7027, for example, interstellar absorption appears to cut down the surface brightness by a factor of about 10! Estimates of the amount of absorption may be made by comparing the Balmer decrement with the Menzel and Baker (1938) "case B" decrement as has been done by Aller (1951). We defer this calculation to a later paper.

We are indebted to Donald MacRae and Jurgens Stock and to M. J. Seaton for communicating their results to us in advance of publication.

REFERENCES

Aller, L. H. 1941, *Ap. J.*, **93**, 236.
Aller, L. H. 1942, *Sky and Telescope*, August.
Aller, L. H. 1951, *Ap. J.*, **113**, 125.
Aller, L. H. 1953, *Ap. J.*, **118**, 547.
Aller, L. H.; Ufford, C. W.; and Van Vleck, J. H. 1949, *Ap. J.*, **109**, 42.
Ambarzumian, V. A. 1933, *Zs. f. Ap.*, **6**, 107.
Andrillat, Henri. 1950, *C.R.*, **231**, 1432.
Andrillat, Henri. 1952, *C.R.*, **234**, 62.
Baker, J. G., and Menzel, D. H. 1938, *Ap. J.*, **88**, 63.
Barbier, D., and Chalonge, D. 1940, *Ann d'ap.*, Vol. **3**, No. 2.
Berman, Louis. 1929, *Harvard Circ.*, No. 335, p. 7.
Berman, Louis. 1930, *Lick Obs. Bull.*, **15**, 98.
Berman, Louis, 1937, *Lick Obs. Bull.*, **18**, 73.
Bowen, I. S. 1939, *Lick Obs. Bull.*, **19**, 1.
Curtis, H. D. 1918, *Lick Obs. Pub.*, **13**, 55.
Garstang, R. 1951, *M.N.*, **111**, 115.
Hebb, M. H., and Menzel, D. H. 1940, *Ap. J.*, **92**, 408.
Johnson, H. L., and Morgan, W. W. 1953, *Ap. J.*, **117**, 313.
Kuiper, G. P. 1938, *Ap. J.*, **88**, 429.
Liller, William. 1954, *Ap. J.* (in press).
MacRae, D., and Stock, J. 1954, *Nature*, **173**, 589.
Menzel, D. H. 1937, *Ap. J.*, **85**, 332.
Menzel, D. H., and Aller, L. H. 1941, *Ap. J.*, **93**, 197; see especially eq. (10), which should be corrected for the error in K, whose numerical value is equal to 3.26×10^{-6}.
Menzel, D. H.; Aller, L. H.; and Hebb, M. H. 1941, *Ap. J.*, **93**, 240.
Minkowski, R. 1930, *Lick Obs. Bull.*, **15**, 98.
Minkowski, R. 1934, *Zs. f. Ap.*, **9**, 202.
Minkowski, R. 1942, *Ap. J.*, **95**, 243.
Page, T. L. 1942, *Ap. J.*, **96**, 78.
Pasternack, S. 1940, *Ap. J.*, **92**, 129.
Plaskett, H. H. 1929, *Harvard Circ.*, No. 335, p. 7.
Seares, Frederick, and Joyner, Mary. 1943, *Ap. J.*, **98**, 312.
Seaton, M. J. 1953, *Proc. R. Soc. London*, *A*, **218**, 400.
Shortley, G. H.; Aller, L. H.; Baker, J. G.; and Menzel, D. H. 1941, *Ap. J.*, **93**, 176.
Vaucouleurs, G. de. 1949, *Ann. d'ap.*, **12**, 287.
White, M. L. 1952, *Ap. J.*, **115**, 71.
Williams, R. C. 1939, *Pub. Obs. U. Michigan*, **7**, 93.
Wilsing, J., and Scheiner, J. 1902, *Ap. J.*, **16**, 234.
Wyse, A. B. 1942, *Ap. J.*, **95**, 356.

A SECOND PHOTOELECTRIC STUDY OF 16 LACERTAE

MERLE F. WALKER*
Berkeley Astronomical Department, University of California
Received February 22, 1954

ABSTRACT

Photoelectric observations of 16 Lacertae in 1952 reveal large night-to-night variations in the amplitude of the light-curve, superimposed upon the 17-day beat-curve. Observations in infrared, yellow, and ultraviolet light, obtained on one night, indicate that the temperature of the star varied by 1000° K during the 4-hour period and that maximum temperature coincides with maximum light. Semiempirical tests of pulsation have been applied by combining the three-color light-curve with simultaneous observations of the radial velocity. The results of the tests do not confirm the pulsation hypothesis.

Photoelectric observations of 16 Lacertae were obtained at Mount Hamilton on 11 nights during the summer of 1952, to extend the investigation of the star begun in 1951 (Walker 1952). The purpose of the investigation was twofold: to improve the value of the beat-period discovered in 1951 (Miczaika 1952; Walker 1952) and to obtain simultaneous photometric and spectroscopic observations which could be used to apply the semiempirical tests of pulsation to the star.

For the purpose of improving the beat-period, the star was observed on 10 nights with the 12-inch Lick refractor and the photometer described previously (Walker 1952, 1953*b*). Since the 1951 observations indicated that there was no appreciable difference in the amplitudes of the yellow and blue light-curves, the star was observed only through a blue filter (Corning No. 5543). 14 Lacertae was employed as the principal comparison star, and its constancy was checked by observations of HD 217227. The intercomparisons of these stars have been published elsewhere (Walker 1953*a*).

In order to apply the tests of pulsation, it is necessary to have simultaneous observations of the light, color, and radial velocity of the star. Unfortunately, as we have just pointed out, the 1951 observations of 16 Lacertae did not reveal a detectable variation in the blue-yellow color index during the 4-hour period, although C. de Jager (1953) has subsequently found that, by forming mean light-curves, a blue-yellow color-variation of one or two hundredths of a magnitude is detectable in these observations. Since the blue-yellow color-variation in hot stars like 16 Lacertae is insensitive to small changes in temperature, it seemed likely that the color-variation could be detected and observed with reasonable accuracy by increasing the color base line. Observations in infrared, yellow, and ultraviolet light of HD 199140 revealed the variation in color very clearly (Walker 1954). Consequently, similar observations of 16 Lacertae were obtained on September 3, 1952, using an infrared-sensitive photometer attached to the Crossley reflector. The photometer and filters were those used in the observations of HD 199140 and have been described elsewhere (Walker 1954). Simultaneous observations of the radial velocity were obtained by D. H. McNamara with the two-prism spectrograph on the 36-inch refractor and a 12-inch camera (dispersion 37 A/mm at $H\gamma$).

The light-curves and velocity-curve are presented in Figures 1–3. Figures 1 and 2 show the blue light-curves obtained with the 12-inch refractor. Figure 3 shows the simultaneous three-color light-curves and velocity-curve. The ordinates of all the light-curves are the magnitude differences, 16 Lacertae *minus* 14 Lacertae, reduced to no atmosphere. The abscissae are heliocentric Julian days.

The times of maximum light observed in 1950, 1951, and 1952 are listed in Table 1,

* Since October, 1952, Carnegie Fellow at the Mount Wilson and Palomar Observatories.

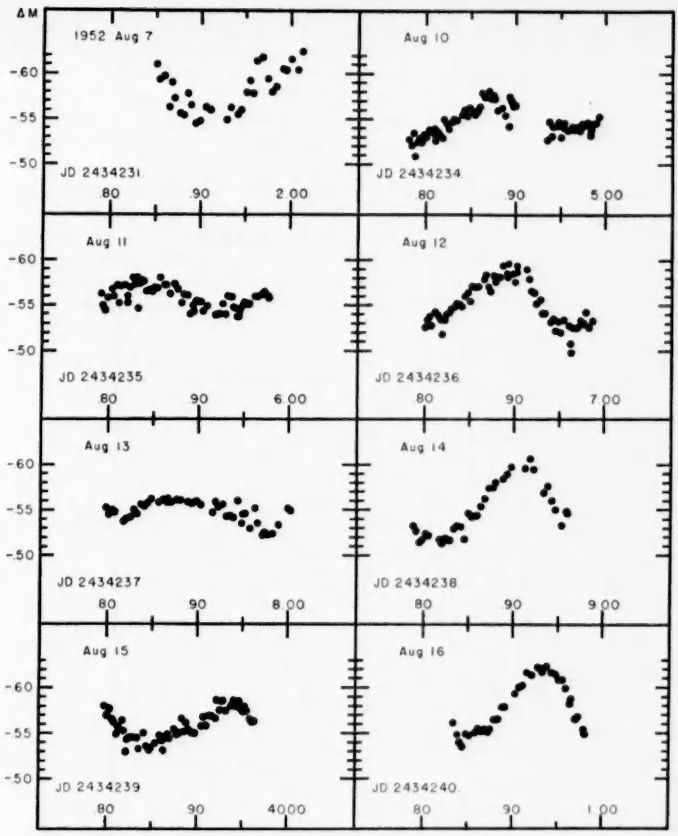

FIG. 1.—Photometric observations of 16 Lacertae in 1952. The ordinates are the blue-magnitude differences, 16 Lacertae *minus* 14 Lacertae, reduced to no atmosphere. The abscissae are heliocentric Julian days.

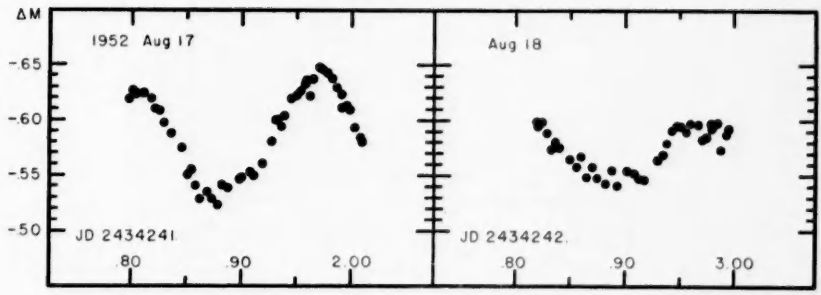

FIG. 2.—Photometric observations of 16 Lacertae in 1952. Ordinates as in Fig. 1

together with the residuals, observed maximum *minus* maximum computed from Max. = Hel. JD 2433505.765 + 0.169165E day. The epoch of maximum light used in the 1951 investigation has been retained for convenience, even though it was not chosen to make the mean residual equal to zero. The same value of the 4-hour period has also been used; the addition of the 1952 observations does not sufficiently increase the length of time over which the star has been observed to make a significant improvement possible.

It is at once evident from the observations that large night-to-night changes occurred both in the amplitude of the light-curve and in the phase of maximum light. These presumably resulted from the variation of the amplitudes of one or both of the two interfering oscillations present in this star. It is likely that the scatter in the amplitudes of the

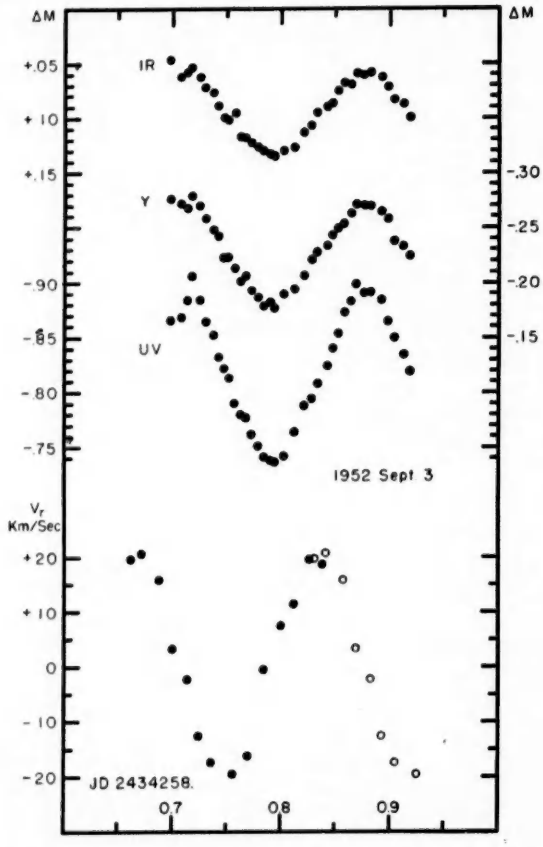

FIG. 3.—Simultaneous three-color light-curves and velocity-curve of 16 Lacertae in 1952. The infrared light-curve is given at the top of the figure, followed by the yellow- and ultraviolet-curves. The ordinates of these curves are the magnitude differences, 16 Lacertae *minus* 14 Lacertae, reduced to no atmosphere. The velocity-curve is shown at the bottom of the figure. Circles represent velocities brought forward one cycle of the star.

light-curves observed in 1950 (Walker 1951) is attributable to this same phenomenon and that these fluctuations were absent or less pronounced in 1951, so that a fairly smooth beat-curve was obtained. The existence of a variable amplitude of one of the oscillations is quite common among the β Canis Majoris stars (Struve, 1952) and apparently can be associated with either the P_1 or the P_2 period. It is not clear from the present observations which of the two oscillations in 16 Lacertae possesses the variable amplitude.

These night-to-night fluctuations in the amplitude of the light-curve make it almost impossible to obtain improved elements of the 17-day beat-curve or to determine its maximum and minimum amplitudes; the observations can be fitted by any period between 17.0 and 17.2 days. The light-ranges observed in 1950, 1951, and 1952, together with the phases computed according to the elements Zero phase = JD 2433870.89 + 17.15E days, are shown in Table 2 and Figure 4. In the figure the crosses represent the

TABLE 1

OBSERVED MAXIMA OF 16 LACERTAE*

Helioc. JD	O−C (Day)	Pnase (P=17.15 Days)	Helioc. JD	O−C (Day)	Phase (P=17.15 Days)	Helioc. JD	O−C (Day)	Phase (P=17.15 Days)
2433			2433			2434		
504.906	−0.013	0.660	872.854	+0.001	0.115	234.871	+0.005	0.223
505.765	.000	.710	873.868	.000	.174	235.841	− .040	.280
505.930	− .004	.719	883.837	− .012	.755	236.896	.000	.341
519.957	− .018	.537	889.930	− .009	.110	237.871	− .040	.398
521.795†	− .041	.645	897.864	− .025	.573	238.911	− .015	.459
523.834	− .032	.764	904.828	+ .003	.979	239.939	− .002	.519
527.921	− .005	.002	910.701	− .045	.321	240.933	− .023	.577
535.830†	− .046	.463	917.830	− .020	.737	241.971	.000	.637
870.826	+ .003	.996	925.801	− .001	.202	242.969	− .017	.696
870.996	+ .004	.006	2434			258.879	−0.009	0.623
871.849	+0.011	0.056	232.015†	+0.025	0.057			

* Max. light = Hel. JD 2433505.765 + 0.169165E day; zero phase = JD 2433870.89 + 17.15E days.
† Low weight.

TABLE 2

THE BEAT-PERIOD OF 16 LACERTAE*

JD	Light-Range (Mag.)	Phase (P=17.15 Days)	JD	Light-Range (Mag.)	Phase (P=17.15 Days)	JD	Light-Range (Mag.)	Phase (P=17.15 Days)
2433			2433			2434		
504.90	0.110	0.660	874.80	0.000	0.228	234.88	0.045	0.224
505.88	.110	.717	875.82	.025	.287	235.88	.032	.282
519.92	.079	.535	883.85	.078	.756	236.89	.066	.341
521.90	.090	.655	889.87	.056	.107	237.90	.039	.400
523.87	.060	.766	897.84	.065	.571	238.87	.088	.456
527.92	.081	.002	904.81	.064	.978	239.88	.047	.515
535.90	.048	.467	910.76	.038	.325	240.91	.074	.575
870.89	.056	.000	917.77	.079	.733	241.90	.117	.633
871.91	.060	.060	925.84	.029	.204	242.91	.051	.692
872.88	.059	.116	2434			258.81	0.092	0.619
873.88	0.036	0.174	231.93	0.066†	0.052			

* Zero phase = JD 2433870.89 + 17.15E days.
† Low weight.

1950 observations, the dots the 1951 observations, and the circles the 1952 observations. The barred circle represents the yellow light-range observed on September 3, 1952.

Figure 5 shows the residuals in the time of maximum light plotted against the phase in the 17-day period. The various symbols have the same meanings as in Figure 4. The small symbols indicate observations of lower weight.

Theoretical curves of the variation in amplitude and of the shift in the time of maximum light have been computed by the formula given by O. Struve (1950). The curve marked A in Figures 4 and 5 was computed for oscillations having ranges $R_1 = 0.040$ mag. and $R_2 = 0.050$ mag.; the curve marked B was computed for $R_1 = 0.035$ mag. and $R_2 = 0.055$ mag. The 1951 observations of the beat-amplitude are best fitted by the

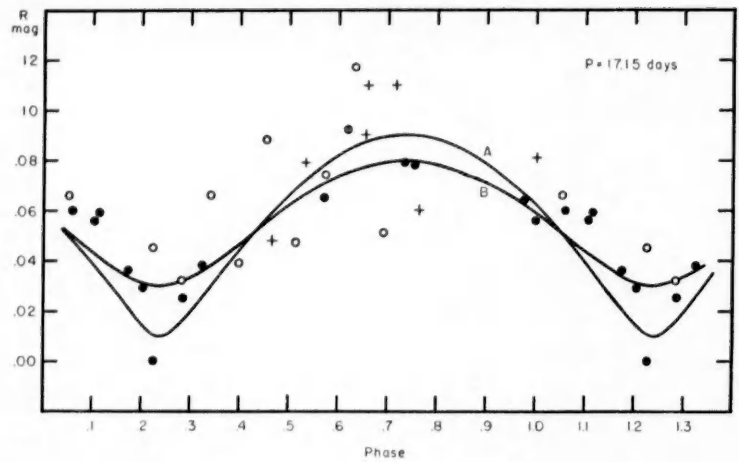

FIG. 4.—The beat-period in the amplitudes of the light-curves. The ordinate is the light-range, the abscissa is the phase computed from Zero phase = JD 2433870.89 + 17.15E days. The crosses represent the 1950 observations, dots the 1951 observations, and circles the 1952 observations. The barred circle represents the yellow light-range observed on September 3, 1952. The curve labeled A is based on $R_1 = 0.040$ mag., $R_2 = 0.050$ mag.; B is based on $R_1 = 0.035$ mag., $R_2 = 0.055$ mag.

latter, while the former gives a better representation of all the observations of the beat-curve and also of the shifts in the times of maximum light. The ratio of the amplitudes of the P_1 and P_2 oscillations is probably $1.2 \leq R_2/R_1 \leq 1.6$.

The three-color light-curves obtained on September 3 show very clearly the color-variation of the star. As in HD 199140 (Walker 1954), there is no indication of a shift in the phase of maximum or minimum light with wave length, and the star is bluest at the time of maximum light, which is also the time of maximum contraction of the star on the pulsation hypothesis. The accuracy of the three-color observations of 16 Lacertae is considerably greater than for HD 199140. In the latter star the accuracy was limited by the thermal noise of the unrefrigerated photocell. Since 16 Lacertae is about 1 mag. brighter than HD 199140, there was a corresponding gain in the signal-to-noise ratio.

If we plot the observed light-range against the reciprocal of the effective wave length of the cell and filter combinations, we obtain a very nearly linear variation of amplitude with $1/\lambda$. There is no suggestion of an abnormal amplitude in one color, such as was found in HD 199140. Furthermore, when we compute the light-variation which we would

expect to observe with our cell and filters if a black body at 20,000° K changed its temperature by 1000°, we obtain within the observational error the amplitudes actually observed in 16 Lacertae, as is shown in Table 3. It has been pointed out in connection with HD 199140 that if the star is pulsating, the observed variation of light-range with $1/\lambda$ ought to be parallel to that computed for some change in temperature but that the observed light-ranges should be smaller by Δm_r, the change in brightness produced by the change in radius. Thus we arrive at the same result as that obtained for HD 199140: If we assume black-body conditions in the star, the observations are not consistent with the pulsation hypothesis; the entire light-variation can be explained as the result of a change in the temperature of the star.

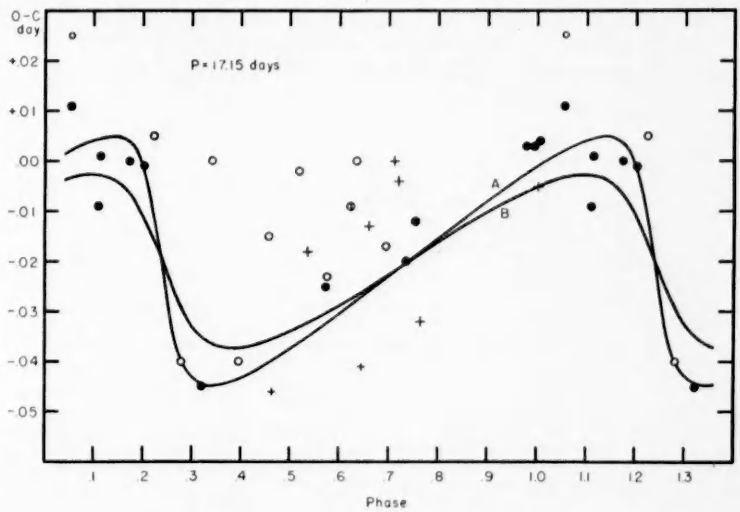

FIG. 5.—Periodic variations in the times of maximum light. The ordinate is the residual, observed maximum *minus* maximum predicted from the formula Max. = Hel. JD 2433505.765 + 0.169165E day. The abscissa is the phase computed from Zero phase = JD 2433870.89 + 17.15E days. Symbols as in Fig. 4. Small symbols indicate observations of lower weight.

TABLE 3

LIGHT-VARIATION OF 16 LACERTAE ON SEPTEMBER 3, 1952

	LIGHT-RANGE (MAG.)		
	IR 0.846μ	V 0.549μ	UV 0.358μ
Observed	0.077	0.094	0.153
Calc. for black body at 20,000° K ($\Delta T = 1000°$)	0.073	0.096	0.144

Let us now apply A. J. Wesselink's (1946) method of points of equal color, which avoids the assumption of black-body conditions. If we assume that there exists a single-valued relationship between the color and the effective temperature of the star, then the change in the magnitude of the star between two phases when it has the same color is that due to a change in radius, Δm_r. This may be compared with the displacement of the surface of the star between the same phases, ΔD, found by integrating the velocity-curve. For a succession of such points, a plot of Δm_r against ΔD should give a straight line whose slope is proportional to the radius of the star. The relationship between Δm_r and ΔD for 16 Lacertae is shown in Figure 6. In HD 199140 it was found that the points, instead of yielding a straight line as required by the pulsation hypothesis, fell all over the diagram. Here, perhaps owing to the greater accuracy of the observations, the points do give a straight line through the origin. Moreover, the points derived from yellow-in-

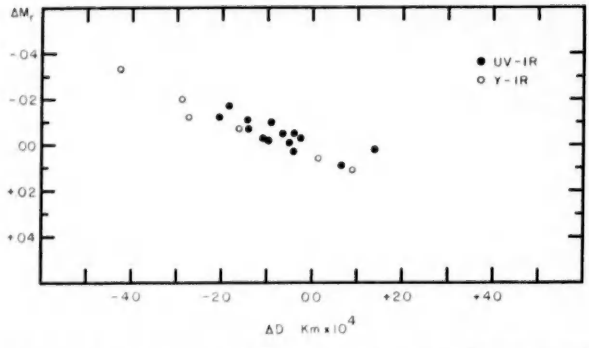

FIG. 6.—Semiempirical test of pulsation in 16 Lacertae, using Wesselink's method of points of equal color. The ordinate is the change in brightness resulting from a change in radius; the abscissa is the displacement of the surface of the star. Dots represent points of equal ultraviolet–infrared color; circles represent points of equal yellow–infrared color.

frared colors agree with those obtained by using ultraviolet-infrared colors. Unfortunately for the concept of pulsation, however, the relationship between Δm_r and ΔD has the opposite sense from what it should have if the pulsation hypothesis were correct. Assuming the limb-darkening coefficient of 16 Lacertae to be 0.5, the observed line corresponds to a radius of *minus* 50 $R_\odot$.

Even though the accuracy of the observations is considerably greater for 16 Lacertae than for HD 199140, this test is probably still very nearly indeterminate, owing to the facts that the light-curves are nearly symmetric about maximum and minimum light and that the contributions to the light-curve from the variation in effective temperature and from the change in radius are 180° out of phase.

Our conclusion regarding the hypothesis of pulsation in 16 Lacertae is thus the same as in the case of HD 199140: Neither test confirms the concept of radial pulsation, but there are weaknesses in both the tests which prevent us from concluding that the concept is incorrect. It seems obvious from the fact that a variation in radial velocity exists that we cannot explain the observations solely as the result of a variation in temperature. Since the results of the tests in both HD 199140 and 16 Lacertae are similar, the observations, if they mean anything at all, might be taken as strengthening the supposition that the stars undergo some sort of nonradial pulsation.

I am indebted to Dr. C. D. Shane for making available the facilities of the Lick Observatory, and to Dr. G. E. Kron for the use of one of his infrared-sensitive photometers. It is also a pleasure to thank Dr. D. H. McNamara for the use of his simultaneous radial velocities, and Dr. H. H. Voigt for assisting me at the Crossley reflector.

REFERENCES

Jager, C. de. 1953, *B.A.N.*, **12**, 88.
Miczaika, G. R. 1952, *Ap. J.*, **116**, 99.
Struve, O. 1950, *Ap. J.*, **112**, 520.
Struve, O. 1952, *Ann. d'Ap.*, **15**, 157.
Walker, M. F. 1951, *Pub. A.S.P.*, **63**, 35.
Walker, M. F., 1952, *Ap. J.*, **116**, 106.
Walker, M. F., 1953*a*, *Ap. J.*, **118**, 481.
Walker, M. F. 1953*b*, *Pub. A.S.P.*, **65**, 39.
Walker, M. F. 1954, *Ap. J.*, **119**, 631.
Wesselink, A. J. 1946, *B.A.N.*, **10**, 91.

THE MAGNETIC VARIABLE HD 188041

HORACE W. BABCOCK
MOUNT WILSON AND PALOMAR OBSERVATORIES
CARNEGIE INSTITUTION OF WASHINGTON
CALIFORNIA INSTITUTE OF TECHNOLOGY
Received February 1, 1954

ABSTRACT

Fifty-seven observations of the magnetic field of HD 188041 have been made at intervals during the last seven years. The field is always of positive polarity but varies between the extreme limits 600 and 4800 gauss, with some irregularities in amplitude, in a period of 226 days. The star is also a spectrum variable in which lines of *Eu* II, *Gd* II, and *Sr* II are stronger when the field is strong; the phase of the intensity-curve for *Gd* II is earlier than the magnetic curve by about 0.1 of the period. When the field is increasing most rapidly, *Gd* II shows a stronger magnetic-field intensity than do other elements, and *Fe* II shows a stronger field than *Fe* I. The velocity shows small random fluctuations.

The star HD 188041[1] = HR 7575 has been variously classified as F0p + A and as A5sp, but it appears not to have been included in recent lists of peculiar A-type stars. There seems to be no modern evidence that the spectrum is really composite. In fact, it is nearly identical to the spectra of β Coronae Borealis (F0p), γ Equulei (F0p), and 73 Draconis (A2p), being rich in sharp lines of the metals, which have rather low central intensities. All these stars are known to have variable magnetic fields (Babcock and Cowling 1953), and 73 Dra (Morgan 1933) is a spectrum variable with a period of 20.27 days, the longest heretofore established. The half-widths of most of the metallic lines in the spectra of these four stars are between 0.1 and 0.2 A; for example, in HD 188041 the rather strong components of the *Mg* II doublet λλ 4481.129–4481.327 are just resolved on plates of 4.5 A/mm dispersion.

When first tested in 1947, HD 188041 was found to have a magnetic field. Numerous subsequent plates show that the field is always of positive polarity but that it varies between the extreme limits +600 and +4800 gauss in a period of about 226 days. Recently it has been found that lines of *Eu* II, *Gd* II, and *Sr* II, which are abnormally strong, vary in intensity with the same period. HD 188041 is therefore closely related to the group of peculiar A stars typified by α^2 Canum Venaticorum, HD 125248, and 73 Dra. It is of somewhat later spectral type than most others of this group and is of particular interest because its period is more than ten times as long as any other for which elements of variation have been determined.

OBSERVATIONS

The spectrograms have been taken in the usual way with the double circular analyzer, in almost all cases with a dispersion of 4.5 A/mm in the second- or third-order grating spectrum provided by the 6-foot cameras of the coudé spectrographs of the 100-inch and 200-inch telescopes. Twenty-one of the plates have been measured by Miss Sylvia Burd, 18 by Mrs. A. J. Deutsch, and 14 by Mr. J. R. Novotny. From 40 to 80 lines between λ 3900 and λ 4500 have been measured for magnetic-field intensity and for radial velocity on each plate. Measures typically include several lines each of *Fe* I, *Fe* II, *Cr* I, *Cr* II, a few of *Ti* II, *Gd* II, and *Eu* II, and scattered lines of *Mn* I, *Mg* I, *Sr* II, *Sc* II, etc. It was not practicable to measure precisely the same list of lines on each plate, but many of the lines are common to nearly all. The various elements are in fairly good accord for field strength, so that the probable error from each plate is between ±100 and ±200 gauss.

Table 1 lists the observations according to number, Julian day, and phase in the 226-

[1] $\alpha = 19^h50^m42^s$; $\delta = -3°15'$ (1950); $m_v = 5.6$.

TABLE 1

MEASURES OF MAGNETIC-FIELD INTENSITY AND OF VELOCITY IN HD 188041 WITH ESTIMATED INTENSITY OF *Gd* II LINES

PLATE	JD 2430000+	PHASE	$H_p \cos a$ (GAUSS)						$-v$ (KM/SEC)	MEAS. BY	INT. *Gd* II
			All Lines	*Fe* I	*Fe* II	*Cr* I	*Cr* II	*Gd* II			
Ce 4730	2366.93	0.194	2090 ± 75	2100	2200:	2100::	2238	.....	20.7	N	3
4761	2397.77	.331	3100	2850	3040	3580	2840	3400	21.1	B	4
4837	2430.70	.477	4145	4060	4110	7400::	1900::	4100	23.3	B	5
4883	2458.69	.600	3375	3580	.....	3060::	3420	2570	20.7	N	5
4946	2489.66	.737	3570 ± 200	3720	4670:	3480:	3490	.....	.....	N	4
5150	2657.98	.482	4790	4360	4970:	5970	3160	4090	22.1	B	5
5186	2693.95	.641	4120	4170	9000::	2510:	4260	1800::	20.2	N	4
5197	2718.90	.751	.....	.....	.....	.....	.....	.....	.....	.....	2
5300	2785.75	.048	1550	1290	1320	2170:	1300	2400	.....	B	2
5768	3114.92	.504	4420	4440	.....	4470	4080	4340	20.7	B	5
5768	3114.92	.504	4850	4435	.....	3200::	4700	5150	20.6	N	...
5948	3173.68	.764	2870	2660	2060	3440	2860	2880::	20.6	B	2
5968	3194.68	.857	2815 ± 120	2460	.....	2360::	2580	.....	22.1	N	2−
6223	3402.98	.779	2690	2380	2540	2760	2960	.....	21.7	B	2
6232	3406.98	.796	2650	2440	2910	2320	1630	.....	22.1	B	2
6250	3430.94	.902	2050	1670	2160	1780	2290	.....	.....	B	1
6271*	3433.97	.916	1400	1070	1260	1120:	1960	.....	.....	B	1
6327	3461.87	.039	1680	1710	2280	800::	1790	.....	23.2	N	2
6335	3462.86	.047	1490	.....	.....	.....	.....	.....	.....	.....	2
6341	3463.87	.048	1605	1370	1740	.....	1290	5900	21.6	N	2
6354	3465.90	.009	.....	.....	.....	.....	.....	.....	.....	.....	2
6368	3488.86	.159	2870	3130	3830	1960::	2150	.....	21.1	N	2+
6387	3492.82	.176	2650	2720	3290	1500::	3430	.....	21.1	N	3
6505	3526.79	.327	3160 ± 160	3150	2940	.....	3400	.....	.....	B	5
6505	3526.79	.327	3550	3330	3640::	.....	3460	.....	21.5	N	...
6538	3549.63	.428	3170	2990	2620	.....	3840	1730::	22.2	N	5+
6610	3574.65	.538	3190 ± 125	2890	.....	.....	3110	.....	22.6	N	5
6666	3609.63	.....	.....	.....	.....	.....	.....	.....	.....	.....	3
6681	3612.63	.706	3100	2720	3990	2230	3730	.....	20.1	N	3
7038	3788.93	.486	3065 ± 185	3090	3830	3240	3390	2650	23.1	D	5
7069	3811.91	.588	2850 ± 125	3180	3760	3140	2140	2680	22.5	D	4
7130	3848.9	.752	2590 ± 110	2260	2940	2640	2460	3820::	21.6	D	2
7210	3856.7	.786	2740 ± 150	2880	1930	3170	2760	1800	21.5	D	2+
7364	3881.8	.897	2290 ± 150	2290	2180	2610	2890	4000	22.1	D	1
Pa 156	3907.7	.012	1485 ± 110	1570	1530	1070	1200	1270	22.1	B	2
206	3940.7	.158	2210 ± 125	2480	1650::	1590	2620	3220	22.3	D	4
347	4145.9	.066	1240 ± 82	1080	1290	1260	1030	.....	21.5	D	2
Ce 8066	4169.9	.172	2585	2080	2280	1760	2520	3830	20.5	B	4
8066	4169.9	.172	2440 ± 130	.....	.....	.....	.....	.....	21.2	D	...
Pa 385	4202.9	.318	2550 ± 160	2650	.....	3720	2100	2630	21.3	D	4+
399	4208.85	.344	2670 ± 120	2520	4400::	2800	2450	2630	22.0	D	4+
Ce 8263	4232.8	.450	3970 ± 160	3770	2440	4150	4150	4280	21.7	D	5
8286*	4236.8	.469	.....	.....	.....	.....	.....	.....	.....	.....	5+
8350	4261.7	.578	3800	3960	3680	4440	3100::	3770	21.6	B	4
8369	4265.7	.596	3060	3130	2000	3250	1650::	4000	21.1	B	4
8441	4294.7	.724	3850	3790	2280	4350	.....	4830	21.3	B	3
Pa 508	4285.7	.685	.....	.....	.....	.....	.....	.....	.....	.....	4
Ce 8464	4317.65	.826	2135 ± 190	1990	1340	1400	2800	.....	22.4	D	2
Pb 941	4527.95	.756	2700 ± 100	2860	2300	2260	2690	5500::	20.4	D	2−
954	4531.92	.774	.....	.....	.....	.....	.....	.....	22.2	B	2+
981	4554.82	.875	2470 ± 160	2510	1800::	.....	2340	.....	21.1	D	2−
1007	4558.86	.893	2160 ± 95	1870	1300::	.....	2390	.....	20.4	D	2−
1045	4582.76	.000	600 ± 150	390	−890	1580	160	1450	21.1	B	2
1060	4585.75	.012	1775 ± 100	1840	1770	1340	180	3600	21.8	D	2+
1060	4609.86	.119	2005 ± 125	1940	2540	1820	2040	4500	21.8	D	3
1157	4646.7	.286	2520 ± 200	2100	1640	2500:	1000:	3320	20.2	B	4
1158R	4646.8	.286	3370 ± 200	2610	1350:	3160	2830	4440	20.8	B	...
1177	4671.7	.392	3680 ± 220	3880	4100	3150	3260	3760	.....	B	5
1242	4706.7	0.549	2465 ± 105	.....	.....	.....	.....	.....	19.9	D	5

* Dispersion 10 A/mm. Dispersion of Ce and Pb plates is 4.5 A/mm, of Pa plates, 2.2 A/mm.

day period, with the magnetic-field intensity, the radial velocity reduced to the sun, and the initials of the measurer. The magnetic-field intensity is $H_p \cos a$, computed as usual on the assumption that the field of the star is that of a dipole located at its center. If the line of sight is parallel to the magnetic axis ($a = 0$), the figure listed is the intensity of the field at the magnetic pole; in contrast, if the field had at all points on the surface a direction parallel to the line of sight, its intensity would be only 0.3 of the given figure.

The results of all the magnetic measurements of HD 188041 have been plotted against Julian day in Figure 1. This shows that the variations in amplitude are nonuniform from

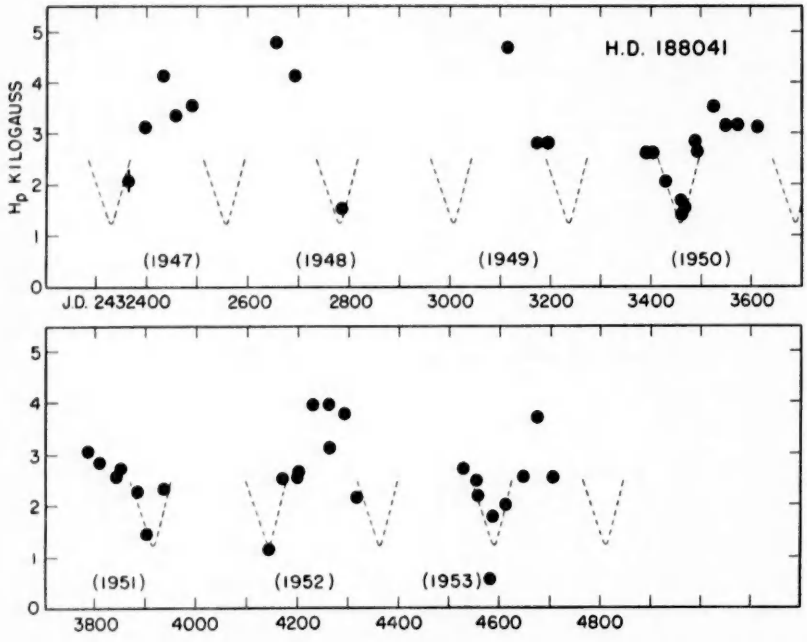

FIG. 1.—Magnetic-field intensity, $H_p \cos a$, plotted against Julian day. The rather sharp minimum recurs at intervals of about 226 days. The amplitude at maximum is nonuniform.

cycle to cycle but that a minimum in magnetic-field intensity recurs at fairly regular intervals. The elements that seem best to represent the recurrence are

$$\text{Magnetic minimum} = \text{JD } 2432323 + 226E.$$

All observations have been plotted against phase in Figure 2, *a*, which further emphasizes the nonuniformity in amplitude and the relatively sharp, well-defined minimum. The question arises to what extent the dispersion of the points represents actual physical differences in the star from cycle to cycle as contrasted with accidental errors of measurement. Three types of evidence bearing on this are as follows:

a) The group of seven plates taken near phase 0.05, as plotted in Figure 2, *a*, all lie within a range of 550 gauss, whereas at magnetic maximum (phase 0.5) results from several plates scatter over a range of nearly 2000 gauss.

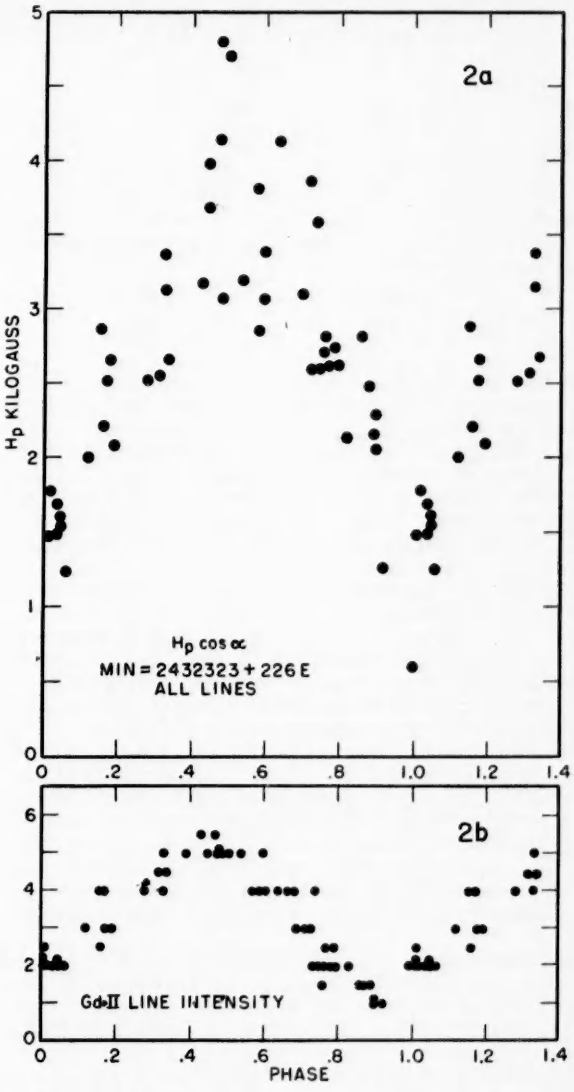

FIG. 2.—*a*, magnetic-field intensity in kilogauss plotted against phase in the period of 226 days. *b*, intensity of *Gd* II lines, in arbitrary units, plotted against phase. The phase of this curve is slightly in advance of the phase of the magnetic curve.

b) Several pairs of plates taken only a few days apart yield nearly similar results, as would be expected when the probable errors of the plates are of the order of ± 100 gauss. For example, the pairs given in the accompanying tabulation may be mentioned.

JD 2430000+	$H_p \cos a$	JD 2430000+	$H_p \cos a$
3173	2870 gauss	3461	1680 gauss
3194	2815	3462	1490
3402	2690	3463	1600
3406	2650	4202	2550
		4208	2670

Another pair shows a greater difference, but the 3-day interval follows immediately what may be a very sharp minimum:

JD 2430000+	$H_p \cos a$
4582	600
4585	1775

c) Three plates (Ce 5768, 6505, and 8066) were measured twice by different individuals with fairly accordant results: 4540–4850, 3160–3550, and 2585–2440 gauss, respectively. The lines were selected at random by each measurer.

d) Because a somewhat different list of lines was measured on each plate, there is a possibility that if the various elements are differently distributed in the star's atmosphere and therefore indicate different effective field strengths, they might thus cause the vertical dispersion in the diagram of Figure 2, *a*. In this case we might expect the scatter to be greater near mid-cycle when the field is strong. To test this idea, the field intensity as indicated by lines of *Fe* I alone has been plotted in Figure 3. The average number of lines of *Fe* I per plate was 17. The resulting pattern is quite similar—indeed, almost indistinguishable—from that of Figure 2, *a*, suggesting that the magnetic fluctuations of Figures 1 and 2, *a*, are real and are not due to difficulties of measurement.

The foregoing considerations substantiate the impression gained from Figure 1 that the magnetic amplitude of the star varies widely from cycle to cycle. Indeed, this figure suggests some remote similarity to the familiar curves of Wolf numbers or sunspot frequency that reflect the changing magnetic activity of the sun.

A scanning of the data suggested that *Gd* II might yield a magnetic intensity greater than the other elements on several of the plates. Consequently, in Figure 4, the difference H_p (*Gd* II) ***minus*** H_p (all lines) has been plotted against phase. The results bear out the impression that between phases 0.3 and 0.6, *Gd* II agrees in field intensity with the other elements but that between phases 0.7 and 0.3, when the average field of all elements undergoes a sharp minimum (and when line intensities of *Gd* II are relatively weak), this element yields a field about 1000 gauss stronger than the others. This difference in magnetic behavior presumably reflects a nonuniform distribution of *Gd* II in the stellar atmosphere.

One second-order spectrum was taken in the green-yellow region, with a special analyzer, at phase 0.286 (Pb 1158). Of the 41 lines measured, 7 of *Gd* II and 1 of *Eu* II gave much greater field strengths than did the other elements. If these rare earths are omitted, the resulting $H_p \cos a$ is 2930 gauss, as compared to 2520 gauss obtained from all lines on Pb 1157 taken only a few hours earlier.

Another systematic effect may be found in the difference in the effective field strength indicated by the ionized and neutral states of the metals *Fe* and *Cr* as a function of phase. The difference H_p (*Fe* II) ***minus*** H_p (*Fe* I) has been plotted in Figure 5 for plates on which three or more lines were measured. Throughout the greater part of the cycle there is considerable scatter, but in the first two-tenths of the cycle, when the effective field is increasing most rapidly, *Fe* II shows a field intensity several hundred gauss stronger than *Fe* I. Seven plates in this interval are consistent in this effect. A rather similar effect, but

with greater amplitude and greater scatter, is shown when a similar plot is made for *Cr* II and *Cr* I.

VELOCITIES AND HYPERFINE STRUCTURE

The radial velocity as well as the field strength has been derived from each plate. The probable error for individual plates averages about ± 0.15 km/sec. The mean velocity of the star from all measured plates is $v = -21.51 \pm 0.08$ km/sec. On purely statistical grounds, the probable error of the mean should be about ± 0.02 if the velocity of the star is constant. It is possible to interpret the plot of the velocities in Figure 6 as an ill-defined double wave having an amplitude of about 1.5 km/sec, with random deviations superposed. Small deviations of instrumental origin are not excluded, but indications are

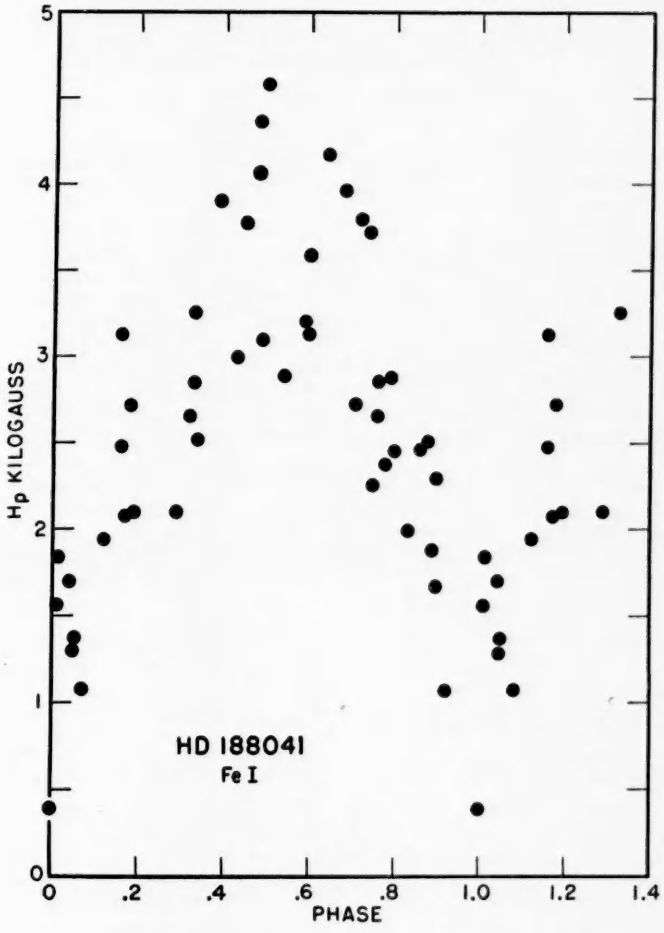

FIG. 3.—Field intensity as measured for lines of *Fe* I alone

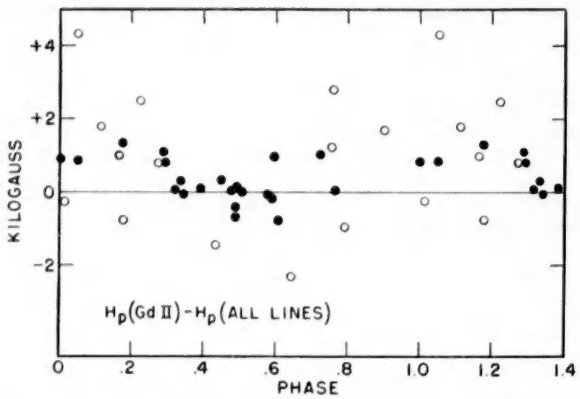

FIG. 4.—The difference in field intensity between lines of *Gd* II and lines of all elements plotted against phase. Open circles, of low weight, are from plates on which only one or two lines of *Gd* II were measured.

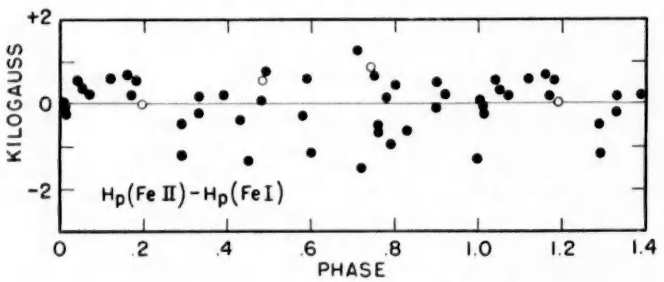

FIG. 5.—Difference in magnetic-field intensity between lines of *Fe* II and lines of *Fe* I. Early in the cycle, while the field is increasing most rapidly, the ionized element shows a greater field strength.

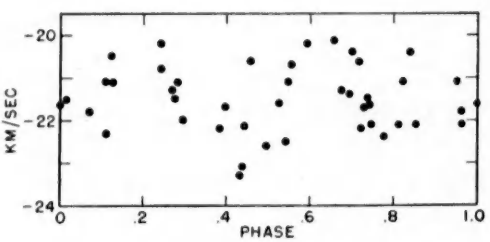

FIG. 6.—Measurements of radial velocity as a function of phase

that irregular fluctuations in the atmosphere of the star may contribute. (If it is supposed that HD 188041 has a diameter twice that of the sun, that it rotates with a period of 226 days, and that the obliquity of its axis is about 35°, then $v_e \sin i = 0.3$ km/sec.)

Of all elements measured for velocity, only *Eu* II seemed to be systematically biased. The average velocity derived from *Eu* II lines was −23.92 km/sec, about 2.4 km/sec more negative than the mean. As has been pointed out elsewhere, the most probable source of this discrepancy seemed to lie in the adopted laboratory wave lengths. It appears that one should employ not the wave length of the principal component as listed in the *Revised Multiplet Table* (C. E. Moore 1945), but the blended wave length, taking account of satellite lines due to hyperfine structure. As A. S. King (1930, 1939) pointed out, most of the prominent lines of *Eu* II in the photographic region are accompanied by satellites on the shortward side. These may shift the effective wave length by several hundredths of an angstrom. The velocity measures of HD 188041 provided a homogeneous body of data from which effective stellar wave lengths of eleven lines of *Eu* II between λ 3930 and λ 4522 were derived (Babcock 1954).

SPECTRUM VARIATIONS

An intercomparison of plates taken at phases of strong and of weak magnetic field shows pronounced changes in the intensities of lines of the rare earths *Eu* II and *Gd* II, these lines, in general, being stronger when the field is strong. The enhancement seems to result primarily from an increase in depth of the profile, with little change in width. There are also large changes in the intensity and profile of λ 4078 and λ 4215 of *Sr* II. With a weak field, these lines are relatively sharp, though deep; with a strong field, they develop shallow wings having the unusual width of 2–3 A. Therefore, HD 188041 is not only a magnetic variable but a spectrum variable closely similar to the spectrum variables of type A that have been described previously (Deutsch 1947).

In addition to the foregoing variations, a slight weakening of a few lines of *Fe* I was noticed with increasing field strength. For the most part, the numerous lines of *Cr* I and *Cr* II seem to remain constant in intensity, although the possibility of a slight enhancement with increasing magnetic field remains open. The weak, shallow wings of the K line of *Ca* II probably change as do the wings of the *Sr* II lines, although with smaller amplitude.

A comparison of Pb 1177 ($H = 3680$ gauss) with Pb 1045 ($H = 600$ gauss) taken 3 months earlier shows a number of intensity variations of which the most conspicuous are listed in the accompanying tabulation. Notations compare the plate of stronger (increasing) field with that of weaker field. This list is representative of other comparisons at similar phases.

λ 3922.9	*Fe* I	weaker and wider	
3930	*Eu* II	slightly stronger	
3996.3	*Gd* II	stronger	
4070.3	*Gd* II	much stronger	
4078	*Sr* II	wide weak wings, shallower core	
4115	*Gd* II	stronger	
4118.5	*Fe* I	much weaker	
4129	*Eu* II	stronger	
λ 4188.1	*Gd* II	stronger	
4191.1	*Gd* II	stronger	
4205	*Eu* II	stronger	
4215	*Sr* II	wide weak wings, shallower core	
4251.7	*Gd* II	stronger	
4347	*Gd* II	stronger	
4383.1	*Eu* II	stronger	
4435.6	*Gd* II	much stronger	

Eye-estimates of the intensity of the *Gd* II lines (principally λ 4251.7) were made on all plates and have been plotted against phase in Figure 2, *b*. The arbitrary units employed are on a scale such that the intensity of the apparently invariant line *Fe* I λ 4250.9 is equal to 4. The variable lines of *Eu* II, while stronger, were more difficult to evaluate than those of *Gd* II. The resulting intensity-curve for *Gd* II is roughly sinusoidal and has the interesting property of a phase shift. This is especially noticeable at minimum, when the line-intensity-curve is earlier in phase than the magnetic curve by 0.05–0.10 of the

period. This effect might be expressed by the statement that the intensity of the *Gd* II lines is enhanced while the magnetic field is increasing most rapidly and that the intensity of these same lines tends to diminish at other phases. The intensities were checked by careful comparisons of pairs of plates on the Hartmann comparator, the pairs being selected for equal magnetic-field intensity on the increasing and decreasing slopes of the magnetic curve. For example, Pb 1157 (phase 0.286, $H = 2520$, increasing) showed all rare-earth lines to be stronger than on Pb 981 (phase 0.875, $H = 2470$, decreasing). The same effect was found on comparing Pb 1157 with Pb 941 (phase 0.756, $H = 2700$, decreasing). Furthermore, the intensities of the variable lines were essentially identical on Pb 1045 (phase 0.000, $H = 600$ gauss, minimum) and on Pb 941. These comparisons bear out the finding that the variable lines are stronger when the field is increasing than when it is decreasing. Several of the comparisons also suggested that the metallic lines were, in general, slightly sharper with rapidly increasing magnetic field than at other phases. These estimates were, of course, made on spectra taken with the polarizing analyzer, so that the very slight Zeeman broadening of the profiles with a strong field is largely removed.

INTERPRETATION

For HD 188041, as for some other magnetic and spectrum variables, the gross features, such as the periodicity in the magnetic field and in the line intensities, can be interpreted in terms of the oblique rotator model. Here the changes are ascribed to the variation in aspect of a rigidly rotating star having a magnetic axis considerably inclined to the axis of rotation and carrying on its surface relatively permanent patches that are spectroscopically anomalous, in the sense that the effective local abundance of particular elements is greatly enhanced. We shall examine the data for HD 188041 with a view to determining how well it can be represented by the rotator model and what points of discrepancy may remain.

It was shown by D. W. N. Stibbs (1950) and by M. Schwarzschild (1950) that if the magnetic axis of a star having a dipolar field makes an angle α with the line of sight, the effective field in integrated light is $H_p \cos \alpha$. Further, following Stibbs, if the axis of rotation of the star makes an angle i with the line of sight and an angle β with the magnetic axis, the value of α is given at any phase of the rotation by

$$\cos \alpha = \cos i \cos \beta + \sin i \sin \beta \cos \theta,$$

where $\theta = 2\pi \times$ phase.

If the data of Figure 2, *a*, are smoothed to make the best fit with a simple harmonic curve, the maximum is about +3500 gauss and the minimum about +1500 gauss, the ratio being roughly 2.3. There is no unique solution for i and β, but a large range of reasonable values is possible, as exemplified by the curves published by Stibbs. For example, if we arbitrarily assume that $i = 30°$, we obtain 34° for β. But, as we have seen, the probable error of a single plate is less than ± 200 gauss; and there seems no reasonable source of large errors that would account for the dispersion in the points of Figure 2, *a*, near magnetic maximum, where the values of $H_p \cos \alpha$ range from 2800 to 4800 gauss. Most probably, then, the deviations in the magnetic maxima are real and reflect changes with time in the physical conditions at the surface of the star, even if we attribute the fundamental harmonic variations to axial rotation in a period of 226 days. Further, the magnetic minimum seems sharper and better defined than the maximum.

In the spectrum of HD 188041, broadening of the lines by axial rotation is practically negligible. The line widths, no greater than 0.2 A, set an upper limit on $v_e \sin i$ of about 7 km/sec. If $R = 2R_\odot$, the line widths then permit any period of rotation greater than about 15 sin i in days. If actually $P = 226$ days, the greatest semi-amplitude that could arise in radial velocity from axial rotation, even on the extreme and obviously incorrect assumption that all absorption lines arise in one small patch, is about 0.4 km/sec. The

greater range indicated by the velocity plot of Figure 6, while it may be due in part to instrumental factors, is not incompatible with the idea of slow, large-scale hydromagnetic turbulence.

The sinusoidal nature of the curve showing intensity of the lines of *Gd* II (Fig. 2, *b*) is by itself readily interpreted on the rotator model; taking the phase shift into account, we should suppose that *Gd* is concentrated in a moderately extensive patch centered some 30° in longitude from the magnetic pole. This picture is in part consistent with evidence of Figure 4, that near magnetic minimum the lines of *Gd* II show a field about 1 kilogauss stronger than the field of the other elements. A curious inconsistency arises at mid-period, however, for on this model we should expect to find at *all* phases and, in particular, near magnetic maximum, a stronger field for *Gd* II than for other elements. But, according to Figure 4, *Gd* II near magnetic maximum shows a field indistinguishable from that of all elements considered together. If, in the endeavor to meet this difficulty, we assume that *Gd* II is spectroscopically effective over essentially the whole positive magnetic hemisphere of the star instead of in a limited patch, we find that, bearing in mind the restricted range of α permitted by the curve of magnetic variation, we are no longer able to account for the large periodic change in the intensity of the *Gd* II lines as plotted in Figure 2, *b*.

No very obvious interpretation of the results of Figure 5 is available. Here the effect is that, for about one-fifth of the period, while the observed field is growing most rapidly, lines of *Fe* II consistently show a field strength greater by a few hundred gauss than the lines of *Fe* I. Yet, except for a very small minority of the lines in *Fe* I, no change in line intensity of either *Fe* II or *Fe* I has been found. Perhaps equally important is the indication that throughout the remainder of the period consistency is lost and rather large, irregular differences prevail between H_p (*Fe* II) and H_p (*Fe* I).

We conclude that the observations are not completely and readily accounted for on the oblique rotator model and that if, despite the difficulties that have been brought out, the fundamental periodic variations are attributed to axial rotation, we must in all probability admit, in addition, the occurrence of intrinsic hydromagnetic fluctuations at the surface of the star.

I am very grateful to Miss Burd, Mrs. Deutsch, and Mr. Novotny for their careful and skilful measurement of the spectrograms.

REFERENCES

Babcock, H. W. 1954, *Ap. J.*, **119**, 463.
Babcock and Cowling. 1953, *M.N.*, **113**, 357.
Deutsch, A. J. 1947, *Ap. J.*, **105**, 283.
King, A. S. 1930, *Ap. J.*, **72**, 22; 1939, *Ap. J.*, **89**, 380.
Moore, Charlotte E. 1945, *A Multiplet Table of Astrophysical Interest* (rev. ed.; Princeton: Princeton University Press).
Morgan, W. W. 1933, *Ap. J.*, **77**, 77.
Schwarzschild, M. 1950, *Ap. J.*, **112**, 222.
Stibbs, D. W. N. 1950, *M.N.*, **110**, 395.

THE ABNORMAL ATMOSPHERE OF AG PEGASI*

G. R. Burbidge and E. Margaret Burbidge
Cambridge, England
Received October 21, 1953; revised January 30, 1954

ABSTRACT

Equivalent widths of all measurable lines in the blue-violet region of the spectrum of AG Peg are given. Nearly all the lines are in emission and are very strong. From the intensities of the Balmer lines an estimate of the extent of the outer atmosphere has been made; this radius is approximately 400 stellar radii. It has been shown that a variable magnetic field of order 10^3 gauss, detected in the *Fe* II lines by H. W. Babcock, was probably present far out in the atmosphere. It is suggested that the field at the surface of the central star may have been several orders larger than this.

I. INTRODUCTION AND OBSERVATIONS

The remarkable emission-line star AG Pegasi[1] has, since 1915, been extensively studied spectroscopically by Merrill (1916, 1929, 1932, 1942, 1951*a*, *b*); Struve and Swings (1940, 1942*a*, *b*, *c*, *d*, 1943, 1944) have also published descriptions of the spectrum, and earlier observations have been summarized by Merrill. This star has become of even greater astrophysical interest because of the recent observations by H. W. Babcock (Babcock and Cowling 1953), which indicate that it has a variable magnetic field.

Two spectrograms were obtained by the authors with the coudé spectrograph on the 82-inch telescope at the McDonald Observatory. The camera giving a linear dispersion of 17½ A/mm between λ 4950 and λ 3650 was used. The dates of the observations were May 7^d46 and May 8^d45, 1953, U.T. The plates were calibrated by means of a new grating spectrograph designed by W. A. Hiltner and built at the Yerkes Observatory. In this spectrograph, light is admitted through a linear wedge-slit; the second order, giving a dispersion of about 13 A/mm, was used, and the width of the calibration on the plate was 1 inch. Two calibration plates were taken for each spectrum, one with a daylight and one with an ultraviolet filter; thus the whole wave-length region from $H\beta$ to beyond the Balmer limit was covered. The calibration plates were of a different size from the spectrum plates; however, they had been especially ordered to be coated with the same batch of emulsion as the spectrum plates used. They were developed side by side with the spectrum plates in Kodak D19, for 2¾ minutes at 65° F, in order to keep down the grain. The emulsion used was Eastman Kodak 103*a*-O. Tracings of the spectra and calibrations were made with the Beals microphotometer at the Yerkes Observatory. Reductions were carried out in the usual way.

On these two spectrograms, all the lines are in emission alone, except for the *He* I triplet lines and *N* III λ 4097, which have strong violet-displaced absorption components alongside the emission lines. The equivalent widths of all the measurable lines are given in Table 1. The first plate was less strongly exposed than the second, in order to avoid overexposing the very strong hydrogen lines so much. Consequently, the continuum is weak on this plate, and lines of wave length shorter than λ 3965 and longer than λ 4472 were not measured on it, with the exception of $H\beta$. For most of the remaining lines, the measures in Table 1 are the means of the two plates. The agreement for the weaker lines is satisfactory, indicating an error of ±12 per cent. The earlier hydrogen lines are more uncertain; they are so intense that they lie well above the straight-line portions of the

* *Contributions from the McDonald Observatory, University of Texas*, No. 237.

[1] HD 207757; BD +11°4673; $\alpha_{1900} = 21^h46^m2$, $\delta_{1900} = +12°9'$.

TABLE 1*

EQUIVALENT WIDTHS

Element	Tabular Wave Length	Equivalent Width (A)	Element	Tabular Wave Length	Equivalent Width (A)	Element	Tabular Wave Length	Equivalent Width (A)
Fe II	4923.92	1.86	[O III]	4363.21	3.05	V II	3916.42	0.29
He I	4921.93	2.65	Fe II	4351.76	1.20	Fe II	3914.48	0.55
Hβ	4861.33	188	Hγ	4340.47	80	V II	3914.33	
Fe II	4731.44	0.30	Fe II	4314.29	0.37	Si I	3905.53	1.01
He I	4713.14	1.68	Ti II	4312.86	0.26	V II	3903.27	0.16
He II	4685.68	10.44	Ti II	4307.90	0.20	Ti II	3900.55	0.29
Fe II	4666.75	0.15	Fe II	4303.17	0.46	Hζ	3889.05	36.9
C III	4651.35		Ti II	4301.93	0.17	He I	3888.65	
C III	4650.16	1.48	Ti II	4300.05	0.16	He I	3888.65 abs.	1.13
C III	4647.40		Fe II	4296.57	0.44	V II	3878.72	0.15
			Ti II	4290.22	0.28	[Ne III]	3868.77	2.32
N III	4641.90	9.44	Fe II	4278.13	0.18	Si II	3862.59	0.42
N III	4640.64		Cr II	4275.57	0.06	Si II	3856.02	0.88
N III	4634.16	5.66	Fe II	4273.32	0.25	Mg II	3850.40	0.29
Fe II	4629.34	1.32	Fe I	4271.76	0.17	Mg II	3848.24	0.22
Fe II	4620.51	0.20	Fe II	4258.16	0.32	Mg I	3838.29	0.74
Fe II	4601.34	0.07	[Fe II]	4243.98	0.29	H9	3835.39	14.87
Fe II	4583.83	2.83	Cr II	4242.38	0.09	Mg I	3832.30	0.35
Fe II	4580.06	0.04	Fe II	4233.17	1.45	Mg I	3829.35	0.20
Fe II	4576.33	0.43	Fe I	4216.19	0.37	Fe I	3827.82	0.13
Si III	4574.78	0.06	Fe II	4178.86	0.96	Fe II	3824.91	0.22
Mg I	4571.10	0.23	Fe II	4177.70	0.29	Fe I	3824.44	
Si III	4567.87	0.16	Fe II	4173.45	0.73	He I	3819.61	1.62
Cr II	4558.66	0.20	Ti II	4171.90	0.17	Si III	3806.56	0.30
Fe II	4555.89	0.80	Ti II	4163.64	0.18	H10	3797.90	10.65
Ti II	4549.62	1.24	He I	4143.76	1.04	Fe I	3787.88	0.05
Fe II	4549.47		Si II	4128.05	0.43	Fe II	3786.37	0.11
Fe II	4541.52	0.74	Fe II	4122.64	0.51	Fe II	3783.35	0.36
Fe II	4534.17	0.55	He I	4120.81	0.74	H11	3770.63	10.18
Ti II	4533.97		Si IV	4116.10	2.40	Fe II	3764.09	0.28
Fe I	4528.62	0.38	Hδ	4101.74	56	Fe I	3763.79	
Fe II	4522.63	0.85	N III	4097.31	2.41	H12	3750.15	6.45
Fe II	4520.22	0.74	N III	4097.31 abs.	0.39	Fe I	3745.69	0.41
Fe II	4515.34	1.62	Si IV	4088.86	3.12	Fe I	3743.36	0.06
Fe II	4508.28	0.67	Fe I	4071.74	0.10	Ti II	3741.63	0.12
Fe II	4491.40	0.59	Ni II	4067.05	0.24	Ca II	3736.90	0.86
Fe II	4489.18	0.39	Fe I	4063.60	0.18	H13	3734.37	4.68
He I	4471.48	7.50	N IV	4057.80	2.59	H14	3721.94	3.48
He I	4471.48 abs.†	0.79	Ti II	4053.81	0.23	Fe I	3719.94	0.18
Fe I	4461.65	0.15	Fe I	4045.82	0.16	Cr II	3715.45	0.40
Fe I	4459.12	0.10	He I	4026.19	3.64	H15	3711.97	4.10
Fe I	4427.31	0.23	He I	4026.19 abs.	0.77	H16	3703.86	2.55
Ti II	4418.34	0.14	Ti II	4012.37	0.13	H17	3697.15	1.83
Fe II	4416.82	0.43	He I	4009.27	0.47	H18	3691.56	1.81
Fe I	4415.12	0.14	Fe II	3981.61	0.07	H19	3686.83	1.69
Fe II	4413.60	0.14	He	3970.07	33.4	H20	3682.81	1.35
Ti II	4409.52	0.05	He I	3964.73	1.20	H21	3679.36	1.48
Ti II	4399.77	0.18	Al I	3961.52	0.19	Cr II	3677.82	0.58
Ti II	4395.85	0.11	V II	3951.97	0.15	H22	3676.36	1.18
Ti II	4390.98	0.18	Fe II	3945.21	0.26	H23	3673.76	1.04
Mg II	4390.58		Al I	3944.01	0.16	H24	3671.48	1.02
He I	4387.93	1.46	Fe II	3938.29	0.86	H25	3669.47	0.91
Fe II	4385.38	0.49	Fe II	3935.94	0.28	H26	3667.68	0.91
Fe II	4384.33	0.39	Ca II	3933.66	1.14	H27	3666.10	0.46
N III	4379.09	0.93	Fe II	3930.31	0.42	H28	3664.68	0.67
Fe I	4375.93	0.33	He I	3926.53	0.44	H29	3663.41	0.64
Fe II	4369.40	0.21	Fe I	3922.91	0.20	H30	3662.26	0.57

* Uncertain measures of lines partially blended with more well-defined lines have not been included. Some lines have not been measured because of small flaws on the plates.

† abs. = absorption component.

characteristic curves in the conversion to intensities, and the logarithmic intensity scale leads to inaccuracy for strong emission lines. We estimate that the absolute measures are reliable only to about 50 per cent, although the relative measures should be better than this.

Merrill has followed in detail the striking spectral changes which this star has undergone since 1920, prior to which it had a Be-type spectrum resembling that of P Cyg. From 1920 until 1950, emission lines arising from atoms in increasingly high stages of ionization have gradually appeared and strengthened, while lines of the ionized metals remained numerous and strong. Also, evidences of a low-temperature spectrum have appeared (e.g., weak *TiO* bands), resembling the "combination" spectra of stars like Z Andromedae.

There are no striking changes in the appearance of the spectrum since the last observations described by Merrill. The principal differences on our plates are: (1) the *C* III blend at λ 4650 is visible as a weak, broad emission; (2) the line at λ 4058, which Merrill identified as probably due to *N* IV, is very much stronger, and the identification seems certain; and (3) the Pickering series of *He* II is probably present as weak, broad emission lines. Thus it appears that the trend toward higher excitation is continuing.

In addition to the progressive changes, Merrill detected a periodic variation in the appearance, strength, and velocities of various lines, the period being about 800 days.

TABLE 2

VELOCITIES GIVEN BY THE EMISSION LINES

Element	No. of Lines	Velocity (Km/Sec)	Element	No. of Lines	Velocity (Km/Sec)	Element	No. of Lines	Velocity (Km/Sec)
H	25	−12.9	*He* II	1	−11.2	*Si* IV	2	−46.8
Metals I	20	−16.6	*N* III	3	−57.5	[*Fe* II]	1	− 3.0
Metals II	71	−16.4	*N* IV	1	−47.3	[*O* III]	1	+ 2.3
He I singlets	7	−15.0	*Si* I	1	−17.2	[*Ne* III]	1	+ 6.1
He I triplets	5	− 7.4	*Si* II	3	− 9.6			

If we assume this length for the cycle, we see from Merrill's curves that at the time of our observations the spectrum should show the maximum number of lines of the ionized metals and should be just past the time of maximum sharpness of the hydrogen lines, as given by the quantum number of the last resolvable Balmer line. On our plates the ionized metal lines were very sharp and numerous. The hydrogen lines near the Balmer series limit are also very sharp, while the earlier members are broadened by their very great intensity. Table 2 gives the mean velocities from the two plates for the various elements, together with the number of lines measured on the stronger plate. The number of lines on the first plate is smaller than that on the second, since the former was underexposed for all except the hydrogen lines. The velocities in Table 2 may be compared with values at the appropriate phase on Merrill's most recent velocity-curves (1951*a*). The velocities of hydrogen and the ionized metals agree well. Our velocities for *He* I and *He* II are 10 km/sec less algebraically than values from the curves, and our velocities for *N* III and *Si* IV are about 45 km/sec less. There are no curves for [*Ne* III] and [*O* III], but velocities in a table given by Merrill average about −50 km/sec, while our values are about +5 km/sec. It appears that the amplitudes, or the mean values, or both, are continuing to vary. The difference in the case of the forbidden lines is most remarkable.

II. THE BALMER DECREMENT AND THE EXTENT OF THE EMITTING REGION

The relative energies emitted in the hydrogen lines were obtained from the equivalent widths in Table 1 by assuming that the continuous spectrum came from an underlying

star radiating as a black body at 50,000°. Estimates of the temperatures of Wolf-Rayet and related stars are notoriously uncertain, but we believe that the temperature of AG Peg should lie near this value (see Zanstra and Weenen 1950). The calculated Balmer decrement agrees approximately with that calculated by Baker and Menzel (1938) for a gaseous nebula at an *electron* temperature of 20,000°. (This temperature is probaby a reasonable value for the electron temperature in the region where the emission lines arise in AG Peg; in any case, the calculated decrement is insensitive to assumed electron temperature.) The values are given in Table 3 and are referred to $H\gamma$ as unity because of the greater uncertainty in the equivalent width of $H\beta$.

Recently we showed (1953*b*) that the Balmer decrement for emission lines from the higher quantum levels in certain normal Be stars differed from the predicted nebular decrement by factors of the order of 10 (about 30 in the case of 12 Aur), in the sense that the lines from higher quantum levels were too strong. We showed that this was perhaps

TABLE 3

THE BALMER DECREMENT

Line	Observed Decrement	Calculated Nebular Decrement (Baker and Menzel)	Line	Observed Decrement	Calculated Nebular Decrement (Baker and Menzel)	Line	Observed Decrement	Calculated Nebular Decrement (Baker and Menzel)
$H\beta$	1.6	2.00	$H13$	0.10	.....	$H22$	0.027	.....
$H\gamma$	1.00	1.00	$H14$	.076	.....	$H23$	.024	.....
$H\delta$	0.87	0.60	$H15$	.090	0.042	$H24$	.023	.....
$H\epsilon$	0.58	0.384	$H16$	.056	.....	$H25$	.021	0.010
$H\zeta$	(0.68)*	0.260	$H17$	.041	.....	$H26$	.021	.....
$H9$	0.27	0.186	$H18$	.041	.....	$H27$	.011	.....
$H10$	0.22	0.138	$H19$	.038	.....	$H28$	.015	.....
$H11$	0.21	.....	$H20$	.031	0.920	$H29$	.015	.....
$H12$	0.14	.....	$H21$	0.033	.....	$H30$	0.013	0.006

* Blended with *He* I.

due to self-absorption effects in the star's tenuous outer atmosphere for lines from the lower quantum levels. Since the Balmer decrement in AG Peg is relatively close (within a factor of 2) to the predicted nebular one, self-absorption effects should be unimportant, and the emitting region must be more tenuous and much more extensive than that around normal Be stars. In a previous paper (1953*b*) we developed an approximate method of determining the extent of such a region, using the Balmer emission lines; and this will be used for AG Peg.

We shall assume that the outer tenuous atmosphere has spherical symmetry and a radius aR_*. From the Inglis-Teller formula (Inglis and Teller 1939), we find that, since the last resolvable hydrogen line is $H30$, then $n_e = 1.5 \times 10^{12}$. Using a value of $T_e = 20{,}000°$ in the extended atmosphere to derive the electron pressure, and a photospheric temperature for the central star of $T = 50{,}000°$, we can use the Saha equation,

$$\log\left(\frac{N_{H^+}}{N_H}\right) = -13.54\,\theta + 2.5\log T - 0.48 - \log p_e + \log W,$$

to determine a relation between the dilution factor W and the degree of ionization and hence N_H (since $N_{H^+} = n_e$). We also have (Burbidge and Burbidge 1953*a*, eq. [11])

$$V N_n = 8\pi^2 c R_*^2 \frac{w}{\lambda^4 A_{n2}\left(e^{h\nu/kT} - 1\right)}$$

for each Balmer line, where V is the total volume of the emitting region, N_n is the number of atoms in level n, and the other symbols have their usual meaning, and

$$V = (a^3 - 1)\tfrac{4}{3}\pi R_*^3.$$

The equivalent widths, w, are measured, and we assume that $R_* = 5\,R_\odot$, which is a reasonable value for a dwarf star of this temperature. [Beals (1951), from estimates of interstellar line strengths, assigned an absolute magnitude of -2.4 to AG Peg.] Hence the quantities in the right-hand side of the equation for VN_n are all known, and we have obtained ΣVN_n for all the Balmer lines excepting $H\alpha$, which in any case would be expected to give the smallest contribution and can easily be neglected. (VN_n increases with increasing n, and, for example, $H\beta$ contributes less than 0.001 of the sum.) Since $\Sigma N_n = N_H$, we are able to substitute a value for N_H determined from the Saha equation, and hence V and therefore a can be found.

For $a \gg 1$ the dilution factor at a distance $(a - 1)R_*/2$ is $W \simeq 1/a^2$; therefore, in practice we initially assumed a value for W to use in the Saha equation and hence determined N_H, which was then used to determine V and a. By a series of successive approximations, we found that a value of $a \simeq 400$ gives reasonable agreement for the parameters involved. Thus the result of this approximate calculation is that the radius of the outer atmosphere of AG Peg is about 400 stellar radii.

This is likely to be a minimum value, for the following reasons: First, the value of n_e obtained from the Inglis-Teller formula may be too large, since by using the formula we have assumed that the whole of the broadening is due to interionic Stark effect, i.e., we have not taken into account any macroscopic motions which may contribute. Second, we have assumed that the hydrogen emission lines arise throughout the whole of the extended atmosphere, while, in reality, recombination will not occur in the region adjacent to the hot stellar surface.

III. THE MAGNETIC FIELD

We think it reasonable to suppose that the *Fe* II emission lines arise in the same part of the extended atmosphere, within broad limits, as do the lines of hydrogen. Reasons for this are that both sets of lines have very sharp and narrow profiles (excluding, of course, the extremely intense earlier Balmer members), in distinction to the high-excitation lines, on the one hand, and the forbidden lines, on the other. The ionization potentials are similar, and *Fe* II emission lines are often associated with hydrogen emission lines in normal Be stars.

Now Babcock detected and measured the magnetic field from the Zeeman effect in the emission lines of *Fe* II (private communication) at a time when they were narrow and strong (as they were when observed by us). Since the variable field measured was of the order of 1000 gauss, it follows that we have here indirect evidence that a magnetic field of this order has at some time existed at a distance of several hundred stellar radii from the surface of the hot star. It would seem to follow on very general grounds that this field has its origin in the central field of the star, which would probably be several orders larger than 1000 gauss. No quantitative argument can be developed at the present time to determine the magnitude of such a field. We can make a very approximate estimate by supposing that the magnetic-energy densities and the material densities are proportional in the outer atmosphere and at the surface of the central star. For this we need to know the photospheric density in the central star, and this cannot be measured. For an *assumed* density of 10^{16} hydrogen atoms/cc and a density of 10^{12} hydrogen atoms/cc for the outer atmosphere (from the Inglis-Teller formula), the method would give a field of the order of 10^5 gauss in the star's photosphere. We can also suppose that the measured field, which is variable, has appeared in the outer regions because of currents circulating in these regions and that it is a transient effect. It is likely that such transient fields would

have their origin in large "spot" regions on the stellar surface. In any case, at the times when these magnetic fields are observed, the magnetic forces will exercise a very powerful influence on the shape and the motions of the tenuous outer region.

IV. CONCLUSIONS

It is important to make some remarks concerning the brightness variations of this star. Slow variations amounting to about 3 mag. have been recorded since 1820 (Payne-Gaposchkin 1950; Rigollet 1947). We have previously discussed the 800-day cycle discovered by Merrill. Rigollet (1947) has published a series of measures of the brightness of AG Peg in 1945 and 1946. He found a range of brightness of $\frac{3}{4}$ mag., and these variations were not inconsistent with an 800-day cycle in brightness as well as in spectrum variations. If the 800-day cycle were taken as representing a pulsation of the central system, then the period would be extremely long compared to any reasonable value for an adiabatic period. The star does not appear to be a giant. As we have remarked before, the assigned absolute magnitude is -2.4. Thus the star is very different from P Cyg, which it resembled spectroscopically before 1920 and which is 4–6 mag. brighter than this.

The most remarkable features are the huge extent of the emitting atmosphere and the probability that sometimes there exists a large magnetic field in the central star. In connection with this latter point, it is interesting to speculate on the probable effect of such a field. One of us (G. R. Burbidge 1954) has recently completed some calculations on the dynamical stability of a star having a magnetic field. These calculations were based on the work of Chandrasekhar and Fermi (1953). For a decay field in a solar-type model, we have found that the critical field for instability is of the order of 10^8 gauss for the lowest mode of excitation ($n = 1$). For a model consisting of a sphere having a uniform electrical conductivity, the surface field is of the same order. Such a calculation gives a rough theoretical upper limit to the surface field in AG Peg, since, although the star has been shown historically to be an unstable object, there has been no violent instability which would be characteristic of dynamical instability.

Chandrasekhar and Fermi (1953) have also shown that a star having a strong magnetic field will tend to take up a spheroidal shape, the degree of flattening depending on the strength of the field. It is possible, therefore, that the system of AG Peg may be flattened to some extent.

Unfortunately, we have no direct evidence of physical conditions at the surface of the central star, since no normal photospheric absorption lines are visible (prior to 1919, there were normal weak absorption lines of *He* I). The origin of the *TiO* bands and other indications of a "combination" spectrum are unknown; they might even arise in a companion star whose orbit might lie some distance within the extended atmosphere of the hot star.

Our attention has been drawn to a recent paper by Tcheng Mao-Lin and Bloch (1952) containing an account of the spectrum of AG Peg in 1951. In this paper a list is given of the intensities of the principal emission lines between *Hα* and *H*9, in arbitrary units. The authors remarked that the Balmer decrement agreed fairly well with the nebular decrement calculated by Baker and Menzel; but agreement over this range is not significant, since departures from the predicted decrement become noticeable usually only for levels of $n > 10$.

They measured the color temperature of the star and derived the low value of 7700°, uncorrected for interstellar reddening, indicating considerable intrinsic reddening similar to that observed in P Cyg and at times in γ Cas. Our assumed temperature of 50,000° was derived from the spectral lines arising deep within the emitting region and may thus be too high for the black-body temperature of the light finally leaving the star. If $T = 25{,}000°$, the decrement given in Table 3 will be practically unchanged. If $T = 10{,}000°$, the values for high n should be approximately halved, and the observed decrement approaches closer to the theoretical nebular one. If $T = 10{,}000°$, the calculated

energies in the Balmer emission lines are too large, and the effect of this alone on the extent of the emitting region would be to reduce it by a factor of the order of 5, although this is an upper limit, since we have not here allowed for the increased effective stellar radius due to lack of transparency of the inner emitting region. Further, the consequent adjustment to the dilution factor and electron pressure in the Saha equation will tend to increase the extent of the emitting region; and, in view of the approximate nature of the calculation, we conclude that the dimensions of the emitting region will not be altered.

The material on which this study is based forms part of a program of spectrophotometry of magnetic stars, begun while the authors were working at the Yerkes and McDonald Observatories. We are deeply grateful to Dr. H. W. Babcock for information and advice about this and other magnetic stars. We wish to thank Dr. L. Goldberg and Dr. D. B. McLaughlin for the use of a plate-measuring machine at the Observatory of the University of Michigan while we were attending the symposium on astrophysics at Ann Arbor. We also wish to thank Dr. S. Chandrasekhar for the stimulation provided by his work and discussions on magnetic objects.

REFERENCES

Babcock, H. W., and Cowling, T. G. 1953, *M.N.*, **113**, 357.
Baker, J. G., and Menzel, D. H. 1938, *Ap. J.*, **88**, 52.
Beals, C. S. 1951, *Pub. Dom. Ap. Obs. Victoria*, Vol. **9**, No. 1.
Burbidge, G. R. 1954, *Ap. J.* (in preparation).
Burbidge, M., and Burbidge, G. 1953*a*, *Ap. J.*, **117**, 407.
Burbidge, M., and Burbidge, G. 1953*b*, *Ap. J.*, **118**, 252.
Chandrasekhar, S., and Fermi, E. 1953, *Ap. J.*, **118**, 116.
Gaposchkin, C. P. 1950, *Harvard Ann.*, **115**, 233.
Inglis, D., and Teller, E. 1939, *Ap. J.*, **90**, 439.
Mao-Lin, T., and Bloch, M. 1952, *Ann. d'ap.*, **15**, 104.
Merrill, P. W. 1916, *Michigan Obs. Pub.*, **2**, 71.
Merrill, P. W. 1929, *Ap. J.*, **69**, 330.
Merrill, P. W. 1932, *Ap. J.*, **75**, 413.
Merrill, P. W. 1942, *Ap. J.*, **95**, 386.
Merrill, P. W. 1951*a*, *Ap. J.*, **113**, 605.
Merrill, P. W. 1951*b*, *Ap. J.*, **114**, 338.
Rigollet, R. 1947, *Bull. Soc. astr. de France*, **61**, 247.
Struve, O., and Swings, P. 1940, *Ap. J.*, **91**, 546.
Struve, O., and Swings, P. 1942*a*, *Ap. J.*, **95**, 112.
Struve, O., and Swings, P. 1942*b*, *Ap. J.*, **95**, 134.
Struve, O., and Swings, P. 1942*c*, *Ap. J.*, **95**, 152.
Struve, O., and Swings, P. 1942*d*, *Ap. J.*, **96**, 254.
Struve, O., and Swings, P. 1943, *Ap. J.*, **97**, 194.
Struve, O., and Swings, P. 1944, *Ap. J.*, **99**, 205.
Zanstra, H., and Weenen, J. 1950, *B.A.N.*, **11**, 165.

THE WIDTH OF *Hα* IN SOLAR FLARES*

LEO GOLDBERG, HELEN W. DODSON, AND EDITH A. MÜLLER
McMath-Hulbert Observatory, University of Michigan, Pontiac, Michigan
Received February 1, 1954

ABSTRACT

It is shown that the observed large widening, at or near maximum, of the *Hα* emission line in certain solar flares can be explained as a consequence of radiation damping and the high abundance of two-quantum *H* atoms in the line of sight. When the effective width of the *Hα* line is calculated according to the theory of self-absorption, the assumption of radiation damping leads to agreement with the observed lines widths when the number of two-quantum *H* atoms lies in the approximate range 10^{15}–10^{16} per cm^2 in the line of sight. If it is assumed that the lateral extension of a flare is large compared with its thickness, the theory predicts that the effective width of *Hα* should be proportional to the square root of sec θ, where θ is the angular distance from the center of the solar disk. Study of the *Hα* line widths of 610 flares reported in the *Quarterly Bulletin* of the I.A.U. for the period January, 1949, through June, 1952, reveals that the average line width increases steadily with increasing central meridian distance of the flares. Furthermore, flares with exceptionally wide lines ($\geq$4.0 A) are observed most often in flares 45° or more from the central meridian. The relation between effective line width and central intensity found by Ellison is explained as primarily a consequence of self-absorption. Finally, the existing observational evidence in favor of the Stark effect as an important cause of the line broadening is examined and found unconvincing.

INTRODUCTION

It is an observed fact that for certain solar flares the *Hα* line is very wide at or near flare maximum. According to Ellison (1953), the *Hα* line width at peak central intensity varies, on the average, from about 3.0 A for a flare of importance 1 to about 16 A for a flare of importance 3+. A width as great as 22 A was reported (Ellison and Conway 1950) for the flare of November 19, 1949. The line width has been found to be roughly proportional to the central intensity up to intensity values equal to about 1.5 times the neighboring continuum, but thereafter the line width increases more rapidly with increasing central intensity (Ellison 1949). The width of *Hα* undergoes variations with time that are in phase with changes in the central *Hα* intensity, the two quantities having simultaneous maxima (Ellison 1950). Usually, the decrease in line width immediately after flare maximum is more rapid than the decrease in central intensity. Except for a weakening in the blueward wing, the widened line is essentially symmetrical with respect to the normal position of *Hα* (Ellison 1949), but, in major flares, it exhibits a central self-reversal. Ellison and Hoyle (1947) attribute the large observed line widths to the Stark effect, on the grounds that thermal widening is unlikely, since it would require a temperature of the order of a million degrees. According to the Kodaikanal observers (Rao *et al.* 1949; Ellison 1949), the Stark-effect hypothesis is contradicted by their observation that *Hα* was wider than *Hβ* in the spectrum of the flare of October 3, 1949. On the other hand, Mustel and Severny (1952) find that the profiles of *Hγ*, *Hδ*, and *Hε*, observed during the flare of August 5, 1949, are qualitatively consistent with Stark broadening, inasmuch as the line widths appear to increase with serial number. The *Hα* profile, however, is best fitted by a thermal Doppler core with $T = 11{,}000°$ K and by wings broadened by radiation damping. It should be mentioned, finally, that Bruce (1949) explains the line broadening as a consequence of the Zeeman effect, a hypothesis which requires magnetic fields of about 10^5 gauss.

Whether or not the Stark effect is an appreciable factor in the line formation, it appears not to have been previously emphasized that the most important cause of the large

* Supported in part by Contract N6-ONR-232-V with the Office of Naval Research.

Hα line widths is the great abundance of two-quantum hydrogen atoms. The half-width of a weak emission line is essentially independent of the number of absorbing or emitting atoms. It can be shown (Mustel and Severny 1952), however, that the optical depth at the center of *Hα* during the maximum of a bright flare is about 500. The line must therefore be strongly self-absorbed, and its width will depend on $(N_2)^n$, where n is equal to $\frac{1}{2}$ for radiation (or collision) damping and to $\frac{2}{5}$ for Stark broadening, and N_2 is the total number of two-quantum *H* atoms in the line of sight.

The importance of the abundance factor may be illustrated by reference to Ellison and Hoyle's (1947) argument in favor of the Stark effect as the widening mechanism for *Hα*. On the assumption that the electron density of the flare gas is 10^{13} per cubic centimeter, they calculate the number of two-quantum *H* atoms per cubic centimeter from the Saha equation with $T = 4830°$ K. They further assume that the thickness of the flare-emitting layer is 500 km, and they obtain $N_2 = 5 \times 10^{16}$ cm^{-2} for the number of two-quantum atoms in the line of sight. With these values of N_2 and the electron density, the absorption coefficient calculated with the Holtzmark formula is as large as 0.2 at a distance of 4.1 A from the center of *Hα*. The calculated broadening is therefore of the same order of magnitude as that which is observed in flares. But this argument for the presence of the Stark effect is not convincing, unless it can be shown that other competing causes of line broadening, which involve fewer assumptions, are inadequate. There is general agreement that thermal broadening alone can be ruled out because of the high temperatures required. On the other hand, the calculation of line-wing broadening by radiation damping requires no assumptions other than of a value for N_2. For example, if we adopt Ellison and Hoyle's value, $N_2 = 5 \times 10^{16}$ cm^{-2}, the absorption coefficient at $\Delta\lambda = 4$ A due to radiation damping alone is 0.17. Hence the agreement with observation which Ellison and Hoyle obtained on the basis of the Stark effect results primarily from their choice of a sufficiently high value of N_2. It will be shown later that the observed large widths of *Hα* in solar flares can be explained as arising from radiation damping alone and that existing data are not adequate to reveal what role, if any, is played by the Stark effect.

DEPENDENCE OF LINE WIDTH ON CENTRAL MERIDIAN DISTANCE

Inasmuch as the width of a self-absorbed emission line depends on the number of absorbing atoms in the line of sight, the width of *Hα* in solar flares may be influenced by the position of the flare on the solar disk. If the lateral extension of the flare is large compared with its thickness, the length of the absorbing (or emitting) column will be proportional to sec θ, where θ is the angular distance of the flare from the center of the solar disk. It is clearly not to be expected that flares with wide *Hα* will be found only close to the limb, since other factors, such as the temperature, pressure, and thickness of the flare-emitting layer, will also have a strong influence on the number of excited *H* atoms. Hence any correlation between line width and central meridian distance will be statistical rather than one-to-one in nature.

Reports of the width of *Hα* at the time of flares are available in the *Quarterly Bulletin* from January, 1949, through June, 1952. During this period, 2295 flares were reported, and measures of *Hα* widths are given for 1138 of them. Since the *Hα* line often undergoes a very brief period of maximum width, it is important to study, first, those flares for which the period of maximum line width and intensity was included in the observation. For most flares, maximum follows very shortly after the start of the flare. We have therefore selected for particular study those flares for which either the start or the maximum was definitely reported as observed and for which concomitant measures of line width are given. There are 610 such flares reported in the *Quarterly Bulletin*. When two or more observers reported measures of *Hα* width at maximum, the values have been averaged. If any subsequent measure of *Hα* width was greater than that reported for

maximum, the greater value was also included in deriving the "maximum" value of *Hα* for the flare in question.

Table 1 and Figures 1 and 2 summarize the data for the width of *Hα* at flare maximum. There is a steady increase in average line width with increasing central meridian distance of the flares. The values range from 2.48 A at the center to 3.93 A at the limb. The fact that *Hα* is much wider, on the average, for flares of importance 2 and 3 than for flares of importance 1 is clearly shown in Figure 2. Nevertheless, flares of importance 1, as well as those of importance 2 and 3, exhibit the dependence of line width on position of the flare on the solar disk. The values for zone 81°–90° suggest that estimates of importance for flares very close to the limb are unreliable.

TABLE 1

AVERAGE WIDTH OF *Hα* AT FLARE MAXIMUM

CENTRAL MERIDIAN DISTANCE	NUMBER OF FLARES			AVERAGE WIDTH OF *Hα* AT FLARE MAXIMUM (A)		
	Imp. 1	Imp. 2 and 3	Total	Imp. 1	Imp. 2 and 3	Total
0°	5	.....	5	2.48	.....	2.48
1°–10°	68	18	86	2.45	3.66	2.71
11–20	54	15	69	2.53	3.29	2.69
21–30	46	23	69	2.56	3.49	2.87
31–40	65	17	82	2.60	4.12	2.91
41–50	53	27	80	2.73	4.03	3.17
51–60	67	24	91	2.80	4.69	3.30
61–70	56	15	71	2.99	5.24	3.47
71–80	31	9	40	2.89	6.00	3.59
81–90	12	5	17	3.80	4.24	3.93
Total	457	153	610	2.71	4.19	3.08

The distribution on the solar disk of flares with wide *Hα* is very different from that of flares in general. All flares reported between January, 1949, and June, 1952 (2295 flares), show slowly decreasing numbers on the solar disk out to a central meridian distance of 70°. The diminution in observed numbers near the limb is then sharp and definite. Similar distributions are found when the counts are restricted to those flares for which *Hα* width has been measured (1138 flares), or to the 610 flares for which the width of *Hα* was measured at maximum. For flares of importance 2 and 3 (354 flares), the diminution in observed numbers with increasing distance from the center is even more marked. In contrast to the above distributions, the percentage of flares for which the width of *Hα* is reported by any observer as ≥ 4.0 A rises to a maximum at the 51°–60° zone (see Tables 2 and 3 and Fig. 3).

If it is assumed that flares occur in equal numbers at all distances from the central medidian, the apparent diminution in the number of flares near the limb must then be taken to indicate an observational effect. The factor required to bring the observed distribution to a uniform display can be determined for each zone. When such factors, derived from the distribution of all (2295) flares, are applied to the observed numbers of flares with *Hα* width ≥ 4.0 A, the percentage distribution of flares with wide lines steadily increases from center to limb (see Fig. 1). When similar studies are made for flares with *Hα* $\geq$ 6, 8, and 10 A, respectively, there is further evidence that exceptionally wide *Hα* lines are observed most often in flares 45° or more from the central meridian.

In the foregoing statistics and figures, flare positions have been divided into nine

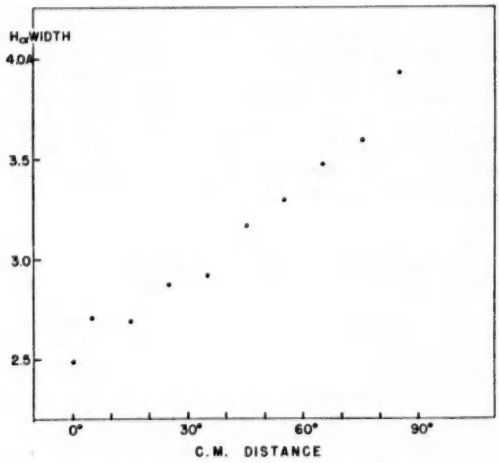

FIG. 1.—Width of *Hα* at flare maximum averaged for 10° intervals of central meridian distance. Based on all flares (610) for which this measurement is given in the *Quarterly Bulletin of Solar Activity*, January 1, 1949—June 30, 1952.

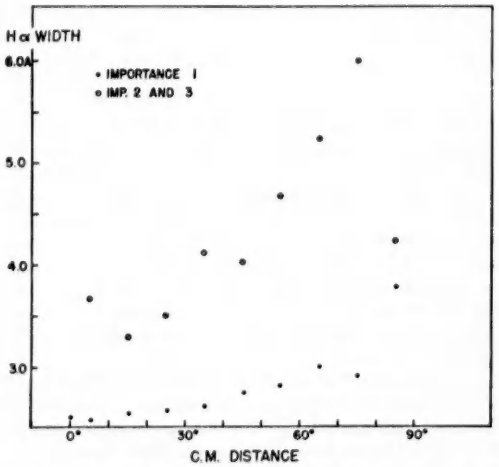

FIG. 2.—Average width of *Hα* at maximum versus central meridian distance for flares in different importance categories. Based on data in *Quarterly Bulletin*, January 1, 1949—June 30, 1952.

TABLE 2

Distribution of Flares on Solar Disk

Central Meridian Distance	Number of Flares Reported in *Quarterly Bulletin*, Jan. 1, 1949—June 30, 1952							
	All Flares	Flares of Imp. 2 and 3	Flares for Which $H\alpha$ Width Was Measured					
			All Cases	With Measurement at Flare Maximum	All Flares with $H\alpha$ Width			
					≤ 4 A	≤ 6 A	≤ 8 A	≤ 10 A
(0°)	(12)	(2)	(6)	(5)	.....	.....	.....	.....
1°–10°	339	57	158	86	8	2	1	.....
11 –20	277	43	139	69	12	1	.....	.....
21 –30	300	54	143	69	12	3	.....	.....
31 –40	287	42	133	82	8	3	.....	.....
41 –50	273	48	140	80	22	6	2	.....
51 –60	276	40	143	91	30	10	2	1
61 –70	247	35	136	71	20	7	3	2
71 –80	160	21	95	40	18	5	2	2
81 –90	124	12	45	17	15	7	1	.....
Total	2295	354	1138	610	145	44	11	5

TABLE 3

Percentage Distribution of Flares on Solar Disk

Central Meridian Distance	Percentage of Flares Reported in *Quarterly Bulletin*, Jan. 1, 1949—June 30, 1952							
	All Flares	Flares of Imp. 2 and 3	Flares for Which $H\alpha$ Width Was Measured					
			All Cases	With Measurement at Flare Maximum	All Flares with $H\alpha$ Width			
					≤ 4 A	≤ 6 A	≤ 8 A	≤ 10 A
(0°)	(0.5)	(0.6)	(0.5)	(0.8)	.....	.....	.....	.....
1°–10°	14.8	16.1	13.9	14.1	5.5	4.6	9.1	.....
11 –20	12.1	12.1	12.2	11.3	8.3	2.3	.....	.....
21 –30	13.1	15.2	12.6	11.3	8.3	6.8	.....	.....
31 –40	12.5	11.9	11.7	13.5	5.5	6.8	.....	.....
41 –50	11.9	13.6	12.3	13.1	15.2	13.6	18.2	.....
51 –60	12.0	11.3	12.6	14.9	20.7	22.7	18.2	20.0
61 –70	10.7	9.9	11.9	11.6	13.8	15.9	27.2	40.0
71 –80	7.0	5.9	8.3	6.6	12.4	11.4	18.2	40.0
81°–90°	5.4	3.4	4.0	2.8	10.3	15.9	9.1	.....

zones, 1°–10°, 11°–20°, etc., and the isolated case 0°. The twelve flares in the zero position have been excluded from the diagrams in the top line of Figure 3. There were no flares with *Hα* as wide as 4.0 A at position 0°.0.

INTERPRETATION OF THE *Hα* LINE WIDTHS

In all discussions of the *Hα* line width in solar flares, it must be remembered that the measured width is not the half-intensity width but is defined by the minimum distance from the line center at which the observer can no longer detect any difference in intensity between the flare emission and the residual emission in the absorption line arising from the undisturbed disk. Relatively few line widths have been measured photo-

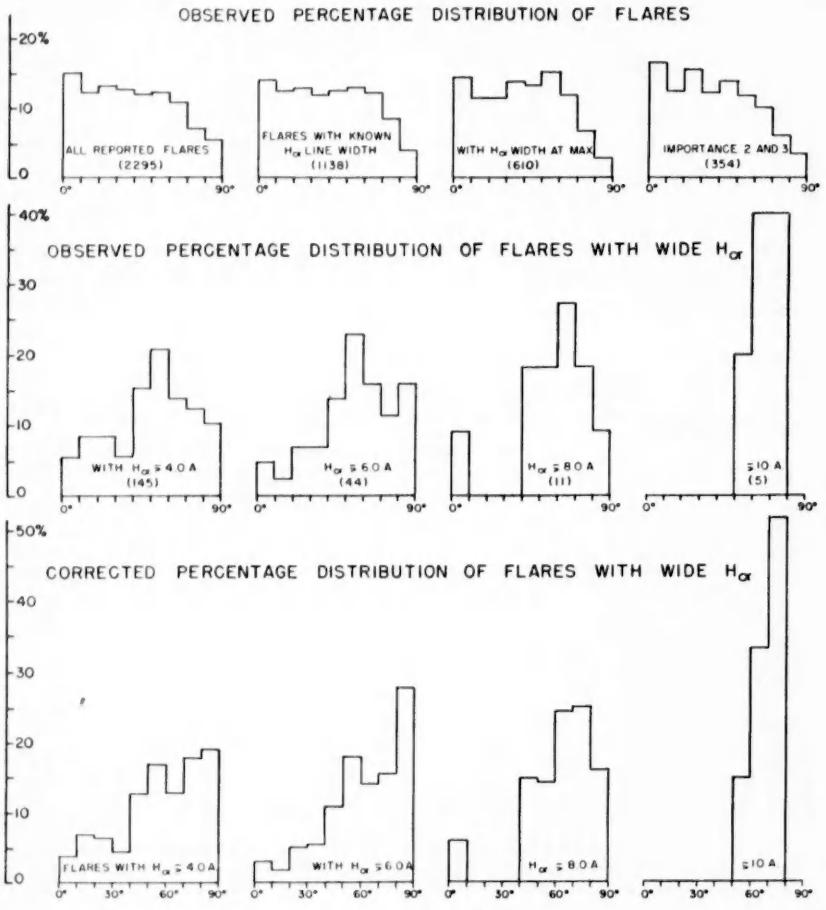

FIG. 3.—Percentage distribution on solar disk of all flares, and flares with *Hα* equal to or greater than 4.0 A. Based on data in *Quarterly Bulletin*, January 1, 1949—June 30, 1952.

graphically; most observations have been carried out visually with the spectrohelioscope. The observer displaces the second slit away from the center of the line until the contrast between the flare and the surrounding disk appears to be zero and then notes the wave-length displacement. The *effective width* is defined as twice this displacement.

In this section we shall derive a theoretical expression for the effective width of $H\alpha$, making use of the theory of self-absorption. As pointed out by van de Hulst (1953), it is important to distinguish between *self-absorption* and *self-reversal*. Self-absorption can occur even in an isothermal gas and arises because radiation emitted by atoms at the far end of a gas column is absorbed by intervening atoms before it can emerge. The effect of self-absorption on an emission line is to suppress the central intensity, which, in fact, cannot exceed the intensity given by the Planck function at the gas temperature. Once the central intensity reaches saturation, the further addition of atoms to the gas column serves only to widen the line. Self-reversal occurs in the presence of a temperature gradient. When a hot mass of gas is surrounded by cooler layers, the emission profiles show absorption lines at their centers. Both self-absortion and self-reversal undoubtedly occur in flares. Self-reversal is conspicuous in many of the $H\alpha$ profiles observed by Ellison (1953) and by Mustel and Severny (1952), although the latter state incorrectly that the central self-reversals are only apparent and that they result from the superposition of the emission profile of the flare on the absorption profile of the undisturbed disk.

For the present, we shall omit consideration of the central self-reversal and assume that the flare-emitting layer is isothermal. We shall assume further that the flare is elevated above the photosphere to the extent that the absorption profile of $H\alpha$ from the disk below is identical with that of the surrounding undisturbed areas. Finally, the thickness of the flare region is supposed to be small compared with its lateral extension, and energy is assumed to be taken from the outgoing beam by absorption only. With these assumptions, the expression for the intensity at each point in the emission profile is similar to that given by Menzel (1931) for the chromosphere, namely,

$$E_\nu = A_\nu e^{-\tau_\nu \sec\theta} + P_\nu (1 - e^{-\tau_\nu \sec\theta}) , \tag{1}$$

with

$$\tau_\nu = N_2 a_\nu . \tag{2}$$

In equations (1) and (2), E_ν is the intensity per unit frequency, A_ν is the residual intensity in the undisturbed $H\alpha$ absorption profile, N_2 is the total number of neutral hydrogen atoms per square centimeter in the first excited state, a_ν is the line-absorption coefficient per excited atom, and θ is the angular distance from the central meridian. P_ν is understood to be a constant over the line and, in thermal equilibrium, is given by the Planck function:

$$P_\nu = \frac{2h\nu^3}{c^2} \frac{1}{e^{h\nu/kT} - 1} , \tag{3}$$

where T is the gas temperature. Even in the general case of nonthermal equilibrium, P_ν is also given by equation (3), in which T is the excitation temperature required to represent the populations of the upper and lower levels by the Boltzmann equation (Suemoto 1951). At the center of a very strong line, where $\tau_\nu \gg 1$, E_ν is equal to P_ν.

Referring to equation (1), we see that the effective line width is defined by the point on the line profile where $E_\nu - A_\nu$ approaches zero. As a practical matter, the observer with the spectrohelioscope can probably distinguish intensity differences of the order of 5 per cent (Ellison 1953). Hence the measured line widths can be assumed to refer to the point on the profile where $E_\nu - A_\nu = 0.05$.

In calculating the effective line width, we shall distinguish between weak lines whose central emission intensities are considerably less than P_ν and very strong lines which are completely saturated at their centers. In both cases we are chiefly interested in the

line wings, where the optical depths are very small. When $\tau_\nu \ll 1$, equation (1) may be written as

$$E_\nu - A_\nu = (P_\nu - A_\nu)\, \tau_\nu \sec\theta\,. \tag{4}$$

For weak lines, $N_2 \sec\theta$ is small, and the absorption coefficient may be assumed to be given by thermal broadening, namely,

$$\tau_\nu = \tau_{\nu_0} \exp\left\{-\left(\frac{\nu-\nu_0}{\Delta\nu_D}\right)^2\right\}, \tag{5}$$

where τ_{ν_0} is the optical depth at the center of the line:

$$\tau_{\nu_0} = \frac{\pi e^2}{m\,c} f \frac{N_2}{\pi^{1/2}\Delta\nu_D}\,. \tag{6}$$

In equations (5) and (6), $\Delta\nu_D$ is the Doppler displacement corresponding to the most probable atomic velocity. Combining equations (4) and (5), we obtain

$$E_\nu - A_\nu = (P_\nu - A_\nu)\, \tau_{\nu_0} \sec\theta \exp\left\{-\left(\frac{\nu-\nu_0}{\Delta\nu_D}\right)^2\right\}. \tag{7}$$

When equation (7) is solved for the line width at intensity E_ν, we have

$$\frac{2\,(\nu-\nu_0)}{\Delta\nu_D} = \frac{2\,(\lambda-\lambda_0)}{\Delta\lambda_D} = 2\left[\frac{1}{0.4343}\log\frac{(P_\nu - A_\nu)}{(E_\nu - A_\nu)}\,\tau_{\nu_0}\sec\theta\right]^{1/2}. \tag{8}$$

For weak lines, the width thus depends only very slightly on $N_2 \sec\theta$ and is, in fact, very nearly constant and equal to $2\Delta\lambda_D$ over a considerable range of the other parameters.

For strong lines, when $N_2 \sec\theta$ is very large, we assume that the line wings will be broadened by radiation damping and hence

$$\tau_\nu = \frac{\pi e^2}{m\,c} f N_2 \frac{\Gamma}{4\pi^2}\frac{1}{(\nu-\nu_0)^2}. \tag{9}$$

Numerically, with the damping constant $\Gamma = 5.66 \times 10^8\ \mathrm{sec}^{-1}$,

$$\tau_\nu = 2.45 \times 10^5 \frac{N_2}{(\nu-\nu_0)^2}. \tag{10}$$

Again making use of equation (4), we find, for the line width,

$$2\,(\lambda-\lambda_0) = 1.42 \times 10^{-8}\left(\frac{P_\nu - A_\nu}{E_\nu - A_\nu}\right)^{1/2}(N_2 \sec\theta)^{1/2}. \tag{11}$$

The *Hα* line at the maximum of a bright flare is undoubtedly saturated, and therefore the line width will be given by equation (11). Since the width is proportional to $(N_2 \sec\theta)^{1/2}$, the abundance factor is of relatively great importance in the line broadening. Also, for flares observed near the limb ($\sec\theta \sim 10$), the line widths are predicted to be greater by about a factor of 3 than for those at the center of the disk. Although existing data are inadequate for a quantitative test, there is little doubt of the presence of the limb effect in Figures 1–3.

Two further points of interest are visible in equation (11). First, the dependence of the line width on $P_\nu - A_\nu$ means that the line width will, in general, be small when $P_\nu \sim A_\nu$, i.e., when P_ν is in the neighborhood of unity. As shown by equation (1), when $P_\nu = A_\nu$, the emission at frequency ν is just balanced by the lowering of the underlying absorption profile. This means that flares will not exhibit very wide *Hα* unless the central

intensity appreciably exceeds the continuum value. Second, the dependence on $E_\nu - A_\nu$ suggests that line widths observed with the spectrohelioscope will vary considerably among different observers, perhaps by a factor of 2, according to their ability to distinguish small differences in intensity.

Equations (8) and (11) may now be employed for the calculation of effective line widths for various values of N_2 and P_ν. As noted above, we define the effective width by the point on the emission profile where $E_\nu - A_\nu = 0.05$. For A_ν we have taken the values given by de Jager (1952) for the undisturbed center of the disk. When more detailed comparison with observation is required, account must be taken of the dependence of A_ν upon θ; but the present calculations will be performed for sec $\theta = 1$. Three values of

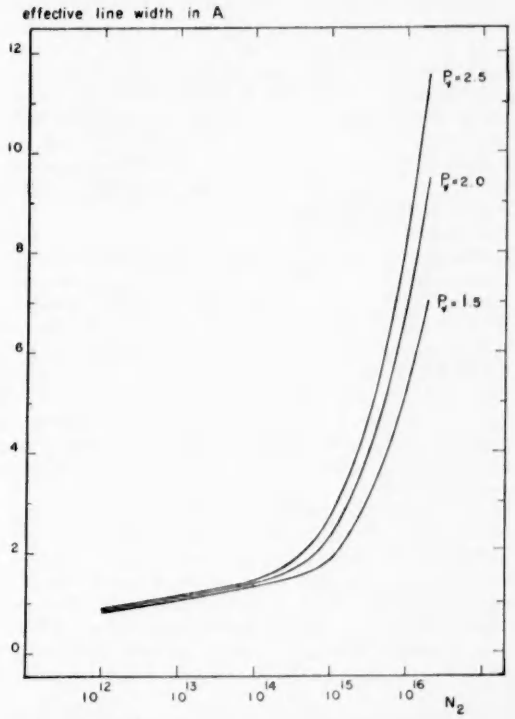

FIG. 4.—Relation between effective line width for $H\alpha$ and number of two-quantum hydrogen atoms

P_ν were chosen, namely, 1.5, 2.0, and 2.5. According to Ellison (1953), these values correspond, on the average, to flares of classes 1, 2, and 3, respectively, although the spread in P_ν is considerable in each class. For $\Delta\lambda_D$ we adopted the value 0.25 A, corresponding to a kinetic temperature of 8000° K. A rough approximation to the temperature is sufficient, since it controls the widths of only the weak lines.

The calculated relation between the effective line width and N_2 is shown in Figure 4. When N_2 is in the neighborhood of 10^{15}, neither equation (8) nor equation (11) is valid, and in this range the line widths were obtained graphically from calculated profiles.

When the dependence of the line width on sec θ is taken into account, it appears from Figure 4 that the observed variation in line width at peak central intensity of from 1 to 16 A corresponds to a variation of about 10^{15}–10^{16} in N_2. By comparison, the value of N_2 determined for the undisturbed chromosphere by Cillié and Menzel (1935) is 2×10^{12}. The curves also suggest an explanation for the observed relation between the effective line width and the central intensity, derived by Ellison (1953) from simultaneous visual observations made with a photometer and line shifter. Ellison has found that, on the average, the effective line width at flare maximum is correlated with the central intensity at maximum. This relation is predicted by theory if we suppose that the lines are saturated at maximum, since the effective line width, for a constant value of N_2, is proportional to $(P_\nu - A_\nu)^{1/2}$, and the central intensity of a saturated line is equal to P_ν. However, a quantitative comparison between theory and observation is not possible without knowledge of the numerical relation between P_ν and the absolute number of excited H atoms.

Ellison has also observed that, following flare maximum, the initial decrease in line width is much more rapid than the decline in central intensity but that later the rates of decline are similar. Presumably, the decline in flare brightness is occasioned by a decrease in both N_2 and P_ν. The time dependence of N_2 and P_ν can probably be derived from the analysis of observed line profiles, but even in the absence of this information the relation between line width and central intensity observed during the decline of a flare can be explained on theoretical grounds.

We may suppose that the decline in flare brightness is caused by a drop in the gas temperature. As the temperature falls, the number of excited H atoms will also decrease, but P_ν, which is proportional to N_3/N_2, will decrease at a much slower rate than N_2, since the absolute number of atoms in either the second or the third excited state is much more sensitive to the temperature than is the ratio of the numbers in the two excited states. At flare maximum the $H\alpha$ line is saturated, and therefore the central intensity will not initially be affected by the decrease in N_2 but will fall at the same rate as P_ν. On the other hand, the line width, as shown by Figure 4, is strongly dependent on N_2 and will therefore decrease very rapidly immediately following maximum. As the temperature continues to fall, N_2 decreases to the point at which the line is no longer saturated; and at this stage the fall in central intensity is accelerated, while the line width decreases more slowly.

Finally, we wish to point out that although radiation damping appears to account for existing observations of $H\alpha$ line widths in solar flares, the observations are neither sufficiently complete nor detailed enough to preclude the possibility that collisional damping and Stark effect may also play roles. The precise contributions of the various sources of line broadening can be established with certainty only after analysis of accurate observational profiles of the lines of the hydrogen Balmer series and of other atomic lines. It will probably be necessary during the course of such studies to take quantitative account of temperature gradients in the flare layers, since the gradients will influence the line shapes.

At present, the observational evidence in favor of the Stark effect is unconvincing. For $H\alpha$, Stark broadening is comparable in magnitude with radiation damping when the electron density reaches 10^{13} cm^{-3}. But Suemoto (1951) finds, from observation of the $H10$ line in the flare of February 28, 1951, that the electron density at the base of the flare was 1.1×10^{12}, assuming an electron temperature of 10,000° K. Even if the temperature is taken to be 50,000° K, the electron density is only 4.1×10^{12}. The only observational evidence that appears, on the surface, to favor the Stark effect as opposed to radiation damping has been offered by Mustel and Severny (1952), on the basis of spectrophotometric profiles, of $H\gamma$, $H\delta$, and $H\epsilon$. The wings of the $H\alpha$ profile appear to fit the hypothesis of radiation damping. However, the Stark effect is invoked to explain the fact that the half-widths of the other series members increase in the order

$H\gamma$, $H\delta$, $H\epsilon$. Unfortunately, the work of Mustel and Severny suffers from two serious errors which appear to invalidate their arguments. First, they have neglected the absorption by the flare layer of the underlying $H\alpha$ absorption profile. This is equivalent to replacing the term $A_\nu e^{-\tau_\nu \sec\theta}$ in equation (1) by A_ν. As pointed out by Suemoto, this procedure introduces an error in the derived emission intensity amounting to $-A_\nu(1 - e^{-\tau_\nu \sec\theta})$, which can be considerable in magnitude unless $P_\nu \gg A_\nu$. Second, the observed profiles appear not to have been adequately corrected for instrumental broadening and/or scattered light, since the profiles given for the Balmer series arising from the undisturbed disk show central intensities of 35–40 per cent, instead of 15–20 per cent. Both errors would tend to decrease the central intensities of the emission lines, which may be in error by as much as 40 per cent of the continuous spectrum. The derived half-widths cannot therefore be considered as real.

REFERENCES

Bruce, C. E. R. 1949, *Nature*, **164**, 280.
Cillié, G. G., and Menzel, D. H. 1935, *Harvard Circ.*, No. 410.
Ellison, M. A. 1949, *M.N.*, **109**, 3.
Ellison, M. A. 1950, *Pub. R. Obs. Edinburgh*, **1**, 53.
Ellison, M. A. 1953, *Pub. R. Obs. Edinburgh*, **1**, 75.
Ellison, M. A., and Conway, M. 1950, *Observatory*, **70**, 77.
Ellison, M. A., and Hoyle, F. 1947, *Observatory*, **67**, 181.
Jager, C. de. 1952, *Recherches astronomiques Obs. Utrecht*, Vol. **13**, Part I.
Menzel, D. H. 1931, *Lick Obs. Pub.*, Vol. **17**, Part I.
Mustel, E. R., and Severny, A. B. 1952, *Rept. Crimean Ap. Obs.*, **8**, 19.
Rao, N. R.; Das, A. K.; Ananthakrishnan, H.; Raheem, K. C. A.; and Sethumadhavan, K. 1949, *Nature*, **164**, 964.
Suemoto, Z. 1951, *Pub. Astr. Soc. Japan*, **3**, 110.
Van de Hulst, H. C. 1953, *The Solar System*, Vol. **1**: *The Sun*, ed. G. P. Kuiper, p. 207.

EMISSION IN HYDROGEN BALMER LINES AND CONTINUUM IN FLASH SPECTRUM OF 1952 TOTAL SOLAR ECLIPSE AT KHARTOUM, SUDAN

R. Grant Athay, Donald E. Billings, John W. Evans,*
and Walter O. Roberts
High Altitude Observatory of Harvard University
and
University of Colorado, Boulder, Colorado
Received December 28, 1953

ABSTRACT

Analysis of the spectrograms of the chromospheric flash obtained at the 1952 solar eclipse in Khartoum, Sudan, presented serious photometric problems. Standardizing exposures made at Khartoum were not successful because of a posteclipse failure of the film-advance mechanism. Characteristic curves obtained from standard lamp exposures made in Boulder after completion of the expedition could not be trusted to represent the photometric properties of the eclipse films and were principally useful as a first approximation to the curves representing the eclipse spectrograms.

Methods were developed that, in spite of these problems, allowed entirely reliable determinations of the characteristic curves of the eclipse films. A thorough, independent check on the consistency and accuracy of the final curves was possible, and its result was entirely satisfactory. Change with wave length of film sensitivity, atmospheric absorption, and optical constants of the spectrographs were evaluated and included in the photometry. The integrated intensities of the hydrogen Balmer lines from $H8$ to $H31$ and at four wave lengths in the Balmer continuum were measured at two points on the east limb on seventeen ultraviolet spectrograms; and the intensities of $H\beta$, $H\gamma$, and $H\delta$ were measured at one of these points on nineteen visible spectrograms. The observations extend from 100 to 6300 km, with a height resolution of 108 km throughout most of the low chromosphere. Preliminary interpretation of the line intensities revealed that the effects of self-absorption were pronounced and also demonstrated that there were large departures from thermodynamic equilibrium, in the sense that the b_n's were greater than 1 at 1000 km and increased with height. A preliminary interpretation of the continuum data gave a chromospheric model characterized by a large increase of temperature with height and a relatively low electron-density gradient. A more detailed analysis of the data is in progress.

I. INTRODUCTION

Spectrographic observations of the flash spectrum at the total solar eclipse in Khartoum, Sudan, on February 25, 1952, were made by the High Altitude Observatory of Harvard University and the University of Colorado. The methods of analysis and the requirements for the optical observations were developed by Thomas (1950). The spectographic equipment was designed and built by Evans and the staff of the High Altitude Observatory especially to fit these requirements and to give the necessary data for the analytical method, namely, detailed spectrophotometric observations of the emission in the hydrogen Balmer and Paschen series. Most of the work reported here was performed by Athay (1953) and has been described in fuller detail in a Ph.D. thesis submitted to the University of Utah.

II. OBSERVATIONS AT THE ECLIPSE

The High Altitude Observatory portion of the Naval Research Laboratory expedition was headed by John W. Evans, who was assisted by Robert H. Lee and Robert H. Cooper. Observations were made with three slitless spectrographs, two having lens systems and one a reflection system for the image-forming elements. The properties of the spectrographs are given in Table 1. A diagonal mirror in the ultraviolet spectrograph,

* Now superintendent, Upper Air Research Observatory, Sunspot, New Mexico.

between the grating and the spherical mirror, diverted the spectrum to the photographic emulsion. This mirror blocked out 40 mm of the short dimension of the grating, leaving an effective surface of 85 × 150 mm.

All three spectrographs were attached to a single sturdy structural spar, mounted equatorially and designed to be guided in hour angle and declination by a precise photoelectric servo-mechanism (Fowler and Johnson 1951) similar to those used at the Climax and Sacramento Peak coronagraph stations. During totality the spar was driven in R.A. only by a fixed oscillator.

The cameras were designed for "jumping-film" observations at a much faster rate than earlier eclipse-goers had attempted. A very low-inertia pneumatic film transport and shutter system was used. This design allowed rapid film transport with a minimum of mechanical motion and vibration. The cameras were all operated by a single control system giving simultaneous exposures.

TABLE 1

CHARACTERISTICS OF HIGH ALTITUDE OBSERVATORY SPECTROGRAPHS

	Wave-length Range	Grating				Image System	Dispersion (A/mm)
		Ruling	Area	Blaze	Ruled by		
Ultraviolet	λλ 5100–3360	900 lines per mm	125×150 mm	λ 3700, 1st order	Bausch and Lomb	Spherical mirror, 60 in. f.l.	7.5
Visual	λλ 6500–3950	600 lines per mm	100×150 mm	λ 5500, 1st order	Bausch and Lomb	Ross lens, 4 in. ap., 60 in. f.l.	11
Infrared	λλ 8680–6200	15,000 lines per in.	125×160 mm	.....	R. W. Wood	Ross lens, 4 in. ap., 60 in. f.l.	11.5

The observing program at the eclipse was as follows: the exposure times in the low chromosphere were 0.3 second with an interval of 0.1 second between the end of one exposure and the beginning of the next. The 0.3-second exposures were started 10 seconds before the computed time of first flash. At the appearance of the flash the program control was started. The 0.3-second exposures were continued for 12 exposures, and then four exposures of 0.9 second and five of 2.9 seconds were taken. After the last 2.9-second exposure, some longer exposures of the corona were made. The same program was reversed for second flash. Preparations of the HAO group were severely hampered by Evans' fall from the equatorial mount, less than 2 weeks before eclipse, which resulted in a very severe leg fracture.

Excellent observing conditions at Khartoum prevailed during eclipse on February 25. The sky was cloudless, the wind velocity moderate, and the seeing good. On February 22, there was a cold frontal passage with a rather severe sandstorm. On the day of the eclipse there was still some blowing sand, but this was confined to the levels a few feet above the surface and below most of the observing equipment. There was still a slight haze left by the dust from the preceding storm. However, the atmospheric transparency was good and showed no evidence of variability. The photopic and spectral attenuation of the atmosphere was measured by the Naval Research Laboratory group (Beck, Lovell, and Hulbert 1953) during the 10 days preceding the eclipse and on eclipse day.

The sandstorm on February 22 forced fine sand into the film transport and shutter system. The operation of this system afterward was somewhat erratic. Fortunately, the operation during the eclipse was quite smooth, though some doubling of exposures occurred. Seventeen ultraviolet and nineteen visible spectrograms at first flash are of good

quality and suitable for accurate photometry. The infrared spectrograms at first flash were underexposed, and, although there is much usable information on them, all the Paschen lines are too weak for accurate photometry on all except the first eight exposures. The high-order lines can be measured on only two of these.

The program for second flash started a few seconds too late, and the longer exposures were overexposed in the ultraviolet and visible cameras. There are, however, ten visible and five ultraviolet spectrograms of good quality. The accidental delay in the program was beneficial to the infrared camera, and some of the Paschen lines are suitable for photometry on ten spectrograms.

The spectrographs were designed so that two images of the spectrum appeared simultaneously side by side in each exposure. The two images were produced with a simple image-dividing system in each spectrograph. The primary image received practically all the light from the grating, and the secondary image received approximately 1/100 of the total light. This simple device greatly increased the amount of usable information on the spectrograms by extending the range of intensities that can be measured, and it provided a basis for checking the accuracy of the photometry, as described below.

Along with the two images of the spectrum, each exposure contained the image of a data panel. The panel included a step-wedge, as a check on photometry, and a system of clocks for measuring exposure times. The step-wedge was illuminated from behind by a constant light-source; the light transmitted by the wedge was filtered to give a band about 400 Å wide.

Figures 1 and 2 are reproductions of visible and ultraviolet spectrograms. The bright regions bordering the primary image were formed by the coronal continuum that extends beyond the moon's limb at right angles to the line of contacts. This continuum overlaps the secondary image of the spectrum and the image of the data panel. In designing the eclipse spectrographs, we overlooked the fact that this continuum would be so intense. This oversight had both beneficial and detrimental effects. The overlap into the secondary image raised the densities in that image above the extreme toe of the characteristic curve, making the determination of intensities more reliable, and introduced no systematic errors, since the light of the overlapped image integrated out of all line intensities in the reduction process. On the other hand, the effects on the data panel were detrimental. In the visible spectra the effect is scarcely noticeable and even for the step-wedge can be reliably corrected. In the ultraviolet, however, the data panels were of little use. In only six spectrograms could the clock images be seen, and none of the wedges was usable. At first, we feared that this was a very serious loss, but, as we shall point out below, the image of the continuum itself allowed us to determine the characteristic curves of the films at all desired wave lengths and also to determine the relative exposures of each image.

III. PHOTOMETRIC METHODS

Two principal methods of photometric standardization of our eclipse films had been planned before the eclipse, with two possible alternatives visualized in case of difficulties with these principal methods. As our program developed, we were forced to rely in part upon the alternative methods, but we are confident that the final results are comparable in accuracy to those expected from the principal methods. In fact, the photometric procedures were carried out in such a way that the accuracy of the results could be checked.

The principal planned methods of standardization were: (1) standard exposures taken on the eclipse films, in Khartoum using both diffuse sunlight and a calibrated tungsten ribbon-filament lamp and collimator of known optical properties as sources; and (2) the standard wedge in the data panel was to serve as a check on the photometry by giving an accurate characteristic curve at one wave length in each spectrograph and for each spectrogram. Posteclipse failure of the film-transport mechanisms destroyed the results of the standardization of part 1 of these methods; and the continuum overlap described

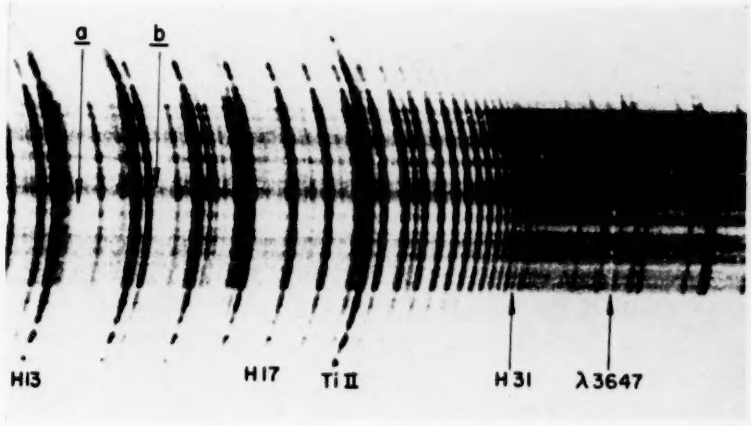

FIG. 1.—Negative print of a portion of ultraviolet spectrogram No. 9. Points *a* and *b* and several Balmer lines are indicated.

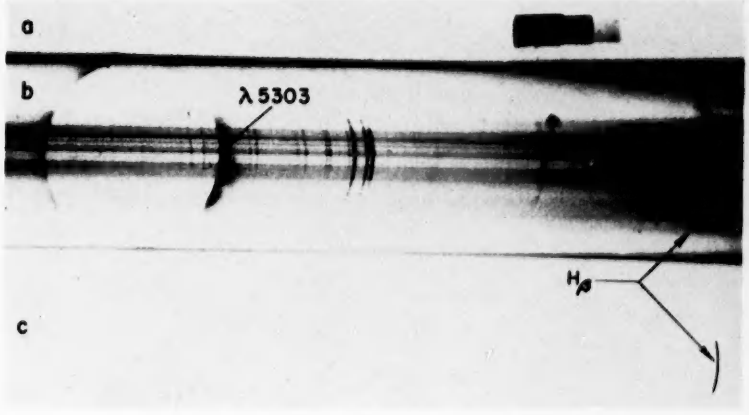

FIG. 2.—Negative print of a portion of visual spectrogram No. 13 showing: *a*, data panel wedge; *b*, primary image; *c*, secondary image.

above resulted in the loss of part 2 in the ultraviolet spectrograph. Part 2 was carried through as planned in the visible and infrared spectrographs.

The alternative methods planned were: (1) standard exposures, on the same film emulsions, from the standard lamp and collimator taken in Boulder after the return trip, and (2) determination of the characteristic curves by considering the primary and secondary images as a two-step wedge. The standard exposures were attempted twice in Khartoum, but both attempts failed, partly because of damage done to the pneumatic system by the sandstorms and partly because of the extreme fatigue of the eclipse party, the handicap of Evans, and the very rigid return schedule.

After the return trip to Boulder, the standard exposures were completed on the same rolls of film used for the eclipse pictures. The processing and exposing conditions used at Khartoum were carefully recorded, and an attempt was made to duplicate these conditions in Boulder. We recognized, however, that the detailed shapes of the characteristic curves obtained from these exposures would be only a first approximation to the proper curves; but the variations of the curves with wave length and the absolute intensities we expected to be able to trust. The detailed shapes of the eclipse characteristic curves at one wave length for the visible and infrared films were easily and most reliably determined from the images of the step-wedge in the data panel. Alternatively, but less reliably and much more tediously, the detailed shapes of the curves at all wave lengths could be obtained from the primary and secondary images. Rather than carry out this process independently, we decided to use the two images to check the accuracy of the curves obtained by the previously described methods.

In spite of our efforts to duplicate the conditions at Khartoum for the standard exposures, there were important differences in the clear-film densities in the two cases. The clear-film areas around the eclipse spectrograms showed densities near 0.23 in all three spectrographs. On the other hand, the standard exposures showed clear-film densities near 0.14 in all three films. However, a detailed comparison of the characteristic curves obtained from the data-panel wedge in the visible spectrograms with the characteristic curves at the same wave length in the standard exposures showed no discernible differences except in the low densities. A check with the primary and secondary images showed unambiguously that the curve given by the data-panel wedge was the proper curve, as was to be expected. Hence, for the visible films, we were able to derive what appeared to be a completely reliable calibration.

A comparison of the characteristic curve obtained from the wedge in the data-panel image in the infrared spectrograms with the characteristic curves at the same wave length obtained from the standard exposures showed no agreement in any parts of the curves. This result was not too surprising, in view of the instability of most infrared films and the severe heat at Khartoum. For this reason, the posteclipse infrared standards were not used. In addition, the secondary images in these spectrograms were too badly underexposed to be of any use. For these films we were faced with the problem of using the charasteristic curve obtained from the data-panel wedge to determine the curves at other wave lengths.

For the ultraviolet films we had the standard exposures, of questionable accuracy, and the primary and secondary images in the spectrograms. Preliminary attempts to construct the curves from the two images showed that this would be a difficult and time-consuming job. Fortunately, we found an unexpected but reliable method for constructing the ultraviolet curves, and we used the same method in the infrared, to extend the data-panel curve to different wave lengths.

In slitless spectrograms each wave length produces a circular image of the corona similar to the image of the green coronal line, λ 5303, showing in Figure 2. The continuum intensity at any point in the spectrograms is a result of the overlapping of these images. At points on the limb $\pm 90^{\circ}$ from the line of dispersion, the images are displaced tangent to the limb, and the effects of the overlapping are much more pronounced. Fur-

thermore, if the line of dispersion is along the line of contacts, the intensity of the continuum at these points and all points farther out from the limb is independent of the position of the moon, so that their intensities should be constant during the short time of the eclipse.

It is well known (Grotrian 1931; Allen 1946) that the coronal continuum is essentially a reproduction of the photospheric continuum and does not change color with height. Hence we should expect that in the image of the continuum extending beyond the moon's limb, at $\pm 90^\circ$ to the line of contacts, the relative intensities are the same function of height at all wave lengths. In other words, the ratio of intensities on any two lines parallel to the line of dispersion and in this image of the coronal continuum is the same at all wave lengths. The validity of this statement can be checked at the two wave lengths appropriate to the characteristic curves obtained from the visible and infrared data-panel wedges.

As was expected, the infrared and visible spectrograms gave the same function of height for the intensity in this image. In addition, the same function of height was obtained regardless of the duration of the exposure or the actual time of the exposure. The exposure times varied over a range of 10 to 1, and the actual measurements of intensity covered the extreme ranges of the curves. The consistency of the results is a rather rigorous check on the accuracy of the curves used.

Once the intensities were known as a function of height above the limb, this image was used to construct characteristic curves at numerous wave lengths for all three films. The ultraviolet curves obtained duplicated the curves obtained from the standard exposures at all wave lengths except for the low densities. A check of the primary and secondary images fully confirmed the curves obtained from the coronal continuum. The visible characteristic curves obtained from the coronal continuum showed a similar duplication of the standards. In both these films the characteristic curves showed considerable change with wave length. In the infrared film neither the standards nor the coronal continuum-curves showed any change in shape with wave length.

The absolute intensity scale was fixed in the visible and ultraviolet films by the straight-line portions of the standard exposure characteristic curves. The absolute intensities include corrections for differential film sensitivity, atmospheric absorption (Beck, Lovell, and Hulbert 1953), spectral emissivity of tungsten (Forsythe and Adams 1945), and the optical constants of the collimator and spectrographs. The standard lamp was calibrated by the National Bureau of Standards both before and after the standard exposures, with no significant changes.

The ultraviolet and visible spectrograms overlapped from λ 3950 to λ 5100. Measurements of the integrated intensity of $H\delta$ showed that the absolute intensity scales agreed to within 0.10 in the $\log_{10}$ of the intensity. The visible scale was adjusted slightly to agree with the ultraviolet. The variation of continuum intensity with wave length in the visible spectrograms gave a good reproduction of the integrated disk continuum as given by Nicolet (1951). In the infrared the absolute intensities could not be determined from the standard exposures; but it was found that the continuum intensity at λ 6375 and the integrated intensity of the red coronal line, λ 6374, which was common to the infrared and visible spectrograms, could both be made to agree with the visible spectrograms on the same intensity scale. There was no evidence of external fogging in either the visible or the infrared spectrograms. However, the ultraviolet spectrograms were noticeably fogged on the long-wave-length end. The fogging was serious enough to affect the continuum intensities in some parts of the spectrograms down to at least λ 3700. The continuum intensities in the center of the spectrograms at λ 3700 are too high, relative to the intensities in the visible spectrogram by a factor of 1.5, but this factor decreases rapidly to ~ 1 near the edges of the spectrograms.

In using the coronal continuum bordering the spectrum, we assumed that there was no measurable effect from fogging at the positions where the measurements in the coronal

continuum were made. Fortunately, as was shown by a detailed comparison of ultraviolet and visible continuum intensities at several wave lengths and positions in the spectrograms, this assumption was justified. The agreement of the resulting characteristic curves with the curves obtained from the standard exposure and the consistency with the primary and secondary images was further support for the accuracy of the characteristic curves.

The fogging in the ultraviolet spectrograms does not affect the measurements of integrated line intensities because the background continuum integrates out in the reduction process. The same is true for the free-bound component of the hydrogen Balmer continuum. These measurements are discussed in the following section.

The corrections for different exposure times were determined from the intensities in the image of the coronal continuum bordering the spectrum. The intensity scale in each spectrogram was adjusted to give a constant intensity at a given point in this image of the corona. To avoid film defects, several points were used and the results averaged. This procedure automatically corrects for variations in exposure times and allows for reciprocity failures of the films.

In our opinion the checks on the characteristic curves made possible by the use of the primary and secondary images of the spectrum and the coronal continuum bordering the spectrograms leaves very little room for doubt about the reliability of the photometric standardization. The internal consistency of the line-intensity data lends further support to these conclusions.

IV. TABULATION OF INTENSITIES

Two points near the line of contacts on the east limb at first flash were traced on all the ultraviolet spectrograms with the microdensitometer at the McMath-Hulbert Observatory. The tracings included the Balmer lines from $H8$ to $H\infty$ and the Balmer continuum from λ 3647 to λ 3500. The two points are marked *a* and *b* in Figure 1. Point *a* is at a heliographic position angle of 67° and point *b* at 65°. This region of the sun's limb showed no signs of prominence activity either during the eclipse or during the days immediately following and preceding the eclipse. Points *a* and *b* were chosen as representative of the average "undisturbed" chromosphere, and the data from the two points show no systematic differences. The red, λ 6374, and green, λ 5303, coronal lines showed moderate maxima at 75°; but the region was small, and the main center of activity had passed the east limb 1 or 2 days before eclipse (Trotter and Roberts 1952). The intensities of $H\beta$, $H\gamma$, and $H\delta$ were traced at point *b* on all the visible spectrograms with the High Altitude microdensitometer.

The microdensitometer tracings were reduced to intensity units, and the line profiles were replotted. The areas under the profiles were measured with a planimeter. Many of the lines were traced more than once at different times and with different sensitivities of the microdensitometer. Of 54 such cases, the maximum difference in the log of the intensity was 0.08, and the probable error of an individual determination was ± 0.027 in the log of the intensity. There are, of course, additional errors due to defects in the emulsions, defective shutter action, and other sources of random errors that cannot be evaluated.

In general, the stronger lines were measured in the secondary images, and the weaker lines in the primary images. The lines of intermediate intensity were measured in the secondary images in the low chromosphere, and in the primary images in the high chromosphere. This had the effect of putting all the lines in density ranges that at one time or another covered a large portion of the characteristic curves. In spite of the fact that some lines were measured first on the lower half of the curve and then on the upper half, the intensities were found to be consistent. This is further evidence for the lack of systematic errors in the photometry.

The Balmer line intensities are tabulated in Table 2. We have made no attempt to cor-

TABLE 2

LINE* AND CONTINUUM† INTENSITIES

POINT *a*

	HEIGHT (KM)																
	530	640	750	1180	1280	1390	1500	1610	1720	1820	1930	2040	2150	2260	2400	3180	3720
*H*8	3.44	3.11	3.14	2.79	2.82	2.79	2.80	2.69	2.63	2.63	2.55	2.46	2.44	2.38	2.44	1.79	1.44
*H*9	3.14	2.91	2.91	2.59	2.54	2.49	2.52	2.47	2.30	2.27	2.20	2.12	1.96	1.92	1.83	1.30	1.08
*H*10	2.98	2.80	2.81	2.50	2.40	2.41	2.34	2.32	2.23	2.15	1.97	1.95	1.85	1.80	1.73	1.22	0.92
*H*11	2.88	2.72	2.75	2.41	2.33	2.27	2.28	2.24	2.07	2.02	1.97	1.88	1.78	1.64	1.60	1.00	0.82
*H*12	2.85	2.69	2.73	2.38	2.28	2.15	2.20	2.13	1.98	1.88	1.81	1.70	1.63	1.66	1.52	0.90	0.55
*H*13	2.83	2.64	2.70	2.31	2.20	2.15	2.12	2.00	1.87	1.74	1.79	1.82	1.50	1.48	1.49	0.84	
*H*14	2.74	2.61	2.66	2.23	1.98	2.06	1.98	1.95	1.78	1.62	1.61	1.69	1.57	1.45	1.40		
*H*15	2.56	2.49	2.48	2.10	1.97	1.89	1.83	1.86	1.67	1.48	1.56	1.48	1.30	1.19	1.27		
*H*16	2.51	2.37	2.48	2.00	1.96	1.82	1.72	1.78	1.56	1.39	1.50	1.38	1.20	1.09	....		
*H*17	2.43	2.30	2.40	2.02	1.86	1.74	1.65	1.68	1.45	1.32	1.46	1.34	1.04	1.06	1.08		
*H*18	2.36	2.27	2.26	1.94	1.73	1.68	1.55	1.52	1.43	1.21	1.33	1.16	0.94	0.97	0.84		
*H*19	2.36	2.29	2.24	1.87	1.70	1.72	1.59	1.60	1.34	1.13	1.33	1.15	0.95	0.88	0.88		
*H*20	2.28	2.20	2.19	1.78	1.66	1.56	1.53	1.46	1.29	1.33	1.21	0.99	0.88	0.78	0.77		
*H*21	2.29	2.17	2.22	1.84	1.55	1.47	1.51	1.39	1.21	1.20	1.11	0.90	0.73	0.74	0.72		
*H*22	2.15	2.05	2.06	1.70	1.53	1.43	1.36	1.24	1.15	1.18	....	0.86	0.70	0.64	0.61		
*H*23	2.12	2.03	2.01	1.55	1.39	1.32	1.22	1.22	1.06	1.02	0.86	0.78	0.70	0.62	0.62		
*H*24	2.09	1.97	1.95	1.48	1.33	1.19	1.19	1.04	0.97	0.93	0.81	0.69	0.58	0.55	0.50		
*H*25	2.10	1.98	1.92	1.47	1.25	1.14	1.09	0.96	0.92	0.77	0.76	0.62	0.56	0.47	0.27		
*H*26	1.93	1.87	1.78	1.40	1.24	1.15	1.02	0.94	0.87	0.73	0.72	0.59	0.52	0.35	0.39		
*H*27	1.95	1.84	1.69	1.20	1.10	1.08	0.89	0.82	0.72	0.64	0.65	0.52	0.35	0.38	0.23		
*H*28	2.01	1.96	1.81	1.17	1.17	1.00	0.91	0.82	0.80	0.63	0.60	0.43	0.42	0.30	0.36		
*H*29	1.78	1.73	1.67	1.14	0.98	0.88	0.81	0.69	0.78	0.45	0.49	0.39	0.28	0.31	0.20		
*H*30	2.14	1.96	1.85	1.22	1.23	0.91	0.82	0.79	0.78	0.52	0.60	0.45	0.38	0.35	0.27		
*H*31	1.59	1.65	1.54	0.93	0.84	0.66	0.63	0.59	0.60	0.36	0.37	0.26	0.22	....	0.14		
λ 4700†				1.65	1.63	1.63	1.65	1.57	1.58	1.59	1.56	1.57	1.57	1.57	1.55	1.57	1.55
λ 3700†		1.60	1.61	1.42	1.39	1.40	1.43	1.27	1.31	1.39	1.36	1.31	1.31	1.36	1.15		
λ 3640†				1.80	1.69	1.71	1.71	1.65	1.56	1.59	1.57	1.48	1.43	1.45	1.23		
λ 3600†				1.78	1.67	1.70	1.70	1.66	1.57	1.61	1.56	1.49	1.44	1.46	1.26		
λ 3550†				1.77	1.65	1.68	1.71	1.62	1.52	1.57	1.53	1.45	1.39	1.41	....		
λ 3500†				1.78	1.53	1.67	1.68	1.59	1.46	1.56	1.55	1.43	....	1.39	....		
λ 3640‡	2.43	2.44	2.37	1.63	1.41	1.44	1.41	1.43	1.43	1.19	1.18	1.03	0.87	0.80	0.54		
λ 3600‡	2.40	2.29	2.42	1.60	1.38	1.43	1.40	1.45	1.26	1.25	1.17	1.07	0.93	0.88	0.70		
λ 3550‡	2.40	2.09	2.28	1.60	1.36	1.41	1.44	1.40	1.18	1.19	1.13	1.00	0.81	0.72	....		
λ 3500‡	2.31	....	2.24	1.63	....	1.41	1.40	1.36	1.06	1.19	1.20	0.98	....	0.71	....		

* Add 12.00 to all line intensities to get $\log_{10}$ of the integrated emission in the line in ergs/sec from a slice of chromosphere bounded by two parallel planes 1 cm apart, which lie in the line of sight and are perpendicular to the sun's limb; and a third plane tangent to the moon's limb along the line of sight. The emission is assumed to be isotropic.

† These continuum intensities are $\log_{10}$ of the total intensity in the continuum from all sources in ergs/sec/unit frequency.

‡ These continuum intensities are $\log_{10}$ of the free-bound emission in the Balmer continuum (see text for derivation).

All values below the solid line are measured in the primary image; those above the line are measured in the secondary image.

TABLE 2—*Continued*

POINT *b*

	Height (Km)															
	100	530	640	750	850	960	1070	1180	1280	1390	1500	1610	1750	2520	3060	$\beta_a \times 10^8$ cm^{-1}
*H*8	3.27	3.10	3.02	3.10	3.08	3.03	3.00	2.88	2.88	....	2.81	2.79	....	2.09	1.74	1.39
*H*9	....	2.88	2.84	2.81	2.80	2.73	2.72	2.65	2.63	2.53	2.53	2.45	2.20	1.70	1.38	1.51
*H*10	3.04	2.82	2.74	2.69	2.69	2.63	2.59	2.49	2.48	2.38	2.39	2.31	2.01	1.55	1.24	1.56
*H*11	2.99	2.73	2.67	2.60	2.60	2.55	2.51	2.39	2.38	2.28	2.27	2.19	1.93	1.49	1.12	1.62
*H*12	2.97	2.75	2.67	2.60	2.59	2.51	2.46	2.35	2.33	2.22	2.15	2.13	1.85	1.38	0.97	1.68
*H*13	2.98	2.73	2.63	2.55	2.54	2.48	2.46	2.31	2.24	2.09	2.08	2.06	1.73	1.25	0.88	1.68
*H*14	2.86	2.68	2.56	2.55	2.45	2.41	2.34	2.21	2.12	2.06	1.93	1.99	1.67	1.20		1.70
*H*15	2.69	2.62	2.40	2.35	2.29	2.25	2.18	2.05	2.01	1.93	1.88	1.84	1.58	1.10		1.73
*H*16	2.64	2.48	2.35	2.30	2.20	2.22	2.08	1.97	1.98	1.84	1.87	1.75	1.52	1.07		1.73
*H*17	2.57	2.37	2.26	2.21	2.17	2.13	2.03	1.90	1.84	1.77	1.69	1.62	1.49	0.92		1.79
*H*18	2.43	2.33	2.17	2.14	2.07	2.01	1.93	1.87	1.79	1.65	1.74	1.48	1.41	0.78		1.85
*H*19	2.45	2.27	2.12	2.14	2.11	1.98	1.92	1.81	1.77	1.66	1.63	....	1.29	0.66		1.91
*H*20	2.42	2.22	2.14	2.07	2.01	1.90	1.78	1.74	1.72	1.62	1.65	1.34	1.18			1.91
*H*21	2.37	2.25	....	2.07	2.01	1.77	1.75	1.66	1.66	1.55	1.48	1.29	1.09			1.96
*H*22	2.35	2.08	2.00	1.92	1.91	1.68	1.68	1.60	1.67	1.50	1.30	1.22	1.07			1.96
*H*23	2.27	2.03	1.92	1.87	1.80	1.59	1.57	1.49	1.42	1.38	1.23	1.12	1.02			1.96
*H*24	2.25	1.99	1.88	1.82	1.78	1.56	1.51	1.43	1.30	1.28	1.19	1.04	0.90			2.05
*H*25	2.26	2.01	1.79	1.80	1.75	1.46	1.47	1.38	1.39	1.25	1.11	0.98	0.89			2.08
*H*26	....	1.86	1.75	1.73	1.69	1.39	1.39	1.28	1.27	1.17	1.03	0.93	0.84			2.05
*H*27	2.18	1.79	1.72	1.66	1.65	1.43	1.35	1.23	1.20	1.11	1.02	0.85	0.79			2.08
*H*28	2.29	1.86	1.78	1.60	1.71	1.34	1.35	1.16	1.16	1.08	0.91	0.80	0.78			2.12
*H*29	....	1.68	1.62	1.54	1.54	1.18	1.26	1.08	1.01	0.87	0.68	0.77	0.74			2.08
*H*30	....	1.97	1.81	1.75	1.71	1.32	1.36	1.12	1.19	1.05	0.77	0.84	0.71			2.12
*H*31	....	1.53	1.52	1.43	....	1.07	1.14	0.94	0.81	0.80	0.63	0.57	0.59			2.12
λ 3700†		1.74	1.65	1.57	1.60	1.50	1.45	1.45	1.45	1.39	1.41	1.42	1.34			
λ 3640†				2.29	2.41	2.16	1.90	1.92	1.86	1.73	1.72	1.68	1.51			
λ 3600†				2.14	2.32	2.12	1.85	1.91	1.85	1.70	1.73	1.70	1.54			
λ 3550†				2.06	2.33	2.06	1.80	1.84	1.79	1.68	1.70	1.66	1.57			
λ 3500†				2.04	2.07	1.97	1.83	1.81	1.75	1.66	1.69	1.65	1.58			
λ 3640‡	2.73	2.39	2.32	2.20	2.08	2.06	1.72	1.75	1.66	1.48	1.45	1.36	1.06			2.19
λ 3600‡	2.74	2.36	2.37	2.01	2.24	2.01	1.65	1.74	1.65	1.44	1.47	1.41	1.15			2.10
λ 3550‡	2.80	....	2.06	1.92	2.25	1.94	1.58	1.64	1.56	1.41	1.43	1.35	1.25			2.10
λ 3500‡	2.80	2.31	....	1.80	1.92	1.82	1.64	1.61	1.51	1.40	1.42	1.35	1.29			2.05

TABLE 2—*Continued*

POINT b—*Continued*

	Height (Km)									
	530	640	750	850	960	1070	1180	1280	1390	1500
$H\beta$	3.68	3.75	3.62	3.69	3.62	3.55	3.66	3.52	3.52	3.45
$H\gamma$	3.66	3.68	3.62	3.63	3.52	3.50	3.56	3.44	3.37	3.31
$H\delta$	3.51	3.55	3.47	3.42	3.35	....	3.36	3.21	3.11	3.02
λ 4700†	1.91	1.87	1.76	1.80	1.76	1.75	1.73	1.65	1.69	1.67

	Height (Km)									
	1610	1750	1980	2250	2520	3060	3870	4680	5490	6300	$\beta_n \times 10^9 cm^{-1}$
$H\beta$	3.36	3.38	3.32	3.22	3.15	2.74	2.25	....	1.08	0.64	1.56
$H\gamma$	3.27	3.20	3.12	2.98	2.78	2.54	1.94	1.23	0.53	....	1.70
$H\delta$	3.04	3.04	2.85	2.70	2.49	2.20	1.60	0.94	0.42	....	1.70
λ 4700†	1.61	1.64	1.69	1.64	1.68	1.58	1.61	1.55	1.58	1.58	....

rect for unresolved blending of other lines with the hydrogen lines. In the case of the higher-order Balmer lines and a few Balmer lines close to non-Balmer lines, the wings are blended with the neighboring lines. These have been corrected by extrapolating the continuum intensity from the nearest well-defined point to include the overlapped region of the lines and then extending the profiles of the lines down to this continuum in such a way that the individual profiles add up to the observed ones and have the same shape as the unblended profiles. All the series lines beyond $H31$ are too badly affected by blends to give reliable intensity measurements. We have made no systematic attempt to identify these lines, but a tentative identification shows that $H36$ is definitely discernible on some spectrograms, and $H37$ is quite probable. The Paschen line measurements are not yet completed.

The effective height of each exposure was assumed to be the point reached by the moon's limb at the middle of the exposure. The heights were measured from the photospheric limb, which was determined by plotting the continuum intensity at λ 3700 for point *b* against the exposure number. The resulting curve showed a sharp increase in slope near exposure No. 3. The shape of the curve indicated that the point of contact should be accurate to within ±30 km of the apparent edge of the photosphere. The continuum intensity at point *a* showed that this point reached contact before the first exposure. The heights were determined for this point from special moon-profile pictures taken at Khartoum for this purpose. The difference in the heights of points *a* and *b* was found to be 700 km, with an uncertainty in each point of about 100 km, due to small variations in the moon profile. A visual estimate of the intensities of the *CN* bands and numerous weak metallic lines gave an average difference between points *a* and *b* of 650 km. The 650-km value was used.

The intensities at four wave lengths in the Balmer continuum and outside the Balmer continuum at λ 3700 and λ 4700 are also included in Table 2. We have tabulated both the total observed continuum intensity from all sources and the intensity of the free-bound emission in the Balmer continuum. The free-bound emission was determined by subtracting the intensity of the non-Balmer continuum from the total intensity. The non-Balmer continuum intensity was determined from the observed intensity at λ 3700 and an empirical correction to the shorter wave lengths. The empirical correction was determined from the image of the coronal continuum bordering the spectrograms.

The plots of log emission versus height are all well represented by straight lines above a certain height. For the higher-order lines, $n \geq 12$, and Balmer continuum, the approximation appears to be good above 500 km. For the lower-order lines there is a marked decrease in the slopes of the lines in the lower chromosphere. For $H9$ the straight-line approximation appears to be good above 2000 km, and for $H\beta$ it appears to be good above 4000 km. In the regions where the straight-line approximation is good, the emission, E_n, in a line or in the continuum can be represented by

$$E_n = E_{n,0}\, e^{-\beta_n h}. \tag{1}$$

The values of β_n are tabulated in Table 2. The values for $n \geq 13$ were measured at 2000 km, for the lines 8–12 at 3000 km, and for lines 4–6 at 5000 km. If one looks at the curves of log E_n versus height at the same height, there is a steady decrease in the slopes of the lines as one goes to lower-order lines. This effect will be discussed in Section V.

The only existing data that afford a good comparison with our data are those of Cillié and Menzel (1935). A comparison with these data shows that our values of β_n are about 30 per cent larger than their values. Both sets of data show the decrease in β_n as n decreases. At corresponding heights the two sets of data show very similar Balmer decrements.[1] The Balmer decrements increase with height in both sets of data.

The absolute intensities of our data in the low chromosphere are greater than those of

[1] The Balmer decrement is defined as $\Delta \log E_n \beta_n^{3/2}/\Delta n$.

Cillié and Menzel by a factor of about 5. This is possibly, for the most part, a real difference in the chromosphere at the two eclipses. Further evidence for real differences in the chromospheric structure can be obtained from a comparison of maximum heights of lines at this eclipse with those reported by Wildt (1947) for four previous eclipses. Wildt gives the maximum height of $H31$ as 1000 km, whereas our data show $H31$ to a height of 2400 km. On the other hand, Wildt gives a maximum height of 4000 km for $H16$, and our spectrograms give 3700 km. This convergence is also shown by the intermediate lines. These results are consistent only if we admit larger height gradients and larger absolute intensities in the low chromosphere at the 1952 eclipse.

Mitchell (1947) has reported similar differences in visual estimates of relative intensities and height gradients in previous eclipses. Cillié and Menzel (1935) have reported large differences between two points on the limb at the same eclipse. A preliminary analysis of a more disturbed region on the west limb at the 1952 eclipse gives higher absolute intensities and much lower height gradients than the east-limb region (Athay, Evans, and Roberts 1954). The evidence strongly suggests that the chromosphere is not in a steady state over large periods of time and that it is not uniform over the solar surface. It is possible that the projected chromosphere at any point on the limb represents an averaging along the line of sight of several regions of temperature and density fluctuations, such as spicules. Our "undisturbed" region may simply be a region in which the averaging produces an apparent uniformity. The degree to which chance alignments of such a nonuniform structure could produce irregularities in the projected chromosphere is an open question. The association of the disturbed region on our west-limb spectrograms with an active center showing enhanced coronal-line emission, flare activity, sunspots, and active prominences clearly suggests that the chromospheric irregularities in this region are caused by a single disturbance, possibly a flare.

V. PRELIMINARY INTERPRETATION OF DATA

The data given in Table 2 are, at the present time, being carefully analyzed by Athay, R. N. Thomas, and S. Matsushima. The analysis is aimed specifically at determination of the following quantities: (1) kinetic temperature and electron density as functions of height; (2) self-absorption, and hence the population of the Balmer ground state, as a function of height; and (3) departures from thermodynamic equilibrium. The results reported in this paper are preliminary estimates of these quantities. The final results will be reported when the analysis is completed.

The notation, geometrical situation, and geometrical approximations used below were given by Thomas (1949) in a previous paper. When the effects of self-absorption and departures from thermodynamic equilibrium are taken into account, the observed emission in a Balmer line is

$$E_n = KC_n \int_h^\infty \int_{-\infty}^\infty b_n N_e N_p T_e^{-3/2} e^{X_n} \exp\left[-a_{n,2} \int_u^\infty N_2(x, y)\, dy \right] dy\, dx\,, \tag{2}$$

where

$$K = h \left(\frac{h^2}{2\pi m k} \right)^{3/2} \tag{3}$$

and

$$C_n = \nu_{n,2} A_{n,2} \frac{\varpi_n}{2}. \tag{4}$$

In the Balmer continuum the effects of self-absorption and departures from thermodynamic equilibrium are negligible, so that equation (2) can be written

$$E_\lambda = 2.63 \times 10^{-33} \int_h^\infty \int_{-\infty}^\infty N_e N_p T_e^{-3/2} e^{X_\lambda} dy\, dx\,. \tag{5}$$

A. CONTINUUM EMISSION

If we assume that $N_p = N_e$, the Balmer continuum emission is a fairly simple function of T_e and N_e, and one can readily obtain estimates of these quantities. The Balmer continuum intensities can, within the accuracy of the data, be represented by exponential functions of height. For this case, equation (5) becomes

$$E_\lambda = 2.63 \times 10^{-33} N_e^2 T_e^{-3/2} e^{X_\lambda} \frac{(2\pi r)^{1/2}}{\beta_\lambda^{3/2}}. \tag{6}$$

Hence, we have

$$T_e = \frac{0.434 h c (\lambda' - \lambda)}{k \lambda \lambda' (\log E_{\lambda'} \beta_{\lambda'}^{3/2} - \log E_\lambda \beta_\lambda^{3/2})} \tag{7}$$

and

$$\log N_e = 13.38 + \tfrac{3}{4} \log T_e + \tfrac{1}{2} \log E_{3640} \beta_{3640}^{3/2}. \tag{8}$$

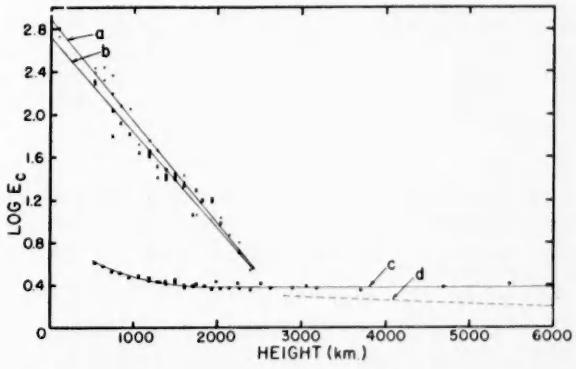

FIG. 3.—Change of continuum intensity with height. *a*, free-bound, λ 3640; *b*, free-bound, λ 3500; *c*, total, λ 4700, *minus* 1.2; *d*, east limb only, λ 4700, *minus* 1.2.

Temperatures determined from equation (7) are extremely sensitive to small errors in the data. If the individual observations at each height are used, the results are so badly scattered that they are meaningless. This is not an indication that the data are poor, but only a reflection of the fact that the observed values of $\Delta \log E_\lambda \beta_\lambda^{3/2}$ are small and that small errors are important. This difficulty can be by-passed by averaging the data. One method of doing this is to plot $\log E_\lambda$ versus height and fit the data with analytical curves. The data at λ 3640 and λ 3500, fitted with straight lines by a least-squares method, are shown in Figure 3. The data at intermediate wave lengths give curves that lie between these two curves. The data at four wave lengths were fitted with straight lines, and values of T_e were computed for all possible combinations of the lines. This method gives six determinations of T_e at each height. The average values obtained are listed in Table 3. The values at each height are subject to considerable error. For example, the equations of the two lines in Figure 3 are

$$\log E_{3640} = 2.89 \pm 0.04 - (0.95 \pm 0.03) \times 10^{-5} h \tag{9}$$

and

$$\log E_{3500} = 2.73 \pm 0.04 - (0.89 \pm 0.03) \times 10^{-5} h. \tag{10}$$

It is readily seen that the probable errors are not small compared with the differences between two equations. This method of analysis has the disadvantage that it undoubtedly introduces systematic errors into the results. On the other hand, this method shows clearly that the temperature increases with height. For an isothermal chromosphere, the two curves in Figure 3 should have the same slope. The probable errors in the slopes, equations (9) and (10), are small enough that an isothermal chromosphere is improbable.

Another method of using the data to obtain temperature information is to average the values of log $E_\lambda/E_{\lambda'}$, for each pair of wave lengths at all heights. A value for the temperature can then be computed for each pair of wave lengths and the results again averaged. This method gives an average chromospheric temperature, at these levels, of 6200° when the observed values of log $\beta_\lambda/\beta_{\lambda'}$ are used. For an isothermal model, which requires log $\beta_\lambda/\beta_{\lambda'} = 0$, an average temperature of 8000° is obtained. It must be admitted that this method of analysis is too rough to give a detailed temperature model for the chromosphere. Fortunately, the electron density determined from equation (8) is not

TABLE 3

T_e AND N_e

Height (km)	400	800	1200	1600	2000	2400
T_e (° K)	4300	4900	5600	6600	9100	11,100
$N_e \times 10^{-11}$	4.2	3.0	2.2	1.5	1.3	0.93

TABLE 4

CONTRIBUTION OF WEST LIMB TO CONTINUUM INTENSITY

Height (km)	3060	3870	5490	6300
$\frac{\text{Total } E_c}{\text{West-limb } E_c}$	3.6	3.5	2.9	2.6

too strongly dependent upon the temperature. The electron densities obtained from the emission at λ 3640 and the temperatures in Table 3 are also given in Table 3.

The intensity in the non-Balmer continuum at λ 4700 shows a surprisingly low height gradient. In fact, the continuum intensity is constant between 1600 and 6000 km, as shown by the curve in Figure 3. This is partly due to the fact that the intensity in the continuum is an integration over the chromosphere and corona extending above the moon's limbs on both sides of the sun. Hence, as the moon covers up an area on the east limb, an area of the same size is uncovered on the west limb. It is possible to separate the contributions from the two limbs by means of the terrestrial absorption bands in the infrared spectrograms, where the exposure was sufficient to show the continuum, because the absorption of the emission from the two sides of the sun occurs at different positions on the films. The contributions from the west limb are tabulated in Table 4, and the corrected curve at λ 4700 is shown by the broken line in Figure 3.

After the corrections for the west-limb contributions are made, the continuum intensity can be expressed as

$$E_c = \int_h^\infty \int_{-\infty}^{\infty} \mathfrak{E}_c \, dy \, dx \, (\lambda) \, , \tag{11}$$

where $dx(\lambda)$ indicates that each height is represented by a different wave length. However, at λ 4700 the photospheric continuum is fairly constant for about 200 A on either side, and the variation in the wave length in equation (11) is unimportant. For this case,

the integration in equation (11) is the same as in equation (5). If we assume that the continuum arises from electron scattering, we have

$$\mathfrak{E}_c \propto N_e. \tag{12}$$

It may be, as Zanstra (1950) has pointed out, that there are contributions to the continuum from free-bound emission from metals, $H-$, and hydrogen Paschen continuum. However, a preliminary analysis of the continuum data showed that these effects were important only in the lowest layers of the chromosphere. Thus we expect that an analysis of the continuum data at λ 4700 will give the electron-density structure of the chromosphere. Once the electron-density structure is known, a more accurate analysis of the temperature structure can be made from the Balmer continuum data. A detailed analysis along the lines proposed independently by Thomas (1950) and Zanstra (1950) is now in progress and will be published at a later date.

In the higher levels of the chromosphere, $h > 2000$ km, the height gradient of the continuum intensity is very small, even after corrections for the west-limb contributions are made. The data indicate changes in $\log E_c$ of the order of 0.03 per 1000 km. Gradients in $\log E_c$ of about 0.01 per 1000 km were found for the lower corona from the measurements of the continuum bordering the spectrograms. We are forced to conclude that the electron-density gradient in the chromosphere above 2000 km is very small and that the line-emission gradients in these regions of the chromosphere result primarily from the increase of temperature with height. This point will be discussed in a following section.

B. LINE EMISSION

Analysis of the line-intensity data can give us results on the effects of self-absorption and departures from thermodynamic equilibrium. The detailed analysis is not completed. However, it is possible to draw some important preliminary conclusions from an over-all look at the data.

If we restrict our discussion to the levels where the approximation of equation (1) is good, we can write for the emission gradient of a line

$$\frac{\partial \ln E_n}{\partial h} = -\beta_n = \frac{2d \ln N_e}{dh} - (\tfrac{3}{2} + X_n)\frac{d \ln T_e}{dh} + \frac{\partial \ln b_n}{\partial h} + \gamma_n(h), \tag{13}$$

where $\gamma_n(h)$ is the change in the gradient due to self-absorption; and, for the Balmer decrements,

$$\frac{\partial \ln E_n \beta_n^{3/2}}{\partial n} = \frac{\partial \ln C_n}{\partial n} - \frac{2X_n}{n} + \frac{\partial \ln b_n}{\partial n} + \frac{\partial \ln \text{abs.}}{\partial n}. \tag{14}$$

The term $2X_n/n$ in equation (14) is negligible for $n > 8$ and $T_e \geq 5000$ K°. The effect of the absorption term is to decrease the decrements. The observations show that the quantity d_n, defined by

$$d_n \equiv \frac{\partial \ln E_n \beta_n^{3/2}}{\partial n} - \frac{\partial \ln C_n}{\partial n},$$

is positive for all values of n in the lowest levels of the chromosphere. This is apparently due to the effects of self-absorption. As the height increases, the values of d_n decrease and become negative for large n. At still greater heights, above 2000 km, they are negative for all $n \geq 17$ and above 3000 km for $n \geq 9$. The negative values can result only from having $b_n > b_{n+k}$; and, since $b_n \to 1$ as $n \to \infty$, we must have $b_n > 1$. The appearance of the negative values of d_n first for the high-order lines and later for the low-order lines results from the greater effect of self-absorption on the low-order lines.

Thomas (1949) and Giovanelli (1948) have shown by theoretical computations that $b_n > 1$ for cases where the electron temperature exceeds the radiation temperature. The observations show the $b_n > 1$ for all heights greater than 1000 km. If we accept the results of Thomas and Giovanelli, we should expect to find a T_e greater than the radiation temperature, $\sim 6000°$ K, at all heights above this level. This is not very discordant with the results in Table 3 if one remembers the large probable errors in those results.

The line-emission gradients are another point of interest. If we combine equations (6) and (13) and ignore the term $X_n d \ln T_e/dh$ for $n > 8$, we can write

$$\beta_\infty - \beta_n = \frac{\partial \ln b_n}{\partial h} + \gamma_n(h) \, . \tag{15}$$

Matsushima (unpub.) has shown that, for the case of an exponential emission gradient,

$$\ln \text{abs.} = \ln \sum_{m=0}^{\infty} (-1)^m \frac{[1 + (\beta_2/\beta_n)]^{-1} (\bar{N}_2 a_{n,2})^m}{(1+m)^{3/2} m!} , \tag{16}$$

where $\bar{N}_2$ is the total number of atoms in the Balmer ground state along the line of sight. Hence,

$$\gamma_n(h) = \beta_2 \bar{N}_2 a_{n,2} \times \frac{\sum_{m=1}^{\infty} (-1)^{m+1} [(1 + m\beta_2/\beta_n)^{-1} (\bar{N}_2 a_{n,2})^{m-1}] / [(1+m)^{3/2} (m-1)!]}{\text{abs.}} , \tag{17}$$

and we see that $\gamma_n(h)$ will show approximately the same height variation as $\bar{N}_2$, which was assumed to be exponential. We could not expect to find line-emission gradients with $\beta_n < \beta_\infty$ and independent of height if $\gamma_n(h)$ was the only perturbing effect. The fact that we observe such results, but only in the higher levels of the chromosphere where self-absorption is small, could be interpreted to mean that the term $\partial \ln b_n/\partial h > 0$, and is an important contribution to the emission gradients of the low-order lines. In fact, this appears to be the only explanation of the steady changes in β_n for $n \geq 9$. The values of β_n for $n < 9$ are measured in the higher layers of the chromosphere where we have no measurements of β_∞. All the low-order lines show changes in the emission gradients in the low chromosphere of the form expected from the absorption term.

For $n \leq 8$, the term $X_n d \log T_e/dh$ may be of importance in determining the emission gradients. The effect of this term is to increase the values of β_n for small n. Such an increase is observed between $H9$ and $H6$, but it should be remembered that there is also a large increase in the height at which β_6 was measured. If this increase in β_6 is due to the increase in X_n, we should expect a much greater increase in β_4, which is not observed. However, departures from the thermodynamic equilibrium and self-absorption both tend to decrease β_n as n decreases, and the effect of the increase in X_n may be masked.

It was pointed out above that the electron-density gradient in the high chromosphere is very low. If we ignore the last two terms on the right of equation (13) for $n = 6$, we have

$$(\tfrac{3}{2} + X_6) \frac{d \ln T_e}{dh} - 2 \frac{d \ln N_e}{dh} = 1.70 \times 10^{-8} ; \tag{18}$$

and, since the continuum intensities at λ 4700, as discussed above, give $d \ln N_e/dh \simeq -0.07 \times 10^{-8}$ cm^{-1} in these levels,

$$\frac{d \ln T_e}{dh} = \frac{1.56 \times 10^{-8}}{1.5 + 0.44 \times 10^4/T_e} . \tag{19}$$

For $10{,}000 < T_e < \infty$,

$$0.35 \times 10^{-8} < \frac{d \log T_e}{dh} < 0.45 \times 10^{-8} \text{ cm}^{-1}. \tag{20}$$

These limits agree reasonably well with the value found by Thomas (1950). Even the lower of these limits on $d \log T_e/dh$ represents a rapid increase of T_e with height. For example, if we use $T_e = 11{,}000°$ K at 2400 km, as given in Table 3, and the lower limit for $d \log T_e/dh$, we get $T_e = 1.01 \times 10^{6}°$ K at 8000 km. At first sight, this value of T_e appears much too high. However, the maximum height of $H\alpha$ at this eclipse appears to be about 8000 km, and we should not be too surprised to find coronal temperatures at this height.

The methods of analysis used above are rather rough, and the results will undoubtedly be modified by the more detailed analysis in progress. Nevertheless, the above results are sufficiently well determined to conclude that the chromosphere above 2000 km is characterized by a large increase in temperature with height and a relatively small electron-density gradient. This is in contrast with previous models of the chromosphere, which have assumed a low temperature gradient and a relatively high electron-density gradient.

It is of further interest to consider the method of obtaining emission gradients used by Wildt (1947). The condition for equal intensity in the Balmer lines, as used by Wildt, is

$$\frac{d \ln E_n \beta_n^{3/2}}{dh} = \left(\frac{\partial \ln C_n}{\partial n} - \frac{2X_n}{n}\right)\frac{dn}{dh} + 2\,\frac{d \ln N_e}{dh} - \left(\tfrac{3}{2} + X_n\right)\frac{d \ln T_e}{dh} + \frac{\partial \ln b_n}{\partial n}\frac{dn}{dh} + \frac{\partial \ln b_n}{\partial h} + \frac{\partial \ln \text{abs.}}{\partial n}\frac{dn}{dh} + \gamma_n(h) = 0. \tag{21}$$

Wildt ignored the b_n terms and worked at levels where the absorption terms were negligible. He then interpreted all of the quantity

$$\left(\frac{\partial \ln C_n}{\partial n} - \frac{2X_n}{n}\right)\frac{dn}{dh}$$

as being due to the electron-density gradient. In view of the above arguments, the neglect of the b_n's and the temperature gradients will lead to erroneous results. In fact, since the lines all show different emission gradients, the values of dn/dh depend upon the intensity under consideration. In Figure 4 the values of $\log C_n - \frac{3}{2} \log \beta_n$ are plotted against heights of equal intensity for three different intensities. The slopes, m, of the resulting straight lines are entered in Figure 4 and are seen to be different for the three cases. In all cases the intensities are in regions where the gradients are exponential, and, as pointed out above, the effects cannot be blamed entirely upon self-absorption. From equations (13) and (21), we get

$$(\beta_n - m)\frac{dh}{dn} = \frac{\partial \ln \text{abs.}}{\partial n} + \frac{\partial \ln b_n}{\partial n}. \tag{22}$$

For $n \geq 19$ and $\log E_n = 13.5$, the left side of equation (22) is negative. The term $\partial \ln \text{abs.}/\partial n$ is positive, and we must conclude that $\partial \ln b_n/\partial n < 0$. This is in agreement with the results obtained from the observed Balmer decrements. Furthermore, this result seems to hold at all chromospheric levels above 700 km. For small n, the left side of (22) is positive, and the effects of self-absorption dominate.

In plotting Figure 4 we have ignored the effect of the term e^{X_n} on the line intensities. For large n and $T_e \geq 5000°$, the neglect is unimportant. For small n, we should evaluate this term in the high levels of the chromosphere. However, we expect high temperatures in the high levels of the chromosphere, and even for small n the neglect of this term is probably not important.

The heights of $H\beta$, $H\gamma$, and $H\delta$ are greater than would be expected from the linear relationship exhibited by the higher-order lines. If we include the e^{X_n} term in the line intensities, the departures from linearity will be smaller, but they cannot be removed with any reasonable values of T_e. Actually, as an inspection of equation (22) will show, we have no reason to expect a linear relationship unless the effects of self-absorption and departures from thermodynamic equilibrium can be neglected. The large heights of the low-order lines are primarily due to the departures from thermodynamic equilibrium as pointed out above. This interpretation of Wildt's analysis was suggested by Thomas (1949). The data show that this interpretation is consistent and can explain the low emission gradients found by Wildt.

We wish to express our thanks to Dr. E. O. Hulbert and Dr. John P. Hagen, of the Naval Research Laboratory, for the many forms of assistance and advice rendered us before, during, and after the expedition. We are particularly indebted to them for aid at the eclipse after Dr. Evans' accident and for the close co-ordination of their radio-noise

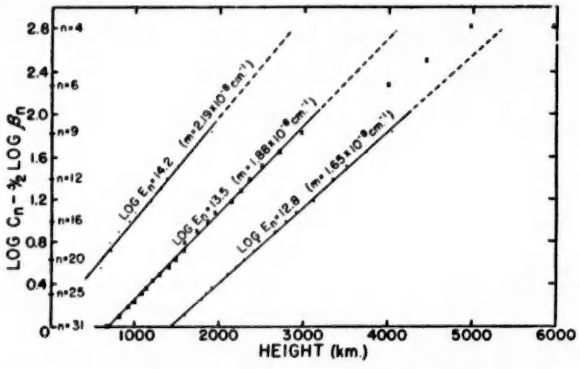

FIG. 4.—Emission gradients obtained from heights of equal line intensity

observations with our optical observations. We also wish to thank Commander W. E. Berg for the excellent manner in which the eclipse expedition was carried out. Our equipment made the difficult trip to the eclipse site in the face of severe complications, on excellent schedule, and without any damage.

In the course of preparing the observing equipment we were forced to turn to many other groups for help. We wish particularly to acknowledge the contributions of the following: (1) Lick Observatory for the use of the Ross lenses; (2) Mount Wilson Observatory for the loan of a mirror blank for the 24-inch spherical mirror; (3) Dr. D. H. Menzel for the use of the infrared grating; (4) Dr. David Richardson and the Bausch and Lomb Optical Company for their excellent and generous work in the preparation of the ultraviolet and visual gratings; (5) Baird Associates for preparation of the optical wedges used in the standardizing program; and (6) Dr. William F. Swann and the Research Department of Eastman Kodak Company for preparing films for the observations. In addition, we wish to thank the whole staff of the High Altitude Observatory, who contributed so freely of their time and talents when schedule problems made it appear that some of our components might not be ready in time for the expedition. We are further indebted to Dr. D. H. Menzel for his help and encouragement throughout all phases of the work, to Dr. R. R. McMath for the use of the microdensitometer at the McMath-Hulbert Observatory, to Mrs. K. M. Virnelson for aid in preparation of the manuscript, and to Dr.

Charlotte Pecker for her help in the reduction of the data. The authors wish to express particular appreciation to Dr. Richard N. Thomas, whose enthusiasm for the problem led initially to planning the expedition and whose unstinting encouragement has been a principal factor in carrying the observational reductions through to a successful conclusion. The methods of interpretation were conceived by Thomas, and results of these studies are in preparation for publication by Thomas and his associates.

This work was supported by the Office of Naval Research and was carried out in cooperation with the Naval Research Laboratory.

REFERENCES

Allen, C. W. 1946, *M.N.*, **106**, 137.
Athay, R. G. 1953, Technical Report, Office of Naval Research Contract Nonr 393(01), available from High Altitude Observatory, Boulder, Colorado.
Athay, R. G.; Evans, J. W.; and Roberts, W. O. 1953, *Observatory*, **73**, 244.
Beck, C. J.; Lovell, D. J.; and Hulbert, E. O. 1953, *J. Opt. Soc. Amer.*, **43**, 405.
Cillié, G. G., and Menzel, D. H. 1935, *Harvard Obs. Circ.*, No. 410.
Forsythe, W. E., and Adams, E. Q. 1945, *J. Opt. Soc. Amer.*, **35**, 108.
Fowler, F. E., and Johnson, D. S. 1951, *Electronics*, **24**, 118.
Giovanelli, R. G. 1948, *Australian J. Sci. Res. A.*, **1**, 360.
Grotrian, W. 1931, *Zs. f. Ap.*, **3**, 199.
Matsushima, S. Unpublished communication.
Mitchell, S. A. 1947, *Ap. J.*, **105**, 1.
Nicolet, M. 1951, *Ann. d'ap.*, **14**, 249.
Thomas, R. N. 1949, *Ap. J.*, **109**, 480.
Thomas, R. N. 1950, *Ap. J.*, **111**, 165.
Thomas, R. N. 1950, *Ap. J.*, **112**, 337.
Trotter, D. E., and Roberts, W. O. 1952, *High Altitude Observatory Reports*, Nos. HAO-NBS-11 and HAO-NBS-15.
Wildt, R. 1947, *Ap. J.*, **105**, 36.
Zanstra, H. 1950, *Proc. Keninkl. Ned. Akad. Wetensch.*, **53**, No. 8, 1 (Circ. No. 1, Astronomical Institute, University of Amsterdam).

ACTIVE REGION PROMINENCES AND THE YELLOW CORONAL LINE*

F. P. Dolder, W. O. Roberts, and D. E. Billings
High Altitude Observatory, Boulder, Colorado
Received November 16, 1953; revised December 30, 1953

ABSTRACT

Regions of the sun characterized by emission of the rarely observed yellow coronal line λ 5694 were found to be positively associated with the following characteristic behavior of prominences at the same location: (*a*) large numbers of associated surge-type prominences; (*b*) predominance of scattered knots; (*c*) formation of continuous streamers; (*d*) downward motion of knots and streamers toward an active center; and (*e*) sharp curvatures and focusing effects in trajectories. On the other hand, the principal observed characteristics of quiescent solar prominences were found to be negatively associated with the regions of yellow coronal-line emission.

INTRODUCTION

The yellow line, λ 5694, in the spectrum of the solar corona differs from the most readily observed coronal lines λλ 5303, 6374, and 6702, in that it is a much more rare phenomenon and in that it is clearly associated with centers of intense solar activity. Waldmeier (1950) and Roberts (1952) have studied prominences associated in time and solar position with yellow-line coronal emission (hereafter called "yellow-line prominences") and have given qualitative descriptions of typical yellow-line prominences. Dolder, Roberts, and Billings (1954) have presented quantitative evidence for the identification of yellow-line emission with solar flares, the most violent of solar active-region phenomena.

Other phenomena, such as active sunspots, intense emission of the common coronal lines, bright solar plages, or prominences of recognizable type, also characterize centers of strong solar activity. A distinctive indicator of active solar regions is the presence of prominences of the types classified by Pettit (1943) as "sunspot prominences" III*a*, III*b*, III*c*, and III*d*. Such prominences exhibit rapid changes, surges, high-curvature loops, and knots of material that appear to converge toward a point on the solar limb generally in the close neighborhood of a sunspot.

In this paper we report a quantitative analysis of the degree of association of these characteristics of sunspot prominences with occurrence of yellow coronal-line emission. We compare, for control, the extent to which the same characteristics are associated with prominences, sunspot and otherwise, that are not located in regions of known yellow-line emission. From our study we conclude that there is sound quantitative justification for association of coronal yellow-line emission not only with flares, as previously reported (Dolder, Roberts, and Billings 1954), but also with specific characteristics of sunspot prominences. We conclude, moreover, that certain of the characteristics of sunspot prominences are more strongly associated than others with the intense solar activity indicated by the yellow coronal line.

OBSERVATIONAL MATERIALS

The basic data resource for this study was coronal spectrograms from the High Altitude Observatory coronagraph at Climax, supplemented by all available similar spectrograms from the Harvard College Observatory program at the Upper Air Research Observatory at Sacramento Peak, New Mexico, for the years 1946–1950 inclusive, some 4500 individual spectra. Dolder carefully examined these spectra independently of any previous measures, searching only for clear-cut instances of emission of the coronal yellow

* The research reported in this paper was supported by the Office of Naval Research.

line. He found 43 such cases. The dates and locations of these cases are given in an earlier publication (Dolder, Roberts, and Billings 1954). In all cases active regions showing sunspots, flares, coronal red and green line-emission maxima, or all three phenomena appeared on the limb near the point of yellow-line emission.

We then collected, from our Climax prominence motion-picture library, 41 prominence sequences selected only on the basis that the films included the locations of coronal yellow-line emission and were taken on or within 2 days of the date of the yellow-line case. For a number of the yellow-line observations we did not have such motion-picture sequences; however, we did have films for 23 of the 43 yellow-line cases. The motion pictures had been photographed in the Climax coronagraph, through a birefringent filter of 4 A half-width centered on the Balmer-α hydrogen line. The rate of photographing was two, three, or six frames per minute.

Finally, for purposes of comparison, we assembled from our library of prominence films another set of motion pictures from which we had removed only the yellow-line prominences. The remainder thus contained a mixture of sunspot-type and other prominences. These comparison films were taken during the winters of 1947–1948 and 1949–1950. We chose pictures taken during winter months because of their generally better quality. The particular winters were chosen to include a period near sunspot maximum, as well as a period somewhat removed from sunspot maximum, and thus to approximate the time distribution with regard to sunspot maximum of the years during which the yellow-line cases occurred. Forty-two prominences were included in the comparison motion picture, taken in the order in which they appeared on the film, without any regard for their size or type. Thirty prominences were included from the winter of 1947–1948, 12 from the winter of 1949–1950. We emphasize that this body of materials may have included unrecognized cases of emission of the yellow coronal line.

METHOD OF GRADING PROMINENCES

In order to obtain a description of the prominences that could be handled by quantitative statistical methods, we decided to grade each prominence numerically according to the degree to which it exhibited certain characteristics. We included, of course, only the prominences at the same position as the yellow-line emission, when the films included several prominences. Two HAO staff members examined the films several times, in a preliminary way, to determine the distinguishable features by which to define a system of categories for numerical grading, including particularly those characteristics that seemed typical of the yellow-line prominences. From this they established the following categories of prominence characteristics for further treatment:

1. Construction of prominence
   - *a*) Scattered knots—isolated concentrations of prominence material not fastened to any other portions of the prominence
   - *b*) Continuous streamers—prominence material fastened together to give the appearance of a solid stream or column of gas
   - *c*) Massive body—the body of the prominence is a large cloud of material such as is usually associated with the "quiescent" prominences
2. Origin of the prominence material
   - *a*) Space—the prominence gas seems to materialize out of "space," coming thus from above the solar limb but not from any visible cloud of material
   - *b*) Suspended cloud—the prominence material seems to come from a cloud of gas above the sun's surface
   - *c*) Body on the sun's surface—the material seems to come from a body attached, in projection at least, to the surface of the sun
3. Focusing effects
   - *a*) At the source of the moving matter—the prominence material seems to originate

at one point and spread out in different directions, thus clearly diverging from the focus

b) At the terminus of the moving matter—the material seems to converge to a point on or near the sun's surface

4. Curvature of trajectory—the trajectory of the moving material is highly curved
5. Number of surges seen—the actual number per unit time of sudden outward ejections of prominence material from the solar surface was noted
6. Direction of motion
   a) Downward—the prominence material appears to be moving toward the sun's limb
   b) Horizontally—the material is moving horizontally
   c) Interacting—the material seems to be moving in opposite directions at the same time
   d) Upward—the material appears to be moving away from the sun's limb

Five different staff members then studied the projected motion pictures of yellow-line prominences, running each film several times and grading each prominence on each characteristic, using numerical grades that ran from 1 to 5—1 if the prominence provided a striking example of the characteristic; 5 if the characteristic was not present at all. One observer, Dolder, finding that his gradings followed closely the averages of the other observers, graded the nonyellow-line prominences alone. Many of the characteristics were not, of course, mutually exclusive, so that, for example, 1*a* and 1*b* tended to occur to a marked degree in the same prominence.

ANALYSIS AND RESULTS

We then applied statistical treatment to the grades given the prominences for two purposes:

1. To determine from the grades of the yellow-line prominences alone whether or not any change takes place in the character of yellow-line prominences during yellow-line emission over the 5-day range included in our study.

2. To measure the extent by which yellow-line prominences differ from nonyellow-line prominences in the characteristics listed.

In carrying out the analysis of the first question we studied the prominence on the day of yellow-line emission and on the 2 days preceding and the 2 days following. Table 1

TABLE 1

Days from yellow-line date	−2	−1	0	+1	+2
No. of films	3	7	21	6	4

shows the number of films used in each case. An average grade was obtained for each characteristic in each time group. These grades showed no clear-cut trend. The negative result of this analysis suggests that yellow-line emission is not a sharply defined step in the evolution of the prominences over an active region. It also suggests that the characteristics typical of a yellow-line prominence are observable when the center of the prominence is not exactly at the limb. The results imply that it should often be possible, from the characteristics of the associated prominences, to identify an active region unambiguously 2 or 3 days before its center rotates onto the visible solar disk.

Tables 2 and 3 summarize the results of our study of the second question. Columns 1 and 2 of Table 2 list the mean grades of the prominences of both groups, derived as described above, and indicate which characteristics differ between the two classes of films. Table 3 lists the mean number of surges per hour, which we consider significantly different for the two classes.

To evaluate the significance of the differences between the yellow-line prominences and the nonyellow-line prominences, we applied the following statistical procedures. We considered the set of yellow-line prominences and the set of nonyellow-line prominences each to be samples drawn from infinite populations of yellow-line cases and nonyellow-line cases, respectively. If we had an infinity of samples of each kind, we would expect the means of the samples to be distributed about the means of their respective populations

TABLE 2

Prominence Characteristics	Yellow-Line* Mean Grade (1)	Nonyellow-Line Mean Grade (2)	$\sigma_{\bar{x}_1-\bar{x}_2}$ (3)	$\Delta M/(\sigma_{\bar{x}_1-\bar{x}_2})$ (4)	Probability of Being from Same Population† (5)
Scattered knots	2.5	3.6	0.27	4.1	4×10^{-5} Y
Continuous streamers	2.6	3.5	.24	3.7	2×10^{-4} Y
Massive body	3.7	2.0	.32	4.7	1×10^{-6} N
Matter from space	1.7	3.6	.31	6.1	1×10^{-6} Y
Matter from suspended cloud	4.4	4.2	.76	0.8	5×10^{-1}
Matter from body on surface	3.8	2.4	.34	4.3	2×10^{-5} N
Focus at source	3.2	4.2	.26	4.0	6×10^{-5} Y
Focus at terminus	2.3	3.4	.27	3.8	1×10^{-4} Y
Curvature of trajectory	2.7	3.5	.25	3.2	1×10^{-3} Y
Downward motion	1.4	2.8	.26	5.5	1×10^{-5} Y
Horizontal motion	3.9	3.2	.29	2.4	2×10^{-2}
Interacting motion	4.5	4.6	.21	0.5	6×10^{-1}
Upward motion	4.1	4.6	0.22	2.0	5×10^{-2}

* Small numbers (1) indicate that the prominence strongly exhibits the characteristics; large numbers (5) that it does not do so.

† Y = Considered significantly small, indicating characteristics typical of the yellow-line prominences; N = Considered significantly small to indicate characteristics typical of nonyellow-line prominences.

TABLE 3

MEAN NUMBER OF SURGES PER 1000 MINUTES

Yellow-line prominences	7.05
Nonyellow-line prominences	2.05
Probability of being from same population	1×10^{-3} Y

according to a normal distribution. The most probable distribution of the means of the samples about the population mean is, in each case, such that $\sigma_{\bar{x}}$, the standard deviation of the sample means from the population mean, is related to the standard deviation within a given sample, σ_x, by

$$\sigma_{\bar{x}} = \frac{\sigma_x}{\sqrt{N-1}},$$

where N is the number of cases in the sample—in our problem, the number of prominence films.

The difference between the means (of pairs of samples) from the same population may also be expected to follow a normal distribution about zero. The standard deviation, $\sigma_{\bar{x}_1-\bar{x}_2}$, of these differences from zero is related to the standard deviations, $\sigma_{\bar{x}_1}$ and $\sigma_{\bar{x}_2}$, of the sample means from the population means by

$$\sigma_{\bar{x}_1-\bar{x}_2} = \sqrt{\sigma^2_{\bar{x}_1} + \sigma^2_{\bar{x}_2}},$$

tabulated in column 3 in Table 2.

Hence, if we assume the yellow-line prominences and the nonyellow-line prominences to be samples from the same population, the probability that a difference equal to, or

greater than, ΔM will occur between the mean grades in the first and second columns of Table 2 is

$$P = 1 - \frac{2}{\sqrt{\pi}} \int_0^z e^{-z^2} dz = 1 - \text{erf}(z), \qquad \text{where} \qquad z = \frac{\Delta M}{\sigma_{\bar{x}_1 - \bar{x}_2}} \cdot \frac{1}{\sqrt{2}},$$

and *erf* (z) represents the normal error function. Values of P for each characteristic are tabulated in Table 2, column 5. We have considered characteristics marked "Y" significantly associated with yellow-line prominences, but not prominences in general. We have considered properties marked "N" significantly absent in yellow-line prominences by comparison with other types of prominences.

DISCUSSION OF RESULTS

By listing the characteristics on which the prominences were to be graded after we had studied the films to be graded, we may have biased the analysis in favor of the results obtained. Consequently, we established rigorous criteria of significance for the probabilities, P, in column 5 of Table 2. We have considered significantly small only those probabilities less than 3×10^{-3}, i.e., the differences between means of samples are greater than three standard deviations of differences from zero. The significant characteristics positively associated, we find, are all those which have been listed by Pettit (1943) as the characteristics of sunspot prominences. Thus we may consider the results as giving quantitative justification of the hypothesis that yellow-line prominences are, in general, of the sunspot type.

Two prominence characteristics very closely associated with yellow-line emission are "matter from space" and "scattered knots." When matter suddenly becomes visible from "space," according to Alfvén (1950), it is probably a consequence of magnetic constriction in an electric discharge, resulting in the aggregation of matter in the discharge. Menzel and Evans (1953) have also suggested that formation of discrete knots is a consequence of magnetic constriction in a discharge. The importance of a third characteristic, "focus at source," suggests that the electric discharges in which prominence material arises are well localized in the solar atmosphere.

The remaining significant characteristics of yellow-line prominences—"downward motion," "focus at terminus," "continuous streamers," and "curvature of trajectories"—suggest further that these discharges take place in a magnetic field which extends outward, diverging from an active center through a considerable region in the corona. A sufficient condition for downward motion of a neutral cloud of ions is that the component of the gravitational field parallel to the magnetic field should exceed opposing forces which might arise from pressure gradients or magnetic-field gradients. Field gradients are involved, since clouds of ions are diamagnetic. Hence the magnetic field which we have just described would, in general, direct prominence material downward and focus it into the active center.

The continuous streams and clear-cut curved trajectories in yellow-line prominences may define magnetic lines of force. They certainly define the motion field resulting from whatever magnetic, electric, and gravitational fields may be present. Motion fields in yellow-line prominences are relatively simple, static, continuous, and extensive. They are simple and static compared to the motion field of eruptive quiescent prominences, which are far from active centers. In such quiescents, the motion of a given knot of matter appears to be compounded of motion of the knot with respect to the velocity field superimposed on a substantial motion of the field with respect to the solar surface (Cape 1953). The recognizable size of the velocity fields determined from prominence motions seems comparable with the extent of the surface magnetic fields observed by Babcock (1952) in the vicinity of active sunspot regions, or with the size of the regions of intense coronal-line emission found near active solar centers (Roberts, Billings, and Liebenberg, unpub.).

Study of motion of individual prominence clouds and attempts like those of Dodson (1948) to derive characteristics of motion fields, even though difficult, are most important. Some such analysis has been carried out at the High Altitude Observatory (Bartlett, Witte, and Roberts 1953), and more are in progress.

We acknowledge with appreciation the opportunity to use coronal spectrograms from the Upper Air Research Observatory at Sacramento Peak, New Mexico, operated by Harvard College Observatory and by the Geophysical Research Directorate of the Air Force Cambridge Research Center. We also express our gratitude for helpful discussions with John W. Evans, Richard N. Thomas, and Donald H. Menzel. Our former colleague, Bruno Witte, devised and helped carry out much of the statistical analysis reported here.

REFERENCES

Alfvén, H. 1950, *Cosmical Electrodynamics* (Oxford: Clarendon Press).
Babcock, H. W. 1952, *Pub. A.S.P.*, **64**, 282.
Bartlett, T. J.; Witte, B.; and Roberts, W. O. 1953, *Ap. J.*, **117**, 292.
Cape, J. A. 1953, "Investigation of Solar Prominences" (M.S. thesis, Montana State College).
Dodson, H. 1948, *M.N.*, **108**, 383.
Dolder, F. P.; Roberts, W. O.; and Billings, D. E. 1954, *Ap. J.*, **119**, 120.
Menzel, D. H., and Evans, J. W. 1953, *Convegno Volta Accademia nazionale dei Lincei*, **11**, 119.
Pettit, E. 1943, *Ap. J.*, **98**, 6.
Roberts, W. O. 1952, *Ap. J.*, **115**, 488.
Roberts, W. O.; Billings, D. E.; and Liebenberg, D. H. "Evolution of Emission-Line Corona" (in preparation).
Waldmeier, M. 1950, *Zs. f. Ap.*, **27**, 73.

BRIGHT LATE M-TYPE STARS NEAR THE GALACTIC EQUATOR

J. J. NASSAU AND V. M. BLANCO
Warner and Swasey Observatory, Case Institute of Technology
Received January 18, 1954

ABSTRACT

A catalogue is given of 384 late M-type stars within a galactic zone 4° wide from longitude 333° through zero to 201°. Of these stars, 67 are known or "suspected" variables. The classification was made on objective-prism plates, utilizing the near infrared spectral region from λ 6800 to λ 8800. The limiting infrared magnitude of stars in the list is about 8.2.

In the course of our surveys of relatively cool stars in the Milky Way, a number of bright (in infrared sense) late M stars were selected, and their positions established with the hope that other investigators may find them useful. The present list includes all stars with infrared magnitude less than 8.2 and spectral classes M5 and later. The region covered is a 4°-wide continuous belt centered at the galactic equator from longitude 333° to 201°. A few stars with galactic latitude slightly outside the limit $\pm 2°$ have been included, as well as some stars fainter than the limiting magnitude.

The surveys were carried out with the 2° objective prism attached to the Burrell Schmidt-type telescope. The spectral region covered is from λ 6800 to λ 8800 and was obtained by using Kodak 1-N emulsion with a No. 89 Wratten filter. The criteria for classification were those established by Nassau and van Albada (1949). The class M5 was selected, since it can be established readily by the presence of the *TiO* bands at λ 8432 and by fully developed *TiO* bands near the telluric A band. This boundary in spectral class divides the M stars naturally into two groups, and, in addition, it makes certain that the selected stars are free from early supergiants. An effort was made to free the list from late M dwarfs, as the infrared spectra do not distinguish between giants and dwarfs. One such star was found. From the known distribution of dwarfs with respect to magnitude, very few, if any, should be found in the present list.

The limiting magnitude of the plates used was about 10.2, so that, in general, the spectra of the stars included in the present list were overexposed. For this reason, spectra of standard stars purposely overexposed were used for the classification. An independent classification for about one-third of the stars was made from spectra of correct exposure which were obtained with the 4° or 6° objective prism. The results indicate no systematic errors, and the difference between the two classifications was rarely more than one spectral subclass, readily accountable when the spectral change of the stars themselves is considered.

The approximate magnitudes were established directly from the spectral plates by means of a graduated scale of spectral images of the appropriate spectral class. The density estimates were calibrated by means of infrared sequences established in the LF regions (McCuskey and Seyfert 1947), which are located in the Milky Way about 20° apart. Since an overlap of nearly 2° was available from plate to plate, the calibration was extended to the individual plates. In addition, the program plates were taken and treated under the same conditions and have the same effective exposure. A rough comparison with *BD* magnitudes indicates that no serious systematic errors are present. The great majority of these stars are bound to be variable, and the principal reason for listing their magnitudes is to establish a limiting magnitude for the catalogue and to aid in their identification. To obtain approximate photographic magnitudes, 5.6 may be added to the infrared magnitudes.

Table 1a

Late M-Type Stars

No.	B.D.		1900	m_1	Sp	l	b	Remarks
1	63°	3	$0^h04^m.1$ +63°24'	4.8	M5	86	+2	
2	62	190	0 56 .9 +62 34	5.7	M5	92	+1	
3	63	173	1 13 .7 +63 30	6.1	M6	94	+2	
4	61	325	1 40 .1 +62 04	6.5	M6	97	+1	BX Cas, M6, SR?
5	61	355	1 49 .2 +61 43	5.1	M7	98	+1	
6	60	382	1 49 .3 +60 28	7.4	M5	98	0	
7	50	829	3 41 .3 +50 32	5.4	M6	117	-2	
8	50	856	3 48 .5 +50 23	7.7	M5	118	-1	
9	49	1130	4 05 .7 +49 27	7.3	M5	121	0	
10	49	1152	4 11 .0 +49 37	5.3	M5	121	+1	
11	45	940	4 22 .9 +45 44	5.2	M6	125	-1	
12	48	1106	4 25 .9 +48 29	8.3	M5	124	+2	
13	44	994	4 29 .3 +44 46	5.4	M5	127	0	YY Per, M3, SP?
14	44	1028	4 41 .8 +44 08	7.9	M5	129	+1	
15	39	1081	4 44 .0 +39 15	6.3	M5	133	-2	
16	38	989	4 52 .7 +38 58	8.0	M5	134	-1	
17	34	946	5 00 .0 +34 43	4.3	M5	138	-2	
18	34	947	5 00 .3 +34 32	7.1	M5	138	-2	
19	34	1011	5 15 .0 +34 05	6.4	M5	141	0	
20	36	1104	5 15 .8 +36 27	5.9	M5	139	+1	
21	33	1029	5 17 .1 +33 26	8.1	M6	141	0	
22	30	903	5 21 .3 +30 38	7.0	M5	144	-1	
23	32	996	5 22 .4 +32 24	5.1	M5	143	0	
24	33	1069	5 23 .7 +33 18	8.1	M7	142	+1	
25	32	1020	5 25 .6 +32 09	7.7	M5	143	+1	
26	30	960	5 31 .6 +30 50	6.4	M5	145	+1	
27	24	898	5 32 .5 +24 57	4.7	M7	150	-2	636
28	28	847	5 34 .8 +28 03	7.6	M7	148	0	AB Tau, M5, SR
29	21	1021	5 46 .8 +21 36	5.9	M5	155	-1	
30	18	997	5 47 .3 +18 57	5.1	M5	157	-2	
31	22	1109	5 51 .0 +22 49	4.4	M6	154	+1	BQ Ori, M5, SR
32	14	1164	6 03 .2 +14 08	5.1	M6	163	-1	
33	13	1145	6 05 .1 +13 04	7.7	M5	164	-1	
34	11	1054	6 06 .0 +11 14	5.5	M6	166	-2	
35	19	1251	6 06 .0 +19 13	7.1	M5	159	+2	
36	12	1055	6 06 .3 +12 30	4.8	M6	165	-1	
37	17	1187	6 09 .6 +17 47	4.4	M5	161	+2	
38	16	1070	6 10 .7 +16 43	6.3	M6	162	+2	
39	8	1312	6 18 .5 + 8 33	7.7	M7	170	-1	
40	3	1231	6 19 .2 + 3 46	6.3	M5	174	-3	
41	3	1233	6 19 .6 + 3 49	4.9	M5	174	-3	
42	6	1258	6 23 .6 + 6 50	7.1	M5	172	0	
43	7	1304	6 23 .7 + 7 29	7.9	M6	172	0	
44	0	1484	6 29 .5 + 0 16	5.8	M5	179	-2	
45	-1	1309	6 33 .5 - 1 34	6.4	M7	181	-2	CY Mon, I
46	1	1506	6 42 .0 + 1 38	5.4	M5	179	+1	861, L
47	-8	1641	6 52 .5 - 8 56	4.9	M5	189	-1	X Mon, M3e, LP
48	-8	1650	6 53 .4 - 8 53	3.8	M5	189	-1	
49	-6	1901	6 57 .8 - 6 23	6.9	M5	188	+1	
50	-7	1699	6 57 .9 - 7 47	5.7	M4	189	0	

Table 1a

Late M-Type Stars

No.	B.D.	1900	m_1	Sp	l	b	Remarks
51	-15° 1686	$7^h06^m.7$ -15°59'	6.8	M5	197	-2	
52	-14 1776	7 08 .8 -14 24	5.4	M5	196	-1	
53	-19 1790	7 12 .6 -19 12	5.2	M5	201	-2	
54	-15 1767	7 15 .2 -15 41	7.0	M8	198	0	
55	-17 1998	7 25 .0 -17 22	4.5	M5	201	+1	
56	-21 4803	17 53 .3 -21 26	5.5	M6	336	0	
57	-15 4775	17 55 .6 -15 21	4.4	M5	341	+2	
58	-22 4508	17 56 .2 -22 29	5.5	M5	335	-1	
59	-21 4828	17 56 .8 -21 59	6.2	M5	336	-1	
60	-16 4697	17 58 .2 -16 57	5.9	M5	340	+1	
61	-20 4974	17 58 .7 -20 48	5.5	M5	337	-1	
62	-15 4805	17 59 .1 -15 43	5.5	M5	341	+1	
63	-19 4839	18 00 .6 -19 53	7.3	M5	338	-1	
64	-19 4850	18 01 .8 -19 49	7.3	M5	338	-1	
65	-11 4543	18 03 .6 -11 49	6.5	M6	345	+2	
66	-18 4822	18 05 .1 -18 53	4.8	M5	340	-1	
67	-13 4896	18 10 .1 -13 14	6.1	M5	344	0	
68	-15 4915	18 12 .6 -15 21	5.8	M5	343	-1	
69	-12 5006	18 14 .4 -12 21	5.4	M5	346	0	
70	-14 5007	18 15 .1 -14 42	5.6	M5	344	-2	
71	-14 5012	18 16 .4 -14 01	5.4	M5	345	-1	
72	-8 4612	18 22 .3 - 8 45	6.6	M5	350	0	
73	-2 4676	18 32 .2 - 2 45	6.3	M6	357	0	CZ Ser, M3, I
74	1 3763	18 39 .6 + 1 47	4.9	M5	2	+1	
75	-2 4745	18 42 .5 - 2 07	6.2	M5	358	-2	AB Aql, M4, I?
76	6 3984	18 52 .5 + 6 34	5.7	M5	7	0	V840 Aql, M5, SR
77	2 3740	18 52 .6 + 2 35	6.0	M5	4	-2	
78	12 3762	18 56 .4 +12 36	6.5	M5	13	+2	
79	4 3952	18 56 .8 + 4 46	5.9	M6	6	-1	
80	8 3970	19 01 .6 + 8 05	4.8	M8	10	-1	R Aql, M7e, M
81	6 4025	19 02 .1 + 6 59	6.1	M6	9	-2	4526, L
82	13 3948	19 08 .1 +13 23	7.3	M5	15	0	
83	19 3967	19 12 .3 +19 16	7.6	M5	21	+2	
84	15 3761	19 14 .0 +15 21	5.4	M5	18	0	
85	17 3940	19 17 .2 +17 28	4.3	M7	20	0	T Sge, M4, I
86	27 3478	19 38 .5 +28 00	7.3	M5	31	+1	
87	29 3730	19 41 .8 +30 01	5.0	M5	33	+2	
88	32 3593	19 46 .8 +32 40	4.8	M8	36	+2	χ Cyg, Mpe, M
89	32 3630	19 52 .0 +33 02	7.4	M5	37	+2	
90	28 3560	19 55 .3 +28 08	7.7	M5	33	-2	
91	32 3664	19 56 .4 +32 20	7.0	M5	37	0	
92	33 3690	19 57 .5 +33 38	4.9	M6	38	+1	V485 Cyg, M7, I
93	29 3877	20 00 .1 +29 31	6.7	M5	35	-2	
94	32 3706	20 02 .6 +33 02	7.4	M5	38	0	V487 Cyg, M3, SR
95	38 3948	20 09 .1 +38 43	6.3	M5	44	+2	
96	37 3831	20 09 .7 +37 26	7.0	M6	43	+1	
97	33 3846	20 14 .0 +33 47	4.0	M5	40	-2	
98	39 4152	20 18 .1 +40 08	5.1	M7	46	+1	V405 Cyg, M6, I
99	37 3946	20 24 .7 +37 28	4.9	M5	45	-1	
100	39 4302	20 41 .2 +40 03	5.7	M6	49	-2	

Table 1a

Late M-Type Stars

No.	B.D.	1900	m_i	Sp	l	b	Remarks
101	45° 3262	$20^h42^m.4$ +45°50'	8.8	M5	53	+1	
102	46 3082	20 49 .0 +46 24	7.1	M7	54	+1	
103	42 3899	20 50 .6 +42 16	6.9	M5	51	-2	
104	44 3649	20 54 .3 +44 24	4.2	M6	53	-1	
105	45 3379	20 59 .4 +46 06	5.9	M6	55	-1	
106	47 3321	21 07 .0 +47 15	4.1	M6	57	-1	
107	48 3348	21 16 .8 +48 56	4.4	M6	59	-1	ADS 14885
108	49 3567	21 33 .0 +49 19	6.9	M5	62	-2	
109	51 3117	21 37 .0 +51 17	6.9	M5	63	-1	5461
110	53 2684	21 37 .3 +53 52	4.8	M7	65	+1	RU Cyg, M8e, SR
111	54 2603	21 38 .8 +54 22	4.9	M5	65	+1	
112	51 3188	21 52 .1 +52 03	5.6	M5	66	-2	
113	53 2748	21 54 .9 +54 05	5.3	M5	67	0	
114	56 2692	22 00 .1 +57 05	6.6	M5	70	+2	
115	57 2487	22 10 .5 +57 31	5.6	M7	71	+1	
116	57 2541	22 24 .7 +57 36	6.7	M5	73	0	
117	60 2438	22 43 .9 +60 44	5.2	M7	76	+2	
118	60 2469	22 57 .4 +61 02	4.6	M6	78	+1	
119	58 2560	23 07 .3 +59 08	5.2	M7	78	-1	V Cas, M6e, M
120	59 2768	23 41 .3 +59 56	5.5	M5	83	-1	ADS 16982 C?
121	59 2806	23 55 .3 +59 48	5.1	M5	84	-2	

Table 1b

. Late M-Type Stars

No.	B.D.		Δx	Δy	1900		m_i	Sp	l	b	Remarks
122	60°	2	4.4	1.4	0^h06^m9	+60°41'	7.1	M6	86	-1	
123	61	38	0.4	1.2	0 14 .8	+61 34	6.8	M6	87	0	CU Cas, M6, SR
124	59	132	3.1	2.6	0 47 .7	+59 41	7.1	M6	91	-2	
125	62	164	1.7	2.8	0 48 .3	+63 01	7.1	M7	91	+1	
126	59	146	1.7	-.5	0 51 .5	+59 48	8.3	M5	91	-2	
127	60	166	2.1	-4.2	1 02 .7	+60 37	8.1	M5	93	-1	
128	59	199	-2.6	0.0	1 04 .3	+59 58	8.1	M6	93	-2	
129	58	213	1.2	2.3	1 12 .4	+59 15	7.9	M5	94	-2	
130	60	230	.5	2.1	1 18 .6	+60 34	5.9	M8	95	-1	BT Cas, M
131	59	271	.7	.5	1 27 .0	+60 12	9.1	M5	96	-1	
132	62	295	-2.3	3.4	1 34 .3	+63 05	8.2	M7	96	+2	
133	60	362	4.8	-.7	1 46 .0	+60 49	8.2	M5	98	0	
134	60	428	-.8	-.5	1 58 .3	+61 10	8.0	M5	99	+1	
135	58	388	-4.4	2.3	2 01 .3	+58 48	7.7	M7	100	-1	
136	58	388	4.2	.5	2 04 .8	+58 42	7.9	M6	101	-2	
137	58	440	1.4	1.2	2 12 .9	+58 54	7.1	M5	102	-1	
138	60	465	-.5	-2.3	2 14 .4	+60 26	7.3	M6	101	+1	DE Cas, SR
139	59	480	0.0	-.6	2 17 .3	+59 30	7.5	M5	102	0	
140	60	481	2.6	-1.0	2 21 .7	+60 58	7.3	M5	102	+1	
141	58	517	-3.6	-.2	2 38 .0	+58 52	7.7	M6	105	0	
142	57	629	2.5	4.2	2 38 .5	+58 20	6.6	M5	105	0	
143	60	579	-.3	-.8	2 43 .3	+60 19	6.9	M7	105	+2	
144	58	523	3.1	0.0	2 43 .6	+58 48	6.4	M7	105	+1	GS Cas, I
145	58	525	-1.0	-1.0	2 45 .3	+58 18	7.9	M5	106	0	
146	57	661	-1.2	1.3	2 47 .9	+57 52	6.9	M6	106	0	
147	58	557	1.4	.7	3 00 .4	+58 39	6.1	M7	107	+1	
148	55	753	-1.4	-1.6	3 05 .8	+55 19	6.1	M7	110	-1	GH Per, M6, SR
149	55	776	2.1	1.8	3 16 .4	+55 52	7.6	M5	111	0	
150	50	834	.5	2.6	3 42 .3	+50 46	7.1	M8	117	-2	AP Per, M7, M
151	51	798	.8	3.5	3 47 .6	+52 19	7.1	M6	117	0	
152	52	759	3.3	2.4	3 58 .9	+52 56	7.3	M6	117	+2	
153	46	857	-5.6	1.2	4 07 .9	+46 34	6.7	M7	123	-2	FV Per, I
154	46	857	-4.3	4.5	4 08 .3	+46 45	6.5	M5	123	-2	
155	46	886	1.6	3.1	4 21 .0	+46 24	7.9	M5	125	0	
156	46	889	.5	2.2	4 2? ?	+46 21	7.9	M6	125	0	
157	43	1075	-2.9	.4	4 41 .5	+44 05	8.1	M5	129	+1	
158	40	1054	4.0	.2	4 42 .7	+40 32	7.4	M6	132	-1	HR Per, M3, I
159	41	990	-.3	-.9	4 45 .5	+41 34	7.9	M6	131	0	
160	40	1074	2.3	2.3	4 47 .1	+41 01	8.0	M6	132	0	
161	35	977	0.0	-2.5	5 00 .0	+35 15	7.7	M7	138	-2	AQ Aur, M
162	35	1004	3.5	3.3	5 05 .8	+36 00	8.3	M5	138	-1	
163	34	967	0.0	-2.3	5 06 .8	+34 30	8.7	M5	139	-1	DV Aur, SR
164	33	984	-1.3	1.4	5 08 .6	+33 38	8.1	M6	140	-1	EN Aur, M3, I?
165	30	852	.5	1.6	5 12 .8	+30 21	6.8	M6	143	-3	
166	34	1001	3.8	.7	5 14 .3	+34 59	8.1	M7	140	0	EE Aur, I
167	34	1010	3.0	-1.6	5 15 .6	+34 34	7.3	M5	140	0	
168	31	963	2.6	.5	5 20 .4	+31 58	7.5	M6	143	0	EG Aur, SR
169	32	996	0.0	-1.0	5 22 .4	+32 21	6.8	M6	143	0	
170	32	1009	1.4	1.4	5 23 .9	+32 43	8.1	M6	143	+1	

Table 1b

Late M - Type Stars

No.	B.D.		Δx	Δy	1900		m_i	Sp	l	b	Remarks
171	29°	949	-1.7	1.7	$5^h32^m.7$	+29°52'	7.1	M7	146	+1	
172	29	949	1.7	.7	5 33 .5	+29 49	7.1	M6	146	+1	
173	21	1008	1.9	.7	5 44 .0	+21 50	7.4	M6	154	-1	QU Ori, I
174	22	1057	-.8	0.0	5 44 .5	+22 26	8.4	M6	154	-1	
175	24	1007	-1.0	2.5	5 47 .2	+24 24	7.6	M5	153	+1	
176	20	1149	4.5	-1.9	5 48 .0	+20 39	8.3	M5	156	-1	
177	20	1172	0.0	1.2	5 49 .9	+20 10	4.8	M8	156	-1	U Ori, M8e, M
178	19	1139	-1.7	-.9	5 50 .3	+19 11	7.5	M6	157	-1	
179	20	1185	.2	3.5	5 51 .0	+20 17	6.5	M6	156	-1	
180	17	1085	.8	1.6	5 54 .7	+17 11	7.5	M6	160	-1	
181	23	1146	1.0	-1.6	5 54 .9	+23 29	8.2	M5	154	+2	
182	16	963	1.0	1.2	5 55 .4	+16 32	5.8	M5	160	-2	
183	15	1029	-2.3	-2.6	5 55 .7	+15 29	7.7	M5	161	-2	V340 Ori, MO, LP
184	21	1102	-2.8	-3.1	5 58 .0	+21 15	8.1	M7	156	+1	V342 Ori, LP
185	17	1109	5.4	-.7	5 59 .2	+17 05	6.5	M5	160	-1	
186	18	1091	-.4	3.0	6 00 .5	+18 43	7.7	M5	159	0	
187	17	1151	-2.6	-3.1	6 04 .1	+17 33	7.5	M7	160	+1	GH Ori, I
188	11	1058	-3.6	-1.2	6 05 .6	+10 59	6.7	M5	166	-2	
189	18	1129	-.9	-2.6	6 07 .4	+18 35	5.3	M7	160	+2	GI Ori, M5, LP
190	9	1160	1.4	1.2	6 10 .3	+ 9 51	7.3	M5	168	-2	
191	10	1081	.6	-.4	6 12 .5	+10 48	7.9	M5	167	-1	
192	14	1235	2.6	-1.4	6 13 .0	+14 21	5.1	M7	164	+1	
193	11	1121	1.2	4.8	6 14 .7	+11 24	7.1	M7	167	0	EO Ori, I
194	13	1219	-3.3	1.9	6 16 .0	+13 17	4.8	M7	166	+1	DD Ori, M6, I?
195	5	1240	1.4	1.2	6 21 .8	+ 5 26	6.9	M5	173	-1	
196	4	1257	.2	-.6	6 21 .9	+ 4 50	8.0	M6	174	-2	
197	10	1145	-.5	-2.4	6 22 .4	+ 9 56	8.1	M6	169	+1	
198	8	1367	1.5	2.6	6 24 .9	+ 8 07	7.4	M7	171	+1	
199	5	1294	-.6	-.5	6 27 .7	+ 5 13	7.9	M6	174	0	
200	-2	1704	-3.1	-2.2	6 34 .5	- 2 23	7.2	M6	181	-2	
201	-5	1787	.1	-.4	6 41 .2	- 5 26	8.2	M6	185	-2	
202	-1	1388	2.8	0.0	6 44 .0	- 1 33	7.4	M6	182	0	880, E
203	-5	1815	-1.6	.8	6 44 .8	- 5 21	8.2	M5	185	-1	
204	-3	1621	3.8	1.7	6 47 .2	- 3 54	7.8	M6	184	0	EG Mon, I
205	-6	1813	.4	.8	6 50 .0	- 6 33	7.7	M6	187	-1	
206	-6	1832	-2.3	.8	6 51 .0	- 6 46	8.1	M6	187	-1	
207	-10	1787	2.6	-.5	6 54 .1	-10 13	7.1	M6	191	-2	
208	-6	1901	-.5	1.7	6 57 .7	- 6 18	7.1	M5	188	+1	
209	-6	1911	1.5	.5	6 59 .0	- 6 44	7.7	M7	188	+1	
210	-8	1722	.3	-.8	6 59 .1	- 8 09	8.5	M7	190	0	
211	-9	1818	2.1	2.8	6 59 .7	- 9 50	6.9	M6	191	0	BQ Mon, RW?
212	-16	1802	3.5	-.7	7 05 .9	-16 06	6.8	M7	197	-2	
213	-19	1783	-1.2	2.8	7 11 .5	-19 10	6.8	M6	201	-2	CQ CMa, SE
214	-17	1913	1.0	1.2	7 14 .9	-17 48	7.6	M6	200	-1	
215	-17	1929	1.0	2.6	7 17 .5	-17 50	6.6	M6	200	0	
216	-18	1819	-1.3	-1.7	7 19 .4	-18 56	7.4	M6	201	0	
217	-17	1984	.6	1.5	7 23 .1	-17 12	7.6	M5	200	+1	
218	-22	4427	.7	2.1	17 42 .3	-22 00	5.2	M6	334	+2	
219	-22	4431	2.8	-3.5	17 44 .2	-22 19	4.8	M6	334	+1	
220	-22	4433	1.4	-7.1	17 44 .4	-23 17	6.2	M5	333	+1	

Table 1b

Late M-Type Stars

No.	B.D.	Δx	Δy	1900	m_i	Sp	l	b	Remarks
221	-20° 4903	-.4	.8	17^h47^m6 -20°19'	7.3	M6	336	+1	
222	-22 4454	-2.4	-5.3	17 48 .4 -23 16	4.6	M5	334	0	V774 Sgr, I
223	-20 4914	1.1	-1.1	17 49 .9 -20 04	6.9	M5	337	+1	
224	-21 4782	-2.0	1.0	17 50 .1 -21 07	6.6	M5	336	0	
225	-17 4953	1.7	1.6	17 50 .2 -17 27	7.9	M6	339	+2	
226	-22 4468	3.1	-.6	17 52 .4 -22 35	6.6	M6	335	-1	
227	-18 4751	-.5	5.1	17 54 .6 -18 18	7.9	M5	339	+1	
228	-22 4489	3.4	.8	17 55 .0 -22 55	5.7	M5	335	-1	
229	-22 4503	-.2	.7	17 55 .8 -22 44	5.7	M5	335	-2	
230	-14 4860	1.3	-.2	17 56 .9 -14 30	7.4	M6	342	+2	
231	-20 4958	2.1	-1.7	17 57 .7 -21 01	6.2	M5	337	-1	
232	-20 4964	1.1	2.2	17 58 .0 -20 19	4.8	M8	337	-1	
233	-22 4551	1.1	1.7	17 59 .4 -22 46	5.5	M5	335	-2	
234	-21 4851	0.0	-.6	18 00 .6 -21 09	6.2	M5	337	-2	
235	-20 4986	.4	-.3	18 00 .7 -20 23	7.3	M5	338	-1	
236	-18 4799	-4.4	1.3	18 01 .6 -18 30	8.1	M5	339	-1	
237	-20 5014	1.2	4.7	18 04 .5 -20 14	8.1	M5	338	-2	
238	-14 4918	1.6	-.9	18 06 .0 -14 30	8.2	M5	343	+1	
239	-19 4886	4.2	-2.1	18 06 .2 -19 58	8.3	M6	339	-2	
240	-18 4825	2.1	-1.7	18 06 .2 -18 53	7.3	M9	339	-2	
241	-19 4894	2.4	-1.7	18 06 .6 -19 10	7.5	M5	339	-2	
242	-19 4894	4.1	.9	18 07 .0 -19 02	7.5	M6	339	-2	
243	-16 4755	-.1	0.0	18 07 .1 -16 18	6.0	M6	342	-1	
244	-10 4629	1.0	-.5	18 07 .8 -10 31	7.8	M7	347	+2	
245	-16 4770	.9	.7	18 09 .7 -16 34	8.2	M5	342	-1	
246	-15 4896	1.0	-1.2	18 10 .1 -15 59	8.0	M6	342	-1	
247	-12 4969	1.7	1.9	18 12 .3 -12 02	8.0	M6	346	0	
248	-12 4982	.7	0.0	18 12 .6 -12 13	7.0	M5	346	0	
249	-15 4915	.7	.3	18 12 .8 -15 20	7.2	M5	343	-1	
250	-14 5007	-2.6	2.5	18 14 .6 -14 35	7.8	M6	344	-1	
251	-12 5009	.2	-1.9	18 14 .8 -12 19	7.6	M5	346	0	
252	-13 4949	2.6	-1.2	18 16 .3 -13 12	7.2	M5	346	-1	
253	-14 5013	1.2	5.4	18 16 .8 -14 09	6.8	M5	345	-2	
254	-13 4959	1.0	1.7	18 18 .0 -12 54	6.6	M6	346	-1	
255	-13 4966	1.4	2.8	18 19 .2 -12 51	7.2	M6	346	-2	
256	-12 5041	3.6	.5	18 20 .2 -12 25	8.0	M6	347	-1	
257	-10 4695	-1.9	.5	18 20 .9 -10 06	6.8	M6	349	-1	
258	-11 4642	7.0	-1.7	18 24 .1 -11 14	8.1	M7	348	-2	
259	-11 4648	1.3	3.1	18 24 .8 -11 22	7.9	M5	348	-2	
260	-8 4622	-1.3	-2.3	18 24 .8 - 8 15	8.1	M6	351	-1	
261	-8 4623	2.2	4.0	18 25 .6 - 8 30	6.8	M5	351	-1	
262	-6 4778	1.4	-.5	18 26 .0 - 6 49	8.2	M6	352	0	
263	-10 4716	1.4	4.9	18 26 .8 -10 00	5.6	M6	350	-2	
264	-0 3505	2.2	-2.4	18 28 .4 - 0 32	8.1	M5	358	+2	
265	-6 4809	1.7	.7	18 31 .7 - 6 28	6.3	M6	353	-1	
266	-5 4732	-2.1	2.6	18 36 .7 - 5 07	7.0	M5	355	-2	
267	4 3870	-1.2	.8	18 40 .6 + 4 31	8.2	M6	4	+2	BY Ser, I
268	0 4013	-.4	-.3	18 41 .0 + 0 11	7.1	M5	0	0	
269	-3 4376	0.0	-1.0	18 41 .2 - 3 04	8.2	M5	357	-2	
270	-1 3568	.5	-.2	18 44 .0 - 0 59	7.7	M5	0	-1	

Table 1b

Late M-Type Stars

No.	B.D.	Δx	Δy	1900	m_i	Sp	l	b	Remarks
271	-1° 3571	-1.9	1.9	$18^h44^m.7$ - 1°36'	6.9	M6	359	-2	
272	6 3951	1.0	4.5	18 45 .3 + 6 59	7.3	M6	7	+2	4407, L
273	1 3828	1.0	1.6	18 52 .4 + 1 17	7.6	M5	3	-2	
274	9 3961	-4.2	-2.9	18 55 .4 + 9 41	7.5	M7	10	+1	
275	8 3951	-4.8	-.8	18 56 .6 + 8 11	7.2	M7	9	0	
276	8 3953	-.5	.5	18 57 .9 + 8 18	5.8	M7	9	0	
277	11 3711	1.8	.6	18 59 .3 +11 41	7.5	M5	13	+1	
278	12 3784	.7	2.3	18 59 .4 +12 43	8.1	M6	14	+2	
279	10 3773	.9	-2.6	18 59 .5 +10 34	7.9	M5	12	+1	
280	8 3970	-3.4	-3.8	19 00 .9 + 7 53	9.1	M9	9	-1	V806 Aql, M
281	10 3804	2.3	-.5	19 05 .5 +10 53	8.2	M6	13	0	
282	16 3768	-.3	-2.7	19 06 .4 +16 47	8.0	M6	18	+2	
283	15 3741	2.4	-.2	19 10 .9 +15 31	8.2	M5	17	+1	
284	11 3794	-3.1	.2	19 13 .0 +11 59	6.7	M6	14	-2	
285	16 3809	-3.1	3.0	19 13 .4 +16 40	7.8	M5	19	+1	
286	16 3809	4.3	2.8	19 15 .0 +16 40	7.6	M6	19	0	4614, I?
287	16 3814	1.4	1.0	19 15 .2 +17 01	6.8	M6	19	0	W Sge, M4e, M
288	14 3872	.2	.5	19 15 .3 +14 32	7.4	M5	17	-1	
289	14 3904	0.0	-.2	19 19 .6 +14 56	8.0	M6	18	-1	
290	22 3710	.8	3.8	19 24 .9 +23 04	8.0	M5	26	+1	
291	18 4100	2.9	0.0	19 26 .4 +18 30	7.6	M6	22	-1	
292	21 3854	2.1	.3	19 34 .0 +21 09	8.0	M6	25	-1	
293	19 4120	-2.9	-.5	19 36 .1 +19 54	8.0	M5	24	-2	
294	22 3786	1.7	.4	19 39 .6 +22 58	6.4	M6	27	-1	
295	27 3492	.2	.8	19 40 .0 +27 31	7.3	M5	31	+1	YZ Vul, M6, M
296	30 3725	-2.6	-1.9	19 40 .9 +30 28	7.7	M6	34	+2	
297	31 3752	.8	.9	19 41 .7 +31 14	6.9	M5	34	+2	EQ Cyg, M
298	28 3473	-2.7	.9	19 41 .8 +28 26	7.7	M5	32	+1	
299	31 3752	2.1	-4.1	19 42 .0 +30 58	7.5	M5	34	+2	
300	25 3995	-.4	2.1	19 46 .1 +26 06	7.3	M6	31	-1	
301	29 3760	3.0	2.2	19 46 .2 +29 14	8.3	M6	33	+1	
302	27 3545	3.3	-.5	19 50 .0 +27 35	7.4	M5	32	-1	
303	27 3560	-.2	-2.2	19 51 .7 +27 46	7.9	M5	33	-1	
304	32 3651	-1.4	-1.3	19 54 .4 +32 56	7.8	M6	37	+1	
305	29 3830	2.1	.9	19 55 .4 +30 08	8.3	M6	35	-1	
306	29 3872	2.6	.7	20 00 .1 +29 40	7.5	M6	35	-2	5007, L
307	36 3907	-1.2	1.7	20 05 .5 +36 38	8.0	M6	42	+1	
308	35 4006	.8	3.3	20 07 .4 +35 49	8.2	M7	41	0	
309	35 4016	.5	-1.7	20 08 .6 +35 40	8.0	M5	41	0	
310	31 3991	.8	-1.3	20 09 .0 +31 57	7.4	M7	38	-2	V557 Cyg, M
311	38 3961	.4	.2	20 10 .4 +39 06	8.0	M7	44	+2	
312	38 4035	-.5	.4	20 17 .9 +39 09	7.8	M5	45	+1	
313	40 4165	.7	-3.0	20 23 .0 +40 53	7.8	M5	47	+1	
314	40 4174	.3	1.2	20 23 .8 +40 45	6.7	M8	47	+1	KZ Cyg, M8e, M
315	37 3950	-1.4	-2.2	20 25 .0 +37 04	7.0	M6	44	-2	
316	42 3769	2.6	-2.4	20 28 .0 +42 11	8.3	M6	49	+1	
317	42 3805	1.3	1.2	20 34 .4 +42 16	7.9	M5	50	0	
318	46 3078	.5	0.0	20 48 .7 +46 58	5.9	M7	55	+1	RZ Cyg, M7, M
319	44 3624	1.2	3.0	20 51 .0 +44 53	7.3	M5	54	0	
320	44 3639	-.3	-1.8	20 52 .9 +44 26	8.1	M6	53	-1	

Table 1b

Late M-Type Stars

No.	B.D.	Δx	Δy	1900	m_i	Sp	l	b	Remarks
321	47° 3240	.7	.7	$20^h55^m.0$ +47°16'	7.8	M7	56	+1	DH Cyg, M
322	47 3243	1.4	1.9	20 56 .0 +47 22	8.0	M5	56	+1	
323	45 3394	1.9	-1.0	21 02 .1 +45 35	6.9	M6	55	-1	V408 Cyg, M3, I
324	44 3709	4.5	1.4	21 04 .8 +45 02	6.9	M5	55	-2	
325	44 3717	4.7	0.0	21 07 .1 +44 49	8.0	M7	55	-3	V527 Cyg, I
326	45 3440	.9	.5	21 08 .3 +46 09	7.8	M5	56	-2	V582 Cyg, M4, I
327	49 3489	2.2	-2.8	21 13 .6 +49 32	6.4	M6	59	0	
328	51 3037	.9	2.6	21 15 .7 +51 44	8.0	M5	61	+1	
329	48 3343	2.1	.9	21 16 .4 +48 42	7.8	M6	59	-1	
330	51 3057	-1.4	1.7	21 20 .3 +52 06	7.6	M6	62	+1	
331	52 2950	.4	-1.9	21 26 .6 +53 01	8.2	M6	63	+1	
332	53 2640	.2	.4	21 28 .6 +53 27	7.6	M5	64	+1	
333	53 2647	-2.6	0.0	21 29 .6 +53 52	5.7	M7	64	+2	
334	49 3548	4.0	1.2	21 29 .9 +50 02	8.2	M5	62	-1	
335	53 2677	1.6	.3	21 36 .8 +54 11	8.6	M5	65	+1	
336	52 3017	-.5	1.2	21 38 .8 +52 37	7.8	M6	64	0	
337	53 2707	-.5	1.0	21 44 .5 +53 42	7.4	M5	66	0	
338	52 3037	2.4	1.4	21 45 .0 +52 26	6.5	M5	65	-1	
339	51 3161	.3	.4	21 45 .7 +51 58	6.7	M6	65	-1	
340	52 3049	.4	3.5	21 48 .5 +52 25	8.2	M5	65	-1	
341	55 2639	1.6	3.4	21 49 .2 +55 30	6.3	M6	67	+1	
342	52 3054	2.3	-2.6	21 50 .6 +52 13	8.2	M5	66	-2	
343	53 2737	-1.7	.4	21 50 .9 +53 16	7.4	M5	66	-1	
344	54 2648	-2.6	-1.9	21 51 .6 +54 43	7.8	M5	67	0	
345	55 2650	1.0	-3.3	21 53 .4 +55 45	8.0	M5	68	+1	
346	52 3071	.7	.8	21 54 .2 +52 22	7.2	M6	66	-2	
347	52 3075	-.7	.5	21 56 .0 +52 42	8.2	M5	67	-2	
348	56 2672	.9	1.9	21 56 .6 +56 53	6.8	M6	69	+2	
349	55 2667	-1.8	-2.4	21 56 .9 +55 23	7.8	M5	68	0	
350	56 2679	1.2	2.6	21 58 .5 +56 29	8.1	M6	69	+1	YY Cep, M?
351	56 2686	.8	0.0	21 59 .6 +56 21	8.1	M5	69	+1	
352	56 2689	-.4	-.2	21 59 .6 +56 58	7.5	M5	69	+1	
353	57 2450	0.0	2.1	22 02 .0 +57 51	7.3	M5	70	+2	
354	52 3105	.7	3.8	22 02 .4 +53 20	7.8	M5	68	-2	
355	55 2687	.7	.2	22 04 .8 +56 02	7.9	M7	70	0	AA Cep, SP?
356	53 2800	3.3	1.2	22 07 .7 +54 08	7.5	M5	69	-2	
357	56 2727	-.5	3.8	22 08 .0 +56 32	5.9	M6	70	0	CU Cep, M6, M
358	53 2834	-3.0	3.3	22 11 .4 +53 42	7.9	M6	69	-2	WZ Lac, LP
359	55 2711	2.1	2.6	22 13 .6 +56 18	7.3	M5	71	0	
360	54 2740	-1.6	2.1	22 16 .1 +55 17	8.5	M5	71	-1	
361	53 2852	.7	.2	22 17 .2 +53 56	7.3	M5	70	-2	
362	54 2746	1.8	1.0	22 18 .1 +54 47	6.9	M6	70	-2	
363	54 2750	.9	1.2	22 18 .5 +55 09	8.3	M6	71	-1	
364	55 2737	.4	3.6	22 19 .5 +55 39	8.1	M5	71	-1	
365	57 2543	-4.7	-.3	22 23 .1 +58 01	7.5	M5	73	+1	
366	56 2783	-.4	-.3	22 24 .3 +57 11	6.7	M5	72	0	
367	59 2556	-3.1	-1.9	22 35 .5 +59 40	7.9	M5	75	+1	
368	56 2825	0.0	4.3	22 35 .8 +57 05	7.9	M5	74	-1	
369	58 2488	-1.6	-1.9	22 46 .0 +59 07	6.9	M5	76	0	
370	60 2450	-1.2	1.2	22 47 .0 +61 14	7.1	M5	77	+2	5623, L?

Table 1b

Late M-Type Stars

No.	B.D.	Δx	Δy	1900	m_i	Sp	l	b	Remarks
371	57° 2676	3.4	.2	$23^h00^m.4$ +58°02'	7.7	M7	77	-1	
372	57 2693	1.2	-3.5	23 03 .7 +57 42	7.9	M7	77	-2	
373	59 2647	-1.3	.7	23 03 .7 +59 47	7.9	M8	78	0	
374	57 2693	3.0	-2.3	23 04 .3 +57 45	8.3	M7	78	-2	
375	61 2405	.2	.7	23 09 .9 +61 42	8.3	M5	80	+1	
376	59 2724	3.6	1.7	23 23 .8 +59 56	8.1	M6	81	-1	
377	57 2749	-1.8	3.5	23 25 .0 +58 25	8.7	M6	80	-2	
378	60 2596	-.2	2.4	23 33 .8 +61 20	7.5	M8	82	0	
379	60 2611	.5	-1.7	23 38 .9 +60 32	7.2	M5	83	-1	
380	60 2625	-3.1	3.1	23 43 .4 +60 28	8.0	M6	83	-1	EM Cas,LP
381	62 2325	1.3	.7	23 51 .1 +62 48	8.2	M6	84	+1	
382	62 2327	3.5	-.3	23 52 .4 +62 18	7.6	M5	85	+1	
383	61 2578	1.7	2.1	23 55 .1 +61 55	7.6	M6	85	0	
384	60 2663	1.8	-1.6	23 59 .6 +60 28	8.4	M6	85	-1	

Tables 1*a* and 1*b* give the final list. Table 1*a* includes all the late M stars which are in the *BD* catalogue. The second table gives a reference *BD* star near the M star and coordinates in millimeters in the scale of the *BD* charts from this reference star. Positive Δx indicates increasing R.A., while positive Δy is in the northward direction. The R.A. and declination for the epoch of 1900 given refer in each case to the M star. The approximate infrared magnitude obtained as described above is designated by m_i. These are followed by the spectral classes and then by the galactic longitude and latitude given to the nearest degree. In the "Remarks" the variable-star designation, the spectral class, and type of variability are obtained from the *General Catalogue of Variable Stars* (Kukarkin and Parenago 1948) and its supplements. The notations used for the types of variability are as follows: *I*, irregular; *LP*, long period; *SR*, semiregular; *RW*, Auriga type; *M*, Mira type; *SP*, short period; *E*, eclipsing, and *L*, unknown, with slow fluctuations in brightness. When a number alone or a number followed by type of variability or spectral class is given, the number refers to the *Catalogue of Stars of Suspected Variability* (Kukarkin *et al.* 1951). The spectral classes given in the "Remarks" are, in general, earlier than the corresponding catalogue classes. This is to be expected, since the previously published spectra refer generally to the time when the stars were at light-maximum.

It should be pointed out that the present survey suffers the expected effects of one epoch of observation. Undoubtedly, some stars within the surveyed region were not included because at the time of observation their spectral classes were earlier than the adopted limit, that is, they were near light-maximum. In addition, some variables are not listed because at the time of observation they were near light-minimum and thus exceeded the adopted magnitude limit.

Our infrared surveys, of which this report constitutes a part, were carried out through grants from the Office of Naval Research. Professor W. W. Morgan has shared in the initial planning of these surveys and has materially assisted us during the progress of the work. For this assistance we are deeply grateful.

REFERENCES

Kukarkin, B. V., and Parenago, P. P. 1948, *General Catalogue of Variable Stars* (Moscow: Academy of Sciences, U.S.S.R.).

Kukarkin, B. V.; Parenago, P. P.; Efremov, U. E.; and Kolorov, P. N. 1951, *Catalogue of Stars Suspected of Being Variable* (Moscow: Academy of Sciences, U.S.S.R.).

McCuskey, S. W., and Seyfert, C. K. 1947, *Ap. J.*, **106**, 1.

Nassau, J. J., and van Albada, B. G. 1949, *Ap. J.*, **109**, 391.

CARBON STARS AT THE GALACTIC EQUATOR IN A ZONE 4° WIDE

J. J. Nassau and V. M. Blanco
Warner and Swasey Observatory, Case Institute of Technology
Received January 6, 1954

A catalogue is given of 271 carbon stars within a galactic zone 4° wide from longitude 333° through zero to 201°. The classification was made on objective-prism plates, utilizing the near infrared spectral region from λ 6800 to λ 8800. Of these stars, 222 are new. A way to separate the N and the R stars is suggested, with the results indicated in the catalogue. The limiting infrared magnitude of the survey is about 11.

The cyanogen bands in the near infrared furnish a ready means for recognizing carbon stars on objective-prism spectra of low dispersion. These stars are the N and R stars grouped in one class by Keenan and Morgan (1941). The present list of such stars was observed on plates taken with the 2° objective prism attached to the Burrell Schmidt-type telescope. The dispersion at the telluric A band with this combination is 3400 A/mm. The spectral range examined was from λ 6800 to λ 8800. No widening was used in the exposures. The *CN* bands at λλ 7945, 8125, and 8320 produce marked weakening in the continuum in this region, while the bands on the short-wave-length side of the A band produce the appearance of a highly reddened star. The segregation of the carbon stars can be made with certainty, even with dense or with very weak spectra. However, when the *CN* bands are very weak, that is, when the star is of class C0, C1, or C2, it is difficult to recognize them with this dispersion, particularly when the spectra are not of the proper density.

In the present list of carbon stars an effort has been made to divide them into the N and R classes by comparing their spectra with the spectra of known N and R stars. Standards were selected from Sanford's list (1944). As far as possible, available plates on which some of the stars in this list were present were utilized. In addition, a number of plates, each with multiple exposures, were taken to provide means for accurate matching of spectra. Thirty-eight stars, of which 18 were of class N and 20 were of class R, were selected as standards.

The weakening of the continuum produced by the absorption of the *CN* bands λλ 7945, 8125, and 8320 was estimated on an arbitrary scale by comparing the spectrum of each star with the spectrum of a standard of approximately the same density. Likewise, the apparent "color" was estimated arbitrarily by the shortening and narrowing of the spectrum on the short-wave-length side of the A band.

The corresponding estimates for each of the thirty-eight stars are plotted in Figure 1, with the *CN* strength as abscissa and the "color" as ordinate. The relative strength of the bands increases with the numerical value of the estimate. Dots represent N stars and crosses R stars.

The distribution of these points suggests an approximate way to separate the N and the R stars. The region nearer the origin is occupied by the class-R stars, which are mostly early type. The N stars occupy the area within the broken lines. The two R stars within the rectangle were both R8, a class also difficult to segregate in other spectral regions. Another discordant classification occurs at the left boundary of the rectangle. The right and upper region of the figure is occupied by class-R stars. The assigned numerical values can be estimated with reasonable consistency. The values given in the figure represent the average of two independent estimates.

The method described above was utilized in segregating the N and the R stars in a belt 4° wide along the galactic equator. The area of 912 square degrees contains 271 carbon stars. Of these, 127 were compared with the standards, and estimates of the strength of the bands were made. For the rest of the stars, either the classification was made without the need of comparison with standards, or the comparison was made, but no estimates were given, as the spectra were too dense or too weak.

Among the 271 stars, 49 were either in Sanford's (1944) or in the Dearborn list (Lee *et al.* 1943, 1947). The spectra of 8 of these stars were too dense for assignment of a numerical estimate of band strength, but comparison with the standard spectra of the same density produced classifications in agreement with the published ones. All gave accordant classifications. For the remaining 41 stars, estimates of band strength were available. Five discordances are present; in addition, star No. 215 (Table 1*b*) was classed as R by Lee and by us and as N by Sanford.

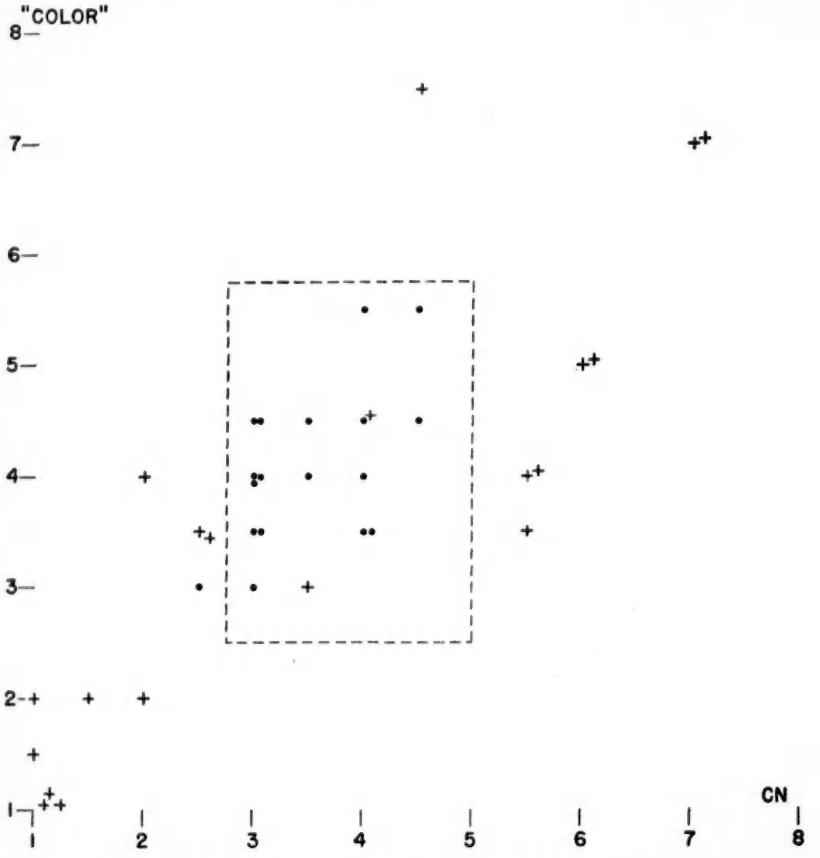

FIG. 1.—Plot of (•) and R (+) standard stars. The *CN* strength is given as abscissa and the "color" as ordinate.

All the 127 stars for which numerical estimates of band strength and "color" were available are plotted in Figure 2. As in the previous figure, the arbitrary estimate of the strength of the *CN* bands is given in the abscissa, and the arbitrary estimate of "color" as the ordinate. The dots indicate that the stars were classed as N, and the crosses as R stars. A circle around a dot or a cross indicates that the classification is in agreement with the published classification. If a disagreement exists, a triangle is placed around the dot or cross.

Tables 1*a* and 1*b* give the list of the 271 carbon stars which are within $\pm 2°$ of galactic latitude from longitude 333° through zero to 201°. A few stars are included which are less than a degree north or south of the latitude limits given. Only stars with very weak *CN* bands are not included, as they are difficult to detect even in spectra of moderate density

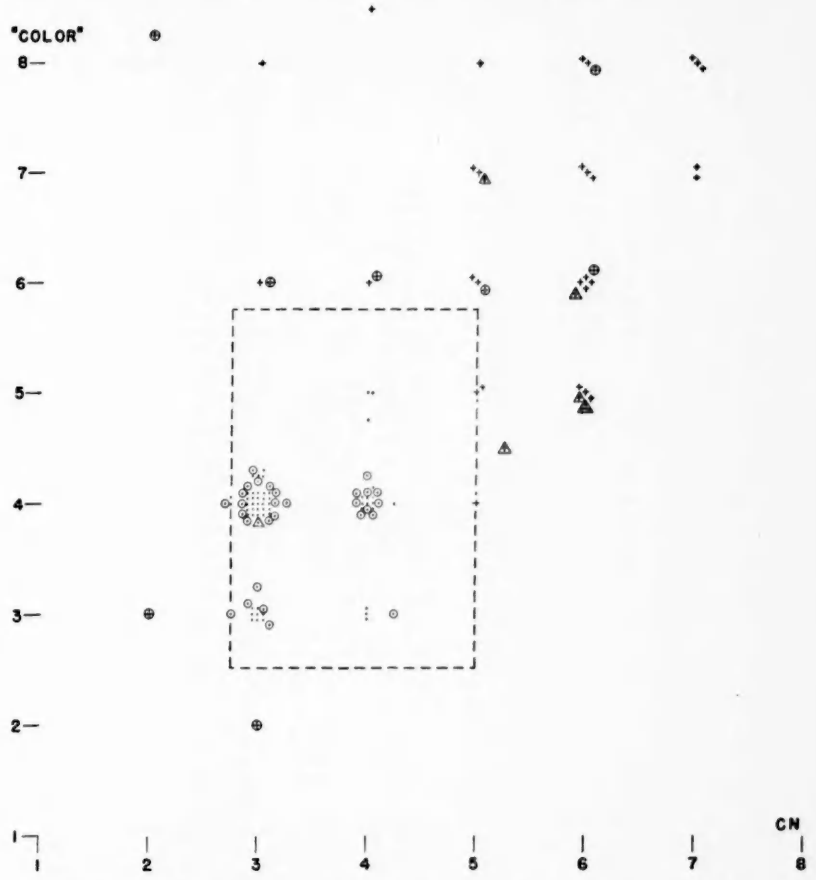

FIG. 2.—Plot of 127 N (•) and R (+) stars. The *CN* strength is given as abscissa and the "color" as ordinate. A circle around a dot or a cross indicates that the classification is in agreement with the published classification. If a disagreement exists, a triangle is placed around the dot or cross.

Table 1a

Carbon Stars

No.	B.D.	1900	m_i	Sp	l	b	Remarks
1	62° 25	$0^h08^m.0$ +62°54'	7.0	R	86	+1	UX Cas, R2*, I?
2	57 702	3 03 .7 +57 31	4.1	R	108	+1	HD 19557, R6*
3	51 762	3 34 .1 +51 11	3.7	N	116	-2	N*
4	50 920	4 03 .9 +51 05	7.8	R	119	+1	FR Per, R3*, I
5	50 961	4 09 .0 +50 23	7.1	N	120	+1	SY Per, Ne*, LP
6	38 955	4 45 .9 +38 20	3.5	N	133	-2	N*
7	38 1035	5 02 .2 +38 52	5.7	N	135	+1	TX Aur, N*, I?
8	35 1046	5 12 .5 +35 41	6.2	N	139	0	HD 34467, N*
9	32 957	5 15 .3 +32 24	5.9	N	142	-1	UV Aur, Ne*, SR
10	34 1044	5 20 .5 +34 04	6.6	N	141	+1	S Aur, N*, LP
11	24 943	5 39 .1 +24 23	5.1	N	151	-1	TU Tau, N*, I
12	8 1363	6 12 .3 + 8 34	6.3	N	169	-2	N*, D38
13	3 1381	6 39 .4 + 3 25	7.3	N	177	+2	CZ Mon, N*, I
14	-4 1708	6 48 .2 - 4 27	3.4	N	185	0	GY Mon, N*, I
15	-7 1742	7 02 .1 - 7 24	3.7	N	189	+1	RY Mon, N*, LP
16	-11 1805	7 03 .4 -11 46	1.7	N	193	0	W CMa, N*, I
17	-17 1866	7 10 .1 -17 13	7.3	N	199	-2	N*
18	-19 4805	17 56 .5 -19 10	6.5	R:	338	0	N*
19	-13 4918	18 12 .7 -13 29	3.2	N	345	0	
20	-15 4923	18 13 .6 -15 39	6.0	R:	343	-2	4006, R6*, I
21	-7 4633	18 31 .7 - 7 41	5.3	N	352	-2	RX Sct, N*
22	5 3950	18 42 .5 + 5 21	5.4	N	5	+2	4376, N*, L
23	10 3764	18 57 .6 +10 06	6.1	N	11	+1	
24	35 4002	20 06 .6 +35 39	6.7	N	41	0	RY Cyg, N*, I?
25	38 3957	20 09 .8 +38 26	4.2	N	44	+2	RS Cyg, Ne*, SR
26	53 2736	21 51 .5 +54 02	6.0	N	67	0	V413 Cyg, D342, N, I
27	60 2432	22 40 .4 +61 12	4.8	N	76	+2	HD 215484, N*
28	59 2564	22 41 .2 +59 22	7.5	R	75	+1	
29	59 2810	23 56 .2 +59 48	1.7	N	85	-2	WZ Cas, N*, SR

Table 1b

Carbon Stars

No.	B.D.		Δx	Δy	1900		m_i	Sp	l	b	Remarks
30	61°	7	-.4	.2	0h03m.7	+62°10'	8.0	R	86	+1	
31	63	22	-.3	-.3	0 11 .9	+63 16	10.0	N	87	+1	
32	60	60	-1.7	-1.1	0 23 .6	+60 34	10.8	N	88	-1	
33	60	71	-1.8	-2.8	0 29 .4	+60 46	8.8	N	89	-1	
34	60	79	-1.2	-1.6	0 33 .8	+60 13	10.8	N	89	-2	
35	62	155	.1	2.3	0 44 .4	+62 45	11.0	C	91	+1	
36	59	132	1.8	1.9	0 47 .0	+59 39	10.4	N	91	-2	
37	62	164	-.1	-1.4	0 47 .6	+62 49	8.3	R	91	+1	
38	62	175	1.7	1.8	0 52 .8	+63 16	10.0	N	92	+1	
39	60	141	-2.5	-1.3	0 53 .3	+60 10	10.4	N	92	-2	AV Cas, M
40	61	198	-1.8	-1.2	0 56 .6	+61 20	8.0	R	92	-1	HO Cas, D240, R, I
41	60	163	-3.1	-.7	0 58 .4	+60 50	9.5	N:	92	-1	
42	59	203	.7	.9	1 06 .7	+59 50	11.2	N	93	-2	
43	59	205	.5	-1.0	1 06 .9	+59 19	10.4	N	94	-2	
44	62	224	1.1	2.4	1 07 .2	+62 26	7.5	R	93	+1	
45	62	236	-1.5	.3	1 12 .2	+62 22	9.2	R	94	+1	
46	61	272	-3.2	-.8	1 22 .0	+61 45	9.2	R	95	0	
47	62	294	.3	-3.5	1 35 .4	+62 35	10.9	N	96	+1	
48	62	292	1.6	0.0	1 35 .7	+63 06	10.1	N	96	+2	
49	60	322	-.9	.4	1 37 .8	+60 19	11.5	C	97	-1	
50	62	301	-1.2	-.3	1 38 .4	+62 27	11.1	N	97	+1	
51	62	303	-.8	-1.7	1 38 .5	+62 37	11.1	N	97	+1	
52	58	299	-.7	.4	1 40 .8	+58 32	11.1	C	98	-2	
53	58	334	.3	1.1	1 49 .8	+58 46	7.6	N	99	-2	X Cas, Ne*, M
54	58	334	.6	2.2	1 50 .0	+58 49	10.5	N	99	-2	
55	59	482	-.5	-2.6	2 17 .4	+59 17	11.0	C	102	0	
56	59	531	2.8	2.3	2 36 .0	+59 58	11.0	C	104	+1	
57	59	550	-1.2	1.9	2 42 .4	+59 36	10.8	N	105	+1	
58	58	521	5.6	1.0	2 43 .0	+58 27	10.6	N	106	0	
59	59	560	.1	.3	2 45 .4	+59 35	10.0	N:	105	+1	
60	58	524	2.9	-.7	2 46 .6	+59 05	8.3	R	106	+1	
61	57	711	-3.9	1.1	3 08 .8	+58 02	9.0	R	109	+2	D 257? N
62	55	773	-.3	-1.9	3 15 .2	+55 40	10.9	C	111	0	
63	52	701	.4	-.1	3 25 .6	+52 23	8.1	R	114	-2	BI Per, D 262, R, I
64	51	760	-2.5	2.0	3 32 .4	+51 48	8.1	R	115	-2	BK Per, I
65	51	791	.8	-1.7	3 45 .6	+51 46	10.0	N	117	0	
66	50	918	-1.2	1.1	4 03 .0	+51 11	9.8	N	119	+1	
67	52	777	2.4	3.6	4 03 .2	+52 26	10.4	N	118	+2	
68	50	926	-.7	-.2	4 04 .8	+50 54	10.6	N	119	+1	
69	48	1057	2.3	-1.7	4 06 .0	+48 06	8.6	R	121	-1	
70	46	864	.5	-.3	4 11 .8	+46 55	9.1	R	123	-1	
71	46	871	.9	-.2	4 14 .2	+46 48	10.7	N	123	-1	
72	47	985	1.0	-2.2	4 16 .4	+47 39	11.3	N	123	0	
73	49	1179	-.5	2.1	4 17 .9	+51 00	11.5	C	121	+2	
74	49	1179	2.0	1.6	4 18 .7	+50 58	9.1	N:	121	+2	
75	44	965	.1	-.6	4 24 .0	+45 02	8.0	R	126	-1	AT Per, I
76	48	1103	-.2	3.3	4 24 .4	+48 46	10.7	C	123	+2	
77	47	1017	-3.7	-4.4	4 31 .2	+47 00	10.8	N	125	+1	
78	41	929	-1.6	2.7	4 32 .8	+41 26	7.3	N	130	-2	AV Per, N*
79	42	1022	1.5	-1.4	4 33 .5	+43 00	9.2	N	129	-1	
80	41	929	2.7	.4	4 33 .8	+41 18	11.0	N	130	-2	

Table 1b

Carbon Stars

No.	B.D.		Δx	Δy	1990	m_i	Sp	l	b	Remarks
81	42°	1048	1.4	-3.0	$4^h40^m.2$ + 42°39'	11.4	C	130	0	
82	38	940	2.7	1.4	4 41 .8 + 39 08	10.7	N	132	-2	
83	45	989	4.3	-.7	4 42 .4 + 45 36	10.2	N	128	+2	
84	39	1077	.2	-1.9	4 43 .2 + 39 45	10.7	N	132	-2	
85	42	1066	0.0	-.7	4 43 .8 + 42 30	10.0	N	130	0	
86	43	1094	.1	.5	4 44 .0 + 43 31	9.2	N	129	+1	
87	43	1104	.3	.5	4 46 .2 + 43 40	10.8	N	130	+1	
88	40	1076	-1.6	-1.0	4 46 .6 + 40 31	10.1	N	132	-1	
89	41	1005	-4.6	1.0	4 47 .6 + 41 18	10.3	N	131	0	
90	41	1004	.2	-1.6	4 48 .8 + 41 42	10.6	C	131	0	
91	42	1121	.4	2.8	4 52 .5 + 42 38	9.9	N	131	+1	
92	38	1008	-3.6	1.8	4 54 .8 + 38 21	11.3	C	135	-1	
93	41	1043	-1.8	-2.4	4 55 .7 + 41 48	9.7	N	132	+2	
94	42	1139	2.3	0.0	4 56 .0 + 42 10	10.1	N	132	+2	
95	37	1039	-.7	.9	4 59 .4 + 37 17	9.2	N:	136	-1	DI Aur, I
96	39	1171	-1.4	-.2	4 59 .5 + 40 02	9.1	N	134	+1	
97	40	1183	.7	.8	5 01 .6 + 40 18	10.5	N	131	+1	
98	39	1198	-3.2	2.0	5 03 .4 + 39 15	8.5	R:	135	+1	
99	39	1196	-.9	1.3	5 03 .4 + 39 43	10.0	N	135	+1	
100	33	965	.8	-2.3	5 03 .8 + 33 53	8.8	R	139	-2	DS Aur, D 174? N, I
101	34	967	3.0	1.4	5 07 .5 + 34 42	11.0	N	139	-1	
102	36	1066	-.4	-.1	5 09 .8 + 36 58	11.4	C	138	+1	
103	30	876	-.9	-1.2	5 18 .0 + 30 26	11.2	N	144	-2	
104	33	1036	-.6	2.2	5 18 .4 + 33 44	9.5	N	141	0	
105	32	983	-2.1	-.2	5 19 .6 + 32 19	11.4	N	143	0	
106	31	964	.8	1.8	5 20 .2 + 31 55	10.4	N	143	0	
107	34	1053	-.1	.8	5 21 .4 + 34 25	10.8	N	141	+1	
108	31	995	-1.1	-.8	5 24 .6 + 31 49	10.6	N	144	0	
109	28	815	-3.0	-.7	5 25 .5 + 28 12	10.6	N	147	-1	
110	29	921	1.1	2.0	5 25 .8 + 29 28	10.6	N	146	-1	
111	32	1019	3.3	-.1	5 26 .0 + 32 52	9.4	R	143	+1	D 180?R
112	29	926	-3.4	1.3	5 26 .1 + 29 37	9.8	R	146	-1	
113	33	1087	-.8	-2.2	5 28 .3 + 33 47	10.4	N	142	+2	
114	30	964	-4.3	-2.7	5 31 .2 + 30 00	9.8	N	146	+1	
115	30	963	1.2	-1.0	5 32 .4 + 30 23	11.2	N	146	+1	
116	28	858	-2.3	-2.0	5 35 .9 + 28 15	10.8	C	148	+1	
117	21	954	-1.4	-1.0	5 38 .6 + 21 51	8.0	R	154	-2	
118	25	960	1.1	.7	5 39 .7 + 25 27	9.9	N	151	0	
119	25	971	.5	.3	5 40 .4 + 25 35	10.5	N	151	0	
120	25	999	-1.1	1.2	5 43 .8 + 25 14	10.7	C	151	0	
121	22	1054	-1.1	1.3	5 44 .0 + 22 14	10.3	N:	154	-1	
122	20	1184	.2	-.3	5 50 .9 + 20 53	8.2	R	153	0	
123	24	1055	-2.8	.6	5 53 .7 + 24 49	9.9	N	153	+2	
124	21	1081	-.3	-.1	5 55 .0 + 21 06	9.8	N	156	+1	
125	18	1082	-.1	-1.3	5 59 .4 + 18 32	9.4	N	159	0	
126	13	1156	-2.2	-2.3	6 05 .8 + 13 00	10.4	C	165	-1	
127	12	1061	-3.1	.7	6 06 .8 + 12 14	9.6	C	165	-1	EI Ori, I ?
128	9	1167	-.2	1.4	6 10 .8 + 9 55	8.9	C	168	-2	728, I?
129	14	1232	1.2	-1.3	6 12 .0 + 14 31	8.9	N	164	+1	D 36, N
130	6	1196	0.0	-.6	6 14 .3 + 6 52	9.8	N	171	-2	

Table 1b

Carbon Stars

No.	B.D.	Δx	Δy	1900	m_i	Sp	l	b	Remarks
131	7° 1254	1.9	2.7	$6^h16^m.5$ + 7°23'	6.3	N:	171	-2	BN Mon, N*, SR
132	8 1312	-.3	.2	6 18.4 + 8 33	9.8	N	170	-1	
133	8 1312	1.3	-1.0	6 18.7 + 8 30	9.2	N	170	-1	D 45? N
134	8 1379	1.5	3.2	6 27.1 + 9 03	10.0	N	171	+1	
135	5 1347	1.4	1.5	6 34.0 + 5 50	10.8	C	174	+1	
136	-1 1343	-.1	1.0	6 37.7 - 1 07	9.7	N	181	-1	
137	-5 1768	-1.3	-3.4	6 39.1 - 5 27	9.8	R	185	-3	
138	+0 1595	.2	-2.4	6 41.9 + 0 42	10.3	N	180	+1	
139	+0 1605	-3.2	-.2	6 42.1 + 0 20	8.5	N	180	+1	DE Mon, D,59,N, I
140	+0 1600	.4	-.2	6 42.5 + 0 47	7.8	N	180	+1	DF Mon, N*, I
141	-5 1830	.8	.8	6 46.6 - 5 08	11.2	C	185	-1	
142	-6 1786	.8	-.4	6 47.6 - 7 02	6.8	N	187	-2	W Mon, N*, I
143	-7 1626	1.6	-1.1	6 50.2 - 7 55	8.3	R:	188	-1	EM Mon, M
144	-9 1738	.9	-1.4	6 52.2 -10 02	10.0	N	190	-2	
145	-5 1910	0.0	-.9	6 55.4 - 5 17	10.8	N	186	+1	
146	-5 1925	-2.4	-2.5	6 56.4 - 5 23	10.6	N	187	+1	EU Mon, I
147	-9 1787	1.1	-.2	6 56.6 - 9 10	10.8	C	190	-1	
148	-9 1825	2.0	-1.4	7 00.0 - 9 28	10.6	C	191	0	
149	-11 1785	-.4	-.4	7 01.4 -11 37	9.8	C	193	-1	
150	-13 1825	1.0	-2.5	7 02.6 -13 39	10.9	N	195	-2	
151	-13 1836	1.5	2.5	7 03.8 -13 19	10.3	N	194	-1	
152	-15 1708	-.5	-.5	7 09.1 -15 23	9.7	N	197	-1	
153	-10 1945	-2.0	-.2	7 10.5 -10 26	10.0	N	193	+2	
154	-12 1866	-.4	.3	7 10.9 -12 41	9.5	N	195	+1	
155	-17 1876	-1.0	1.3	7 11.1 -17 23	8.3	N	199	-1	N*
156	-16 1887	-.7	1.0	7 14.2 -16 03	9.3	N	198	0	
157	-18 1794	-.9	.3	7 16.2 -19 01	9.7	N	201	-1	
158	-15 1780	0.0	-1.8	7 17.2 -15 25	9.5	N	198	+1	
159	-22 4454	-7.2	-5.8	17 47.2 -23 18	10.4	N:	333	0	
160	-22 4454	6.6	-4.3	17 50.0 -23 12	10.0	N:	334	-1	
161	-17 4987	-3.1	3.0	17 55.1 -17 00	8.7	N	340	+2	
162	-14 4855	.2	0.0	17 56.3 -14 20	9.3	N	342	+3	
163	-13 4845	1.4	-3.4	18 00.0 -13 17	10.5	N	343	+2	
164	-14 4885	2.3	2.0	18 01.4 -14 37	7.0	N	343	+1	
165	-16 4786	-4.2	.8	18 10.1 -16 31	8.9	R	342	-1	
166	-11 4588	0.0	1.0	18 12.6 -11 48	10.0	N	346	0	
167	-9 4731	-1.2	1.7	18 20.3 - 9 25	10.6	N	349	0	
168	-6 4759	1.9	1.3	18 20.6 - 6 19	11.1	N	352	+1	
169	-10 4699	1.3	-2.2	18 22.4 -10 14	11.0	N	349	-1	
170	-6 4768	-.2	.9	18 22.6 - 5 59	8.2	R	353	+1	
171	-6 4785	-.6	.3	18 26.8 - 6 31	9.9	N	353	0	
172	-8 4631	1.0	2.1	18 28.1 - 8 32	10.9	C	351	-1	
173	-2 4658	1.2	-3.6	18 29.8 - 2 11	11.3	N	357	+1	
174	+0 3971	-.8	3.5	18 29.8 + 0 47	10.8	C	0	+3	
175	-3 4329	1.1	1.0	18 33.0 - 2 57	10.9	N	357	0	
176	-2 4711	.8	.2	18 37.1 - 2 23	11.3	C	358	-1	
177	3 3781	1.2	-.2	18 38.1 + 3 59	10.1	N	3	+2	
178	+0 4005	-2.8	-2.1	18 38.9 - 0 03	11.4	N	359	0	
179	1 3782	-2.4	-2.8	18 41.8 + 0 58	11.4	C	359	-1	
180	1 3798	1.1	-.3	18 47.0 + 1 28	10.5	R	2	-1	

Table 1b

Carbon Stars

No.	B.D.	Δx	Δy	1900	m_1	Sp	l	b	Remarks
181	7° 3943	1.1	2.1	$18^h58^m.4$ + $7^{\circ}22'$	9.4	R	9	-1	Extremely red
182	13 3899	-1.6	-3.3	19 00 .6 +13 32	8.6	N	14	+2	
183	13 3926	.3	1.9	19 05 .8 +14 02	10.0	N	15	+1	
184	14 3831	-2.8	2.2	19 08 .2 +14 33	10.1	N	16	+1	
185	18 3997	.8	-1.1	19 10 .1 +18 25	8.7	N	20	+2	
186	17 3904	-.2	.8	19 11 .0 +17 14	8.5	N	19	+1	
187	16 3857	.9	.3	19 23 .1 +17 01	10.7	C	20	-1	
188	18 4117	-.7	-1.4	19 28 .2 +18 28	8.3	R	22	-1	4712, L?
189	26 3601	-1.2	1.4	19 31 .6 +26 21	8.1	N	29	+2	AR Vul, I
190	27 3446	1.9	1.5	19 33 .6 +28 03	10.4	N:	31	+2	Overlapped
191	27 3452	.7	3.4	19 35 .1 +27 23	10.0	N	30	+2	
192	28 3438	2.4	1.2	19 38 .8 +28 49	11.0	N	32	+2	
193	30 3707	-1.2	-.4	19 39 .2 +30 05	10.6	C	33	+2	
194	25 3983	-1.3	-2.2	19 44 .6 +25 53	7.8	R	30	-1	
195	30 3768	-1.3	-.2	19 46 .2 +30 46	8.4	N	35	+1	
196	32 3629	-.7	.2	19 51 .8 +32 14	10.7	N	36	+1	V467 Cyg, SR
197	30 3816	-1.1	.2	19 52 .6 +30 32	10.6	C	35	0	
198	31 3855	-.6	2.7	19 53 .0 +31 28	11.1	N	36	0	
199	33 3694	-.3	-.8	19 58 .2 +33 19	10.7	N	38	+1	
200	30 3863	-.3	-4.0	19 58 .4 +30 28	6.9	N	36	-1	4995, N*, E?
201	34 3883	-1.8	.2	20 04 .2 +35 01	10.5	N	40	+1	
202	34 3883	3.8	-1.8	20 05 .6 +34 55	8.4	N:	40	0	
203	35 4006	.6	2.8	20 07 .4 +35 48	7.9	R	41	0	V429 Cyg, D217, R, LP
204	33 3793	.4	2.5	20 07 .8 +33 48	11.1	N	40	-1	
205	33 3793	2.4	.7	20 08 .2 +33 42	9.7	N	40	-1	
206	36 3970	-1.1	-2.2	20 11 .8 +36 42	7.9	R	42	0	V432 Cyg, D218, R, I
207	37 3876	.4	-.1	20 14 .8 +37 09	6.7	R	43	0	WX Cyg, Ne*, M
208	33 3861	.2	-.1	20 16 .0 +33 53	10.7	N	41	-2	
209	40 4161	-1.0	.7	20 21 .6 +40 24	10.5	N	47	+1	
210	37 3934	.2	-2.6	20 23 .0 +37 57	7.9	R	45	-1	
211	42 3790	.3	-1.0	20 31 .6 +42 49	11.4	N	50	+1	
212	45 3219	2.8	-.5	20 32 .3 +45 08	9.6	N	52	+2	
213	43 3710	.6	-1.2	20 42 .2 +43 07	9.0	R:	51	0	
214	46 3067	-2.0	2.5	20 46 .0 +46 26	10.6	N	54	+1	
215	44 3596	1.2	1.3	20 46 .9 +45 02	7.1	R	53	0	DS Cyg, N*, I, D330, R
216	42 3920	1.2	-1.6	20 54 .2 +42 22	10.6	C	52	-3	
217	45 3355	-1.1	1.1	20 55 .8 +45 17	10.6	N	54	-1	
218	47 3243	.3	-1.0	20 55 .8 +47 13	8.5	R	56	+1	
219	47 3251	-1.3	-2.1	20 56 .8 +47 17	8.8	R	56	0	
220	45 3370	.6	-1.4	20 59 .0 +45 44	10.3	N	55	-1	
221	44 3701	.8	.7	21 03 .0 +44 54	11.3	N	55	-2	
222	49 3465	-1.2	2.6	21 03 .6 +49 31	11.1	N	58	+1	
223	45 3421	-.9	-.5	21 04 .2 +45 23	10.5	N	55	-2	
224	46 3201	-.6	2.6	21 05 .2 +47 00	9.0	R	57	-1	V573 Cyg, M
225	46 3204	1.9	-1.3	21 06 .6 +46 20	8.6	R	56	-1	V577 Cyg, LP
226	47 3350	.3	-3.5	21 12 .6 +47 15	9.7	N	58	-1	
227	49 3492	-2.5	1.6	21 13 .4 +49 59	10.5	N:	60	0	
228	47 3410	-.9	.8	21 22 .8 +48 11	11.3	N	60	-2	
229	49 3536	1.6	3.1	21 27 .2 +49 24	10.5	N	61	-1	
230	52 2966	-3.4	-.7	21 28 .2 +52 36	11.3	N	63	+1	

Table 1b

Carbon Stars

No.	B.D.	Δx	Δy	1900	m_1	Sp	l	b	Remarks
231	53° 2655	-1.1	-2.7	$21^h33^m.4$ +54°04'	10.9	N	65	+1	
232	53 2703	-1.4	-.1	21 42 .4 +53 39	9.1	N	66	0	
233	51 3143	.3	1.3	21 43 .0 +52 06	7.1	N	65	-1	D 339, R
234	52 3043	.8	-1.2	21 46 .6 +52 10	8.7	N	65	-1	
235	54 2640	-2.2	.9	21 48 .4 +54 37	7.9	R	67	+1	
236	52 3053	-.6	1.1	21 49 .4 +53 01	9.1	N:	66	-1	
237	52 3065	-1.5	-.3	21 51 .8 +52 25	9.1	N	66	-2	
238	57 2427	1.0	2.2	21 52 .6 +57 10	10.8	N	69	+2	
239	55 2650	1.6	-3.9	21 53 .4 +55 43	10.3	N	68	+1	
240	52 3070	2.4	6.5	21 54 .0 +53 20	9.1	N	67	-1	
241	54 2655	-1.4	-1.4	21 54 .4 +54 25	10.1	N	67	0	
242	52 3070	4.7	-1.3	21 55 .0 +52 54	9.9	N	67	-1	MQ Cyg, M
243	54 2654	2.0	3.2	21 55 .4 +55 01	9.9	N	68	0	
244	54 2672	-2.9	-3.0	21 57 .8 +54 04	11.5	C	68	-1	
245	53 2768	2.5	1.0	21 58 .8 +53 22	9.7	N	67	-1	
246	55 2701	1.2	-.2	22 08 .9 +55 16	9.0	R	70	-1	
247	53 2830	.9	.2	22 12 .4 +54 02	8.0	N	69	-2	
248	53 2834	.5	-.2	22 12 .8 +53 31	9.2	N	69	-2	
249	55 2738	-.4	2.1	22 19 .4 +56 12	10.6	N	71	-1	
250	58 2427	.3	-2.0	22 20 .2 +58 14	10.0	N	72	+1	
251	57 2531	2.0	-1.3	22 23 .0 +57 40	10.6	N	72	0	
252	55 2766	-1.0	-.5	22 28 .0 +55 13	10.4	N	72	-2	
253	57 2558	-1.7	2.8	22 28 .7 +58 06	6.4	N	73	0	N*
254	58 2449	.5	.9	22 28 .8 +59 02	9.8	N	74	+1	
255	57 2571	1.8	-3.1	22 34 .5 +57 57	10.4	N	74	0	
256	57 2578	1.9	-1.1	22 36 .1 +58 07	11.0	N	74	0	
257	55 2803	-.1	1.6	22 41 .1 +56 05	5.7	N	74	-2	DV Lac, N*, I
258	58 2479	-.6	-2.0	22 42 .4 +59 03	8.6	N	75	0	
259	57 2606	2.5	.3	22 43 .6 +57 47	10.8	C	75	-1	
260	59 2574	-2.2	-1.7	22 44 .0 +59 27	9.8	N	76	+1	
261	56 2878	-.4	2.4	22 46 .1 +57 00	10.0	N	75	-2	
262	58 2486	.9	.7	22 46 .3 +58 17	9.8	N	75	-1	
263	59 2585	-.2	-.2	22 47 .4 +60 02	10.0	N	76	+1	
264	60 2537	.3	-.7	23 20 .8 +60 46	10.0	N	80	0	
265	61 2472	-1.3	-1.8	23 27 .8 +61 34	7.0	N	82	+1	DS Cas, D362, N, I
266	61 2493	-.3	-.7	23 34 .8 +61 50	10.9	N	82	+1	
267	62 2316	2.1	-2.2	23 48 .8 +62 10	10.3	N	84	+1	
268	59 2805	1.1	1.3	23 55 .6 +59 19	11.1	N	84	-2	
269	60 2652	.6	1.7	23 55 .8 +61 02	10.9	N	85	0	
270	59 2815	.2	.1	23 57 .0 +59 25	10.1	N	85	-2	
271	60 2664	.4	1.2	23 59 .0 +60 23	9.1	R	85	-1	

and impossible to detect in dense or in very weak spectra. The two tables differ in one respect only. The first lists all carbon stars which are in the *BD* catalogue. The second gives a reference *BD* star near the carbon star and co-ordinates in millimeters in the scale of the *BD* chart from the reference star to the carbon stars. Positive Δx indicates the direction of increasing R.A., and positive Δy indicates the direction of the north.

The infrared magnitudes, designated by m_i, are approximate and are given to furnish added means of identification. They were estimated from the density of the spectra. To obtain approximate visual magnitudes, 3.6 may be added to the infrared magnitudes. This value was derived by establishing the relation between the *BD* magnitude and ours.

Three classes of stars are given in the spectrum column, N, R, and C. Among the first two classes a few misclassifications may exist, particularly when the estimated values are close to the boundaries of the division between the two classes and in view of the results obtained above. Stars having spectra near the limiting magnitude of the plate were classed as C. However, regardless of the density of a spectrum, the weakening of the continuum produced by the presence of the *CN* bands λλ 7945, 8125, and 8320 was observed with certainty in all stars included in the two tables. The last two columns give the galactic longitude and latitude to the nearest degree. The sources for the "Remarks" were the following:

a) *Sanford's* (1944) *catalogue.*—The asterisk after a spectral class denotes his classification.

b) *Lee's* (1943, 1947) *catalogue.*—The "D" followed by a number and a spectral class denotes that the class was obtained from the Dearborn catalogue. A question mark after the number indicates that the given co-ordinates leave some doubt as to the identification of the star.

c) *The General Catalogue of Variable Stars* (Kukarkin and Parenago 1948).—Here the notations are as follows: *I*, irregular; *LP*, long period; *SR*, semiregular; *M*, Mira-type; and *L*, unknown type with slow fluctuations of brightness.

d) *The Catalogue of Stars Suspected of Variability* (Kukarkin *et al.* 1951).—A number followed by a type of variability was obtained from this catalogue. The notations are the same as given above.

A discussion of the surface distribution of the stars given in this table is to be presented separately, in order that it may include carbon stars at high galactic latitudes as well as other relatively cool stars.

We are indebted to the Office of Naval Research for financial assistance in carrying out our infrared surveys of which this is a part. It is a pleasure also to thank Dr. W. W. Morgan, who shared in the initial planning of the surveys and who has materially contributed during the progress of the work.

REFERENCES

Keenan, P. C., and Morgan, W. W. 1941, *Ap. J.*, **94**, 501.
Kukarkin, B. V., and Parenago, P. P. 1948, *General Catalogue of Variable Stars* (Moscow: Academy of Sciences, U.S.S.R.).
Kukarkin, B. V.; Parenago, P. P.; Efremov, U. E.; and Kolorov, P. N. 1951, *Catalogue of Stars Suspected of Being Variable* (Moscow: Academy of Sciences, U.S.S.R.).
Lee, O. J.; Baldwin, R. B.; Hamlin, D. W.; and Kinnaird, R. F. 1943, *Pub. Dearborn Obs.*, Vol. **4**, Part 16.
Lee, O. J., and Bartlett, T. J. 1947, *Pub. Dearborn Obs.*, Vol. **5**, Part 3.
Lee, O. J.; Gore, G. D.; and Bartlett, T. J. 1947, *Pub. Dearborn Obs.*, Vol. **5**, Part 7.
Sanford, R. F. 1944, *Ap. J.*, **99**, 145.

VARIATIONS IN THE STELLAR LUMINOSITY FUNCTION
VI. A REGION IN MONOCEROS

S. W. McCuskey
Warner and Swasey Observatory, Case Institute of Technology
Received January 15, 1954

ABSTRACT

Spectral types, red color indices, and photographic magnitudes have been observed in an area of 16.4 square degrees centered at R.A. 6^h51^m; Dec. $-1°.3$ (1950). The distribution of 2983 stars according to photographic magnitude is summarized in Table 1. The color indices, summarized in Table 3, indicate no absorption to a distance of 500 parsecs, followed by a gradient of 1.1 mag/kpc to 2500 parsecs. Space densities as a function of distance are given in Table 7. Figure 3 illustrates the luminosity functions constructed for distances of 100, 200, 400, and 600 parsecs. These functions show little variation with distance and do not differ greatly from the standard van Rhijn function (van Rhijn 1936).

The Milky Way in Monoceros is a relatively smooth region, where obscuring matter in concentrated form is inconspicuous. For this reason it serves as an excellent area in which to investigate the changes in the stellar luminosity function with distance from the sun. The region under discussion in this paper, designated as "LF9," is the last of the luminosity-function regions to be investigated. Results of the other studies, with the exception of LF5, have already been published (McCuskey and Seyfert 1947; McCuskey 1949; Nassau and MacRae 1949; McCuskey 1951, 1952).

Region LF9 is a circular area of 16.4 square degrees centered at R.A. 6^h51^m; Dec. $-1°.3$ (1950); $l = 182°$, $b = +2°$. On the Ross and Calvert *Atlas of the Milky Way*, chart 36, it may be found 9.8 cm from the right-hand edge and 15.8 cm from the bottom. Spectral types and photographic magnitudes have been determined for nearly 3000 stars in this area. Blue-red color indices have been observed for the majority of the early-type stars. An analysis of these data with regard to the stellar density functions for various spectral groups and variations in the luminosity function forms the content of the present paper.

OBSERVATIONAL DATA

Table 1 gives a statistical summary of the spectral-type distributions as a function of apparent photographic magnitude. In general, for stars with $m < 11.0$, the spectral types and luminosity classes depend upon estimates from three plates of varying exposure times. In most of the luminosity-classification work, direct comparisons were made between the star to be classified and standard stellar spectra of the same dispersion taken with the same telescope. All plates were taken with the 4° or the 2° prism attached to the Schmidt-type 24–36-inch telescope of this observatory. For the faintest stars, the spectral classification depends upon estimates from two plates.

Criteria for classification of spectral types and luminosity groups are those published by Nassau and van Albada (1947). The nomenclature for luminosity classes is that of Morgan, Keenan, and Kellman (1943). For the fainter stars, luminosity classes could not always be assigned. These are indicated in Table 1 by the numbers in parentheses. The low situation of LF9 in the Cleveland sky, with the resultant decrease in the limiting magnitude of our plates, is reflected in the rather large number of unclassified objects fainter than $m_{pg} = 11.5$.

Photographic magnitudes have been measured on four Kodak IIa-O plates taken with the 24–36-inch telescope. A sequence for calibration, established by Bok and his co-workers (private communication), was available in SA98, which lies within the area

TABLE 1

DISTRIBUTION OF OBSERVED SPECTRAL TYPES IN LF9
(Area 16.4 Square Degrees)

m_{pg}*	B0, B1	B2	B3	B5	B8	B9	A0	A2, A3	A5	F0†			F2			F5			F8			G0		
										III	IV	V	III	IV	V	III	IV	V	III	IV	V	III	IV	V
≤6.0	0	0	1	0	1	0	0	1	0	0	0	1	0	0	0	0	0	0	0	0	0	0	0	0
6.25	0	0	0	0	0	0	0	0	0	0	0	1	0	0	0	0	0	0	0	0	0	0	0	0
6.75	0	0	0	0	2	0	0	0	0	0	0	1	0	0	0	0	0	0	0	0	0	0	0	0
7.25	1	0	1	0	2	0	0	1	1	1	0	0	0	0	0	0	0	0	0	0	0	0	0	0
7.75	0	0	0	1	2	1	1	0	2	0	0	0	0	0	1	0	0	0	0	0	0	0	0	1
8.25	0	0	1	1	6	3	2	3	3	0	1	0	0	0	0	0	0	1	0	0	0	0	0	0
8.75	2	1	2	2	13	11	7	5	6	1	1	2	0	0	1	0	1	0	0	0	0	0	0	1
9.25	1	1	2	8	11	7	10	7	3	0	2	4	0	0	0	1	1	1	0	0	3	0	1	4
9.75	0	1	2	12	20	12	12	16	8	0	4	6	0	(1)	1	1	2	4	1	0	4	0	1	1
10.25	0	2	2	8	23	19	30	21	12	0	(1)	12	1	(1)	6	3	3(1)	4	0	(1)	7	0	1(1)	8
10.75	2	0	3	13	31	25	50	18	8	2	(7)	6	0	(7)	1	3	(2)	3	2	(5)	7	1	(17)	13
11.25	0	1	2	30	42	28	100	32	15	0	(25)	0	1	(15)	2	0	(8)	0	0	(18)	4	2	(71)	2
11.75	1	1	0	23	20	42	152	51	11	0	(24)	0	0	(5)	0	0	(5)	1	0	(13)	0	0	1(111)	0
12.25	0	0	0	1	5	10	81	19	2	0	(5)	0	0	0	0	0	(1)	0	0	(1)	0	0	(35)	0
Total	7	7	16	99	178	158	445	174	71	4	70	33	2	29	12	8	24	14	3	38	25	3	239	30

m_{pg}*	G2			G5			G8			K0			K2, K3			K5			M0, M2			M5, M8†			Unclassified‡	All Stars
	III	IV	V	III	IV	V	III	IV	V	III	IV	V	III	IV	V	III	IV	V	III	IV	V	III	IV	V		
≤6.0	0	0	0	0	0	0	0	0	0	0	0	0	0	0	0	0	0	0	0	0	0	0	0	0	0	4
6.25	0	0	0	0	0	0	0	0	0	0	0	0	0	0	0	0	0	0	0	0	0	0	0	0	0	1
6.75	0	0	0	0	0	0	0	0	0	1	0	0	0	0	0	0	0	0	0	0	0	0	0	0	0	4
7.25	0	0	0	0	0	0	0	0	0	0	0	0	1	0	0	0	0	0	0	0	0	0	0	0	0	8
7.75	0	0	0	0	0	0	1	0	0	0	1	0	0	0	0	1	0	0	0	0	0	0	0	0	0	12
8.25	0	0	0	1	0	0	0	0	0	2	0	0	0	0	0	0	0	0	0	0	0	0	0	0	0	24
8.75	0	0	0	0	0	0	0	1	1	2	0	0	1	1	0	1	0	0	0	0	0	0	0	0	2	65
9.25	0	0	0	0	3	2	3	5	0	3	0	0	3	1	0	0	0	0	0	0	0	0	0	0	4	91
9.75	0	0	0	4	2	1	9	2	0	4	2	0	2	0	0	0	0	0	0	0	0	3	0	0	7	145
10.25	1	2	3	5	2	1	7	2	0	6	4	1	4	3	0	0	0	0	1	0	0	1	0	0	15	225
10.75	0	(3)	5	7	1(1)	9	13	2(3)	2	11	1(1)	0	0	0	0	2	0	0	2	0	0	0	0	0	20	309
11.25	0	1(17)	3	5	2(10)	5	27	1(11)	3	10	1(8)	1	1	(3)	0	0	(3)	0	3	0	1	1	0	0	28	543
11.75	0	(17)	1	6	(22)	2	11	(30)	0	19	(40)	0	0	(10)	0	0	(3)	0	2	(3)	0	1	0	0	174	802
12.25	0	(7)	0	1	(7)	0	4	(13)	0	1	(40)	0	0	(5)	0	0	(3)	0	0	(1)	0	0	0	0	508	750
Total	1	47	12	29	50	20	75	70	6	59	98	2	12	23	0	4	9	0	8	4	1	6	0	0	758	2983

* The entries under m_{pg} refer to half-magnitude intervals, e.g., 7.01–7.5, 7.51–8.0, etc.
† Parentheses around entries for the fainter stars of spectral class F0 and later indicate those for which no luminosity class could be assigned.
‡ Unclassified stars are those for which overlaps or other defects made classification impossible, as well as those few supergiants, OB stars, and stars with composite spectra included in the field.

covered by LF 9. Through the kindness of Dr. D. A. MacRae, selected sequence stars ranging in brightness from $m = 7$ to $m = 11$ were observed photoelectrically, to fix more accurately the zero point and the scale of the sequence. The four plates from which magnitudes of the field stars were obtained were measured with the iris-diaphragm photometer of this observatory, which has been described by Cameron (1951). As determined from the internal agreement of the measures from the four plates, the probable error of a final magnitude is ± 0.05 mag.

Similar measurements of three Kodak 103*a*-E plates taken with the same telescope and with a Wratten No. 22 filter yielded photored magnitudes for 1042 early-type stars and 67 late-type dwarfs. Again the provisional photored sequence in SA98, provided by Bok and collaborators, was used, after a revision of its zero point and scale had been made photoelectrically. The probable error of a final photored magnitude of a field star is ± 0.05 mag. Further comments regarding the magnitude systems are given later in the discussion of the color indices.

TABLE 2

DISTRIBUTION OF SPECTRAL TYPES FROM *Henry Draper Catalogue* FOR REGION SURROUNDING LF9

(Area 100 Square Degrees)

m_{pg}	Spectral Type									All Stars
	B0–B2	B5	B8–A0	A2–A5	F0–F5	F8–G0	G5	K0–K2	K5–M	
6.51–7.00	1	1	6	1	0	1	0	2	1	13
7.01–7.50	1	2	9	0	4	0	0	5	0	21
7.51–8.00	4	4	20	8	4	3	1	4	0	48
8.01–8.50	7	3	61	14	7	4	3	7	1	107
8.51–9.00	3	1	91	55	29	6	3	15	4	207
9.01–9.50	1	1	131	65	45	19	12	40	7	321

A word or two about the photoelectric measures would be in order. One star of the sequence was selected as a zero-point star, and its visual magnitude, V, was determined by comparison with two standard stars, β Cnc and η Hya, of the list published by Johnson and Morgan (1953). Comparison on two nights yielded values of V which differed by only 0.01 mag. Nine stars of the sequence were also measured on two nights, to check the scale. The photoelectric yellow magnitudes, determined by MacRae, were converted to the International Photovisual System by the relation $V = Y_0 - 0.054\ C_0 +$ constant, where Y_0 is our measured yellow magnitude and C_0 is our color index, reduced to outside the atmosphere. The V magnitudes and the colors, $P - V = 0.335 + 1.137\ C_0$, are essentially on the International System, as defined by the work of Stebbins, Whitford, and Johnson (1950). The blue-yellow color indices were converted into blue-red indices by means of the relation R.I. $= 1.33\ (P - V)$. From these relations the photographic and photored magnitudes of the provisional sequence were revised and used for calibration of the plate measurements. A description of the photoelectric equipment with which this work was done has been given by MacRae, Harris, and Rogerson (1952).

In order to strengthen the spectral-type data for statistical analysis, two other sources were used. Counts according to spectral type and photographic magnitude have been made in the *Henry Draper Catalogue* for an area of 100 square degrees surrounding LF9. These data are presented in Table 2. Furthermore, for the very brightest stars, the counts in the *Henry Draper Catalogue* made by Seydl (1929) for the galactic-latitude zone 0° to $\pm 10°$ have been reduced to counts per 100 square degrees and used to supple-

ment the local data. These counts have been summarized in the first paper of this series (McCuskey and Seyfert 1947).

General star counts for a small area in LF9 have been published (McCuskey 1945) in a previous study of the general galactic density gradient in this region. These counts extend to $m_{pg} = 17.1$ and include, in an area of 0.73 square degrees, 2613 stars. Supplemented by general counts derived from Table 1, these have been used to obtain a strengthened solution for the general space-density function in this area.

ANALYSIS OF THE COLOR DATA

Table 3 presents the average observed blue-red color indices for LF9. Included also are the normal red indices and the mean absolute magnitudes required for determining the run of color excesses with distance. These data have been taken from a paper by Nassau and MacRae (1949). The lower part of the table contains red indices for the late-type dwarf stars. Several lines of evidence indicate that the red indices exhibited in Table 3 are somewhat too blue. In the first place, we observe that the average red index for the A5 stars with $m_{pg} < 10$ is -0.07 mag., whereas the intrinsic index is 0.00 mag.

TABLE 3

AVERAGE OBSERVED RED INDICES IN LF9

SPECTRUM	R.I. NORM.	M_{pg}	m_{pg} 8.01–9.00	9.01–9.50	9.51–10.00	10.01–10.50	10.51–11.00	11.01–11.50	11.51–12.00	12.01–12.50
B0, B1	−0.62	−4.0	−0.11(2)	−0.69(1)	.....	.....	+0.18(2)	.....	+0.39(1)	.....
B2	−0.61	−2.8	− .24(1)	.....	−0.16(1)	−0.43(2)	.....	+0.12(1)	+ .13(1)	.....
B3	−0.57	−2.2	− .37(2)	− .30(2)	− .55(2)	− .42(2)	+0.18(2)	− .17(2)	.....	.....
B5	−0.50	−1.4	− .49(3)	− .49(8)	− .49(12)	− .48(8)	−0.26(12)	− .02(26)	− .01(21)	+0.15(1)
B8	−0.40	−0.4	− .41(18)	− .45(11)	− .53(21)	− .29(23)	−0.12(32)	− .10(38)	+ .01(18)	+ .16(4)
B9	−0.33	0.0	− .41(15)	− .41(9)	− .31(11)	− .27(19)	−0.20(26)	− .04(25)	+ .02(39)	+ .13(10)
A0	−0.20	+0.4	− .25(9)	− .31(8)	− .30(12)	− .19(30)	−0.15(48)	− .04(91)	+ .05(135)	+ .14(67)
A2, A3	−0.06	+1.0	− .32(8)	− .26(7)	− .16(11)	− .17(18)	−0.03(17)	+ .04(30)	+ .06(47)	+ .14(17)
A5	0.00	+1.7	− .12(8)	+ .04(3)	− .07(8)	− .04(10)	−0.02(5)	+ .07(12)	+0.05(5)	+0.21(2)
F8 V	+0.40	+3.9	.....	+ .52(2)	+ .29(2)	+ .25(6)	+0.44(3)	+ .38(1)	.....	.....
G0 V	+0.46	+4.3	+ .31(1)	+ .29(3)	+ .31(1)	+ .29(3)	+0.36(7)	+ .48(2)	.....	.....
G2 V	+0.60	+4.6	.....	.....	.....	+ .54(4)	+0.54(6)	+ .62(2)	.....	.....
G5 V	+0.84	+5.2	.....	+0.47(2)	+0.54(2)	+ .82(2)	+0.50(2)	+ .86(5)	.....	.....
G8 V	+1.04	+5.9	+0.84(1)	.....	.....	+0.94(1)	+1.03(2)	+0.96(7)	.....	.....

These stars are within 500 parsecs of the sun and, if anything, should be reddened slightly by interstellar material. Second, the average color excess of the late-type dwarf stars is -0.09 mag. These stars are presumably close by and should have color excesses of zero, on the average. In the third place, five of the sequence stars of spectral classes B8–A0, for which colors have been obtained photoelectrically, have an average color excess on the blue-yellow (P–V) system of -0.06 mag. These stars are of photographic magnitude 8.6–10.6 and hence are at distances of between 500 and 1200 parsecs. Presumably they, also, are reddened somewhat by interstellar material and should have small positive color excesses, if any. The zero point of the system of blue magnitudes used in the present analysis does not appear to be the source of this discrepancy. This has been examined indirectly by means of the catalogue of photovisual magnitudes of bright stars published in *Harvard Mimeograms*, Series III, No. 1.

The *HPv* magnitudes from the Harvard catalogue for 27 stars in LF9 were converted into International Photographic magnitudes, *IPg*, by the relation given in the introduction to the catalogue. The *IPv* magnitudes which enter into this reduction do not differ significantly from the V magnitudes recently published by Johnson and Morgan (1953). The *IPg* magnitudes were then compared with our adopted m_{pg} in LF9. We find for the 27 stars $IPg - m_{pg} = -0.01$ mag. These stars range in spectral class from B3

to K5. Since our m_{pg} system was based on photoelectric measures essentially on the International System, we conclude that no large zero-point error is present.

The evidence seems to point to some systematic error in the red magnitudes which may well arise from the photoelectric measures and conversion to the photored system. The possibility of a systematic error due to position of the star on the photographic plate was examined. If the color indices of the A5 stars with $m_{pg} < 11.5$ are averaged by quadrants of the circular field, we find a range from R.I. = +0.06 to −0.08 mag., with a mean for the whole field of −0.02 mag. The size of the variation is of the same order of magnitude as the systematic blueness exhibited by the colors. Since the average color indices of Table 3 are for stars distributed over the entire field, the positional effects largely average out. For the late-type dwarf stars in particular, the distribution over the field was chosen initially to avoid zonal effects on the plate. The cause of the zero-point discrepancy remains obscure. For the present we shall simply correct the zero point of the color indices by +0.09 mag. before using them in evaluating the absorption in LF9.

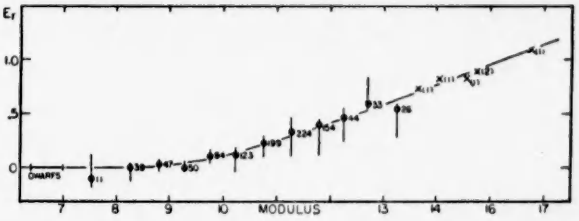

FIG. 1.—Average red color excess (E_r) is the ordinate; photographic distance modulus is the abscissa. Number of values entering each average and the range in values at each point are indicated by the numbers and the vertical lines. Crosses at large values of $m - M$ refer to individual stars, with one exception.

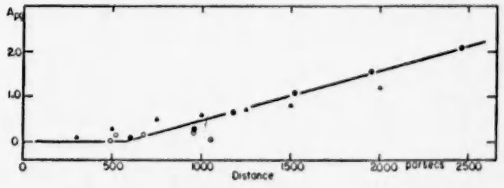

FIG. 2.—Total photographic absorption (A_{pg}) as a function of true distance. The solid points are derived from the color-excess-curve of Fig. 1. Triangles refer to absorption values deduced by Bok and Rendall-Arons. Open circles have been obtained from the photoelectrically observed colors of a few sequence stars.

Figure 1 shows the trend of the average red color excesses, E_r, with photographic distance modulus. Absolute magnitudes used in computing the moduli are listed in Table 3. The weighted average value of E_r for half-magnitude intervals in modulus is plotted, together with a vertical line indicating the greatest and least values of E_r which have entered the means. Numbers indicate the number of individual red excesses entering each mean. Crosses in the range $m - M$ = 13–16 are values essentially for individual stars of high luminosity.

The relationship shown in Figure 1 has been converted into one giving A_{pg}, the total photographic absorption, as a function of the true distance. A ratio $A_{pg}/E_r = 2.6$ was used for this purpose. The resulting run of absorption with distance is shown in Figure 2, where LF9 appears to be a relatively clear region within 500 parsecs of the sun. There-

after, the increase in photographic absorption is linear with a gradient of 1.1 mag/kpc.

We may compare this result with that obtained by Bok and Rendall-Arons (1945). By means of color excesses of B8–A7 stars in several areas throughout Monoceros and an analysis of the early B stars, they deduced the run of photographic absorption indicated by the triangles in Figure 2. Their region D contains our LF9. A small part of LF9 extends into their region C, where they found the absorption to be about 0.5 mag. greater at all distances than in region D. Table 4 summarizes the values of A_{pg} found by our measures (second col.) and their results for region D (third col.).

In the last column of Table 4 is given the run of the absorption as determined independently from the B-star data of Stebbins, Huffer, and Whitford (1940). A factor $A_{pg} = 9\bar{E}_1$ was used to convert their color excesses into total photographic absorption. The stars used in the analysis are distributed over 15° of galactic longitude and 12° of latitude. A few of the B stars in this area have been classed as OB by Nassau and

TABLE 4

SUMMARY OF ABSORPTION VALUES IN LF9

r (Parsecs)	Our Data (LF9)	Bok and Arons (Region D)	Stebbins, Huffer, and Whitford (B Stars)	r (Parsecs)	Our Data (LF9)	Bok and Arons (Region D)	Stebbins, Huffer, and Whitford (B Stars)
500	0	0.3	0.3	2000	1.5	1.2	1.8
1000	0.4	0.6	0.8	2500	2.1	.....	2.3
1500	1.0	0.8	1.3				

Morgan (1951). For these I have adopted $\bar{M}_v = -5.0$ and have recomputed the modulus in establishing the absorption-curve from the B-star data. It would appear from Table 4 that LF9 is in a relatively clear portion of the Monoceros area, although the run of A_{pg} with distance is not markedly different from the surroundings in the Bok and Rendall-Arons region D. For purposes of analysis, we shall assume that the absorption is negligible out to a distance of 500 parsecs. Thereafter, there is a linear increase in A_{pg} of 1.1 mag/kpc; and that this rate extends as far as our analysis may be considered valid, to about 3000 parsecs for the early-type stars.

PERCENTAGE OF DWARFS AMONG LATE-TYPE STARS

The observed numbers of dwarf stars among the brighter apparent magnitudes for the spectral groups F8–G2, G5, and G8–K3 are too small to be of statistical significance. As one estimate, therefore, we have computed the percentages of dwarf stars among the brighter stars by extrapolation from the observed numbers of faint dwarfs. We assume for this estimate that the dwarf stars are distributed uniformly in space within the volume of about 300 parsecs radius encompassed by our data. From the observed numbers of dwarf stars with $m_{pg} = 9$–11, the numbers for $m_{pg} < 9$ can be computed. We may also use, for a second estimate, the summary of percentages of dwarfs deduced from the previous studies of the LF regions and published by McCuskey (1952).

On the basis of these data and assumptions, the percentages of dwarf stars as a function of apparent magnitude have been computed and are exhibited in Table 5. These percentages for the G5 and the G8–K3 stars are in good agreement with the percentages deduced from proper-motion studies. For the early G stars, the adopted percentages of dwarfs are considerably higher than those found by earlier studies of their motions. In the work cited above (McCuskey 1952), however, this discrepancy has been traced to the inclusion of many G5 stars in the group called G.

VALUES OF LOG $A'(m)$ FOR ANALYSIS

Table 6 summarizes the spectral-type groupings and distributions in apparent magnitude in a form for space-density analysis. Here $A'(m)$ is the number of stars per 100 square degrees with magnitude $m - \frac{1}{4}$ to $m + \frac{1}{4}$. The values of log $A'(m)$ have been obtained by grouping the distributions of Table 1 and Table 2 and smoothing the results graphically. Luminosity classes IV and V have been grouped under "d" for the F8–G2 stars; for class G5, the stars in IV have been divided equally between classes "g" and "d"; for the G8–K3 stars, classes III and IV have been grouped under "g."

TABLE 5

ADOPTED PERCENTAGE OF DWARF STARS IN LATE SPECTRAL CLASSES

F8–G2		G5		G8–K3	
m	Per Cent Dwarfs	m	Per Cent Dwarfs	m	Per Cent Dwarfs
<7	75	6– 8	22	6– 8	3
7–9	85	8–10	32	8–10	4
>9	95	10–12	60	10–12	5

TABLE 6

ADOPTED VALUES OF LOG $A'(m)$ IN LF9

m_{pg}	B0, B2	B3, B5	B8–A0	A2–A5	F0–F5	F8–G2		G5		G8–K3		gK5–M
						g	d	g	d	g	d	
4.0	9.37	9.10	9.20	9.25	8.80							
4.5	9.62	9.30	9.55	9.47	9.02							
5.0	9.88	9.49	9.89	9.70	9.31							8.60
5.5	0.13	9.68	0.23	9.90	9.60							8.85
6.0	0.37	9.85	0.55	0.13	9.88	8.85	9.28	9.15	8.55	9.78	8.28	9.12
6.5	0.56	0.02	0.82	0.37	0.16	9.10	9.58	9.44	8.88	0.08	8.58	9.40
7.0	0.70	0.23	1.09	0.67	0.43	9.35	9.88	9.71	9.21	0.38	8.88	9.65
7.5	0.80	0.53	1.38	1.01	0.61	9.59	0.26	0.00	9.57	0.68	9.18	9.90
8.0	0.88	0.92	1.63	1.30	1.00	9.86	0.61	0.30	9.90	0.97	9.48	0.18
8.5	0.92	1.30	1.90	1.57	1.28	0.10	0.94	0.60	0.24	1.29	9.80	0.44
9.0	0.95	1.60	2.12	1.81	1.58	0.35	1.29	0.88	0.58	1.62	0.10	0.70
9.5	0.96	1.80	2.33	2.01	1.88	0.61	1.64	1.09	0.92	1.86	0.40	0.95
10.0	0.98	1.92	2.53	2.20	2.11	0.85	1.97	1.28	1.27	2.11	0.70	1.17
10.5	1.00	2.02	2.73	2.30	2.30	1.10	2.30	1.46	1.57	2.29	0.95	1.36
11.0	1.02	2.10	2.93	2.38	2.40	1.35	2.62	1.64	1.80	2.48	1.20	1.53
11.5	1.04	2.16	3.12	2.45	2.48		2.96	1.82	2.00	2.68	1.40	1.70
12.0	1.06	2.20	3.32	2.50	2.53		3.28	2.00	2.18	2.88	1.60	1.85

SPACE-DENSITY FUNCTIONS IN LF9

The data given in Table 6 have been analyzed by the numerical (m, log π) method (Bok 1937), in which the absolute-magnitude distribution for any spectral group has been assumed to be Gaussian. Mean absolute magnitudes and dispersions used in the analysis are the same as those used in the other papers of this series. They have been published by Nassau and MacRae (1949).

Table 7 summarizes the density functions, corrected for interstellar absorption according to the curve shown in Figure 2. The entries of the table are the numbers of stars per 1000 cubic parsecs at given distances from the sun. Among the prominent features of the galactic structure in this region we may mention the following:

1. The number of B0–B5 stars decreases with distance in the first 500 parsecs from the sun and then increases to a value at 1000–1200 parsecs comparable to the density in the solar neighborhood. Beyond 1200 parsecs these stars diminish in number until, at 2500 parsecs, the density is approximately one-fourth that near the sun. Since LF9 lies at $l = 182°$, $b = +2°$, it is an area immediately adjacent to the part of the sky in which Morgan, Whitford, and Code (1953) have found an aggregate of blue giant stars. Thus the concentration found here at 1000–1500 parsecs may be a part of the spiral arm, shown so effectively in Figure 1 of their paper.

TABLE 7

SPACE-DENSITY FUNCTIONS IN LF9
(Number of Stars per 1000 Cubic Parsecs)

Distance (Parsecs)	Spectral Group											
	B0, B2	B3, B5	B8–A0	A2–A5	F0–F5	dF8–G2	dG5	dG8–K3	gF8–G2	gG5	gG8–K3	gK5–M8
25	.....	.....	0.075	1.10	1.90	2.4	3.5	10.0	0.020	0.042	0.20	0.042
50	.....	.....	.090	0.80	1.67	2.5	5.2	10.0	.020	.042	.20	.040
75	.....	0.0140	.110	0.45	1.45	2.7	7.0	10.0	.020	.042	.20	.039
100	0.00100	.0130	.120	0.34	1.20	2.9	7.5	8.7	.020	.042	.20	.037
200	.00100	.0080	.140	0.39	2.00	3.4	3.5	2.0	.017	.042	.20	.031
300	.00084	.0045	.122	0.38	1.28	4.0	1.8	0.9	.013	.041	.20	.026
400	.00060	.0028	.110	0.32	0.90	4.4	0.9	(0.5)	.011	.038	.20	.026
500	.00056	.0018	.112	0.27	0.45	5.0	0.5	.....	.010	.034	.20	.025
600	.00068	.0024	.150	0.21	0.30	7.3	(0.4)	.....	.011	.029	.20	.024
800	.00097	.0078	.134	0.119	0.14	.....	.....	.....	.015	.026	.17	.021
1000	.00116	.0123	.121	0.071	0.06	.....	.....	.....	.019	.026	.15	.018
1200	.00098	.0135	.145	0.039	0.05	.....	.....	.....	.024	.026	.16	.018
1400	.00075	.0105	.173	0.039	0.05	.....	.....	.....	.028	.028	.18	.018
1600	.00052	.0078	.204	0.030	.....	.....	.....	.....	0.032	0.031	0.20	0.018
1800	.00040	.0066	.216	.....	.....	.....	.....	.....	.....	.....	.....	.....
2000	.00031	.0064	.200	.....	.....	.....	.....	.....	.....	.....	.....	.....
2500	.00019	.0052	0.306	.....	.....	.....	.....	.....	.....	.....	.....	.....
3000	0.00014	0.0045	.....	.....	.....	.....	.....	.....	.....	.....	.....	.....

2. There is an increase in the number of B8–A0 stars per unit volume from the vicinity of the sun to a distance of 2500 parsecs. The density triples in this distance, and the local fluctuations are comparatively minor. There is some indication that the gradient is steeper in the last 500 parsecs of this range. Bok and Rendall-Arons (1945) find in their region D a high density of B8–A0 stars at distances ranging from 200 to 500 parsecs. Our results confirm the concentration found by them and indicate an extension to greater depths of space.

3. The analysis here given for LF9 also confirms the negative density gradient among the A2–A5 stars found by Bok and Rendall-Arons. Between 100 and 500 parsecs we find a decrease in density from 0.34 to 0.27, while the authors mentioned have found 0.34–0.23 for the A1–A7 stars.

4. There is some evidence for a sharply defined concentration of F0–F5 stars between 100 and 300 parsecs. The density at 200 parsecs is equal to that in the immediate solar neighborhood, but there appears to be a sharp minimum in between. Beyond 250 parsecs

the F stars decline rapidly in number until at 1000 parsecs they are only one-thirtieth as numerous as in the vicinity of the sun.

5. From 100 to 500 parsecs the dwarf stars of classes G5 and G8–K3 decrease in number. It should be emphasized, however, that the incompleteness of the spectral data increases the uncertainty of the density values at these greater distances. The F8–G2 dwarf stars appear to increase with distance, slowly at first and then more rapidly, until at 500 parsecs they are twice as numerous as in the neighborhood of the sun.

6. The giant stars of all late spectral classes combined diminish in number by 30 per cent in the first 1000-parsec interval from the sun. Thereafter, the density remains sensibly constant to a distance of 1600 parsecs for the G5, G8–K3, and K5–M giants. The giant stars of classes F8–G2, however, increase in number somewhat until, at 1500 parsecs, they are 1.5 times as numerous as they are near the sun. The relatively constant density for all the spectral groups combined confirms the result published by Bok and Rendall-Arons (1945). They find an average density of 0.26 stars per 1000 cubic parsecs for the distance interval 50–400 parsecs, while we find in LF9 an average density of 0.29 for this same span.

TABLE 8

VALUES OF LOG $A(m)$ FROM GENERAL STAR COUNTS

m	log $A(m)$	m	log $A(m)$	m	log $A(m)$
8	0.30	12	2.00	16	3.24
9	0.85	13	2.35	17	3.52
10	1.29	14	2.68		
11	1.66	15	2.97		

TABLE 9

RELATIVE DENSITY FUNCTION FROM GENERAL STAR COUNTS

Distance (r) (Parsecs)	$D(r)$	Distance (r) (Parsecs)	$D(r)$	Distance (r) (Parsecs)	$D(r)$
100	1.00	600	1.05	1600	0.85
200	1.53	800	1.05	1800	1.23
300	1.35	1000	1.10	2000	1.55
400	1.20	1200	1.10	2500	1.60
500	1.10	1400	0.95		

RELATIVE DENSITIES FROM GENERAL STAR COUNTS

By combining the totals for all spectral classes in Table 1 and the data for Area 12 published by McCuskey (1945) in a previous survey, we have star-count data which yield an over-all picture of the relative density function in this area. Values of log $A(m)$[1] are given in Table 8. For the range $m = 7$ to $m = 12$ these are, on the average, 0.15 greater than those published in the reference cited.

The commonly accepted luminosity function published by van Rhijn (1936) has been used to compute the relative space-density function. Corrections for absorption according to the curve shown in Figure 2 have been applied, and the resulting space-density function is exhibited in Table 9, where $D(r)$ is the density relative to that in the solar neighborhood. In making the calculation, the variation in the general luminosity func-

[1] $A(m)$ is the number of stars with magnitude $m - \frac{1}{2}$ to $m + \frac{1}{2}$ per square degree.

tion with distance from the galactic plane has been taken into account. Bok and MacRae (1941) have published (m, log π) tables convenient for this purpose.

There is some evidence for a concentration of stars between 100 and 400 parsecs which is undoubtedly caused by the excess in dG and dK stars ($+4 < M_{pg} < +7$) in this area. The luminosity functions shown in Figure 3 indicate a small surplus of these stars relative to the standard van Rhijn function. Beyond 500 parsecs the general density remains sensibly constant to a distance of 1500 parsecs. Beyond 1500 parsecs there is evidence for a strong and extensive concentration of stars extending to the limit of reliability of our data. The density at distances of 2000–2500 parsecs is 1.5 times that near the sun. This, again, is a reflection of the increasing density of B8–A0 stars in this particular area. Bok and Rendall-Arons (1945) have pointed out a stellar concentration within 500 parsecs of the sun in Monoceros in their region D, within which LF9 lies. At greater distances their results indicate a constant density of 1.0 to 1600 parsecs, which is in good agreement with the present analysis.

TABLE 10

LUMINOSITY FUNCTIONS IN LF9
(log $\varphi(M) + 10$)

M_{pg}	DISTANCE (PARSECS)					
	100	200	400	600	Standard	Bok-Arons
−3	3.75	3.70	3.41	3.48	.....	.....
−2	4.51	4.36	4.03	4.06	4.75	.....
−1	5.25	5.23	5.05	5.16	5.07	.....
0	5.82	5.86	5.77	5.86	5.68	5.83
+1	6.29	6.33	6.27	6.24	6.34	6.38
+2	6.64	6.72	6.61	6.49	6.77	6.70
+3	6.95	7.10	6.95	6.93	6.86	6.84
+4	7.25	7.35	7.34	7.49	7.19	.....
+5	7.47	7.36	7.32	7.49	7.35	.....
+6	7.74	7.40	6.98	6.96	7.50	.....
+7	7.69	7.17	(6.59)	(6.48)	7.53	.....

THE LUMINOSITY FUNCTION IN LF9

We can compute from the density functions of Table 7 a general luminosity function at those distances where the spectral data are relatively complete. The assumption is made that the absolute magnitudes of the stars of each spectral group are distributed about the mean M_0 in a Gaussian fashion, with the same dispersion σ_0 that was used in calculating the densities originally. Summation over the spectral groups for each M yields a number which is converted into log $\varphi(M)$, where $\varphi(M)$ is the number of stars with M between $M - \frac{1}{2}$ and $M + \frac{1}{2}$ per cubic parsec. Luminosity functions computed for distances of 100, 200, 400, and 600 parsecs are given in Table 10, together with the standard van Rhijn function for comparison. We also list in the last column of the table the luminosity function calculated by Bok and Rendall-Arons at 100 parsecs. The agreement with ours is very satisfactory. Figure 3 shows our results graphically.

Figure 3 indicates that there is no serious difference in the mean between the local luminosity functions and that usually adopted for star-count analyses. A small excess of stars with $-1 < M < +1$ in the local functions over the van Rhijn function is evident, but it is not so large as has been found in some of the other areas of the LF series. Fluctuations in log $\varphi(M)$ with distance are not excessive in the absolute-magnitude

range -2 to $+4$, where our data are most reliable. It should be noted that in making the calculation for log $\varphi(M)$ at 600 parsecs, the density of dG5 stars was assumed to be 0.4, and the density of dG8–K3 stars to be 0.5. These are extrapolated values, and hence the calculated values of log $\varphi(M)$ for $M > 3$ at distances of 400 and 600 parsecs are somewhat uncertain.

In conclusion we may say that this area in Monoceros is perhaps the most homogeneous of any of the LF regions investigated. How these results fit into an over-all picture of the variation in the luminosity function with distance and with galactic longitude is reserved for a future discussion.

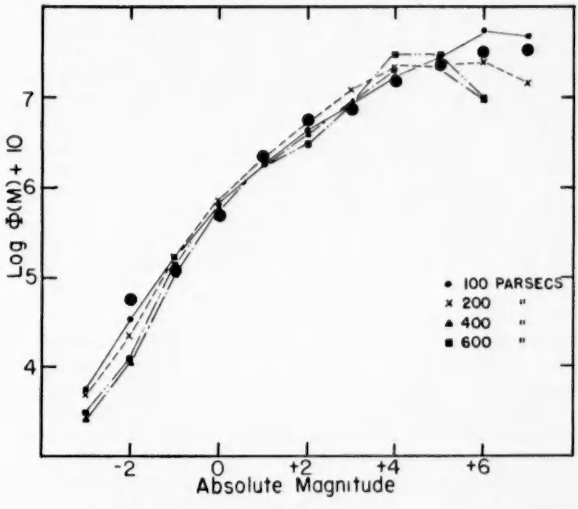

FIG. 3.—Luminosity functions in LF9. Ordinate is log $\phi(M) + 10$; abscissa is absolute photographic magnitude. Large circles indicate the standard van Rhijn general luminosity function normally used for star-count analyses. Functions for distances of 100, 200, 400, and 600 parsecs are indicated by the legend.

It is a pleasure to thank Dr. B. J. Bok for placing his unpublished sequence data in SA98 at my disposal.

REFERENCES

Bok, B. J. 1937, *Distribution of the Stars in Space* ("Astrophysical monograph"), pp. 26–31.
Bok, B. J., and MacRae, D. A. 1941, *Ann. New York Acad. Sci.*, **42**, 252.
Bok, B. J., and Rendall-Arons, J. M. 1945, *Ap. J.*, **101**, 280.
Cameron, D. M. 1951, *A.J.*, **56**, 92.
Johnson, H. L., and Morgan, W. W. 1953, *Ap. J.*, **117**, 313.
Johnson, H. L., and Morgan, W. W. 1953, *Ap. J.*, **117**, 318.
MacRae, D. A.; Harris, D. L.; and Rogerson, J. B. 1952, *A.J.*, **57**, 19.
McCuskey, S. W. 1945, *Ap. J.*, **102**, 32, Table 6, Area 12.
McCuskey, S. W. 1949, *Ap. J.*, **109**, 139.
McCuskey, S. W. 1949, *Ap. J.*, **109**, 414.
McCuskey, S. W. 1951, *Ap. J.*, **113**, 672.
McCuskey, S. W. 1952, *Ap. J.*, **115**, 479.
McCuskey, S. W. 1952, *A.J.*, **57**, 147.
McCuskey, S. W., and Seyfert, C. K. 1947, *Ap. J.*, **106**, 1.
Morgan, W. W.; Keenan, P.; and Kellman, E. 1943, *An Atlas of Stellar Spectra* (Chicago: University of Chicago Press).

Morgan, W. W.; Whitford, A. E.; and Code, A. D. 1953, *Ap. J.*, **118**, 318.
Nassau, J. J., and Albada, G. B. 1947, *Ap. J.*, **106**, 20.
Nassau, J. J., and MacRae, D. A. 1949, *Ap. J.*, **110**, 40.
Nassau, J. J., and MacRae, D. A. 1949, *Ap. J.*, **110**, 45.
Nassau, J. J., and Morgan, W. W. 1951, *Ap. J.*, **113**, 141.
Seydl, O. 1929, *Pub. Prague*, No. 6.
Stebbins, J.; Huffer, C. M.; and Whitford, A. E. 1940, *Ap. J.*, **91**, 20.
Stebbins, J.; Whitford, A. E.; and Johnson, H. L. 1950, *Ap. J.*, **112**, 469.
Van Rhijn, P. J. 1936, *Groningen Pub.*, Vol. **47**.

THE VISCOSITY AND THERMAL CONDUCTIVITY OF A COMPLETELY IONIZED GAS

SYDNEY CHAPMAN
The Observatory, University of Michigan,* and
Geophysical Institute, University of Alaska
Received March 2, 1954

ABSTRACT

The general formulae for the first approximations to the viscosity μ and thermal conductivity λ of a mixed gas are evaluated for a completely ionized gas. The results are expressed in terms of μ and λ for "corresponding" purely ionic or purely electronic neutral gases, composed of equal numbers of positive and negative similar ions, or of positive and negative electrons, of the same temperature and number density (supposing that such particles could continue to exist together without transformation or recombination); the symbols for μ and λ for such gases will be distinguished by the subscripts i and e. Numerical illustrations are given in two cases. For ionized atomic hydrogen, μ is practically the same as μ_i, and μ_e is much smaller; λ is about $\frac{1}{2}\lambda_e$, and λ_i is much smaller. For a gas composed of completely stripped atoms of atomic number 20 and atomic weight 40, the ionic fields of force are strong, their effective diameters are large, and their mean free paths small; the values of μ_i, and (particularly) of λ_i, are much less than those of μ_e and λ_e. The ions reduce μ to about $\mu_e/30$, and λ to about $\lambda_e/50$.

INTRODUCTION

It has been suggested to me by Professor L. H. Aller that astrophysicists would welcome explicit formulae for the viscosity and thermal conductivity of a completely ionized gas; hence this note. It deals only with a gas in a space free from a magnetic field, and the ions are supposed to be all of one kind, each of mass Mm and charge Ne (esu), where m denotes the mass and e the numerical value of the charge of an electron. If n is the number density of the ions, the electrons number Nn per cubic centimeter, the gas being neutral. It is supposed that only binary encounters need be considered; this implies (Chapman 1922) that $kn^{-1/3}T$ is large compared with N^2e^2; this condition is satisfied, for example, if T is 6000° K, and N is 1, provided that n is less than 10^{15}, or if T is 10^7 and N is 30, provided that n is less than 10^{20}.

The necessary general formulae which are here developed approximately for this special type of gas are now most accessible in the book by Cowling and myself (1951), though they were first published in 1916 (Chapman 1916, 1917). Much cross-reference is needed to pass from the general formulae to this special approximate case; page and formula references to that book are given here to assist the reader to follow the procedure adopted.

The symbols μ and λ for the coefficients of viscosity and thermal conduction will here signify the first approximations to these coefficients (according to the Chapman-Enskog theory), as these are what are mainly considered here; these symbols will refer to the actual ionized gas, and the same symbols with subscript i or e will be used for the corresponding (first approximations to the) coefficients for a simple gas composed of the ions alone or the electrons alone—supposing that such gases composed of charges of one sign only could hold together; in fact, the symbols μ_i and λ_i may be interpreted as those for a gas composed of equal numbers of similar ions of *opposite* sign (and likewise for the electronic coefficients μ_e and λ_e), supposing that such ionic (or electronic) gases could continue to exist without recombination.

The repulsive force κ/r^2 between two electrons, between an electron and an ion, or be-

* Visiting professor, under the sponsorship of the U.S. Signal Corps.

tween two ions, distant r apart, is e^2/r^2, $-Ne^2/r^2$, or N^2e^2/r^2, respectively; the change of sign in the second case does not affect the numerical integrals (Chapman 1922) involved in the formulae.

The formulae for μ_e, μ_i, λ_e, and λ_i may be written (p. 172, eq. [1], taking $\nu = 2$):

$$\mu_e = V\sqrt{m}\,, \qquad \mu_i = \frac{V}{N^4}\sqrt{(Mm)}\,,$$

where

$$V = \frac{5}{8A_2(2)}\left(\frac{kT}{\pi}\right)^{1/2}\left(\frac{2kT}{e^2}\right)^2;$$

and

$$\lambda_e = Cm^{-1/2}, \qquad \lambda_i = \frac{C(Mm)^{-1/2}}{N^4},$$

where (p. 39, eq. [2])

$$C = \frac{15kV}{4}.$$

(The symbols V and C are chosen as the initials of viscosity and conductivity.)

When x, given by $4kT(Nn)^{-1/3}/N^2e^2$, is large, $A_2(2)$ is given with adequate accuracy (p. 179) by

$$A_2(2) = 2\left[\ln(1+x^2) - \frac{x^2}{1+x^2}\right],$$

and an associated integral, later required, is similarly given by

$$A_1(2) = \ln(1+x^2).$$

APPROXIMATIONS FOR THE IONIZED GAS

In the present case the mass ratio M is large, namely, WM_0, where W denotes the atomic weight of the ions and M_0 is the value of M for a proton. In the development of the general formulae for μ and λ and of the various terms and factors that appear in them, quantities of order $1/M$ compared with unity will be neglected, though those of order $1/M^{1/2}$ will be retained, as also those of order N/M or more, for consideration when N is of order $M_0^{1/2}$ (that is, 43) or more.

In the general formulae for μ (p. 167, § 9.84, eq. [2]) and λ (p. 166, eq. [2]) the subscript 1 will be taken to refer to the ions and 2 to the electrons; as the gas is neutral, $n_{12} = n_1/n_2 = 1/N$, $n_{21} = N$; the approximations 1 and $1/M$ will be used for the factors M_1 and M_2, which are strictly $M/(M+1)$ and $1/(M+1)$. Similarly, Mm will be adopted as the value of m_0 (strictly $Mm + m$).

The numbers A and B occurring in the formulae are given for the present case by page 172, equations (11); here $\nu = 2$, and x is large, so that $A_2(2)/A_1(2)$ is very close to 2. Hence

$$A = \tfrac{2}{5}, \qquad B = \tfrac{3}{5}.$$

A quantity E, of the same dimensions as viscosity, occurs in the formulae and may be represented to the present degree of approximation as follows (p. 172, eqs. [12.1]; $x_{12} = Ne^2$, $\nu = 2$):

$$E = \tfrac{2}{5}N^2\mu_i(2M)^{1/2}.$$

THE COEFFICIENT OF VISCOSITY FOR THE IONIZED GAS

The formula for μ (p. 167, § 9.84, eq. [2]) can be expressed thus:

$$\frac{\mu}{\mu_i} = \frac{a + bN + cN^2}{a + dN + (cN^2\mu_i/\mu_e)},$$

where, making the indicated approximations,

$$a = 1 + \tfrac{3}{2} MA = \frac{3M}{5}, \qquad c = 1 + \frac{3}{2}\frac{A}{M} = 1,$$

$$b = \frac{3E}{4\mu_i} + \frac{3E}{4\mu_e} + 2 - 3A,$$

so that

$$\frac{bN}{a} = 2^{1/2}\left(\frac{1}{N} + \frac{N^3}{M^{1/2}}\right) + \frac{4N}{3M}.$$

Also

$$d = \frac{3E}{4\mu_e} + \frac{2A\mu_i}{EM_1M_2},$$

so that

$$\frac{dN}{a} = \frac{1/N + 10/3NM^{1/2}}{2^{1/2}}.$$

Hence

$$\frac{\mu}{\mu_i} = \frac{1 + (1/N + N^3/M^{1/2})/2^{1/2} + 4N/3M + 5N^2/3M}{1 + (1/N + 10/3NM^{1/2})/2^{1/2} + 5/3N^2M^{1/2}}.$$

Professor T. G. Cowling, to whom I showed this note in draft, points out that if the term $4N/3M$ in the numerator of the last expression is neglected, as may be permissible, the expression can (owing to the factorizability of the denominator) be put as the sum of two terms, namely,

$$\frac{\mu}{\mu_i} = \frac{1}{1 + 5\sqrt{2}/(3NM^{1/2})} + \frac{N^3M^{-1/2}}{\sqrt{2} + 1/N}.$$

He remarks that the first term here is the ionic contribution to μ/μ_i, and the second term is the electronic contribution; "the terms in the denominators represent the obstruction to the transport of momentum by ions and electrons, due to collisions with other ions and electrons. This form shows incidentally that, as one would expect, the ionic contribution is almost unaffected by collisions with electrons. The advantage of this form is that it can be generalized to apply when several different kinds of ions are present; one merely adds the contributions due to each kind. Each has in its denominator a sum of terms representing the different types of collision undergone by the type of particle making that contribution, so that collisions with neutral atoms as well as with other ions and electrons can be taken into account. The approximations involved in deriving such additive formulae are cruder than when a simple binary mixture of ions and electrons is being considered, but only in extreme cases could the error so introduced be as much as 1 per cent."

VISCOSITY: ILLUSTRATIVE SPECIAL CASES

For completely ionized atomic hydrogen, N is 1, M is M_0, and the result is $\mu = 0.96\mu_i$ (note that in this case $\mu_e = \mu_i/43$). For a gas composed of completely stripped ionized atoms, for which W is $2N$ and M is $2NM_0$,

$$\frac{\mu}{\mu_i} = \frac{1 + 1/2^{1/2}N + N^{5/2}/2M_0^{1/2} + 5N/6M_0}{1 + 1/2^{1/2}n + 5/3N^{3/2}M_0^{1/2} + 5/3N^{5/2}2^{1/2}M_0^{1/2}}.$$

For example, $\mu = 21\mu_i$ if N is 20 (note that in this case $\mu_e = 591\mu_i$).

THE THERMAL CONDUCTIVITY FOR THE IONIZED GAS

The formula for λ (p. 166, eq. [2]) can be expressed thus:

$$\frac{\lambda}{\lambda_e} = \frac{\alpha + \beta/N + \gamma\lambda_i/N^2\lambda_e}{\alpha + \delta/N + \gamma/N^2},$$

where, making the indicated approximations,

$$\alpha = R_2 = 12\frac{\sqrt{2}}{5N^2}, \qquad \beta = \frac{R'_{12}}{\lambda} = \tfrac{16}{25}M^{1/2} + \frac{16}{25N^4},$$

$$\gamma = R_1 = \frac{26N^2}{25}(2M)^{1/2}, \qquad \delta = R_{12} = \tfrac{39}{5} + \tfrac{16}{25}M^{1/2}.$$

Hence

$$\frac{\lambda}{\lambda} = \frac{1 + 15/2N(2M)^{1/2} + 13/4N^3(2M)^{1/2} + 1/N^4M^{1/2}}{1 + 13N/4\sqrt{2} + 15/2N(2M)^{1/2} + 195/16M^{1/2}}.$$

This expression, as Professor Cowling points out (see also Note I of the second edition of our book), can be expressed as the sum of two contributions, ionic and electronic, as in the case of μ/μ_i, namely,

$$\frac{\lambda}{\lambda_e} = \frac{N^{-4}M^{-1/2}}{1 + 15/(2^{3/2}NM^{1/2})} + \frac{1}{1 + 13N/4\sqrt{2}}.$$

Similar remarks apply to the generalization of this formula to an ionized gas containing different kinds of ions, as in the case of μ/μ_i. The expression shows that, as one would expect, the ionic contribution to the conductivity is always small.

CONDUCTIVITY: ILLUSTRATIVE SPECIAL CASES

For completely ionized atomic hydrogen gas, this gives $\lambda = 0.324\lambda_e$ (note that in this case $\lambda_e = 43\lambda_i$). For a gas composed of completely stripped ionized atoms, for which W is $2N$ and M is $2NM_0$ and for which N is 20, it appears that $\lambda = \lambda_e/47$ (and in this case $\lambda_e = 7 \times 10^6\,\lambda_i$).

FURTHER APPROXIMATIONS

The preceding formulae have all related to the first term in the Chapman-Enskog expressions for μ and λ. The general expressions for the next degree of approximation to μ and λ for a mixed gas are still more complicated. Only by specializing these formulae for the completely ionized gas, will it be possible with certainty to determine how much the preceding formulae for μ and λ will be modified in the next approximation. But it seems likely that, according as μ is determined mainly by μ_i or μ_e, and λ by λ_e, the further

approximations to μ and λ will be affected in much the same way as the next approximation affects μ_i or μ_e and λ_e, respectively.

As regards μ_i and μ_e, the next approximation increases the first one in the ratio (p. 173, eq. [2])

$$1 + \tfrac{27}{178} \quad \text{or} \quad 1.15$$

and further approximations seem unlikely to produce an over-all increase of more than 25 per cent over the first.

As regards λ_e, according to page 173, equation (3), the next approximation is greater than the first in the ratio 1.25:1, and later ones may increase this ratio to about $\frac{4}{3}$ or perhaps 1.4.

It does not seem likely that the increases over the first approximations to μ and λ will be nearly so great as for the Lorentz approximations given on page 191, equations (5) and (6), which give only a part of μ and λ.

MAGNETIC FIELDS

In the presence of a magnetic field the preceding formula for λ is applicable to heat conduction parallel to the field, but not transverse to it. The viscous stresses are also modified by the field. The extension of the analysis to those cases may be made along the lines indicated on pages 236–238, but will not be included here.

REFERENCES

Chapman, S. 1916, *Proc. R. Soc. London A*, **93**, 1.
Chapman, S. 1917, *Phil. Trans. R. Soc. London A*, **217**, 115.
Chapman, S. 1922, *M.N.*, **82**, 294.
Chapman, S., and Cowling, T. G. 1951, *Mathematical Theory of Non-uniform Gases* (Cambridge: At the University Press). (2d edition).

THE SOLAR INTERNAL OPACITY AND CONSTITUTION*

I. EPSTEIN AND L. MOTZ
Rutherfurd Observatory, Columbia University
Received February 8, 1954

ABSTRACT

A model solar interior, based on the assumption that the energy is generated by both the proton-proton and the carbon cycles, is calculated with the aid of opacity formulae which include the effects of metals, electrons, and hydrogen. The equilibrium model, self-consistent in the opacity, obtained by an iterative process in a double eigen-value problem, is characterized by $X = 93.1$ per cent, $Y = 6.7$ per cent, and $Z = 0.2$ per cent. The central temperature of this model is 12,850,000°, while the density is 98. A convective core exists to the extent of about 8 per cent of the solar radius. This core includes 4 per cent of the mass and has generated within it 29 per cent of the total energy. The proton-proton reaction is found to provide all the energy generated in this model.

I. INTRODUCTION

Previous calculations (Epstein 1951; Epstein and Motz 1953) on the sun's internal constitution have indicated an abundance of hydrogen far in excess of amounts justifying the neglect of the contribution of hydrogen to the opacity. This source of opacity is due to the free-free transitions of electrons in the field of ionized hydrogen. New opacity tables were derived, the method of calculation being that of Strömgren (1932). With these formulae, which included the effects of the metals and of electron scattering, and with energy-generation laws used in previous calculations, an equilibrium model for the sun was computed.

II. SOLUTION

Under the initial assumption that the relative abundances by weight of hydrogen and the metals are in the ratio 90 : 1, the following formulae were derived for κ_i (the photoelectric ionization opacity, including free-free transitions of hydrogen):

$$\begin{aligned} \log \kappa_i &= 13.209 - 1.683 \log T + \log Z , && \log T \leq 6.04 , \\ \log \kappa_i &= -0.584 + 0.600 \log T + \log Z , && 6.04 < \log T < 6.35 , \\ \log \kappa_i &= 12.779 - 1.504 \log T + \log Z , && \log T \geq 6.35 \end{aligned} \tag{1}$$

Together with the expression for the electron-scattering opacity,

$$\kappa_e = (1.5)\ (0.19)\ (1 + X) , \tag{2}$$

and the energy-generation formulae,

$$\log \epsilon_p = \log \left\{ \frac{3.82}{100} \left(\frac{X}{0.316} \right)^2 \left(\frac{1}{15 \times 10^6} \right)^4 \left(\frac{\mu H}{k} \right) \right\} + \log P + 3 \log T , \tag{3}$$

$$\log \epsilon_c = \log \left\{ 1.0 \times 10^{-143} \left(\frac{\mu H}{k} \right) \left(\frac{XZ}{4} \right) \right\} + \log P + 19 \log T , \tag{4}$$

an equilibrium configuration was sought by the method used in "A Two-Energy Source Solar Model" (Epstein 1951). No such equilibrium model was found, but the best solution obtainable indicated a hydrogen abundance of about 98 per cent. This optimum

* This work was supported in part by a contract with the Office of Naval Research, Nonr-266(19).

model, although not an equilibrium one, was then employed to yield a second approximation to the opacity, which differed considerably and systematically from formulae (1) above. A second series of numerical integrations was then made, using the opacity in the second approximation. It was found that the model was extremely sensitive to the relative abundances of hydrogen and the metals. In all, five sets of integrations of the double eigen-value problem were made, the opacity being altered each time by the results of the previous iteration. A final equilibrium model, self-consistent in the opacity (the opacity derived from the model agreeing with the opacity used to obtain the model to within 0.03 in log $[\kappa_i + \kappa_e]$ at worst) was obtained for $X_0 = 0.931$, $Y_0 = 0.067$, $Z_0 = 0.002$. The details of this equilibrium model are presented in Table 1. The corresponding opacity

TABLE 1

A. SOLUTION FOR THE RADIATIVE ENVELOPE OF THE SUN

log r	log P	log T	log M_r	log L_r	log ρ	U	V	$(n+1)$	log κ_i/κ_e*
10.78	10.75	5.57	33.30	33.58	−3.02	0.00	37.54	4.87	+1.20
10.74	11.92	5.81	33.30	33.58	−2.09	0.00	23.68	4.90	+0.96
10.70	12.74	5.98	33.30	33.58	−1.44	0.03	17.67	4.87	+0.80
10.66	13.37	6.11	33.30	33.58	−0.94	0.07	14.11	4.11	+0.77
10.62	13.88	6.24	33.29	33.58	−0.56	0.13	11.39	3.74	+0.83
10.58	14.29	6.35	33.29	33.58	−0.26	0.20	9.50	3.86	+0.88
10.54	14.65	6.44	33.28	33.58	+0.01	0.29	8.40	4.31	+0.73
10.50	14.97	6.51	33.26	33.58	+0.26	0.40	7.63	4.77	+0.64
10.46	15.26	6.57	33.24	33.58	+0.49	0.54	6.96	4.79	+0.55
10.42	15.52	6.62	33.22	33.58	+0.70	0.70	6.34	4.71	+0.47
10.38	15.77	6.67	33.19	33.58	+0.90	0.88	5.74	4.59	+0.40
10.34	15.98	6.72	33.15	33.58	+1.06	1.08	5.15	4.44	+0.33
10.30	16.18	6.77	33.10	33.58	+1.21	1.29	4.56	4.25	+0.26
10.26	16.35	6.81	33.05	33.57	+1.34	1.50	4.00	4.04	+0.21
10.22	16.50	6.85	32.98	33.57	+1.45	1.70	3.47	3.83	+0.15
10.18	16.63	6.88	32.91	33.56	+1.55	1.89	2.98	3.63	+0.10
10.14	16.74	6.91	32.83	33.54	+1.63	2.07	2.53	3.44	+0.06
10.10	16.83	6.94	32.74	33.52	+1.69	2.22	2.14	3.26	+0.02
10.06	16.91	6.96	32.65	33.48	+1.75	2.36	1.79	3.09	−0.01
10.02	16.97	6.99	32.56	33.44	+1.78	2.47	1.50	2.96	−0.05
9.98	17.03	7.01	32.46	33.39	+1.82	2.57	1.25	2.84	−0.07
9.94	17.07	7.02	32.35	33.33	+1.85	2.65	1.04	2.74	−0.09
9.90	17.11	7.04	32.24	33.27	+1.87	2.71	0.86	2.66	−0.11
9.86	17.14	7.05	32.13	33.19	+1.89	2.77	0.71	2.59	−0.13
9.82	17.17	7.06	32.02	33.11	+1.91	2.82	0.59	2.53	−0.15

* In the column headed "log κ_i/κ_e," κ_e is not the electron scattering itself but 1.5 times this value, provided that the opacity arising from photoelectric ionizations exceeds the electron-scattering opacity. This is true for all log r in this model.

B. VALUES AT CENTER OF CONVECTIVE CORE ATTACHED TO RADIATIVE ENVELOPE AT LOG $r_f = 9.79$

log P_c	log T_c	log ρ	U	V	$(n+1)$
17.30	7.11	1.99	3.00	0.00	2.50

formulae, replacing those of the first approximation and given in equations (1), are

$$\begin{aligned} \log \kappa_i &= 9.231 - 0.995 \log T + \log Z, && \log T \leq 6.03, \\ \log \kappa_i &= -0.588 + 0.438 \log T + \log Z, && 6.03 < \log T < 6.40, \\ \log \kappa_i &= 12.324 - 1.414 \log T + \log Z, && \log T \geq 6.40, \end{aligned} \tag{5}$$

and are derived from Table 2, which gives the guillotine factor as a function of temperature and density, and the relation

$$\kappa_i = 3.90 \times 10^{25} \rho T^{-3.5} (1 + X)\ (1 - X - Y)\ (\bar{l})^{-1}\,. \tag{6}$$

The mass- and luminosity-fits at the interface between the convective core and the radiative envelope in the final model are excellent, and the polytropic index goes smoothly into its proper value of 1.50 at $r_f = 6.15 \times 10^9$ cm, which is 8 per cent of the

TABLE 2

GUILLOTINE FACTORS $\log_{10} i$ FOR THE EQUILIBRIUM MODEL OF THE SUN*

$T \times 10^{-6}$	$\log_e [G(T)/N_e] = \psi/kT$					
	2	3	4	5	6	∞
0.625	0.5820	0.3905	0.1926	−0.0435	−0.0259	−0.4180
0.714	.5881	.4152	.2447	− .1169	− .0340	− .0349
0.833	.6230	.5064	.3215	− .2120	− .1332	− .0547
1.0	.6976	.5481	.4254	− .3150	− .2383	− .1469
2.5	.4838	.2589	.0688	− .0523	− .1262	− .2769
3.0	.5636	.3638	.2181	+ .1381	+ .0861	− .0445
5.0	.6320	.4560	.2812	+ .1310	+ .0272	− .0621
6.0	.7663	.5940	.4800	+ .3960	+ .3492	+ .3150
7.5	.7341	.6140	.4992	+ .4018	+ .3370	+ .2636
9.0	.8056	.7424	.6950	+ .6702	+ .6587	+ .6519
10.0	0.7679	0.6625	0.5540	+0.4346	+0.3835	+0.3185

* Hydrogen: 93.1 per cent; metals: 0.2 per cent, distributed into oxygen (60 per cent) and Russell mixture (40 per cent). Form of table is same as that of M. H. Harrison (1948).

solar radius. The core includes 4 per cent of the solar mass, and 29 per cent of the energy is generated within the core. The high rate of energy production by means of the proton-proton reaction allows less than 1 per cent of the energy to be generated by means of the carbon cycle.

REFERENCES

Epstein, I. 1951, *Ap. J.*, **114**, 438.
Epstein, I., and Motz, L. 1953, *Ap. J.*, **117**, 311.
Harrison, M. 1948, *Ap. J.*, **108**, 310.
Strömgren, B. 1932, *Zs. f. Ap.*, **7**, 118.

THE PROPAGATION OF SHOCK WAVES IN SELF-GRAVITATING GAS SPHERES

ZDENĚK KOPAL
Department of Astronomy, University of Manchester*
Received November 23, 1953

ABSTRACT

The aim of the present paper has been to investigate the existence and properties of progressing waves in self-gravitating gas spheres which arise as a result of a single central explosion. It is shown that if the kinetic energy released by such an explosion is very small in comparison with the gravitational and thermal energy of the gas sphere in its equilibrium (pre-explosion) state, the system of partial differential equations governing a compressible spherical flow can be made to depend on a single variable $\xi = t^{\psi}/r$, where t denotes the time; r, the radial distance; and ψ is a constant which, in the case of flow headed by a shock wave, is related to the exponent α of the equilibrium density distribution $\rho \sim r^{-\alpha}$ by $\psi = 2/\alpha$.

The finiteness and positivity of the equilibrium pressure in front of the shock wave is found to require that $1 < \alpha < 3$; while the finiteness and positivity of the total energy contents inside the shock has restricted the range of possible variation of α to $1.5 < \alpha < 2.5$ in spheres consisting of monatomic gas. The case $\alpha = 2.5$ (corresponding to $\psi = \frac{4}{5}$) is singular for any value of γ and has already been treated in a preceding paper of this series. To each value of α within the limits of the foregoing inequality there corresponds a flow characterized by a definite constant Mach number M. An analysis of the relation between α and M based on extensive numerical integrations reveals, moreover, that, for shocks of great strength, the values of α are very insensitive to M and approach their upper limit asymptotically; while with diminishing M, the constant α decreases until, for approximately $M = 1.6$, $\alpha = 2$, corresponding to $\psi = 1$, i.e., to a shock whose radius increases uniformly for all time. Detailed numerical integrations have been undertaken for seven particular values of M, and a summary of the results is given.

Ultimately, in the appendix to this paper we shall prove that no progressing flow of the "second type" (i.e., one for which $\xi = e^{\psi t}/r$) can arise as the result of a central explosion releasing small fractional amounts of kinetic energy, unless the Mach number of the ensuing flow were infinite.

I. INTRODUCTION

In a previous communication the present writer and his collaborators (Carrus *et al.* 1951*a*, *b*)[1] have investigated the propagation of spherical shock waves in self-gravitating gas spheres and found that the disturbances produced by instantaneous central explosions will propagate outward as waves of the progressing type if the equilibrium density ρ_0 of the respective configuration in its undisturbed state varies as the inverse $\frac{5}{2}$ of the radial distance r. This whole investigation was, however, restricted in one important respect, namely, we enforced the requirement that the total energy (i.e., the sum of the kinetic, thermal, and gravitational energies) interior to the expanding shock be independent of the time. While it is true that an instantaneous explosion will liberate a constant amount of kinetic and thermal energy, the gravitational energy inside a gas sphere characterized by a continuous density distribution will, in general, vary with increasing distance from the center, and, as the shock expands, its amount should vary with the time. The solutions constructed in Paper II corresponded to the special case of an equilibrium density distribution for which the total amount of energy between the instantaneous radius $R(t)$ of the shock and the contact discontinuity $a(t)$ limiting the flow on the inside was represented as remaining constant for a gas flow of the progressing type. Reasons were discussed in Section V of Paper II why solutions of this type may represent a highly idealized approximation to the early phases of the explosion in the central regions of a star.

* The major part of this work was performed at the Massachusetts Institute of Technology in Cambridge, Massachusetts, and was supported by Contract N5ori-O7843 with the Office of Naval Research of the U.S. Navy Department.

[1] These papers will hereafter be referred to as "Paper I" and "Paper II," respectively.

The aim of the present paper will be to approach the hydrodynamical problem of stellar explosions from a somewhat different direction, which can be briefly described as follows. Suppose that, as in Papers I and II, $p_0(r)$, $\rho_0(r)$, and $m_0(r)$ denote the equilibrium pressure, density, and mass interior to r, respectively, and that

$$H = 4\pi \int_0^R \left(\frac{1}{\gamma - 1} \frac{p_0}{\rho_0} - \frac{Gm_0}{r} \right) \rho_0 r^2 dr \tag{1}$$

represents the thermal plus gravitational energy inside a sphere of radius R (with γ denoting, as before, the ratio of specific heats of the gas constituting our sphere and G, the constant of gravitation). Moreover, suppose that $R(t)$ stands for the radius of an expanding shock wave produced by a sufficiently strong central explosion; if so, the quantity $H(R)$ as defined by the foregoing equation will become an implicit function of the time. Let us set out now to seek such solutions of the hydrodynamical equations governing the disturbed field of flow which are of the progressing-wave type and for which the total energy E inside $R(t)$ is, not constant as in Papers I or II, but the same function of the time as $H[R(t)]$.

The foregoing assumption should render the corresponding field of flow relevant to two distinct physical situations. Our solution may then represent the effects of non-instantaneous explosions, implying an energy release increasing with time, or it may represent the limiting case of a flow produced by an arbitrary explosion liberating an amount of energy which—large as it may be in absolute units—remains negligible in comparison with the gravitational and thermal energy stored originally inside a volume of radius R. From the physical point of view, the first alternative is probably of little interest; for its realization would require the fulfilment of very special conditions which the laws of nuclear-energy liberation are unlikely to satisfy. The second alternative appears, however, much more interesting to the astrophysicist; for it is well known (Biermann 1939) that the actual amount of energy liberated by a single nova outburst represents but an insignificant fraction (of the order of 10^{-5}–10^{-4}) of the energy stored inside a star, so that, whatever the actual manner of the energy release may be, the total amount of energy $E[R(t)]$ will remain sensibly the same function of the time as $H[R(t)]$.

The problem which we thus propose to confront will consist of setting up the governing equations and of investigating their solutions for motion which follows if the center of our compressible-gas configuration is disturbed by a radially symmetrical explosion. If this explosion is sufficiently energetic, the expanding field of flow will again be headed by a shock wave whose strength depends on the initial conditions in a manner which we propose to explore. In order to simplify our task, we shall—as in Papers I and II—again limit ourselves to the investigation of solutions of the *progressing type*, i.e., of motions for which the velocity, pressure, and density of the disturbed field of flow can be made to depend on a sole variable $\xi = t^{\psi}/r$, where r denotes the radial distance, t the time, and ψ a suitably chosen constant. The form of the fundamental equations of the problem, together with our foregoing energy requirement, will then specify the value of ψ which will be different for different strengths of the assumed shock front; and if the motion is to be of the progressing type, the equilibrium density of the undisturbed configuration in front of the shock wave is not arbitrary but must fulfil a certain condition depending on ψ. Even so, however, the quantitative form of the corresponding solutions can be studied only by numerical means; for, although the partial differential equations of the general problem reduce to ordinary differential equations for flow of the progressing type, they remain conspicuously nonlinear, and the essential features of the problem are, in fact, governed by the nonlinear terms. Under such circumstances, all known formal methods cease to be of much avail, and numerical integrations again afford the only avenue of approach. In the sections which follow we shall, successively,

set up the equations of the problem, together with their appropriate boundary conditions, and then formulate the restrictions imposed on the behavior of the total energy (and mass) interior to the assumed shock wave. Next the results of the numerical integrations will be given, and their bearing on our physical problem discussed. Ultimately, in the appendix to this paper, we shall prove that the choice of $\xi = t^{\psi}/r$ leads to the *only* family of progressing waves of our problem satisfying the present energy requirement; for should we resort to the progressing waves of the "second type" (discovered in the appendix to Paper II) for which $\xi = e^{\psi t}/r$, the present problem does not admit of any solution headed by a shock wave of finite strength, the Mach numbers of all existing solutions becoming infinite.

II. EQUATIONS OF THE PROBLEM

As in the previous papers, let u, p, and ρ denote the radial velocity, pressure, and density of a compressible fluid at a distance r from the origin and at a time t. If, moreover, m denotes the mass interior to r, G the constant of gravitation, and γ the ratio of specific heats of the fluid (which will hereafter be regarded as constant), the Eulerian hydrodynamical equations governing a spherically symmetrical flow of polytropic gas under the influence of its own gravitation reduce to

$$\frac{\partial u}{\partial t} + u\frac{\partial u}{\partial r} + \frac{1}{\rho}\frac{\partial p}{\partial r} + \frac{Gm}{r^2} = 0\,, \tag{2}$$

$$\frac{\partial m}{\partial r} - 4\pi\rho r^2 = 0\,, \tag{3}$$

$$\frac{\partial \rho}{dt} + u\frac{\partial \rho}{\partial r} + \rho\left(\frac{\partial u}{\partial r} + \frac{2u}{r}\right) = 0\,, \tag{4}$$

$$\frac{\partial}{\partial t}(p\rho^{-\gamma}) + u\frac{\partial}{\partial r}(p\rho^{-\gamma}) = 0\,. \tag{5}$$

The system of partial differential equations (2)–(5) is one of fourth order and second degree, in two independent variables; and in the case of a flow headed by a shock wave, its initial conditions are defined over a moving boundary. In order to normalize the independent variables, we first set

$$r = R_0 x\,, \tag{6}$$

$$t = (2\pi G\rho_c)^{-1/2}\tau\,, \tag{7}$$

where R_0 and ρ_c denote an arbitrary radius and density which may (though not necessarily) be identified with the radius of the undisturbed configuration and with its central density. Moreover, in order to single out, as in Papers I and II, the solutions corresponding to the flow of the progressing type, we set

$$u = (2\pi G\rho_c R_0^2)^{1/2}\frac{x}{\tau}U(\xi)\,, \tag{8}$$

$$p = 2\pi G\rho_c^2 R_0^2\frac{x^2}{\tau^4}P(\xi)\,, \tag{9}$$

$$\rho = \frac{\rho_0}{\tau^2}\Omega(\xi)\,, \tag{10}$$

$$m = 4\pi\rho_c R_0^3\frac{x^3}{\tau^2}\mathfrak{M}(\xi)\,, \tag{11}$$

and introduce the functions $U(\xi)$, $P(\xi)$, $\Omega(\xi)$, and $\mathfrak{M}(\xi)$, depending, by definition, on x and τ only through the combination

$$\xi = \frac{\tau^{\psi}}{x}, \tag{12}$$

where ψ stands for an arbitrary constant. Not all these four functions are, incidentally, independent of one another; for it follows from their definition that

$$\mathfrak{M}(\xi) = \xi^3 \int_{\xi}^{\infty} \frac{\Omega(\xi)}{\xi^4}\, d\xi . \tag{13}$$

When we introduce equations (8)–(11) into equations (2)–(5), this latter fundamental system will assume the form

$$\xi U'(\psi - U) + U(U-1) + \frac{P}{\Omega}\left(2 - \xi \frac{P'}{P}\right) + 2\mathfrak{M} = 0 , \tag{14}$$

$$\xi \mathfrak{M}' - 3\mathfrak{M} + \Omega = 0 , \tag{15}$$

$$(\psi - U)\,\xi P' + [(3\gamma + 2)\,U - 4 - \gamma \xi U']\,P = 0 , \tag{16}$$

$$(\psi - U)\,\xi \Omega' + (3U - 2 - \xi U')\,\Omega = 0 . \tag{17}$$

With regard to the boundary conditions of our problem, we shall assume again, by hypothesis, that the original disturbance has been sufficiently energetic for the flow to be headed by a shock wave propagating outward with a velocity V. If, moreover, the subscripts 0 and 1 refer to the values of the respective quantities immediately in front of and behind the shock wave, the Rankine-Hugoniot conditions assert that

$$u_1 = \frac{2V}{\gamma + 1} - \frac{2\gamma p_0}{(\gamma + 1)\,\rho_0 V}, \tag{18}$$

$$p_1 = \frac{2\rho_0 V^2 - (\gamma - 1)\,p_0}{\gamma + 1}, \tag{19}$$

$$\rho_1 = \frac{(\gamma + 1)\,\rho_0^2 V^2}{(\gamma - 1)\,\rho_0 V^2 + 2\gamma p_0}. \tag{20}$$

In addition, since $u_1 < V$, no mass can possibly overtake the shock, and, in consequence,

$$m_1 = 4\pi \int_0^R \rho r^2 dr = 4\pi \int_0^R \rho_0 r^2 dr , \tag{21}$$

where $R \equiv R(t)$ denotes the radius of the shock front.

In what follows let ξ_1 characterize the position of the shock front of radius $R = (R_0/\xi_1)\tau^{\psi}$. If so, the velocity V of the shock will be given by

$$V = \frac{dR}{dt} = (2\pi G \rho_c R_0^2)^{1/2} \frac{dx}{d\tau} = (2\pi G \rho_c R_0^2)^{1/2}\, \psi \frac{x}{\tau} \tag{22}$$

by equation (12). Moreover, let the pressure p_0 and density ρ_0 in the undisturbed medium in front of the shock wave vary as

$$p_0 = 2\pi G \rho_c^2 R_0^2 \pi(x) , \tag{23}$$

$$\rho_0 = \rho_c \sigma(x) , \tag{24}$$

so that

$$c_0^2 = 2\pi\gamma G\rho_c R_0^2 \frac{\pi(x)}{\sigma(x)} \tag{25}$$

denotes the corresponding local velocity of sound. If so, the Rankine-Hugoniot conditions (18)–(20) permit us to solve for the values of U, P, Ω, and therefore $\mathfrak{M}$, immediately behind the shock; and, doing so, we obtain

$$U(\xi_1) = \frac{2\psi}{\gamma+1}\left(1-\frac{1}{M^2}\right), \tag{26}$$

$$P(\xi_1) = \frac{\tau^4\pi(x)}{x^2(\gamma+1)}\left[2\gamma M-(\gamma-1)\right], \tag{27}$$

$$\Omega(\xi_1) = \frac{(\gamma+1)\tau^2\sigma(x)}{\gamma-1+2/M}, \tag{28}$$

where

$$M^2 = \frac{V^2}{c_0^2} = \frac{\psi^2}{\gamma}\left(\frac{x}{\tau}\right)^2\frac{\sigma(x)}{\pi(x)} \tag{29}$$

denotes the square of the Mach number of the corresponding shock wave. If this wave is to be of the progressing type, the right-hand sides of equations (26)–(28) must be functions of ξ alone; and this will be true, provided that the expressions

$$\left(\frac{x}{\tau}\right)^2\frac{\sigma(x)}{\pi(x)}, \qquad \frac{\tau^4}{x^2}\pi(x), \qquad \tau^2\sigma(x), \tag{30}$$

depend only on ξ.

Now let the density ρ_0 in the undisturbed fluid in front of the shock wave vary, by hypothesis, as some inverse (nonnegative) power a of the distance from the center, so that

$$\sigma(x) = x^{-a}, \tag{31}$$

and, in consequence of the hydrostatic equilibrium prevailing in front of the shock,

$$\pi(x) = \frac{x^{2(1-a)}}{(3-a)(a-1)} + C, \tag{32}$$

where C denotes a constant of integration. If we introduce these equations into equations (26)–(29), we find that *both sides of all three Rankine-Hugoniot conditions (26)–(29) become functions of ξ alone, provided that*

$$a\psi = 2 \qquad \text{and} \qquad C = 0, \tag{32a}$$

when

$$U(\xi_1) = \frac{4}{a(\gamma+1)}\left(1-\frac{1}{M^2}\right), \tag{33}$$

$$P(\xi_1) = \frac{4\xi_1^a}{a^2\gamma M^2}\left(\frac{2\gamma M^2}{\gamma+1}-\frac{\gamma-1}{\gamma+1}\right), \tag{34}$$

$$\Omega(\xi_1) = \frac{(\gamma+1)\xi_1^a}{\gamma-1+2M^{-2}}; \tag{35}$$

while, by equation (21),

$$\mathfrak{M}(\xi_1) = \frac{\xi_1^a}{3-a}, \tag{36}$$

where the Mach number

$$M^2 = \frac{4\,(3-\alpha)\,(\alpha-1)}{\alpha^2\gamma\,\xi_1^{\alpha}}. \tag{37}$$

Now the positivity and finiteness of the equilibrium pressure $\pi(x)$, as defined by equation (32), obviously requires that the constant α as introduced by equation (31) should obey the inequality[2]

$$1 < \alpha < 3\,; \tag{38}$$

and any value of α so constrained will also render M real (provided, of course, that ξ_1 will later also prove to be real and positive).

It should also be noted that a polytropic equation of state $\pi \sim \sigma^{1+1/n}$ with $n = \alpha/(\alpha-2)$, obtained by elimination of x between equations (31) and (32) for $C = 0$, does *not* render n the customary polytropic index or σ a solution of Emden's equation; for we made no attempt to render the equilibrium configuration a self-gravitating one. Its existence implies merely that the specific heat of gas in front of the shock remains constant, though *not* necessarily zero. Therefore, it does not follow that we must have $1 + 1/n = \gamma$ in the equilibrium state. The use of equation (5) implies—as in Papers I and II—that the gas motion initiated by the shock wave is regarded to be adiabatic; but we have no need to assume that $\pi \sim \sigma^{\gamma}$ in front of the shock.

III. SOLUTION OF THE EQUATIONS

Equations (14)–(17), subject to the boundary conditions (33)–(36), are much too involved to admit of an analytical solution, so that, in order to investigate the properties of an expanding gas flow governed by such equations, recourse must be had to numerical integrations. Before embarking upon them, we may observe that, as they stand, the boundary conditions (33)–(36) (and, consequently, all solutions which are to be based upon them) involve three independent parameters: α (or ψ), γ, and ξ_1. The reader should notice, however, that, unlike Papers I and II, we are no longer allowed to set $\xi_1 = 1$ arbitrarily at the shock wave—since all our units have already been normalized—but must treat it as an independent quantity. The ratio of specific heats depends, of course, on the composition of the gas constituting our configuration; and, once a fixed value of γ has been adopted, α (or M) and ξ_1 remain the only arbitrary constants specifying a two-parameter family of solutions. To each pair of ξ_1 and α there will correspond a gas flow headed by a shock wave of strength characterized by the Mach number M as given by equation (38).

Of all such existing solutions, we wish now to single out those satisfying the requirement set forth in the introduction, namely, that the amount of energy within a sphere of any given radius be sensibly the same before and after the explosion. Moreover, since the shock front always travels faster than any material which received its impulse from its passage (and therefore no particle can escape outside it), the total mass within it must remain equal to that contained within the same volume in the equilibrium (pre-explosion) stage. Now the mass m interior to a radius R in this latter stage is evidently equal to

$$m = 4\pi \int_0^R \rho_0 r^2 dr = \frac{4\pi\rho_c R_0^3}{3-\alpha}\, x^{3-\alpha}, \tag{39}$$

[2] The laws of density (31) and pressure (32) then lead, of course, to infinite density and pressure at the center of our configuration. These singularities cause, however, no real difficulty; for we can imagine—as in Paper II—that eq. (31) holds good only to a small distance from the center within which the density remains finite. This avoids the physical difficulty, without appreciably altering either the mass within any significant radius or the values of the gravity and pressure.

while, after the explosion,

$$m_1 = 4\pi \int_0^R \rho r^2 dr = 4\pi \rho_c R_0^3 \tau^{3\psi-2} \int_{\xi_1}^{\infty} \frac{\Omega d\xi}{\xi^4}. \tag{40}$$

Now by equation (12) we may, however, write

$$x^{3-\alpha} = \xi^{\alpha-3} \tau^{(3-\alpha)\psi}; \tag{41}$$

and, if equation (34) holds good, $(3-\alpha)\psi = 3\psi - 2$, which makes both m and m_1 vary proportionally to the same power of τ. If, moreover, they are to remain equal for any value of τ, the coefficient of proportionality in equations (39) and (40) must also be equal, and we should have

$$\frac{\xi_1^{\alpha-3}}{3-\alpha} = \int_{\xi_1}^{\xi_2} \frac{\Omega d\xi}{\xi^4}, \tag{42}$$

which is found to be fulfilled for a *finite* value of the upper limit ξ_2 as defined by the foregoing equation. The existence of such a limit implies—as in Paper II—that our field of flow will inclose an empty sphere of radius $x_2 = \tau^{\psi}/\xi_2$, which represents the distance to which a particle originally at the center has traveled in the time τ.

The restriction on the energy proposed earlier in this section can be formulated as follows. The total energy E inside a shock wave of radius R is known to be given by

$$E = 4\pi \int_0^R \left(\tfrac{1}{2}\rho u^2 + \frac{p}{\gamma-1} - G\frac{m\rho}{r} \right) r^2 dr; \tag{43}$$

and if we introduce the variables defined by equations (8)–(11), we may rewrite this as

$$E = 8\pi^2 G \rho_c^2 R_0^5 \tau^{5\psi-4} F(\xi_2), \tag{44}$$

where

$$F(\xi) = \int_{\xi_1}^{\xi} \left[\frac{1}{2}\frac{\Omega U^2}{\xi^2} + \frac{P}{(\gamma-1)\xi^2} - 2\xi\Omega \int_{\xi_1}^{\xi} \frac{\Omega}{\xi^4} d\xi \right] \frac{d\xi}{\xi^4} \tag{45}$$

specifies the amount of energy contained within a spherical shell of radii ξ_1 and ξ_2. On the other hand, the total energy (thermal and gravitational) within the same volume in the equilibrium (pre-explosion) state was already given by equation (1), and in terms of our normalized variables it becomes equal to

$$H = 8\pi^2 G \rho_c^2 R_0^5 \int_0^{x_1} \left(\frac{\pi}{\gamma-1} - \frac{2\sigma}{x} \int_0^x \sigma x^2 dx \right) x^2 dx, \tag{46}$$

which, for $\sigma(x)$ and $\pi(x)$ of the form (31) and (32), can be readily integrated to yield

$$H = 8\pi^2 G \rho_c^2 R_0^5 \frac{[(2\alpha-1) - 2(\gamma-1)\alpha] x_1^{5-2\alpha}}{(\gamma-1)(3-\alpha)(\alpha-1)(5-2\alpha)}, \tag{47}$$

the positivity of which requires that

$$\frac{1}{2(2-\gamma)} < \alpha < \frac{5}{2}. \tag{48}$$

By equation (12) we may, in turn, write

$$x_1^{5-2\alpha} = \xi_1^{2\alpha-5} \tau^{(5-2\alpha)\psi} \tag{49}$$

and if equation (34) holds good,

$$(5-2\alpha)\psi = 5\psi - 4\,, \tag{50}$$

which makes both E and H vary as the same power of τ. If, moreover, E and H are to be equal at all times, it follows that the coefficients of τ in each must also be equal, i.e., that

$$\frac{2\alpha - 1 - 2(\gamma-1)\alpha}{(\gamma-1)(5-2\alpha)(3-\alpha)(\alpha-1)}\,\xi_1^{2\alpha-5} = F(\xi_2)\,. \tag{51}$$

The foregoing equation (51) represents an additional relation between ξ_1 and α which our solution must satisfy if the flow governed by it is to be of the desired type; and its existence reduces our former two-parameter family of solutions to a one-parameter one. To every value of M there will, in general, correspond a single characteristic value of α (and ξ_1) which satisfies equation (37). As we have seen, the positivity and finiteness of the equilibrium pressure in front of the shock wave have restricted such possible characteristic α's to lie between 1 and 3. The positivity and finiteness of the total energy inside the shock, furthermore, narrowed this range to $1.5 < \alpha < 2.5$ for γ corresponding to a monatomic gas. The case $\alpha = 2.5$ (corresponding to $\psi = \frac{4}{5}$) is singular for any value of γ and has already been treated in Paper II. We saw that, in this case, progressing supersonic flow can be constructed for *any* (constant) value of the Mach number, several examples of which were investigated in detail.

Numerical integrations of equations (14)–(17),[3] containing the clue to the solution of our problem, may now be undertaken in the following manner. We shall assume (throughout this work) that our configuration consists of monatomic gas (i.e., that $\gamma = \frac{5}{3}$), and in each case begin by adopting a fixed value of M. Let us next select a trial value of α, which, by means of equation (37), leads to a certain value of ξ_1. Now we are ready to embark on actual integration of equations (14)–(17), starting from the initial conditions (33)–(36) which can be expressed in terms of the adopted trio of M, α, and ξ_1. The integration may then be continued until, for a certain value of $\xi = \xi_2$, equation (42) is satisfied. When this happens, $\Omega(\xi_2)$ as well as the logarithmic derivative of $P(\xi)$ becomes infinite, which means that we have arrived, as in Paper II, at a contact discontinuity inclosing an empty sphere which has been effectively evacuated by the explosion. The integration can obviously be continued no longer; and therefore we turn to equation (51) to find out whether or not the solution just found also meets our energy equation. If not, the solution must be repeated—starting from a different value of α—until condition (51) is verified.

The results of such integrations which have passed the test of equation (51) for seven distinct Mach numbers ranging from $M^2 = 3$ to $M^2 = 500$ are summarized in Table 1, whose individual columns indicate, successively, the M^2 of the Mach number; the corresponding value of α; ξ_1 as evaluated from equation (37); the value of ξ_2 specifying the location of the contact discontinuity; $\mathfrak{M}(\xi_1)$ and $F(\xi_2)$ according to equations (36) and (51), respectively; the jump in pressure p_1/p_0, density ρ_1/ρ_0, and temperature T_1/T_0 across the corresponding shock, as given by the equations

$$\frac{p_1}{p_0} = \frac{2\gamma M^2 + 1 - \gamma}{\gamma + 1}\,, \tag{52}$$

$$\frac{\rho_1}{\rho_0} = \frac{\gamma + 1}{\gamma - 1 + 2M^{-2}}\,, \tag{53}$$

[3] In order to perform the actual integration, we find it again advantageous—as in Paper II—to eliminate $\mathfrak{M}$ between equations (14) and (15) by differentiation, which results in a second-order equation for $U(\xi)$, and to solve the latter equation from the initial value of $U'(\xi_1)$ obtained from eq. (14) by taking account of eq. (37).

$$\frac{T_1}{T_0}=\frac{(2\gamma M^2+1-\gamma)(2M^{-2}+\gamma-1)}{(\gamma+1)^2}; \tag{54}$$

while the last two columns give the ratios of u_1/V and the adiabatic constant $K = p\rho^{-\gamma}$ on either side of the shock wave, as given by

$$\frac{u_1}{V}=\frac{2}{\gamma+1}\left(1-\frac{1}{M^2}\right) \tag{55}$$

and

$$\frac{K_1}{K_0}=\frac{1-\gamma+2\gamma M^2}{(\gamma+1)^{\gamma+1}(\gamma-1+2M^{-2})^{-\gamma}}, \tag{56}$$

TABLE 1

THE RESULTS OF INTEGRATION

M^2	a	ξ_1	ξ_2	$\mathfrak{M}(\xi_1)$	$F(\xi_2)$	p_1/p_0	ρ_1/ρ_0	T_1/T_0	u_1/V	K_1/K_0
3...	2.118	0.4402	0.7177	0.19938	1.53556	3.50	2.000	1.75	0.5000	1.102
10...	2.429	.2461	.4053	.05813	9.501	12.25	3.077	3.98	.6750	1.882
20...	2.47	.1842	.3048	.02891	22.97	24.75	3.479	7.11	.7125	3.099
50...	2.489	.1271	.2133	.01154	64.11	62.25	3.773	16.50	.7350	6.810
100...	2.4949	.09629	.1634	.005764	132.3	124.75	3.884	32.13	.7425	13.00
200...	2.4975	.07297	.1250	.002881	268.6	249.75	3.942	63.36	.7463	25.37
500...	2.499	0.05059	0.08739	0.001152	669.1	624.75	3.976	157.13	0.7485	62.61

respectively. As is well known, the corresponding change of the entropy s across the shock wave can then be found from the equation

$$s(\xi_1)-s_0=\frac{\mathfrak{R}}{\gamma-1}\log\frac{K_1}{K_0}, \tag{57}$$

where $\mathfrak{R}$ denotes the universal gas constant.

IV. DISCUSSION OF THE RESULTS

The main outcome of the present investigation is the data collected in Table 1. In order to view them in proper perspective, however, let us recall once more the salient physical premises on which the present work was based. This paper represents a continuation of our earlier investigation of the propagation of shock waves in self-gravitating gas spheres, which differs from Papers I and II in the conditions imposed upon the behavior of the total energy of our flow. Whereas, by enforcing in our earlier work a time independence of the total energy inside an expanding shock, we have not only rendered the initial explosion instantaneous, but we have, in effect, considered the amount of energy released by such an explosion to be so large that the thermal and gravitational energy stored inside our configuration was negligible in comparison. As we have seen, however, such an assumption proved compatible with the existence of a progressing-wave solution headed by a spherical shock of finite strength, provided that the equilibrium density in front of the flow fell off as the inverse $\frac{5}{2}$ of the radial distance.

In the present paper we have adopted a diametrally opposite approach: namely, we have allowed the initial internal energy of our configuration to be so large in comparison with that released by the explosion (whether or not the latter is instantaneous becomes now clearly irrelevant) that the total amount of energy remains essentially unaffected by the explosion. Such an assumption also permits us to construct solutions of our problem in the form of expanding spherical shock waves; and as in Paper II, such flows are

limited, on the inside, by a contact discontinuity inclosing a volume effectively devoid of matter. The requisite finite pressure inside such a volume can be maintained only if we regard the "bubble" produced by the original explosion as excessively hot. The events following an explosion of thermonuclear origin might approximate the physical situation which we have in mind.

There is but little room for doubt that all cases of astrophysical interest should be intermediate between the two extremes which we have thus considered—and probably much closer to the situation envisaged in this paper. Unlike the assumption of the constancy of total energy (which was at the basis of our previous work in Papers I and II), our present allowance for the energy variation proves also to be less restrictive in one respect, namely, it admits of not only one but a whole family of equilibrium models in which a disturbance of requisite strength may propagate outward in the form of a progressive flow headed by a shock. In more specific terms, the existence of such a flow turns out to be consistent with *any* value of the constant α, specifying a one-parameter family of equilibrium configurations, provided only that it obeys the inequality (48). On the other hand, while the singular value $\alpha = 2.5$ (corresponding to $\psi = \frac{4}{5}$), which was at the basis of our work in Paper II, was found consistent with a progressing supersonic flow characterized by *any* Mach number, in the present investigation each value of α within the limits of (48) is associated with only *one* specific value of M.

Numerical details of seven distinct cases of such a flow, corresponding to seven assumed round values of M^2, are given in Table 1. An analysis of the relation between M and α based on these results reveals that while, for shocks of great strength, the values of α are very insensitive to any change in M and approach their upper limit of 2.5 in an asymptotic manner, with diminishing M the constant α decreases until, for approximately $M = 1.6$, α becomes equal to 2, corresponding to $\psi = 1$, i.e., to a shock whose radius increases uniformly for all time.[4] It is the first time in our investigations that we have thus succeeded in constructing the case of a *uniform* propagation of a (relatively weak) shock which is of the nature of a progressing wave. Any such case is, however, astrophysically important because of the fact that the radial-velocity observations of most novae in the course of their outbursts indicate velocities of expansion which—different as they may be from star to star—remain more or less constant within periods of the order of several days. It is interesting, therefore, to note that the progressing-wave solutions of our fundamental system of equations (2)–(5) can actually match the observations in this respect, even though for only a rather limited range of (constant) Mach numbers indicative of weak shocks.

APPENDIX

In the appendix to Paper II we proved that, apart from equation (12), there exists one (and only one) other functional relationship between x and τ which, introduced in equations (2)–(5), would lead to a spherically symmetrical flow of the progressing type, namely,

$$\xi = x\, e^{\psi\tau}\,, \tag{58}$$

where ψ denotes an arbitrary constant. The aim of the present appendix will be to explore the particular form which our fundamental equations (2)–(5) will assume in this case and to prove that a progressing flow governed by such equations cannot be headed by a shock wave of *finite* strength, propagating through a gas sphere initially in hydrostatic equilibrium,[5] the only admissible solutions being characterized by infinite Mach numbers.

[4] Equations (31) and (32) disclose that, for $\alpha = 2$, the medium in front of the shock will become isothermal.

[5] This statement holds true, moreover, regardless of whether our gas sphere is a self-gravitating one or whether its gravitational potential arises from a central point-mass.

In order to do so, let us set

$$u = (2\pi G\rho_c R_0^2)^{1/2} x\, U(\xi)\,, \tag{59}$$

$$p = (2\pi G\rho_c^2 R_0^2)\, xP(\xi)\,, \tag{60}$$

$$\rho = \rho_c \Omega(\xi)\,, \tag{61}$$

$$m = (4\pi\rho_c R_0^3)\, x^3 \mathfrak{M}(\xi)\,, \tag{62}$$

which, on insertion in equations (2)–(5), define the functions $U(\xi)$, $P(\xi)$, $\Omega(\xi)$, and $\mathfrak{M}(\xi)$ as solutions of the following simultaneous system:

$$\xi U'(\psi + U) + U^2 + \frac{P}{\Omega}\left(2 + \xi\frac{P'}{P}\right) + 2\mathfrak{M} = 0\,, \tag{63}$$

$$\xi\mathfrak{M}' + 3\mathfrak{M} = \Omega\,, \tag{64}$$

$$\xi P'(\psi + U) + [\gamma\xi U' + (3\gamma + 2)\, U]\, P = 0\,, \tag{65}$$

$$\xi\Omega'(\psi + U) + (3U + \xi U')\,\Omega = 0\,, \tag{66}$$

of the ordinary differential equations containing ξ as the sole independent variable.

With regard to the boundary conditions of our problem, we shall assume again that the initial disturbance has been sufficiently strong for the flow caused by it to be headed by a shock wave propagating with the velocity

$$V = \frac{dr}{dt} = -(2\pi G\rho_c R_0^2)^{1/2}(\psi x)\,, \tag{67}$$

where a positive value of ψ clearly implies an inward-going shock, and $\psi < 0$ an outward-going one. Suppose, moreover, that, as in Section II, the undisturbed density ρ_0 outside the shock varies as

$$\rho_0 = \rho_c x^{-\alpha}\,, \tag{68}$$

where α denotes a (positive) constant. In consequence of the hydrostatic equilibrium prevailing in regions undisturbed by the explosion, the initial (undisturbed) pressure p_0 should vary as

$$p_0 = \frac{2\pi G\rho_c^2 R_0^2}{(3-\alpha)(\alpha-1)}\,[x^{2(1-\alpha)} - C]\,, \tag{69}$$

where C is an integration constant, and the value of α introduced through equation (68) must obey the inequality $3 > \alpha > 1$ in order to render the pressure positive.

Consider, then, the first one of the Rankine-Hugoniot conditions as represented by equation (18): on insertion of equations (67), (68), and (69), equation (18) will assume the form

$$xU(\xi_1) = -\frac{2\psi x}{\gamma+1} + \frac{2\gamma x^{\alpha-1}(x^{2-2\alpha} - C)}{\psi(\gamma+1)(3-\alpha)(\alpha-1)}\,, \tag{70}$$

which will cease to depend on x only if $C = 0$ and $\alpha = 0$. This latter condition is, however, at variance with the inequality (38), and would evidently cause the pressure p_0, as defined by equation (69), to be negative!

This dilemma can be escaped only if we assume our shock to be so strong that the equilibrium pressure p_0 in equation (18) can be ignored in comparison with the pressure p_0 prevailing immediately behind the compression wave. If so, the whole expression (69) becomes immaterial, and the value of α is no longer constrained by inequality (38). Moreover, the Mach number $M \to \infty$, and all three Rankine-Hugoniot conditions (18)–(20) do become independent of x, provided that $\alpha = 0$, i.e., if

$$\rho_0(x) = \rho_c = \text{Constant}\,; \tag{71}$$

for then, immediately behind the shock wave ($\xi = \xi_1$),

$$U(\xi_1) = -\frac{2\psi}{\gamma+1}, \tag{72}$$

$$P(\xi_1) = \frac{2\psi^2}{\gamma+1}, \tag{73}$$

$$\Omega(\xi_1) = \frac{\gamma+1}{\gamma-1}, \tag{74}$$

without imposing any restriction on ψ; and these conditions, together with equation (36), will single out the particular solutions of equations (2)–(5) in which we are interested.

The total mass inside a sphere of radius r in the equilibrium state was clearly given by

$$m = \tfrac{4}{3}\pi\rho_0 r^3 = \tfrac{4}{3}\pi\rho_c (R_0 \xi e^{-\psi\tau})^3; \tag{75}$$

while, after the explosion, the mass inside a shock wave of equal radius will be

$$m_1 = 4\pi\rho_c (R_0 e^{-\psi\tau})^3 \int_{\xi_2}^{\xi_1} \Omega(\xi)\, \xi^2 d\xi. \tag{76}$$

Since no mass particle can escape the shock, the foregoing expressions for m and m_1 must evidently be equal, and their equality imposes a condition—analogous to equation (42)—requiring that

$$\int_{\xi_2}^{\xi_1} \Omega(\xi)\, \xi^2 d\xi = \tfrac{1}{3}\xi_1^3. \tag{77}$$

On the other hand, the total energy inside our equilibrium gas sphere of negligible pressure will consist of its potential energy only and be given by

$$H = -4\pi G \int_0^r m\rho r\, dr = -\tfrac{16}{15} G (\pi\rho_c)^2 (R_0 \xi e^{-\psi\tau})^5; \tag{78}$$

while following the explosion, we have, inside the same volume,

$$E = 8G(\pi\rho_c)^2 (R_0 e^{-\psi\tau})^5 \int_{\xi_2}^{\xi_1} \left(\frac{\Omega U^2}{2} + \frac{P}{\gamma-1} - \frac{2\Omega}{\xi^3} \int_{\xi}^{\xi_1} \Omega \xi^2 d\xi \right) \xi^4 d\xi. \tag{79}$$

The requisite equality of H and E then imposes a second condition—analogous to equation (51)—of the form

$$\int_{\xi_2}^{\xi_1} \left(\frac{\Omega U^2}{2} + \frac{P}{\gamma-1} - 2\,\frac{\Omega}{\xi^3} \int_{\xi}^{\xi_1} \Omega \xi^2 d\xi \right) \xi^4 d\xi = -\tfrac{2}{15}\xi_1^5. \tag{80}$$

In order to obtain these results, we had to commit ourselves regarding the form of ρ_0 and p_0 (leading to $M = \infty$); but the constants ξ_1, ξ_2, and ψ have so far remained arbitrary. Whether or not a flow envisaged in the preceding paragraphs can actually exist depends on whether or not solutions of equations (63)–(66) can be found, by a suitable choice of ξ_1 and ψ, which depart from the initial conditions (72)–(74) and fulfil both equations (77) and (80) for one and the same value $\xi = \xi_2$. Numerical integrations which have been carried out so far for $\gamma = \frac{5}{3}$ appear to indicate that such solutions do indeed exist for a discrete spectrum of negative values of ψ; but their numerical values have not yet been isolated with sufficient accuracy to warrant publication.

In conclusion of this appendix we wish to point out that the foregoing problem does admit of at least one *closed* solution of the following form. A glance at equation (77) reveals that our present mass condition will be clearly satisfied by

$$\Omega(\xi) = 1 , \tag{81}$$

which, in turn, can be reconciled with equation (74), provided that

$$\gamma = \infty . \tag{82}$$

Now if, consistent with equation (81), Ω is to be independent of ξ, it follows from equation (66) that

$$\xi U' + 3U = 0 , \tag{83}$$

which can be integrated to yield

$$U(\xi) = k\xi^{-3} , \tag{84}$$

k being a constant. This latter equation can, however, be reconciled with equations (72) and (82) only if $k = 0$, thus rendering

$$U(\xi) = 0 . \tag{85}$$

If so, however, it follows at once from equation (65) that

$$\xi P'(\xi) = 0 , \tag{86}$$

implying that $P(\xi) =$ Constant, which, in the light of equations (73) and (82), must again be equal to zero[6]—so that the only admissible solution of equation (86) becomes

$$P(\xi) = 0 . \tag{87}$$

Finally, the reader can verify by substitution that a solution of the form $\Omega(\xi) = 1$, $P(\xi) = U(\xi) = 0$, also satisfies the energy condition (80), provided that $\xi_2 = 0$. Unfortunately, however, this whole solution corresponds physically to an incipient shock in incompressible matter ($\gamma = \infty$), and, as such, it appears, therefore, of little or no astrophysical interest.

In conclusion, the writer wishes to record his indebtedness to Mr. Pierre A. Carrus for effective assistance in the course of this investigation. The numerical integrations underlying the results of Table 1 were carried out at the Massachusetts Institute of Technology in the years 1951–1952 and were supported by Contract N5ori-0743 with the Office of Naval Research of the U.S. Navy Department.

REFERENCES

Biermann, L. 1939, *Zs. f. Ap.*, **18**, 344–361.
Carrus, P. A.; Fox, P. A.; Haas, F.; and Kopal, Z. 1951*a*, *Ap. J.*, **113**, 193–209.
Carrus, P. A.; Fox, P. A.; Haas, F.; and Kopal, Z. 1951*b*, *Ap. J.*, **113**, 496–518.

[6] This is, however, not necessarily true of the limiting value of the product of γP, depending on the temperature behind the shock, which, in the light of assumptions made so far, remains wholly arbitrary.

ON THE ELONGATION OF A FLUID SPHERE IN A UNIFORM EXTERNAL MAGNETIC FIELD*

GURO GJELLESTAD†
Yerkes Observatory, University of Chicago
Received February 16, 1954

ABSTRACT

It is shown that a nonmagnetic homogeneous incompressible fluid sphere of infinite electrical conductivity in a uniform external magnetic field will tend to become a prolate spheroid in the direction of the given field. It is further shown that in a magnetic field of the order of 7×10^{-6} gauss in the spiral arm, even the largest clouds ($R \sim 50$ psc) may be appreciably elongated, while smaller clouds will be squeezed into long, thin, rodlike shapes.

Chandrasekhar and Fermi (1953*b*) have shown that a fluid sphere with a uniform internal magnetic field and an external dipole field is unstable and tends to become oblate spheroidal. Later the present author studied an oblate fluid spheroid (Gjellestad 1954) with magnetic fields of the same characteristics as Chandrasekhar and Fermi's and found that a unique series of oblate spheroids stable to the fundamental P_2-deformation (making the spheroids more oblate) could be established, depending upon the five physical parameters of the problem, namely, the strength of the given magnetic field, the mass, the density, the eccentricity, and the major half-axis of the spheroid. It was further shown that under certain conditions clouds in the spiral arms would be squeezed into highly oblate shapes ("magnetic pancakes").

In this paper we shall study a problem which is, in a sense, the reverse of those mentioned above, namely, the gravitational stability of a fluid sphere of infinite electrical conductivity in an external magnetic field, no *initial internal field being present in the sphere*. The method used is essentially the same as that used in the two papers referred to above, namely, to make a small deformation of the body and calculate the change in the total energy due to this deformation. The change in the total energy consists of two terms, one representing the change in the gravitational potential energy, and the other the change in the magnetic energy. It will be shown that the change in the magnetic energy is proportional to a small quantity ϵ, while the change in the gravitational energy is proportional to the square of this quantity. The signs of the two energy terms are such that the body will tend to become a *prolate* spheroid in the direction of the given field.

I. FORMULATION OF THE PROBLEM

Assume a uniform and constant magnetic field of infinite extension in empty space. An incompressible homogeneous fluid nonmagnetic sphere with infinite electrical conductivity is assumed to be at rest in this magnetic field. Since the sphere had initially no internal magnetic field and the conductivity is infinite, the field cannot penetrate into the sphere. The presence of the sphere requires an additional field to satisfy the boundary condition that the normal component of the magnetic field is continuous on the sphere. A dipole field with its axis opposite to the uniform field and of the same absolute magnitude at the poles satisfies this requirement. To this dipole field corresponds a uniform field in the space occupied by the sphere, which will exactly cancel the original field.

* The research reported in this paper has been supported in part by the Geophysics Research Directorate of the Air Force Cambridge Research Center, Air Research and Development Command, under Contract AF 19(604)-299 with the University of Chicago.

† Research and tutorial fellow of University of Oslo (Institute of Theoretical Astrophysics, Blindern-Oslo, Norway).

If the components in the radial and transverse direction of the magnetic field, ${}^0\boldsymbol{H}$, are given by ($\mu = \cos\theta$, where θ is the polar angle)

$$ {}^0H_r = H\left[1-\left(\frac{R}{r}\right)^3\right]\mu \quad \text{and} \quad {}^0H_\theta = -H\left[1+\frac{1}{2}\left(\frac{R}{r}\right)^3\right](1-\mu^2)^{1/2} \quad (r \geqslant R)\,, \tag{1} $$

the magnetic pressure, p_m, will be

$$ p_m = \frac{|{}^0\boldsymbol{H}|^2}{8\pi} = \frac{H^2}{8\pi}\left\{\left[1-\left(\frac{R}{r}\right)^3\right]^2\mu^2 + \left[1+\frac{1}{2}\left(\frac{R}{r}\right)^3\right]^2(1-\mu^2)\right\}. \tag{2} $$

At the surface of the sphere this reduces to

$$ [p_m]_{\text{surface}} = \frac{9}{4}\frac{H^2}{8\pi}(1-\mu^2) \qquad (r=R)\,, \tag{3} $$

showing that the pressure vanishes at the poles, while it has its maximum value, $9H^2/(32\pi)$, at the equator. The corresponding expressions for the external and internal pressures, $p_m^{(e)}$ and $p_m^{(i)}$, respectively, in the problem studied by Chandrasekhar and Fermi (1953*b*) are easily found to be (cf. their eqs. [123] and [124]):

$$ [p_m^{(e)}]_{\text{surface}} = \frac{H^2}{32\pi}(3\mu^2+1) \qquad \text{and} \qquad [p_m^{(i)}]_{\text{surface}} = \frac{H^2}{8\pi}. \tag{4} $$

The difference in the external and internal pressure is thus, in their case,

$$ [p_m^{(e)}]_{\text{surface}} - [p_m^{(i)}]_{\text{surface}} = -\frac{3H^2}{32\pi}(1-\mu^2)\,. \tag{5} $$

This difference has its minimum value at the equator and is zero at the poles. Comparing equations (3) and (4), we should expect that the effect of the magnetic field in the problem to be studied here must be the opposite of that in the Chandrasekhar-Fermi case, namely, to make the sphere *prolate*. We shall now proceed to show this in a more rigorous way, following the method developed by Chandrasekhar and Fermi (1953*b*).

We shall perform a small quasi-static deformation of the sphere, changing its form from one given by the equation

$$ r = R \tag{6} $$

to one given by

$$ r = R + \epsilon P_n(\mu) \qquad (n>1)\,, \tag{7} $$

where ϵ is a small constant ($|\epsilon|/R \ll 1$), R is the radius of the sphere, and $P_n(\mu)$ is a Legendre function of the first kind and of order n. With the assumptions made above, we may treat the problem as axially symmetrical. Spherical polar co-ordinates (r, θ, φ) will be used, the z-axis being the polar axis of the co-ordinate system and the origo at the center of the sphere. The given uniform field will be taken as the direction of the z-axis.

II. THE MAGNETIC FIELD

The internal magnetic field is at any time zero, while the following requirements must be satisfied by the external magnetic field, $\boldsymbol{H}$,

$$ \operatorname{div}\boldsymbol{H} = 0 \qquad \text{and} \qquad \operatorname{curl}\boldsymbol{H} = 0 \qquad [r \geqslant R + \epsilon P_n(\mu)]\,. \tag{8} $$

These equations must be valid at any time. When $r \to \infty$, the field must be uniform, that is,

$$ H_r \to H\mu \qquad \text{and} \qquad H_\theta \to -H(1-\mu^2)^{1/2} \qquad (r\to\infty)\,. \tag{9} $$

When $\epsilon \to 0$, the external field is given by equations (1). A fourth requirement to be satisfied by the external field is that the normal component of the field to the deformed surface of the body must vanish to the first order in ϵ.

The general solution, satisfying equations (8) and the requirements when $r \to \infty$ and $\epsilon \to 0$, can be given the following form, correct to the first order in ϵ,

$$H_r = H\left[1 - \left(\frac{R}{r}\right)^3\right]\mu + H\frac{\epsilon}{R}\sum_{n=1} a_n n(n+1)\left(\frac{R}{r}\right)^{n+2} P_n(\mu) \tag{10a}$$

and

$$H_\theta = -H\left[1 + \frac{1}{2}\left(\frac{R}{r}\right)^3\right](1-\mu^2)^{1/2} + H\frac{\epsilon}{R}\sum_{n=1} a_n n\left(\frac{R}{r}\right)^{n+2} P_n^1(\mu)\,. \tag{10b}$$

The expansion coefficients, a_n, are determined by the last boundary condition, that the normal component of the magnetic field to the deformed surface be continuous. The normal component of the magnetic field (10) to the deformed boundary is, to the first order in ϵ (cf. Chandrasekhar and Fermi 1953*b*, eq. [142]),

$$\begin{aligned}\{H_r\}_{R+\epsilon P_n} + \{H_\theta\}_R \frac{\epsilon}{R} P_n^1(\mu) &= H\left\{1 - \left[\frac{R}{R+\epsilon P_n}\right]^3\right\}\mu \\ &\quad + H\frac{\epsilon}{R}\sum_{n=1} a_n n(n+1) P_n(\mu) - H(1+\tfrac{1}{2})(1-\mu^2)^{1/2}\frac{\epsilon}{R}P_n^1(\mu) \qquad (11) \\ &= H\frac{\epsilon}{R}[3\mu P_n(\mu) - \tfrac{3}{2}(1-\mu^2)^{1/2} P_n^1(\mu)] + H\frac{\epsilon}{R}\sum_{n=1} n(n+1)\, a_n P_n(\mu)\,.\end{aligned}$$

The boundary condition for the magnetic field requires that expression (11) vanish. Thus we must have

$$\begin{aligned}\sum_{n=1} n(n+1)\, a_n P_n(\mu) &= \tfrac{3}{2}(1-\mu^2)^{1/2} P_n^1(\mu) - 3\mu P_n(\mu) \\ &= -\frac{3}{2(2n+1)}[(n+1)(n+2)P_{n+1}(\mu) - (n-1)nP_{n-1}(\mu)]\,.\end{aligned} \tag{12}$$

Because of the orthogonality of the Legendre functions in the interval -1 to $+1$, equation (12) gives

$$a_{n-1} = \frac{3}{2(2n+1)} \quad \text{and} \quad a_{n+1} = -\frac{3}{2(2n+1)}, \tag{13}$$

while

$$a_l = 0 \quad \text{for} \quad l \neq n \pm 1\,. \tag{14}$$

Introducing equations (13) and (14) into equations (10), we finally find, for the magnetic field,

$$\begin{aligned}H_r &= H\left[1 - \left(\frac{R}{r}\right)^3\right]\mu + \frac{\epsilon}{R} H \frac{3}{2(2n+1)} \\ &\quad \times\left[(n-1)n\left(\frac{R}{r}\right)^{n+1} P_{n-1}(\mu) - (n+1)(n+2)\left(\frac{R}{r}\right)^{n+3} P_{n+1}(\mu)\right].\end{aligned} \tag{15a}$$

and

$$H_\theta = -H\left[1+\frac{1}{2}\left(\frac{R}{r}\right)^3\right](1-\mu^2)^{1/2}+\frac{\epsilon}{R}H\frac{3}{2(2n+1)} \times\left[(n-1)\left(\frac{R}{r}\right)^{n+1}P^1_{n-1}(\mu)-(n+1)\left(\frac{R}{r}\right)^{n+3}P^1_{n+1}(\mu)\right], \tag{15b}$$

correct to the first order of ϵ.

III. THE CHANGE IN THE MAGNETIC ENERGY

To the first order in ϵ, the change, $\Delta\mathfrak{M}$, in the magnetic energy is, according to equations (15),

$$\begin{aligned}\Delta\mathfrak{M} = &\iiint_{R+\epsilon P_n\geq r\geq R}\frac{H^2}{8\pi}\left\{\left[1-\left(\frac{R}{r}\right)^3\right]^2\mu^2+\left[1+\frac{1}{2}\left(\frac{R}{r}\right)^3\right]^2(1-\mu^2)\right\}r^2\,dr\,d\mu\,d\varphi\\ &+\iiint_{r\geq R}\frac{H^2}{8\pi}\frac{\epsilon}{R}\frac{3}{2n+1}\left\{\left[1-\left(\frac{R}{r}\right)^3\right]P_1(\mu)\left[(n-1)\,n\left(\frac{R}{r}\right)^{n+1}P_{n-1}(\mu)\right.\right.\\ &\left.-(n+1)\,(n+2)\left(\frac{R}{r}\right)^{n+3}P_{n+1}(\mu)\right]-\left[1+\frac{1}{2}\left(\frac{R}{r}\right)^3\right]P^1_1(\mu)\\ &\left.\times\left[(n-1)\left(\frac{R}{r}\right)^{n+1}P^1_{n-1}(\mu)-(n+1)\left(\frac{R}{r}\right)^{n+3}P^1_{n+1}(\mu)\right]\right\}r^2\,dr\,d\mu\,d\varphi.\end{aligned} \tag{16}$$

Evaluating the integrals on the right-hand side, correct to the first order in ϵ, we find that $\Delta\mathfrak{M}$ reduces to

$$\Delta\mathfrak{M}_2 = -\tfrac{1}{4}H^2R^3\frac{\epsilon}{R} \qquad (n=2) \tag{17a}$$

and

$$\Delta\mathfrak{M}_n = 0 \qquad (n\neq 2). \tag{17b}$$

IV. DISCUSSION OF THE STABILITY OF THE SPHERE

The change in the gravitational energy, $\Delta\Omega$, due to a general P_n-deformation has been calculated by Chandrasekhar and Fermi (1953*b*, eq. [152]) and is given by

$$\Delta\Omega = \frac{3(n-1)}{(2n+1)^2}\frac{GM^2}{R}\left(\frac{\epsilon}{R}\right)^2, \tag{18}$$

where M is the mass of the sphere and G is the gravitational constant. The change in the gravitational energy is seen to be of the second order in ϵ and is always *positive*, while the change in the magnetic energy is seen, from equations (17), to be of the first order in ϵ for a P_2-deformation and of higher order for all other deformations, as in the case studied by Chandrasekhar and Fermi (1953*b*).

According to equations (17) and (18), the total change in energy, $\Delta\mathfrak{E}_2$, due to a P_2-deformation, is given by

$$\Delta\mathfrak{E}_2 = \Delta\Omega_2+\Delta\mathfrak{M}_2 = \frac{3}{25}\frac{GM^2}{R}\left(\frac{\epsilon_2}{R}\right)^2-\tfrac{1}{4}H^2R^3\frac{\epsilon_2}{R}, \tag{19}$$

where we have inserted subscripts 2 to emphasize that we are now dealing with a P_2-deformation. For a P_2-deformation tending to make the sphere *prolate* ($\epsilon > 0$), the

change in the magnetic energy is *negative*. We can accordingly conclude that the sphere is unstable in the presence of the external magnetic field and tends to a *prolate* spheroidal shape. (In the case studied by Chandrasekhar and Fermi [1953*b*] one will remember that a *negative* ϵ made $\Delta\mathfrak{W}_2$ *negative*, and thus the sphere in their case tended to become *oblate* spheroidal.)

As a function of ϵ_2, $\Delta\mathfrak{E}_2$ has a minimum for a value of ϵ_2 determined by the equation

$$\frac{6}{25}\frac{GM^2}{R^3}\epsilon_2 - \tfrac{1}{4}H^2R^2 = 0\,, \tag{20}$$

or

$$\frac{\epsilon_2}{R} = \frac{25}{24}\frac{H^2R^4}{GM^2}\,. \tag{21}$$

On substituting $M = \frac{4}{3}\pi\rho R^3$ and introducing the numerical value for G, the following expression is obtained from equation (21):

$$\frac{\epsilon_2}{R} \approx 0.89 \times 10^6\left[\frac{H}{\rho R}\right]^2. \tag{22}$$

TABLE 1

$H = 1$

ρ	R	10	20	50	100	200
10	ϵ_2/R	*	*	*	*	0.30
50	ϵ_2/R	*	*	0.18	0.048	.012
100	ϵ_2/R	*	0.30	0.048	0.012	0.003

TABLE 2

$H = 10$

ρ	R	10	20	50	100	200
10	ϵ_2/R	*	*	*	*	*
50	ϵ_2/R	*	*	*	*	*
100	ϵ_2/R	*	*	*	*	0.30

Measuring ρ in units of the average interstellar density, $\bar{\rho} = 2 \times 10^{-24}$ gm/cm^3, H in units of the average magnetic field in spiral arms, $H_S = 7 \times 10^{-6}$ gauss, as estimated by Chandrasekhar and Fermi (1953*a*), and R in parsecs, equation (22) assumes the form

$$\frac{\epsilon_2}{R} \approx 1.21 \times 10^6\left[\frac{H}{\rho R}\right]^2. \tag{23}$$

From this formula one can get a rough idea about the effect of the magnetic field in spiral arms on highly conductive spherical clouds which have always been in the spiral arms but may for some reason have been shielded off from the interstellar magnetic field or nonmagnetic clouds which might come into the spiral arms from the outside after the spiral-arm magnetic field has been established.

Tables 1 and 2 have been derived from equation (23). The tables give corresponding values of R and ϵ_2/R for two different values of H ($H = 1$ for Table 1 and $H = 10$ for Table 2), and for three different values of ρ, $\rho = 10$, 50, and 100. For the columns

marked with an asterisk, formula (23) is not valid ($\epsilon_2/R > 1$). From examining the tables, we find that the interstellar magnetic field in spiral arms may affect appreciably the shapes of even the largest highly conductive nonmagnetic clouds, making them prolate spheroidal along the direction of the magnetic field, while smaller clouds, with no initial internal magnetic fields, will be squeezed into long, thin, rodlike shapes ("spaghetti").

It may be questioned whether a situation such as that discussed above has a counterpart in our Galaxy. From a theoretical point of view it still remains to be shown that nonmagnetic clouds can move into a magnetic field of the strength of the spiral-arm field, or, alternatively, a mechanism must be found to show that a cloud which was present in the spiral-arm field when it was formed might have been shielded off from the general field. And with respect to the possibility of detecting a possible effect of the spiral-arm field on nonmagnetic clouds, it may perhaps seem doubtful whether one can, at the present time, observe the effect by direct means. The assumed high electrical conductivity requires some kind of ionization mechanism, and the apparent shape of an observed luminous cloud will probably depend more upon the ionization source for the cloud than on its real physical shape. There are, however, objects in the sky which one may expect, by statistical considerations, to spend some of their lifetime in spiral arms, presumably having come from the outside of the arms, namely, planetary nebulae. There is no direct observational evidence that any of the known planetary nebulae are at the present time in the spiral arms (individual distances cannot be obtained with a sufficient degree of accuracy), nor is there any direct observational evidence that if they are there, they may have come from outside the arm. However, planetary nebulae seem now to have been definitely identified as population II objects and with a high concentration toward the galactic center and a moderate, but quite pronounced, concentration toward the galactic plane (Minkowski 1951). The observational evidence, including knowledge of the radial velocities, leading to their identification as members of population II, seems to indicate the possibility that some of them may at any time be passing through a spiral arm. This assumption is supported by Dr. W. Fricke, who has studied the radial-velocity distribution of the planetary nebulae. According to his estimates, about 50 per cent of the planetaries for which velocities were available would be in or between spiral arms (Fricke, private communication, 1953). The model studied above is, of course, too simple to be taken as a representation of a planetary nebula, but if a planetary nebula should at the present time be in a spiral arm and it did not have an initial internal magnetic field, one would expect it to behave, in a general way, like the clouds studied above. It should be pointed out that the time necessary for an appreciable deformation of a spherical cloud in an external magnetic field to take place is not known. That would require a calculation to a higher order in ϵ and is beyond the scope of the present paper.

I am indebted to Dr. W. Fricke for information on his unpublished investigation of the velocity distribution of the planetaries, and to Dr. Hugh M. Johnson for valuable discussions on various aspects of the problems concerning the application of the derived general results to cosmic clouds and, in particular, for calling my attention to the planetary nebulae. In conclusion, it is a pleasure to express my deep-felt gratitude to Dr. S. Chandrasekhar for his stimulating interest in the investigation presented here. I also wish to express my sincere thanks to the Yerkes Observatory, University of Chicago, for hospitality during the current academic year.

REFERENCES

Chandrasekhar, S., and Fermi, E. 1953*a*, *Ap. J.*, **118**, 113.
Chandrasekhar, S., and Fermi, E. 1953*b*, *Ap. J.*, **118**, 116.
Gjellestad, G. 1954, *Ap. J.*, **119**, 14.
Minkowski, R. 1951, *Pub. Obs. U. Michigan*, **10**, 25 (a symposium on "The Structure of the Galaxy").

NOTES

POLARIZATION OF A HEAVILY OBSCURED CLUSTERING OF OB STARS IN CYGNUS*

The clustering of OB stars reported by Münch and Morgan (1953) has been observed for interstellar polarization. The list of stars and the observed data are given in Table 1. The first and second columns refer to the number of each star assigned by Münch and Morgan (1953) and the BD number, if any, respectively. The next five columns give the 1900 positions, the galactic co-ordinates, and parallactic angle. The positions were taken from the *Bonner Durchmusterung* if a star is in that catalogue. Otherwise, the positions were determined from a direct photograph taken with a 5-inch Ross lens. The eighth and ninth columns give the amount of polarization in magnitudes and the position angle of

TABLE 1

JOURNAL OF OBSERVATIONS

No.	BD	1900		l	b	ϕ	p	θ	θ'	a_V
		α	δ							
1	.....	20^h27^m5	+41° 10′	47.81	+0.49	51.96	0.062	81.8	133.7	5.19
2	.....	20 27.7	+41 10	47.84	+ .45	51.93	.040	71.5	123.4	4.23
3	+40° 4212	20 28.0	+40 52	47.64	+ .23	51.88	.130	106.2	158.1	5.76
4	+40 4219	20 28.6	+41 06	47.89	+ .28	51.78	.051	77.6	129.4	4.44
5	+40 4220	20 28.8	+40 58	47.80	+ .17	51.75	.083	80.5	132.2	5.97
6	.....	20 29.2	+41 05	47.95	+ .18	51.68	.039	55.6	107.3	4.59
7	.....	20 29.7	+41 00	47.94	+ .06	51.60	.079	93.9	145.5	5.28
8	+40 4227	20 29.7	+40 58	47.91	+ .04	51.60	.023	85.9	137.5	4.83
9	.....	20 29.6	+40 55	47.87	+ .02	51.62	.056	51.4	103.0	6.78
10	+41 3804	20 30.2	+41 12	48.16	+ .11	51.52	.008	50.6	102.1	5.49
11	+41 3807	20 30.6	+41 16	48.26	+0.10	51.45	0.075	159.1	30.6	5.25

the plane of vibration, respectively. The following column, θ', is the position angle of the plane of vibration in galactic co-ordinates. The last column is the visual interstellar absorption as published by Johnson and Morgan (1954). Figure 1 is a plot of the positions of the stars and their observed polarizations.

From an inspection of the table it is immediately obvious that the interstellar polarization and absorption are not correlated. For example, stars 3 and 10, with the greatest and least polarization, have very similar interstellar absorption. In fact, the polarization does not appear to be correlated with anything, unless the polarization of star No. 11 can be considered negative, since its plane of vibration is approximately perpendicular to all the others. Then it is apparent that the polarization decreases with an increase in galactic longitude and that the polarization increases with increasing position angle of the electric vector. A long exposure (4 hours on Eastman 103*a*–O emulsion) with a 5-inch *F*/7 Ross lens does not show any obvious rapid changes in obscuration. This is suggested, of course, by the absence of a correlation in interstellar absorption of the individual stars with position. Except for the polarization observations, all the evidence supports the conclusion that these stars form an O-association. It appears, therefore, that the variation in polarization in the group is not a consequence of polarization and depolarization within a series of clouds but rather a result of nonuniformity in orientation of the polarizing particles

* *Contributions from the McDonald Observatory, University of Texas*, No. 238.

within a cloud or clouds.[1] This nonuniformity may be identified with the discontinuities in the direction of the interstellar magnetic field proposed by Fermi (1954) in his discussion of his new acceleration mechanism for cosmic radiation. For an adopted distance of 1.5 kiloparsecs, the minimum dimension of the association is approximately 13 parsecs, which is reasonable for the size of a cloud.

W. A. HILTNER

YERKES AND MCDONALD OBSERVATORIES
February 18, 1954

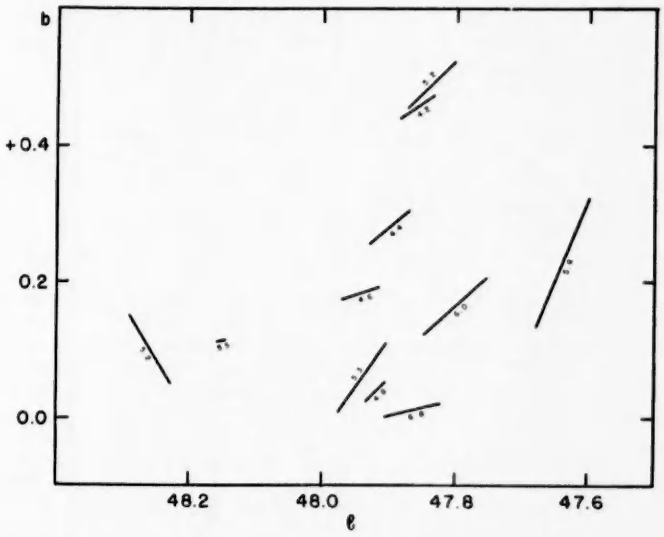

FIG. 1.—Polarization of the OB association in Cygnus. The length of each line representing a star is proportional to the amount of polarization, and the direction of the line represents the plane of vibration. The number beside each line corresponds to the visual interstellar absorption in magnitudes.

REFERENCES

Fermi, E. 1954, *Ap. J.*, **119**, 1–6.
Johnson, H. L., and Morgan, W. W. 1954, *Ap. J.*, **119**, 344–345.
Münch, L., and Morgan, W. W. 1953, *Ap. J.*, **118**, 161–162.

[1] It does not necessarily follow that the lines of force differ in direction within the cloud by 90°, since the lines of force may be nearly parallel to the line of sight and hence a small change in their direction within the association may produce the observed planes of vibration.

NOTE ON THE SPECTRUM OF 16 LACERTAE

Received February 23, 1954

1. The Mount Wilson coudé spectrograms of this star, which were previously used for the determination of its radial velocities (Struve, McNamara, Kraft, Kung, and Williams 1952), have been treated in the same manner as an earlier series of spectrograms of β Canis Majoris (Van Hoof and Struve 1953). Microphotometer tracings of the original spectrograms were obtained at the Institute of Nuclear Physics of the University of

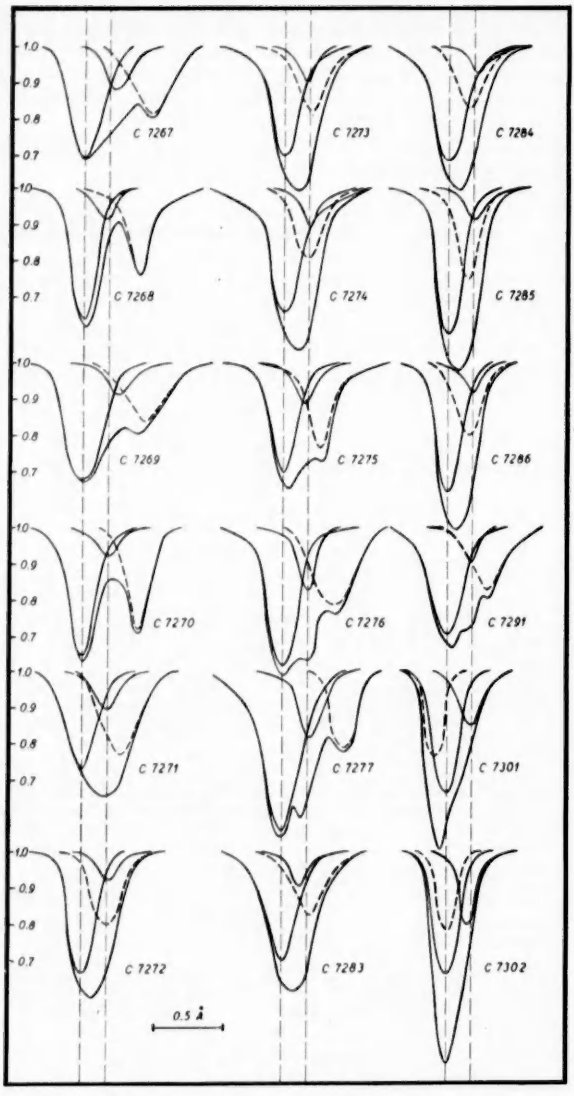

FIG. 1.—Profiles of the line *Ca* II K in 16 Lacertae, observed on August 16, 17, and 18, 1951. The observed profiles have been decomposed into two interstellar (stationary) components (*continuous lines*) and one stellar component (*dashed line*). The individual profiles labeled in the diagram by their plate numbers have the following dates and universal times: Aug. 16, 1951: C 7267, 7:31; C 7268, 7:50; C 7269, 8:12; C 7270, 8:35; C 7271, 9:00; C 7272, 9:27; C 7273, 9:54; C 7274, 10:23; C 7275, 10:50; C 7276, 11:18; C 7277, 11:47. Aug. 17, 1951: C 7283, 5:22; C 7284, 5:49; C 7285, 6:16; C 7286, 6:26; C 7291, 8:52. Aug. 18, 1951: C 7301, 10:47; C 7302, 11:18.

Louvain. On these tracings the distances were measured, in millimeters, between three hydrogen lines and several other near-by lines, chosen in such a way as to eliminate any small remaining differences in the linear dispersions of the individual tracings. The lines chosen for this purpose were as follows:

For $H\gamma$: *O* II 4317, *O* II 4320, *O* II 4346, *O* II 4349, *O* II 4351
For $H\delta$: *O* II 4072, *O* II 4076, *O* II 4119, *He* I 4121
For $H\epsilon$: *O* II 3954, *He* I 3965, *O* II 3973, *N* II 3995

The results of these measurements indicate a small tendency of the hydrogen lines to lag behind the other lines in radial velocity. This lag, amounting to $0.04P$, is of the same order of magnitude and in the same direction as in β Canis Majoris.

On the ascending branch of the velocity-curve the hydrogen lines are systematically displaced toward the red when compared with the other lines, by about 0.4 ± 0.1 mm on our tracings; on the descending branch the hydrogen lines are displaced toward the violet, also by about 0.4 ± 0.1 mm. Since the scale of the tracings is 12.1 km/sec per millimeter, the resulting velocity shifts are ± 4.8 km/sec.

2. On the tracings the duplicity of the *Ca* II K line, noticed by Struve and his collaborators (Struve *et al.* 1952), is clearly seen, and its varying aspect is paralleled by that of *Ca* II H. But Struve's former statement that "the *Ca* II line shows rapid changes in intensity and sharpness . . . which probably represent real and rather drastic variations in the atmosphere of the star" needs revision.

Figure 1 shows that the composite profile lends itself to a decomposition into three elementary lines, of which the strongest and the weakest remain at rest, thus disclosing their interstellar origin, while the one of intermediate strength follows closely the Doppler shifts of the other star lines and therefore represents the true stellar component. This latter component does not appear to undergo changes in intensity larger than can be accounted for by the errors in the intensity determinations, which is also true of its changes in width.

The mean intensity of the stellar component, averaged over all the tracings, is $A_\lambda = 0.053$ A. Its quasi-constancy makes it similar to the other star lines.

Of the two interstellar lines, the fainter one has an intensity of $A_\lambda = 0.019$ A and a radial velocity of $v = -1.0$ km/sec, reduced to the sun. When corrected for a solar motion of 20 km/sec toward an apex at $\alpha = 18.0$ hours, $\delta = 30°$, this leaves a peculiar radial velocity of $+9.4$ km/sec. The latter value suggests that this line cannot come from uniformly distributed interstellar calcium but must be ascribed to a local moving cloud.

The stronger interstellar line has an average intensity $A_\lambda = 0.085$ A, and a peculiar radial velocity of $v = -4.5$ km/sec. If this value represents the effect of differential galactic rotation of the continuous interstellar matter, it would indicate a distance of 1500 parsecs for the star, a value which is not entirely consistent with the low intensity of the line.

A. Van Hoof
M. De Ridder
O. Struve

University of Louvain (Belgium)
and
Berkeley Astronomical Department

REFERENCES

Struve, O.; McNamara, D. H.; Kraft, R. P.; Kung, S. M.; and Williams, A. D. 1952, *Ap. J.*, **116**, 81.
Van Hoof, A., and Struve, O. 1953, *Pub. A.S.P.*, **65**, 158.

PHYSICAL AND GALACTIC CHARACTERISTICS OF PLANETARY NEBULAE

In this note the writer discusses an apparent correlation between the physical characteristics of planetary nebulae (the spectrum, the temperature of the central star, T_s) and the galactic z-distance and peculiar radial velocity, v_{rp}. A characteristic of the spectrum for which there are many data is the ratio of intensities of the N_2 ([O III] 4959) and $H\beta$ emission lines. This ratio is a measure of the degree of excitation and of T_s (Stoy 1933). Setting $H\beta = 0$ mag., the ratio may be expressed as m_{N_2} mag. Aller (1941, 1951), Berman (1936), and Minkowski (1942) give data of m_{N_2} for 79 nebulae, of which 30 are common to Aller and Berman, 6 to Aller and Minkowski, and none to Berman and Minkowski. The difference in m_{N_2} between observers of the same nebulae is Berman − Aller = $+0.31 \pm 0.32$ mag. and Minkowski − Aller = $+0.67 \pm 0.58$ mag. (mean ± M.D.). In view of the photometric differences, which arise partly from observation of different sections of the nebulae, let us consider at present only the 36 nebulae for which a mean of two values of m_{N_2} can be taken after adding +0.31 mag. to the values of Aller and −0.36 mag. to the values of Minkowski.

Data of T_s, z, and v_{rp} are available for each of the above 36 nebulae. T_s may be defined in several ways, but it is based here on the difference between the apparent photographic magnitudes of the nebula and its central star (Berman 1937); z is derived from the mean (Minkowski 1951) of the distances, r, catalogued by Berman (1937) and Pa-

TABLE 1

GROUPED MEAN DATA OF 36 PLANETARY NEBULAE

Group	n	$m_{N_2} \pm$ p.e. (Mag.)	$T_s/1000 \pm$ p.e. (° K)	$\lvert z \rvert \pm$ p.e. (Psc.)	$\lvert v_{rp} \rvert \pm$ p.e. (Km/Sec)	$r \pm$ p.e. (Kpc.)
a	12	-1.82 ± 0.06	68 ± 5	340 ± 40	25 ± 4	2.9 ± 0.2
b	12	$-1.25 \pm .03$	50 ± 4	490 ± 70	30 ± 5	$2.2 \pm .2$
c	12	-0.47 ± 0.10	37 ± 2	620 ± 90	32 ± 4	2.6 ± 0.5

renago (1946); and v_{rp} is the radial velocity in Wilson's *General Catalogue of Stellar Radial Velocities* corrected for a solar motion of 30 km/sec toward $l = 40°$, $b = 0°$, and for the effect of differential galactic rotation. Bottlinger (1933) has tabulated the radial velocity of differential galactic rotation, $v(B/A, V_c, R, l - l_0)$, on his theory of the galactic potential. Here A and B are the rotational constants, and V_c is the circular velocity at R, the distance from the sun to the galactic center, which is at longitude l_0. His tables are constructed for $B/A = -1.0$ (I) and -0.6 (II). These values are larger than the normal ratio, -0.33; but Oort (1942) has shown that the normal ratio is too small for high-velocity objects, while $A - B$ remains the same. Therefore, let us derive v on Bottlinger's cases I and II, each with $R = 6.8$, 8.0, and 9.4 kpc. For each combination let $V_c = 27\,R$ km/sec/kpc and $l_0 = 325°$. Since $v \sin^2 b$ is as large as 5 or 10 km/sec in only 4 of the 36 velocities, a correction for galactic latitude was found to be unnecessary. Table 1 gives v_{rp} according to Bottlinger's case II and $R = 8.0$ kpc. In Table 1 the 36 nebulae are divided into three groups: (*a*) $m_{N_2} \leq -1.50$ mag.; (*b*) -1.50 mag. $< m_{N_2} < -0.99$ mag.; and (*c*) $m_{N_2} \geq -0.99$ mag. Means of m_{N_2}, $T_s/1000°$ K, $|z|$, $|v_{rp}|$, and r are taken in each group. Figure 1 shows the individual points on which the table is based. The table and diagram suggest a correlation between all the parameters except r. As m_{N_2} increases 1.35 mag., T_s drops by nearly half, z about doubles, and v_{rp} increases. An increase of mean v_{rp} from group *a* to group *c* is likewise found with the other combinations

of B/A and R which have been mentioned. Proper-motion data are too scarce and uncertain to be used to investigate peculiar space motions.

The correlation of z with m_{N_2} is the essential point of this note. The increase of v_{rp} with m_{N_2} supports the reality of this correlation, while the tabulated values of r show that these increases do not depend on a systematic change in distance from the sun. There are relatively few observational data of other close forbidden/Balmer line-intensity ratios. However, if White's (1952) data of [N II] 6584/$H\alpha$ for 22 planetary nebulae are divided into two equal groups according to [N II] 6584/$H\alpha > 0$ or $= 0$, respectively, the corresponding mean parameters T_s, z, and v_{rp} again vary in the same direction as they do with m_{N_2}. The spectra of the central stars of planetary nebulae are known in too few instances to correlate them with T_s or m_{N_2}.

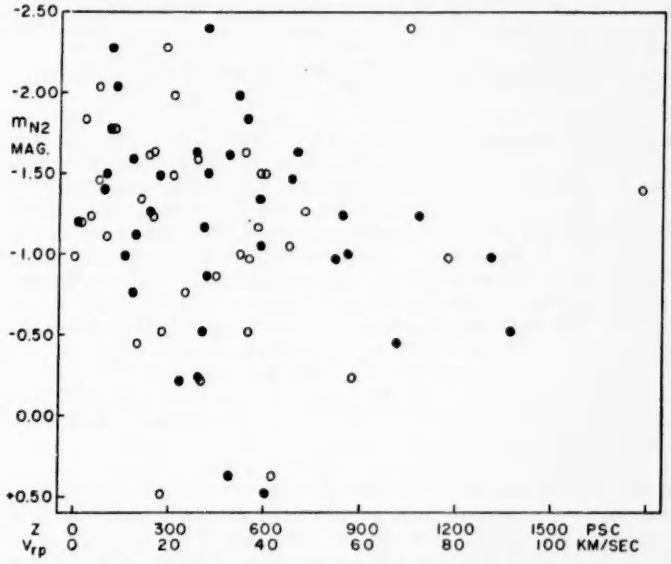

FIG. 1.—The data of 36 planetary nebulae. The absolute galactic z-distance (*filled circles*) and the absolute peculiar radial velocity, v_{rp} (*open circles*), are plotted against the magnitude m_{N_2} of the N_2 emission relative to $H\beta$.

Interstellar reddening is inadequate to explain the observed variations of the relative intensities of lines as close together as 100 A. The motion and expansion of planetary nebulae in the galactic gas stratum is an inappreciable source of collisional excitation near the galactic plane. The writer has found no other selection effect which will predict the correlation given above. He concludes, therefore, that the evidence favors a real correlation between certain physical and spatio-kinematical characteristics of the planetary nebulae.

The writer wishes to thank Dr. A. Blaauw for advice and encouragement in the preparation of this note.

HUGH M. JOHNSON

YERKES OBSERVATORY
January 27, 1954

REFERENCES

Aller, L. H. 1941, *Ap. J.*, **93**, 236.
Aller, L. H. 1951, *Ap. J.*, **113**, 125.
Berman, L. 1936, *M.N.*, **96**, 890.
Berman, L. 1937, *Lick Obs. Bull.*, **18**, 57.
Bottlinger, K. F. 1933, *Veröff. Univ. Sternw. Berlin-Babelsberg*, Vol. **10**, No. 2, Table 2.
Minkowski, R. 1942, *Ap. J.*, **95**, 243.
Minkowski, R. 1951, *Pub. Obs. U. Michigan*, **10**, 25.
Oort, J. H. 1942, *B.A.N.*, **9**, 334.
Parenago, P. P. 1946, *Astr. J. U.S.S.R.*, **23**, 69.
Stoy, R. H. 1933, *M.N.*, **93**, 588.
White, M. L. 1952, *Ap. J.*, **115**, 71.

PHOTOSPHERIC MAGNETIC FIELDS PRECEDING OTHER SOLAR ACTIVITY

The magnetograms of the sun published by Babcock (1953) for July 10, 1953, and July 19, 1953, show an interesting relation of extensive magnetic fields to other solar activity not only at the time of the magnetic observation but also on solar rotations immediately following the dates of the magnetograms. If we compare the July 19 magnetogram with solar-activity maps (D'Azambuja 1953; Trotter and Roberts 1953) for solar rotation No. 1335, June 24, 1953—July 21, 1953, we see two extensive photospheric magnetic fields which correspond to active regions shown on the maps. The high magnetic fields near the west limb and south of the equator clearly correspond to the sunspot and plage region at solar longitude 75°, latitude 10° S., designated 53-Q in HAO solar-activity summaries (Trotter and Roberts 1953). Such correspondence between photospheric magnetic fields and sunspot and plage regions has been noted by H. W. and H. D. Babcock (1952). Similarly, the fields north of the equator and about 2 days west of the central meridian correspond to the coronal region at longitude 45°, latitude 10° N., designated 53-H (Trotter and Roberts 1953).

There was neither disk nor coronal activity during rotation No. 1335 corresponding to the large magnetic fields just north and south of the equator and about 2 days east of the central meridian. One rotation later, however, this previously quiet portion of the sun became quite active. The region designated 53-S appeared at 15° longitude, 10° N. latitude and during its lifetime of two rotations produced more flares than any other region through the summer months. Very near it, 0° longitude, 5° S. latitude, another region, 53-T, appeared for one rotation. Hence we conclude that in regions 53-S and 53-T photospheric magnetic fields preceded sunspots, flares, plage, and coronal-line emission by at least one solar rotation.

The magnetogram of July 10, 1953, shows the extensive magnetic fields to be less intense than they were on July 19. With the exception of a rather large dipole in the Southern Hemisphere near the central meridian, what magnetic activity there was appeared in a rather large region centered just north of the equator and east of the central meridian. Again, during solar rotation 1335, there was no sunspot or coronal activity in that region. However, on the next rotation, the rather large region 53-R appeared at 120° longitude, 15° N. latitude. 53-R lasted for five rotations, displaying sunspots, plages, flares, and red and green coronal-line emission during its lifetime.

These conclusions are obviously drawn from a very small sample of Dr. Babcock's magnetograms, but they suggest that the use of such observations may be of the greatest

importance in prediction of solar-terrestrial relationships, as well as in understanding the basic physical processes involved in the formation of active solar centers.

DONALD E. BILLINGS

HIGH ALTITUDE OBSERVATORY OF HARVARD UNIVERSITY
and
UNIVERSITY OF COLORADO

REFERENCES

Babcock, H. W. 1953. *Ap. J.*, **118**, 387.
Babcock, H. W., and Babcock, H. D. 1952. *Pub. A.S.P.*, **64**, 282.
D'Azambuja, M. 1953. *L'Astronomie*, **67**, 324.
TROTTER, D., and ROBERTS, W. O. 1953. *HAO-21, Solar Activity Summary III*. Boulder, Colo.: High Altitude Observatory.

A NOTE ON THE MOTION OF AURORAL STREAMERS

It was pointed out recently by Meinel and Schulte (1953) that: "The long-recognized westward drift of auroral features was found to occur only during the evening hours. The drift was observed to be always eastward during the morning hours." In this connection an observation that I made during the great display of March 22, 1920, may be of interest. Though the effect differed in slight details, there is no doubt that the same phenomenon was concerned. The relevant passages from the report published at that time are brief enough to be quoted in full (1920):

"During the display I noticed the following curious facts: Before midnight, in the northwest quarter of the sky, streamers forming in the north drifted slowly toward the west; in the northeast quarter, try as I would, I could not determine any definite drift. After midnight, in the northeast quarter, there was a drift from north to east, but I could detect no drift in either direction in the northwest quarter."

If this phenomenon is common to all displays, it would indeed be surprising if it had not been observed and reported (perhaps as obscurely as my own observation) several times before 1920. A search of the literature might yield a considerable amount of useful data.

DEAN B. MCLAUGHLIN

UNIVERSITY OF MICHIGAN

REFERENCES

Meinel, A. B., and Schulte, D. H. 1953, *Ap. J.*, **117**, 454.
McLaughlin, D. B. 1920, *Pop. Astr.*, **28**, 309; reprinted in *Month. Weath. Rev.*, **48**, 388.

THE TEMPERATURE OF THE LOW CHROMOSPHERE

Wooley and Allen (1950) have proposed a model for the solar chromosphere in which the temperature is constant at the photospheric boundary value for heights up to 5000 km and then increases steeply with height until $T = 10^6$° K is attained in the corona. Throughout the isothermal layer, the hydrogen is entirely neutral, and the top of the layer is believed to coincide with the region in which ionization of hydrogen begins to set in. At a height of 6000 km, where the hydrogen is half-ionized, the temperature has increased to 6300° K; and 10 km higher the temperature is 36,000° K, and the ionization of hydrogen is complete. The Wooley-Allen model is based chiefly on two lines of reasoning. First, because of the very high abundance of neutral hydrogen in the lower chromosphere, the optical depth in the Lyman continuum is also high; hence the gas must be in

radiative equilibrium, and, since its opacity shields it from the ultraviolet radiation of the corona, its temperature must approximate that of the photosphere. Second, the model is consistent with the required number of Lyman-continuum quanta, as deduced from ionospheric measurements. A temperature as high as 6000° K throughout the low chromosphere would give far too many ultraviolet quanta.

The purpose of this note is to call attention to the fact that recent observations of Lyman-α radiation from high-altitude rockets by Byram, Chubb, Friedman, and Gailar (1953) furnish strong additional evidence in support of a temperature model of the Wooley-Allen type. The rocket observations consist of absolute-intensity measurements in the Lyman-α region, made with photon counters and continuously telemetered to the ground from altitudes up to 128 km. The total flux per square centimeter at the top of the atmosphere was found to be 0.10 ergs/sec. From the observed constancy of the air-absorption coefficient with altitude and the fact that laboratory measurements show that the atmospheric "window" centered on Lyman-α is exceedingly narrow, Byram *et al.* conclude that the Lyman-α emission line must be less than 1 A in width. They also obtain the result that the radiation intensity in the neighboring continuum must be less than that of a black body at $T = 4600°$ K.

The first conclusion that can be reached from these observations is that the chromosphere cannot be isothermal throughout the region in which hydrogen is neutral, since otherwise the line width would depend only on the square root of the total number of one-quantum hydrogen atoms per unit radial cross-section, which is extremely high. From the table of chromospheric density distribution given by van de Hulst (1953), we find that this number is 1.3×10^{23} cm^{-2}. If we now calculate the width of Lyman-α at half-intensity from the theory of self-absorbed emission lines, broadened by radiation damping (Goldberg, Dodson, and Müller 1954), we obtain the value 155 A, which is independent of temperature. If this value is to be reduced even by a factor of 100, the total number of atoms would have to be lowered by a factor of 10,000, which seems out of the question. This conclusion is independent of any assumed value of the temperature.

The only reasonable assumption that appears to account for the narrow width of Lyman-α is that the line is formed in a region of the chromosphere in which the temperature increases rapidly with height. Let the optical depth in the line, at a point x measured inward from the top of the chromosphere, be τ_ν. Then

$$\tau_\nu = \int_0^x n_1 a_\nu dx , \tag{1}$$

where n_1 is the local concentration of ground-level hydrogen atoms in cm^{-3} and a_ν is the absorption coefficient per atom at frequency ν. The flux F_ν at any point in the profile is given by

$$F_\nu = \int_0^t P_\nu e^{-\tau_\nu} d\tau_\nu , \tag{2}$$

where t_ν is the optical depth at the base of the chromosphere and P_ν is the Planck function at the Boltzmann temperature, defining the ratio of populations in the first and second energy levels of hydrogen. Because of the exponential factor in equation (2), there will be very little contribution to the flux from optical depths greater than unity. We interpret the results of Byram *et al.* to mean that the radiation at the center of Lyman-α comes from the very top of the neutral hydrogen layer, where the temperature is greater than 4600° K, and that, at a distance from the line center not exceeding $\frac{1}{2}$ A, the radiation effectively comes from a lower layer, which is at a temperature $< 4600°$ K.

We assume that the temperature decreases with depth from its value, yet to be established, at the top of the neutral hydrogen layer to a lower limit of 4600° K, which we identify with the boundary temperature of the photosphere. In order to determine the

approximate geometrical height at which the boundary temperature is reached, we set $\tau_\nu = 1$ at $\Delta\lambda = \frac{1}{2}$ A and calculate the total number of ground-level H atoms in the line of sight from equation (1). The absorption coefficient per atom for radiation damping at $\Delta\lambda = \frac{1}{2}$ A is 1.65×10^{-18}, and hence the total number of atoms is 6.1×10^{-7} cm^{-2}. From van de Hulst's (1953) table of density distribution we find, by graphical integration, that this number is reached at a height of 4000 km.

It is also possible to estimate the temperature at the top of the neutral hydrogen layer at $h = 6000$ km from the measurement of the total flux in the line, which amounts to 4.6×10^3 ergs/sec cm^2 of the solar surface. In the absence of information on the line shape and also because a factor of 2 in the Planck intensity corresponds to only about 200° in temperature, we assume that the line profile is rectangular in shape, the length of the base being 1 A, or 2.03×10^{12} sec^{-1}. The central intensity is therefore 2.3×10^{-9} ergs cm^{-2} sec^{-1} per unit frequency, which corresponds to $T = 6030°$ K, in good agreement with the Wooley-Allen model. If the line width is taken as $\frac{1}{2}$ A, the resulting temperature is 6250° K.

It can be concluded that the photon counter measurements of Lyman-α radiation from the sun are consistent with a model chromosphere in which the temperature is at first constant with height at the boundary value of the photosphere up to a height of at least 4000 km and thereafter increases to the approximate value $T = 6000°$ K at height 6000 km. The temperature may rise even more steeply if the width of Lyman-α is less than the assumed value of 1 A, which is an upper limit.

LEO GOLDBERG

McMATH-HULBERT OBSERVATORY
UNIVERSITY OF MICHIGAN
PONTIAC, MICHIGAN
May 1, 1954

REFERENCES

Byram, E. T.; Chubb, T.; Friedman, H.; and Gailar, N. 1953, *Phys. Rev.*, **91**, 1278.
Goldberg, L; Dodson, H. W.; and Müller, E. A. 1954, *Ap. J.*, **120**, 83.
van de Hulst, H. C. 1953, *The Solar System*, ed. G. P. Kuiper, Vol. 1: *The Sun* (Chicago: University of Chicago Press), p. 238.
Wooley, R.v.d.r., and Allen, C. W. 1950, *M.N.*, **110**, 358.

ERRATUM

In *Ap. J.*, **119**, 456, 1954, the detection of galactic emission at a wave length of 10 cm by Piddington and Minnett, *Australian J. Sci. Res. A*, **4**, 459, 1951, was inadvertently overlooked. Therefore, the words "and the galactic background" should be deleted from line 4, page 456, and in the next line the number 25 should replace the number 21. On page 456, line 20, specific intensity equals $3.14 \times 10^{-21} T_B$ instead of $3.14 \times 10^{-25} T_B$.

ANNOUNCING

THE ASTROPHYSICAL JOURNAL SUPPLEMENT SERIES

These *Supplements* are intended to provide a medium for the publication of extensive investigations, such as wave-length lists of stars of special interest, photometric data, results of numerical integrations pertaining to stellar interiors, model stellar atmosphere calculations, and theoretical investigations not immediately related to astronomical problems.

Supplement No. 4

"Photometric Investigation of the Eclipsing Binary UX Ursae Majoris." H. L. JOHNSON, BARBARA PERKINS, and W. A. HILTNER.

Detailed photoelectric observations of the eclipsing binary UX Ursae Majoris in three colors (ultraviolet, yellow, and blue) obtained during the years 1951–53 are discussed with regard to variations with color and time.

(Published June, 1954. Price, $1.25)

Supplement No. 5

"On Nuclear Reactions Occurring in Very Hot Stars. I. The Synthesis of Elements from Carbon to Nickel." F. HOYLE.

The nuclear reactions that occur when stellar material is heated to progressively higher and higher temperatures are considered. It is shown that the temperature range from 10^8 deg. K to 2×19^9 deg. K brings in nuclear reactions that provide for the synthesis of all elements from carbon to zinc, with the exception of nitrogen.

(Ready August, 1954. Price, $1.25)

Supplement No. 6

"On the Dissipation of Gas and Volatilized Elements from Protoplanets." HAROLD C. UREY.

In this paper Dr. Urey attempts to use known thermodynamic properties of chemical substances in order to estimate the conditions under which the earth and other terrestrial planets may have been formed in the past. He concludes that condensation from a high-temperature cloud is impossible and makes suggestions of other possible ways by which the chemical conditions can be met within the framework of current astronomical thinking.

(Ready August, 1954. Price, $1.25)

An abstract of each supplement will be published in THE ASTROPHYSICAL JOURNAL. The Supplements will appear irregularly, and may be purchased separately or by subscription. Each volume of Supplements will consist of approximately 500 pages.

Subscriptions

$8.00 per volume

Canada, $8.75. Foreign, $9.50.

To members of the American Astronomical Society, $6.00 per volume.

Orders now accepted.

THE UNIVERSITY OF CHICAGO PRESS

5750 ELLIS AVENUE CHICAGO 37, ILLINOIS

Announcing

MEASUREMENTS OF DOUBLE STARS, III

By GEORGE VAN BIESBROECK

PUBLICATIONS OF THE YERKES OBSERVATORY, VOLUME VII, PART VI

"This work lists measurements of the position angles and separations of about 2,500 close double stars, mostly in the years 1935 to 1951, with the 40-inch Yerkes refractor and the 82-inch McDonald reflector. New orbits are given for 19 binary systems, and new dynamical parallaxes are published for many slow-moving pairs."—*Sky and Telescope*

244 pages, paper, $10.00

THE UNIVERSITY OF CHICAGO PRESS

5750 ELLIS AVENUE CHICAGO 37, ILLINOIS

THE OBSERVATORY

FOUNDED 1877

* * *

A Magazine presenting current developments in Astronomy by means of Articles, Correspondence, Notes on discoveries and Reviews of important astronomical books. The papers read at the Meetings (Astronomical & Geophysical) of the Royal Astronomical Society and the discussions which follow are also fully reported.

* * *

Annual subscription for 6 issues, post free, £1 (U.S.A. and Canada, $3.00) should be sent to

The Editors, ROYAL GREENWICH OBSERVATORY

Herstmonceux Castle, Hailsham, Sussex, England